Departamento de Ingeniería Química. Universidad de Sevilla

DEVELOPMENT OF NOVEL SCAFFOLDS FROM NANOSTRUCTURED BIOPOLYMER MATRICES WITH APPLICATIONS IN TISSUE ENGINEERING

Desarrollo de andamios de matrices de biopolímeros estructuradas con aplicaciones en Ingeniería Tisular

Víctor Manuel Pérez Puyana

DEVELOPMENT OF NOVEL SCAFFOLDS FROM NANOSTRUCTURED BIOPOLYMER MATRICES WITH APPLICATIONS IN TISSUE ENGINEERING

Memoria presentada para optar al grado de Doctor por:

Víctor Manuel Pérez Puyana

Directores:

Dr. D. Antonio Guerrero Conejo

Dr. D. Alberto Romero García

Sevilla, Octubre de 2019

Departamento de Ingeniería Química

Universidad de Sevilla

La Tesis Doctoral titulada “Development of novel scaffolds from nanostructured biopolymer matrices with applications in Tissue Engineering”, realizada por D. Víctor Manuel Pérez Puyana para optar al grado de Doctor con Mención Internacional por la Universidad de Sevilla, se presenta con la aprobación de los Directores y el Departamento de Ingeniería Química de la Universidad de Sevilla.

Directores:

Dr. D. Antonio Guerrero Conejo

Dr. D. Alberto Romero García

Director de Departamento de Ingeniería Química

Dr. D. Felipe Cordobés Carmona

Doctorando,

Víctor Manuel Pérez Puyana

Agradecimientos

Han pasado 4 años, con sus 1349 días, sus 32376 horas, 1942560 minutos y 116553600 segundos. Parecía que no iba a llegar, pero aquí está. Es el momento de escribir los agradecimientos de mi tesis y todavía no sé por dónde empezar.

La gente que me conoce sabe que me gusta contar historias como si fueran cuentos dejando *frases célebres* por el camino. Ya que para la elaboración de esta tesis he intentado seguir este mismo principio, para escribir estos agradecimientos voy a intentar seguirlo también. En todo cuento y/o historia hay unos personajes que son los responsables del correcto transcurso de la misma. En mi caso, esta tesis ha sido posible gracias a la ayuda y apoyo de muchísima gente, los cuales son los verdaderos protagonistas de esta historia y a los que quiero agradecer (ahora que no me está viendo nadie).

En primer lugar, quiero dedicar mi tesis doctoral a mi familia, la cual siempre me apoya y está ahí cuando se necesita, desde los mayores como son mis tíos Elías y Nieves hasta los más enanos (el bueno de Elías, el travieso de Lucas, el loco de Sergio y la indescriptible Patricia). Sin embargo, hay dos personas a las que quiero hacer una mención especial, dos personas de las que todo lo que diga se queda corto para lo que me inspiran y me hacen sentir. Dos personas sin las cuales estoy seguro de que no estaría donde estoy (no solo biológicamente hablando), que me hacen ser mejor persona y mi ejemplo de futuro. Por supuesto que estoy hablando de mis PADRES, aquellos que verdaderamente me han sufrido día tras día mis caras largas, mis chispazos, mis momentos de "no se me publica nada" y mis innumerables días de llegar tarde y sin ganas de hablar; y ellos siempre con una buena cara y con una paciencia que ni el santo Job. **¡GRACIAS!**

Además de a mi familia, no quiero dejar atrás a mi otra "familia". Esos amigos que me han acompañado (y aguantado) durante este tiempo, con sus días de *chichas*, sus sesiones de Cineeeee, o sus tardes de café, cerveza y cena. **¡GRACIAS!**

Pero ahí no queda la cosa ya que durante estos 4 años donde he pasado más tiempo ha sido en la Facultad de Química, concretamente en el Departamento de Ingeniería Química. ¡La de horas que he echado ahí…!, horas que han pasado como segundos gracias a las personas que componen el departamento, personas que me han ayudado desde que comencé con mi Trabajo Fin de Grado y que me hacían ir a trabajar con ganas. De todos ellos, quiero hacer especial mención a cuatro, las cuales más han colaborado y ayudado a realizar esta tesis. En primer lugar a Antonio, por su confianza a la hora de contar conmigo para trabajar en el grupo y por sacar siempre tiempo de donde no tiene para ayudarme siempre que le molesto con alguna pregunta o paper o capítulo de tesis que leer. También quiero agradecérselo a Alberto, sin el cual (estoy completamente seguro) no habría crecido como lo he hecho, y no solo me refiero en el ámbito profesional. Y no me puedo olvidar de Mercedes y José Fernando. Mercedes es una super ingeniera que me aguanta lo indecible y que vale mucho más de lo que ella se imagina, una persona que llegará a donde ella se proponga pero que tiene un pero… es bética (nadie es perfecto). En cuanto a José Fernando, podría decir muchas cosas, pero las descripciones se me dan *regulinchi* así que solo diré que es un crack. **¡GRACIAS!**

Pero no solamente he trabajado en Sevilla, sino que también he pasado 9 meses en Maastricht (Holanda) desarrollando mi tesis. Y si he podido pasar tanto tiempo allí ha sido gracias a Lorenzo y Paul, que no solo me aceptaron en 2017 sino que consintieron aguantarme durante 2018 y

2019. Sin temor a equivocarme puedo decir que Maastricht es y será mi segunda casa, una ciudad en la que he vivido muchísimas experiencias que me han hecho crecer como persona. Una ciudad en la que holandés no he aprendido, pero he realizado grandes avances en italiano y portugués, sobre todo portugués. Defino mi estancia en Maastricht como una experiencia que me ha hecho conocer a grandísimas personas con las que he vivido numerosas aventuras, cervezas y tardes de relax en el parque. Tendría una lista enorme de amigos a los que podría nombrar pero me quedo, sin duda, con dos artistas con los que he pasado algunos de los mejores momentos allí, ellos son sin duda Shivesh y Tristan. **¡GRACIAS!**

Y me gustaría finalizar diciendo, *plagiando* a un sabio, que los resultados son los resultados. Los que van a ver a continuación han sido los míos después de esta aventura que he vivido durante los últimos 4 años, por lo que me gustaría también agradecerle a usted, sí a usted, por dedicar parte de su tiempo en leer este documento que he elaborado con tanto esfuerzo y cariño. **¡GRACIAS!**

Y eso es todo, un ciclo que termina y que da paso a una nueva aventura, pero eso… eso ya será un problema de mi yo del futuro.

INDEX

Chapter 1: Background

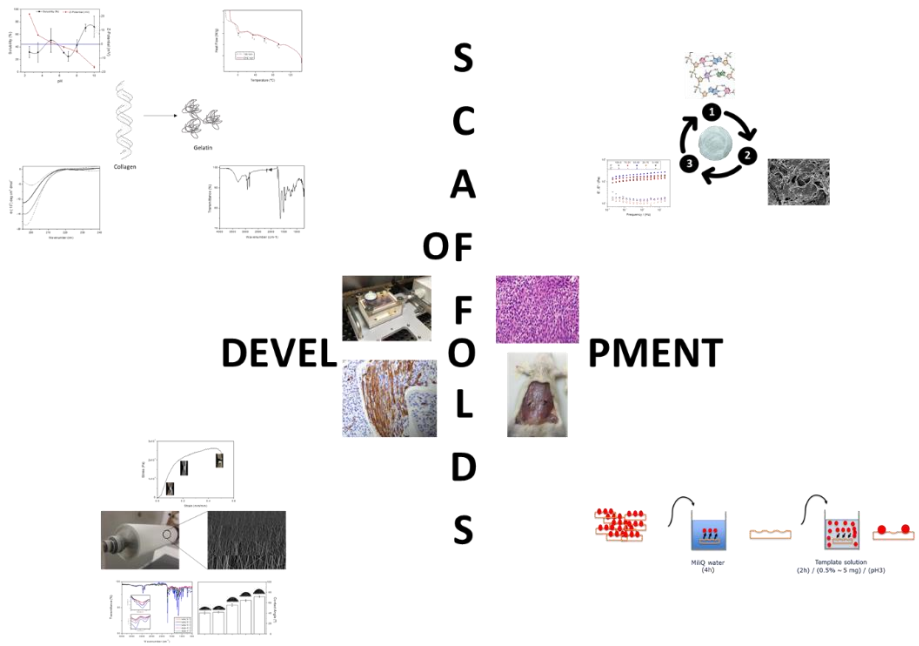

1.1 Introduction

This thesis is based on the development and characterization of polymer-based biomaterials through different techniques for their potential application in Tissue Engineering (TE). During the reading of the thesis some questions concerning this field will be solved, but first of all, what is a biomaterial?

From the multiple definitions given, highlighted those applied to regenerative medicine from 3 authors. Williams in 1987 defined a biomaterial as "a substance or combination of substances, excluding the medicines, which come from a natural or synthetic origin and could be used during a period of time as everything or a part of a system that increases or replaces any tissue, organ or function inside the body". Later, Black in 1992 defined the term biomaterial as "a material of natural origin or produced by the human being which is used to manage or to replace the functions of the tissues of the human body". Recently, a biomaterial was defined as "a material designed to repair or to re-establish the functionalities of a biological defective system" (Ramakrishna et al., 2016). The biomaterials have evolved along the history improving their characteristics. This fact allowed scientists to establish different generations of biomaterials:

- First Generation: The first generation is characterized by the use of *biologically tolerable* materials, such as stainless steel, cobalt-chromium (CoCr) alloys and polymethyl methacrylate (PMMA), which form a fibrous tissue that isolates the implant from the environment and prevents its close union with bone. In this generation, a high priority was given to the treatment of infectious diseases, septic injuries and the application of antibiotics. Efficient treatment of both conditions and materials was indispensable.

- Second Generation: After the Cold War and with a considerable increase in global life expectancy, the use of materials with little rejection in the organism and with the least number of side effects and the longest possible durability became a priority. This generation extends from 1980 to 2000 and is characterized by the development of *bioactive* biomaterials (bioactive silicon and hydroxyapatite glasses) and *biodegradable* (polymers and composites), with the ability to interact with the surroundings, as the medium proteins, that environ the material, allowing an integration of the fabric on the surface of the material. As none of the metals used in the design of prostheses is bioactive per se, within this second generation, metals with surfaces coated with bioactive ceramics and modifications on the surface to induce the adhesion of proteins stand out. During this second generation, bioabsorbable materials, such as biodegradable polymers, also stand out. This is where the accepted definition of a biomaterial is coined: non-viable material with which a medical device is manufactured that interacts with biological systems (Williams, 2009). The same author also defines a very important concept, which is *biocompatibility*: the ability of a material to fulfill a certain function with an adequate response from the host in a specific application (Williams, 2009).
- Third Generation: The third generation of biomaterials are designed considering that they will be in contact with living tissues and that the surface properties of such materials, such as topography, surface charge and all aspects related to the chemistry of their surfaces, are fundamental for a positive response. This entails adequate functionalization of the free surfaces of these biomaterials to facilitate adhesion, proliferation and cell differentiation under

optimal conditions. The implantation of a device in the human organism requires that it be guaranteed its total recognition by the complex physiological system. The surfaces of the biomaterials can be hydrophilic or hydrophobic. This property conditions that the proteins are absorbed by the surface of the material in question, which is directly related to the tolerance of the organism to the material. At this point we start looking for materials that change from biostable to bioresorbable for better implant osteointegration, that is, the body is able to metabolize and resynthesize into compounds that can be absorbed, such as proteins, or they can be discarded completely. These materials are designed to interact and integrate with the biological environment and degrade by hydrolytic or even enzymatic action.

- Fourth Generation: Fourth generation biomaterials combine high functionality with the rise of new multidisciplinary advances that bring us closer and closer to the synthesis of materials that not only adapt to the human body but also imitate it remarkably. In addition to an improvement in terms of the development of those materials already exposed in previous generations, our focus is now on two booming fields that shed some light on the future of biomaterials. These are nanomedicine (application of nanotechnology in medicine) and biomimicry (it is the science that studies nature as a source of inspiration, making use of new technologies to solve those human problems that nature has solved).

On the other hand, the field of development of biomaterials evolved with Tissue Engineering. So, here another question comes, what is Tissue Engineering?

Although the terms "Tissue Engineering" and "Regenerative Medicine" have become interchangeable (the field tries to focus on cures rather than on treatments for complex and often chronic diseases), the concept of Tissue Engineering is integrated into the field of Regenerative Medicine. Regenerative Medicine has long been only an unattainable dream, but with the technological advances and the audacious intellect of several scientists, this great branch of medicine opens the way to the future, developing cures and treatments against major diseases that have limited us until now. But this medical science does not work alone since it joins with others such as advanced cell therapy, genetic engineering and tissue engineering, which are the main fields that can lead to compliance with the goals proposed by this branch of current medicine.

The term "Tissue Engineering" was coined in 1988 being defined as "a new field of investigation, of rapid development, which aim is the production of tissues" (Skalak and Fox, 1988). Nowadays, Tissue Engineering is defined as “the science of the design and fabrication of new tissues for the functional reestablishment of altered organs and the substitution of damaged structures because of traumatism or diseases” (Reddi, 2000), so it is a growing multidisciplinary field with many medical applications and it has the potential to create tissues from scaffolds where cell insertion occurs. The starting point of Tissue Engineering can be set in the pioneering studies of Yannas and Vacanti in the 80s, who conceived the idea of giving the cells a scaffold/frame/matrix so that they could grow and form a tissue (Langer and Vacanti, 1993; Yannas and Burke, 1980). However, Tissue Engineering has suffered an exponential growth since 2000 (Ghosal et al., 2014; Kakkar et al., 2014; Offeddu et al., 2015; Sachlos and

Czemuszka, 2003). This evolution can be observed in the number of related publications shown in Figure 1.1.

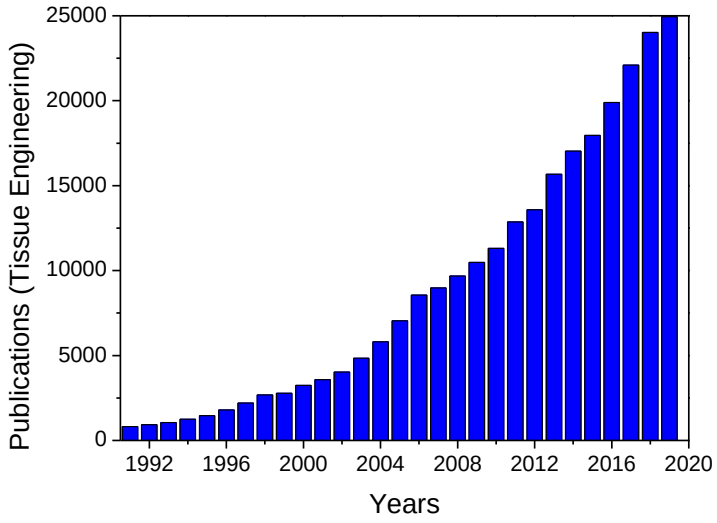

Figure 1.1. Evolution of publications concerning Tissue Engineering. Data obtained from Scopus and Web of Science

The application of Tissue Engineering techniques represents a great advance in the fields of cell therapy and Regenerative Medicine, being one of the advances in biomedicine with greater impact in the health sector. According to the Tissue Engineering Market Research Report from 2017, the investment made in the development of new tissue engineering techniques has grown rapidly from 950 million US $ in 1997 to 7100 million in 2017, foreseeing a growth at a constant rate with a compound annual rate of 17,22% during the period of 2017-2022 review (Nerem, 2010). These forecasts have been confirmed by a recent report by the consulting firm Goldman Sachs, which states that the investment of venture capital funds in the regenerative medicine sector has increased from 296 million in 2011 to 807 million 2016, with an annual growth rate of 34%.

In general, Tissue Engineering is based on three main elements, elements which are essentials for the development of tissues. These elements are stem cells to evolve the tissue, growth factors to stimulate the growth of the cells setting up the optimal conditions and biomaterials as three-dimensional structures to support cell adhesion and growth (Lin et al., 2015). For Tissue Engineering, the biomaterials used for cells regeneration, in conjunction with the cells and growth factors, are called scaffolds. So, what is a scaffold and which properties should satisfy?

A scaffold is a polymer matrix which is degradable and bioabsorbable which its principal function is to serve as an anchor platform for cells adhesion, allowing their growth. In addition, they could have other functions as transport, store and release the growth factors as well as stimulating specific cellular responses (contributing to the structural and mechanical integrity of the region). Moreover, the scaffolds should exhibit some properties or satisfy certain conditions (Vallet-Regi and Munuera, 2000):

- Biocompatibility: it is the crucial property for these three-dimensional structures (matrices) to be considered as scaffolds. It is related to the quality of a material of being compatible with the biological environment that surrounds it, so, its aptitude to interact with the tissues without damaging. A material which could be considered as biocompatible is that one that should be kept inside a few acceptable limits of compatibility, since it is practically impossible to find a completely inert material. In addition, and concerning the biodegradability, the derivative products must also be necessarily biocompatible and without toxicity.

- Biodegradability: These matrices must be biodegradable and absorbable, but with a speed of degradation similar to the regeneration and extension of the tissue formed.
- Porosity: The scaffolds must present porous spaces to shelter to cells and active factors, besides favoring the penetration or bioconductivity of the tissue formed. Depending on what type of cells it shelters, the ideal size of pore ranges between 40 and 150 μm or 200 and 400 μm (Li and Cooper, 2011; Van Vlierberghe et al., 2011). Apart from the pore size, good interconnectivity between the pores is always sought. The porosity presented by the scaffold is a fundamental and exclusive parameter since depending on the applications considered it must present different characteristics, but a distribution of well-interconnected pores is necessary in most TE applications in order to achieve a better nutrient transport and facilitate cell migration.
- Mechanical Resistance: The scaffolds must present a suitable mechanical resistance to be able to act as supporting structures during the period necessary for tissue growth. For it, besides assembling the set of previous properties, it is essential that the scaffolds belong to the group of viscoelastic materials. To evaluate the mechanical resistance of a material it is necessary to study the relation between a variable that realizes of the application of a force or system of forces, as the stress, or relation between the applied force and the area on it is applied, and another that evaluates the strain produced (γ) or the strain rate ($\dot{\gamma}$). All these behaviors are evaluated across Rheology, or science that studies the existing relation between the external forces that act on a body and the deformation that produce. One of the most widespread forms of characterization of these materials is through

"dynamic" tests with low amplitude efforts. In this type of tests, a sinusoidal strain is applied such that the structure of the material remains unchanged, defining the linear viscoelastic zone of the material. In this area, the response (deformation or stress) is also sinusoidal and independent of amplitude. Within the dynamic tests, the relationships between stress and strain of compression, tensile, flexion or shear can be studied, properly selecting the geometry of the specimen and the form of application of the stress or deformation. The most important parameters of this type of test are: *Elastic Modulus* (E'), which represents the ability of the material to store energy elastically; *Viscous Modulus* (E"), which measures the ability to dissipate energy; and the *Loss Tangent* (tan δ), which is the relationship between both modules and marks the predominance of the elastic or viscous nature of the material (Equation 1.1):

$$\tan(\delta) = E''/E' \qquad (1.1)$$

Apart from the properties previously mentioned, there are others which could be profitable enough for the suitable use of three-dimensional matrices as scaffolds. These properties are a high specific surface (in order to allow a high cell density), suitable surface topography (involved in cell attachment on the scaffold) and weak antigenicity (produce no rejection, so, immune response in tissues).

1.2 Hypothesis and main objectives

A general overview of the different stages involved in the development of scaffolds can be seen in the following scheme (Figure 1.2):

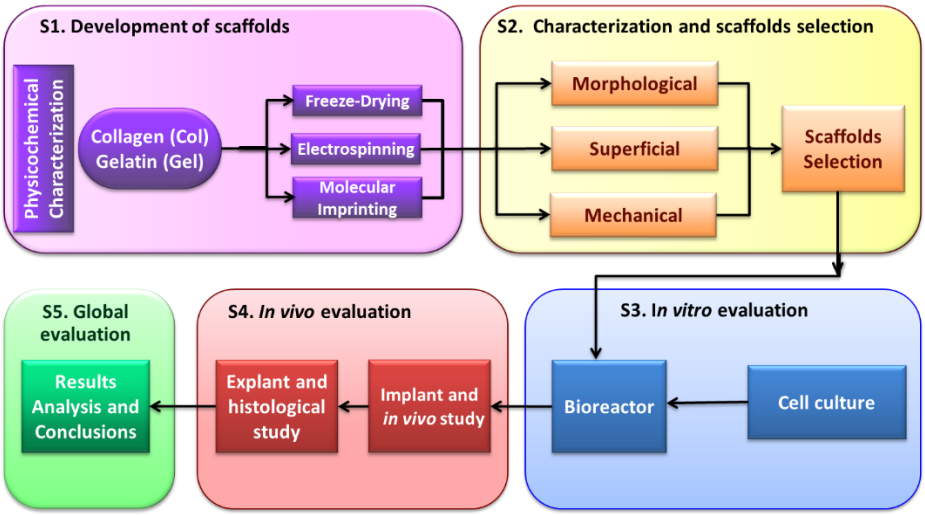

Figure 1.2. Stages (S) in the development of scaffolds for Tissue Engineering

Thus, the initial hypothesis consists of the development of scaffolds with adequate characteristics of porosity, mechanical resistance and biodegradability, which are viable for the development of muscular and biocompatible tissues, from combinations of collagen and gelatin with either natural polymers (chitosan) or synthetic polymers (PCL). The proposal involves the use of classical polymer processing techniques such as freeze-drying, combined with novel techniques aimed at optimizing the properties of matrices such as the electrospinning or molecular imprinting techniques.

Taking this hypothesis as the general objective, the following specific objectives are proposed for its achievement:

- Physicochemical characterization of the raw material: Collagen (CG) and Gelatin (GE).

- Development of a biocompatible and biodegradable porous matrix that serves as scaffolds for TE based on collagen and/or gelatin by means of the three techniques studied: Freeze-Drying, Electrospinning and Molecular Imprinting.
- Characterization of the morphological, superficial and mechanical properties of scaffolds depending on their formulation and processing.
- Optimization of the processing conditions in its different stages, which together with the previous objectives will allow selecting the most promising scaffolds.
- Select those scaffolds with the greatest potential for their application in Tissue Engineering.
- In vitro study of differentiated muscle cells in the selected scaffolds together with growth factors.
- Study of the in vivo behavior of the scaffolds after its implantation in animals (biocompatibility and contractibility) and its histological pattern after the explant.

1.3 Raw material

Interestingly, regardless of the application, choosing an appropriate raw material to be used or obtaining scaffolds with an optimal internal structure have a positive effect over cell activity, so it is evident that the selection of a suitable raw material is crucial for optimum cell growth (Sachlos and Czemuszka, 2003). In this way, scaffolds might be natural or synthetic but it is essential that they present their specific properties during the whole running time (Vallet-Regi and Munuera, 2000). It is interesting to point out that nowadays synthetic polymers are the most commonly used because it is possible to select and control easily the final properties of the scaffolds. However, most of the synthetic polymers present the disadvantage of being toxic or rather non biocompatible (Geutjes et al., 2006). For that reason, the most interesting options are those based on natural polymers.

Among the different natural polymers to be used, proteins and polysaccharides (i.e. collagen, fibrin, elastin, alginate, chitosan, etc.) can be highlighted due to their biological properties. Proteins are a diverse and complex group of macromolecules formed from the combination of 20 amino acids, being as abundant as necessary for life since at least 50% of the dry weight of the cells are proteins. Proteins have several functions that support life, among which are structural support (collagen), biocatalysts (enzymes), cell movement (actin and myosin), defense (keratin), hormonal regulation (insulin), transport (hemoglobin) and reserve essential nutrients as sources of Nitrogen (casein and ovalbumin) (McKee et al., 2003).

From all the existing proteins, collagen is the most abundant protein in animal tissues (constituting more than 30% of the total protein content), and it is commonly found in bones, skin and ligaments. It is a fibrous

protein (composed by myofibrillar proteins) with a typical amino acid profile, constituted mainly by glycine, proline and hydroxyproline which all represent almost 45 % of the total composition. Its basic unit is formed by 3 polymeric chains giving rise to a compact triple helix.

Collagen has many potential applications, in particular in the pharmaceutical industry. Moreover, a new application has emerged using collagen in the last few years, due to its properties such as biocompatibility, biodegradability, high stress resistance, the inclusion of cell adhesion sequences or its ability to mimic biological structures. Thus, collagen has recently been considered an excellent choice as raw material for obtaining porous matrices for Tissue Engineering (Aguirre-Chagala et al., 2017; Davidenko et al., 2015; Gaspar et al., 2011; Merrett et al., 2012; Muthukumar et al., 2016; Oryan et al., 2018).

On the other hand, collagen can be denatured by acidic or alkaline processing and thermal denaturation to yield acidic gelatin (Gelatin Type A) or basic gelatin (Gelatin Type B) (Ohyabu et al., 2013). The main difference between both is the isoelectric point (in the range between 8-9 or 4-5 for types A and B, respectively). Although its main application is in food manufacturing, gelatin is also widely used as a scaffold material because of its advantages in TE applications (Aldana and Abraham, 2017; Chen et al., 2016). It is characterized by its high biocompatibility, bioresorbability, non-immunogenicity, and its beneficial functional properties. Studies reveal that gelatin does not elicit any noticeable antigenic responses upon implantation and promotes cellular growth (Allam et al., 2012).

1.4 Scaffold fabrication techniques

There are numerous techniques for scaffolds fabrication as the ones based on 3D printing as rapid prototyping or melt molding (Hochleitner et al., 2015; Stratton et al., 2018; Thomson et al., 1995); solvent-based techniques as solvent casting (Mikos et al., 1993) or phase separation (Ren et al., 2017); and others more specific as self-assembly (Zhang, 2003). Among these possible techniques mentioned to produce scaffolds, three different techniques will be developed to achieve the hypothesis and the main objectives detailed before: Freeze-Drying, Electrospinning and Molecular Imprinting. The main advantage of these techniques is their possibility to be used with natural polymers since many of the techniques which involve harsh chemicals and large temperature ranges cannot be used because the bioactivity and functionality cannot be preserved.

1.4.1. Freeze-Drying

Although other techniques like 3D printing allow obtaining scaffolds with better structural properties, Freeze-drying technique allows obtaining 3D porous scaffolds with a global porosity higher than 90% and pore sizes in the range between 20 and 400 µm (Teimouri and Azadi, 2016). It is based on the freezing of a polymer solution followed by the sublimation of the solvent, obtaining matrices with an interconnected porous microstructure.

The evolution of the technique over the years can be seen in Figure 1.3. Its origin is found in 1909 when Shackell freeze-dried different biological materials. It is important to mention that it was not until 1927 when the first patent was registered by Tival. Later, in 1934, Flosdorf prepared the first stable structures *via* Freeze-Drying. However, it was in

1990 when De Groot et al. developed the first composite based on combinations of Polyurethane and Poly(L-lactic acid) (PU/PLLA) for Tissue Engineering (de Groot et al., 1990). Five years later, the first freeze-dried scaffold was produced (Whang et al., 1995). Since then, the application of this technique in Tissue Engineering has grown exponentially (Brougham et al., 2017; Fereshteh, 2017).

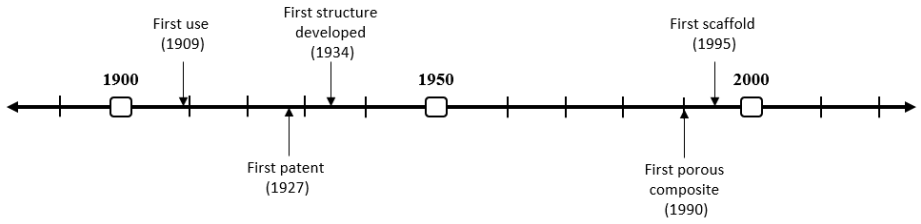

Figure 1.3. Timeline of the evolution of 'Freeze-Drying' over history

A parameter to measure the evolution of the technique over the years and its influence in science is based on the number of publications related. Figure 1.4 shows the number of publications concerning 'Freeze-Drying' since the year 2000.

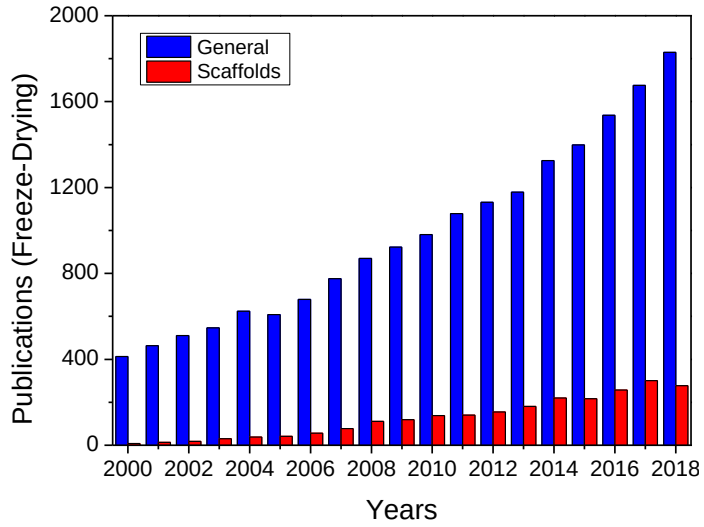

Figure 1.4. Evolution of the number of publications related to 'Freeze-Drying'. Data obtained from Scopus and Web of Science

An exponential growth is observed in the number of publications passing from 400 to more than 1700 in 2018 (blue bars). A study of the specific use of Freeze-Drying to produce scaffolds for TE has also been performed and showed in Figure 1.4 (red bars). An increase over the years is observed, although for their use to fabricate scaffolds, this increase has been smoothed and even decreased (comparing the publications of 2017 and 2018).

1.4.2. Electrospinning

Electrospinning is a technique that allows the formation of continuous ultrafine membranes formed by polymeric fibers. The process consists of the application of a high voltage to induce the evaporation of the solvent of a polymeric solution, leading to the formation of micrometric and nanometric fibers on a metallic surface called the collector.

A timeline with the main events concerning electrospinning is shown in Figure 1.5.

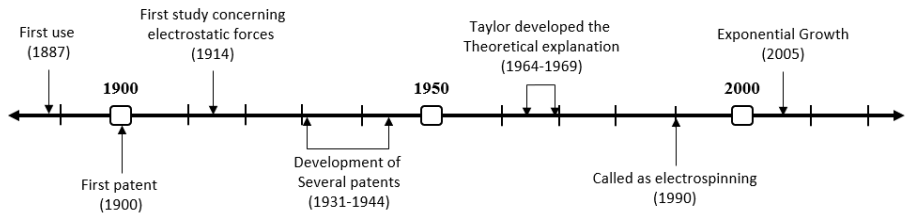

Figure 1.5. Timeline of the evolution of 'Electrospinning' over history

The beginnings of electrospinning go back to the beginning of the 20th century, being patented between 1900 and 1902 by scientists J.F. Cooley and W.J. Morton (although in those years the technique was not known by the name that is used at the moment). Later, between 1931-1944, Firmhals got 22 patents on the mechanism (Tucker et al., 2012). However, it was not until 1964 when sir Geoffrey Ingram Taylor presented his theoretical explanation of the technique and the known

'Taylor's cone' (Taylor, 1964). The technique was performed to produce materials with different applications as filters, although the technique did not receive its name until 1990.

On the other hand, Figure 1.6 shows the evolution of the number of publications concerning electrospinning. Once again, an exponential growth is observed since 2006 but with a higher hit that the previous technique as the number of publications reached almost 4000 in 2018. Interestingly, the impact of this technique over tissue engineering is also higher since a quarter of the publications concerning electrospinning are devoted to the development of scaffolds.

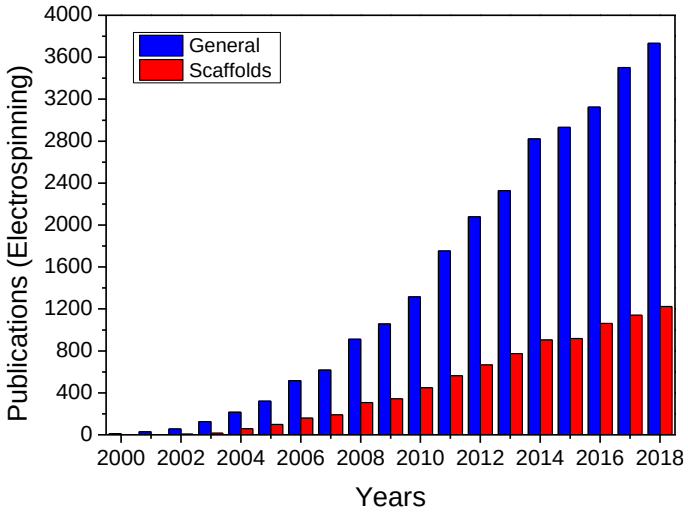

Figure 1.6. Evolution of the number of publications related to 'Electrospinning'. Data obtained from Scopus and Web of Science

According to the results, there is growing inertia based on the development of 3D electrospun scaffolds for TE. To achieve this purpose, different approaches are being studied: Modify the electrospinning process to redesign the collector (to produce 3D structures instead of flat membranes scaffolds) or combine the electrospinning process with others as melt plotting or 3D printing.

The rise of this field is related to the fourth generation of biomaterials, together with another growing field such as Nanomedicine. It is one of the most promising aspects within the many technological advances still under study since it offers the possibility of diagnosing and treating diseases at the cellular and molecular level. Nanomedicine contains five main disciplines: analysis tools, nanoimaging, nanomaterials, new therapeutic delivery systems and drugs, as well as regulatory and toxicological aspects related to clinical practice.

1.4.3. Molecular Imprinting

The technique called Molecular Imprinting consists of "the construction of ligand selective recognition sites in synthetic polymers where a template (atom, ion, molecule, complex or a molecular, ionic or macromolecular assembly, including micro-organisms) is employed in order to facilitate recognition site formation during the covalent assembly of the bulk phase by a polymerization or polycondensation process, with subsequent removal of some or all of the template being necessary for recognition to occur in the spaces vacated by the templating species" (Chen et al., 2011).

Although the origin of the technique is found in the 1930s with the pioneering studies of Polyakov, it was not until ten years later when Pauling presented the first theoretical approach. In 1949, Dickey achieved an MI process properly performed on silica gel and between 1960 and 1975, the concepts of *alternative molecular imprinting* and *covalent molecular imprinting* were introduced with the studies of Michael and Wulff & Sarhan (concepts described in Chapter 5). Already in the 1990s, the first molecularly imprinted membranes were obtained with the inclusion of nanoparticles (Figure 1.7).

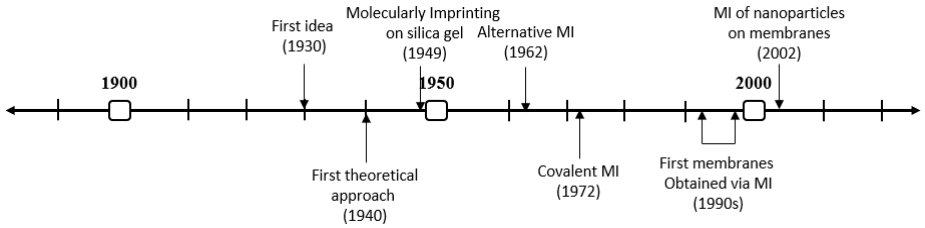

Figure 1.7. Timeline of the evolution of 'Molecular Imprinting' over history

According to the results shown in Figure 1.8, the publications concerning molecular imprinting are sensibly lower compared to the fields of Freeze-Drying (Figure 1.4) or Electrospinning (Figure 1.6), with a lower impact on Tissue Engineering. This fact may be due to the success in achieving molecularly imprinted structures by using small molecules, although imprinting of biomacromolecules (i.e. proteins) is still challenging.

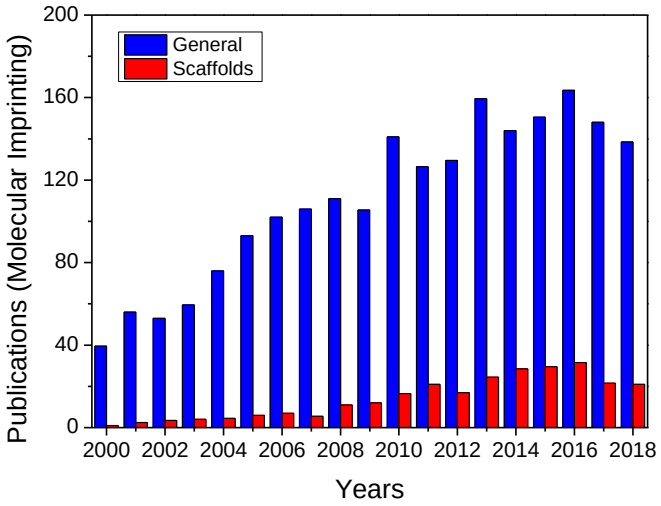

Figure 1.8. Evolution of the number of publications related to 'Molecular Imprinting'. Data obtained from Scopus and Web of Science

In addition, a combinatorial study has been performed by searching the publications which merge the techniques of electrospinning and molecular imprinting, in other words, perform the molecular imprinting over electrospun structures.

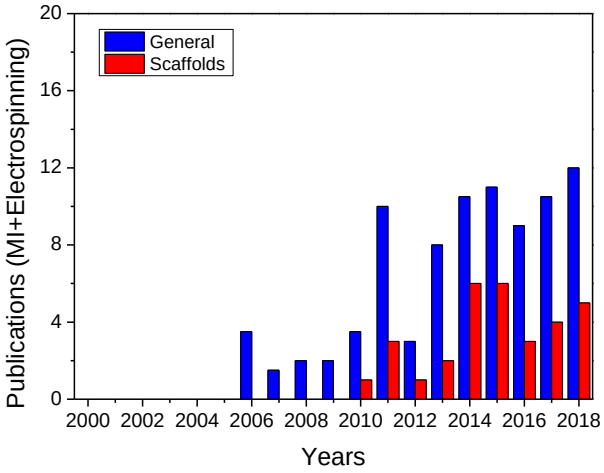

Figure 1.9. Evolution of the number of publications related to 'Molecular Imprinting+Electrospinning'. Data obtained from Scopus and Web of Science

The results (Figure 1.9) evidenced the relatively new and innovative process which combines both techniques to produce molecular imprinted structures. The number of publications reached a maximum at 10-12, half of them related to scaffolds.

Related publications

- Perez-Puyana, Víctor Manuel; Félix Ángel, Manuel; Romero García, Alberto; Guerrero Conejo, Antonio (2019). Collagen as a potential biopolymer for the production of porous matrices (scaffolds) with application in Tissue Engineering (Chapter 8). In: *Materials for Biomedical Engineering – Absorbable Polymers*. ElSevier Science, pp. 217-244. DOI: 10.1016/B978-0-12-818415-8.00008-5

References

Aguirre-Chagala, Y.E., Altuzar, V., León-Sarabia, E., Tinoco-Magaña, J.C., Yañez-Limón, J.M., Mendoza-Barrera, C., 2017. Physicochemical properties of polycaprolactone/collagen/elastin nanofibers fabricated by electrospinning. Mater. Sci. Eng. C 76, 897–907.

Aldana, A.A., Abraham, G.A., 2017. Current advances in electrospun gelatin-based scaffolds for tissue engineering applications. Int. J. Pharm. 523, 441–453.

Allam, E., Bottino, M.C., Al-Shibani, N., Jack Windsor, L., 2012. Collagen scaffolds: Tissue engineering and repair, Type I Collagen: Biological Functions, Synthesis and Medicinal Applications.

Brougham, C.M., Levingstone, T.J., Shen, N., Cooney, G.M., Jockenhoevel, S., Flanagan, T.C., O'Brien, F.J., 2017. Freeze-Drying as a Novel Biofabrication Method for Achieving a Controlled Microarchitecture within Large, Complex Natural Biomaterial Scaffolds. Adv. Healthc. Mater. 6, 1–7.

Chen, L., Xu, S., Li, J., 2011. Recent advances in molecular imprinting technology: current status, challenges and highlighted applications. Chem. Soc. Rev. 40, 2922–2942.

Chen, S., Zhang, Q., Nakamoto, T., Kawazoe, N., Chen, G., 2016. Gelatin Scaffolds with Controlled Pore Structure and Mechanical Property for Cartilage Tissue Engineering. Tissue Eng. Part C. Methods 22, 189–198.

Davidenko, N., Schuster, C.F., Bax, D. V, Raynal, N., Farndale, R.W., Best, S.M., Cameron, R.E., 2015. Control of crosslinking for tailoring collagen-based scaffolds stability and mechanics. Acta Biomater. 25, 131–142.

de Groot, J.H., Nijenhuis, A.J., Bruin, P., Pennings, A.J., Veth, R.P.H., Klompmaker, J., Jansen, H.W.B., 1990. Use of porous biodegradable polymer implants in meniscus reconstruction. 1) Preparation of porous biodegradable polyurethanes for the reconstruction of meniscus lesions. Colloid Polym. Sci. 268, 1073–1081.

Fereshteh, Z., 2017. Freeze-drying technologies for 3D scaffold engineering, Functional 3D Tissue Engineering Scaffolds: Materials, Technologies, and Applications. Elsevier Ltd.

Gaspar, A., Moldovan, L., Constantin, D., Stanciuc, A.M., Sarbu Boeti, P.M., Efrimescu, I.C., 2011. Collagen-based scaffolds for skin tissue engineering. J. Med. Life 4, 172–177.

Geutjes, P.J., Daamen, W.F., Buma, P., Feitz, W.F., Faraj, K.A., Van Kuppevelt, T.H., 2006. From Molecules to Matrix: Construction and Evaluation of Molecularly Defined Bioscaffolds, in: Tissue Engineering. Springer, Boston, pp. 279–295.

Ghosal, K., Latha, M.S., Thomas, S., 2014. Poly(ester amides) (PEAs)—scaffold for tissue engineering applications. Eur. Polym. J. 60, 58–68.

Hochleitner, G., Jungst, T., Brown, T.D., Hahn, K., Moseke, C., Jakob, F., Dalton, P.D., Groll, J., 2015. Additive manufacturing of scaffolds with sub-micron filaments via melt electrospinning writing. Biofabrication 7, 35002.

Kakkar, P., Verma, S., Manjubala, I., Madhan, B., 2014. Development of keratin-chitosangelatin composite scaffold for soft tissue engineering. Mater. Sci. Eng. C 45, 343–347.

Langer, R., Vacanti, J.P., 1993. Tissue Engineering. Science (80-.). 260, 920–926.

Li, W.-J., Cooper, J.A., 2011. Fibrous Scaffolds for Tissue Engineering, in: Biomaterials for Tissue Engineering Applications. Springer, Vienna, pp. 47–73.

Lin, X., Huang, J., Shi, Y., Liu, W., 2015. Tissue Engineering and Regenerative Medicine in Applied Research: A Year in Review of 2014. Tissue Eng. Part B Rev. 21, 177–186.

McKee, T., McKee, J.R., de Buitrago, J.M.G., 2003. Bioquímica: la base molecular de la vida. McGraw-Hill, Interamericana.

Merrett, K., Ljunggren, M.K., Mondal, D., Griffith, M., Rafat, M., 2012. Collagen Type I: A promising scaffold material for Tissue Engineering

and Regenerative Medicine, in: Type I Collagen. pp. 1–42.

Mikos, A.G., Sarakinos, G., Leite, S.M., Vacanti, J.P., Langer, R., 1993. Laminated three-dimensional biodegradable foams for use in tissue engineering. Biomaterials 14, 323–330.

Muthukumar, T., Aravinthan, A., Sharmila, J., Kim, N.S., Kim, J.H., 2016. Collagen/chitosan porous bone tissue engineering composite scaffold incorporated with Ginseng compound K. Carbohydr. Polym. 152, 566–574.

Nerem, R.M., 2010. Regenerative medicine: the emergence of an industry. J. R. Soc. Interface 7 Suppl 6, S771–S775.

Offeddu, G.S., Ashworth, J.C., Cameron, R.E., Oyen, M.L., 2015. Multi-scale mechanical response of freeze-dried collagen scaffolds for tissue engineering applications. J. Mech. Behav. Biomed. Mater. 42, 19–25.

Ohyabu, Y., Yunoki, S., Hatayama, H., Teranishi, Y., 2013. Fabrication of high-density collagen fibril matrix gels by renaturation of triple-helix collagen from gelatin. Int. J. Biol. Macromol. 62, 296–303.

Oryan, A., Kamali, A., Moshiri, A., Baharvand, H., Daemi, H., 2018. Chemical crosslinking of biopolymeric scaffolds: Current knowledge and future directions of crosslinked engineered bone scaffolds. Int. J. Biol. Macromol. 107, 678–688.

Ramakrishna, S., Ramalingam, M., Kumar, T.S.S., Soboyejo, W.O., 2016. Biomaterials: A Nano Approach. CRC Press.

Reddi, A.H., 2000. Morphogenesis and tissue engineering of bone and cartilage: inductive signals, stem cells, and biomimetic biomaterials. Tissue Eng. 6, 351–_359.

Ren, K., Wang, Y., Sun, T., Yue, W., Zhang, H., 2017. Electrospun PCL/gelatin composite nanofiber structures for effective guided bone regeneration membranes. Mater. Sci. Eng. C 78, 324–332.

Sachlos, E., Czemuszka, J.T., 2003. Making tissue engineering scaffolds work. Review: the application of solid freeform fabrication technology to the production of tissue engineering scaffolds. Eur. Cells Mater. 5, 29–40.

Skalak, R., Fox, C.F., 1988. Tissue engineering : proceedings of a workshop held at Granlibakken, Lake Tahoe, California. Liss, New York, pp. 26–29.

Stratton, S., Manoukian, O.S., Patel, R., Wentworth, A., Rudraiah, S., Kumbar, S.G., 2018. Polymeric 3D printed structures for soft-tissue engineering. J. Appl. Polym. Sci. 135, 45569.

Taylor, G.I., 1964. Disintegration of water drops in an electric field. Proc. R. Soc. London A 280, 383–398.

Teimouri, A., Azadi, M., 2016. Preparation and characterization of novel chitosan/nanodiopside/nanohydroxyapatite composite scaffolds for tissue engineering applications. Int. J. Polym. Mater. Polym. Biomater. 65, 917–927.

Thomson, R.C., Wake, M.C., Yaszemski, M.J., Mikos, A.G., 1995. Biodegradable polymer scaffolds to regenerate organs, in: Peppas, N.A., Langer, R.S. (Eds.), Biopolymers II. Springer Berlin Heidelberg, Berlin, Heidelberg, pp. 245–274.

Tucker, N., Stanger, J.J., Staiger, M.P., Razzaq, H., Hofman, K., 2012. The history of the science and technology of electrospinning from 1600 to 1995. J. Eng. Fiber. Fabr. 7, 63–73.

Vallet-Regi, M., Munuera, L., 2000. Biomateriales: Aquí y Ahora. Editorial Dykinson.

Van Vlierberghe, S., Dubruel, P., Schacht, E., 2011. Biopolymer-Based Hydrogels As Scaffolds for Tissue Engineering Applications : A Review. Biomacromolecules 12, 1387–1408.

Whang, K., Thomas, C.H., Healy, K.E., Nuber, G., 1995. A novel method to fabricate bioabsorbable scaffolds. Polymer (Guildf). 36, 837–842.

Williams, D.F., 2009. On the nature of biomaterials. Biomaterials 30, 5897–5909.

Yannas, I.V., Burke, J.F., 1980. Design of an artificial skin. I. Basic design principles. J. Biomed. Mater. Res. 14, 65–81.

Zhang, S., 2003. Fabrication of novel biomaterials through molecular self-assembly. Nat. Biotechnol. 21, 1171–1178.

Chapter 2: Characterization of the different collagen/gelatin protein concentrates to be used as raw material for the production of scaffolds

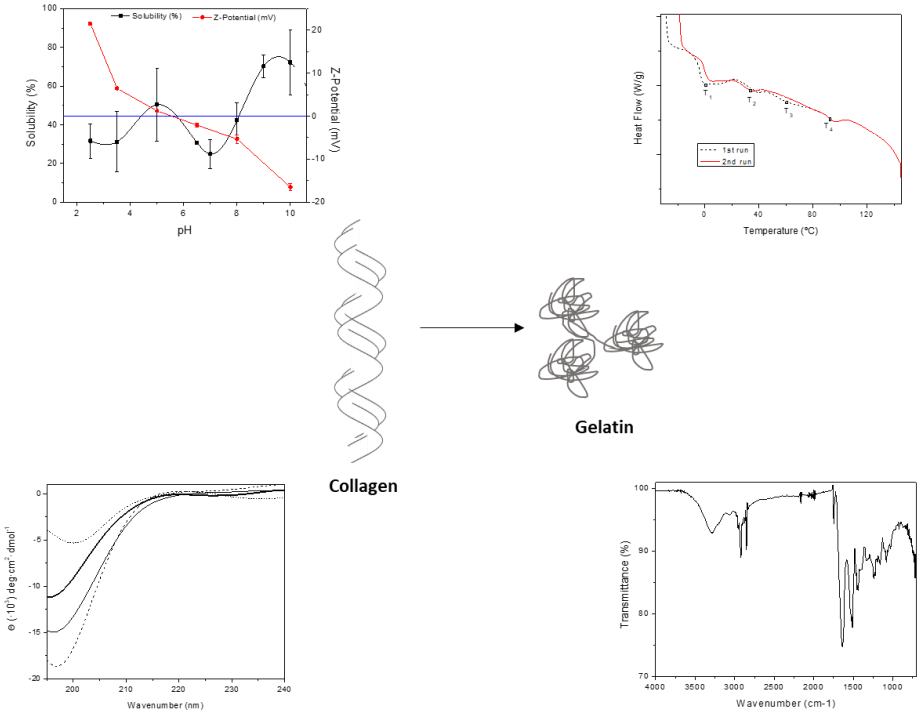

2.1 Introduction

Nowadays, most studies in regenerative medicine focus on the development of 2D and 3D structures to act as promising scaffolds for Tissue Engineering (TE), due to the increasing importance of TE in the recovery and care of diseases (Langer and Vacanti, 2016). However, the efficiency of the process is quite linked to the properties of the scaffold. As a matter of a fact, these properties are closely related to the raw material used for the fabrication of the scaffold.

The scaffolds can be produced from either synthetic or natural polymers, depending on the properties to be promoted (synthetic for better mechanical properties or natural for a better biocompatibility) (Aldana and Abraham, 2017; Deng et al., 2018). Polysaccharides (chitosan, alginate, agarose, etc.) and proteins (collagen, gelatin, fibrin, fibronectin, etc.) are the most commonly used biopolymers for the development of scaffolds (Khajavi et al., 2016; Pok et al., 2014; Stratton et al., 2018; Zhang et al., 2016).

The use of protein concentrates as raw material for scaffolds requires the knowledge of some basic characteristics as their chemical and amino acid composition, surface charges or structure. First, it is important to evaluate their composition in order to corroborate the active matter (real protein) that they contain. The evaluation of their chemical composition may include the protein and lipids content, as well as the moisture of the sample. The analysis of the amino acid composition is also interesting because it allows to know the amino acids present in higher proportions in order to plan the modification of the structure. In this sense, as example, the content in proline or hydroxyproline gives information about the stabilization of the protein. Moreover, amino acids like

methionine or cysteine give information about the sulfur content, involved in the protein aggregation by forming disulphide bonds.

The different amino acids are connected by forming sequences (chains), establishing four different structural levels depending on the organization of these chains with each other: Primary structure, which consists of a linear combination of monomers called amino acid joined by a type of bond called peptide bond. The secondary structure is originated from the folding of the primary structure by means of the formation of α-links (α-helix) and β-structures (β-sheets) (Figure 2.1):

- α-helix: This structure is formed by the winding of the polypeptide chain around an imaginary longitudinal axis to the center of the proper helix, leaving the groups out of the dextrogyre helical skeleton.
- β-sheets: It is formed by the alignment of two or more segments of the polypeptide chains, which are extended in zigzag, joining together through hydrogen bonds. Adjacent polypeptide chains of a β-sheet may be parallel or antiparallel, depending on whether they have the same amino-carboxy or opposite orientation; the repetition period is smaller for the parallel sequence (6.5 Å compared to 7 Å for the antiparallel sequence).

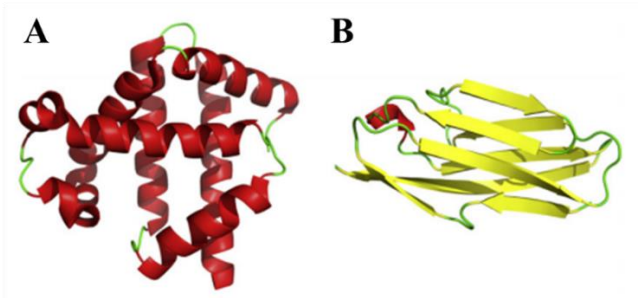

Figure 2.1. Secondary structures of proteins: (A) α-helix and (B) β-sheet. Image obtained from Reeb and Rost (2019)

The tertiary structure is the definitive three-dimensional structure for most proteins, obtained by the folding of the polypeptide chain due to the formation of additional bonds (hydrogen bonds, hydrophobic bonds or disulphide bonds). Finally, the quaternary structure is formed by the coupling of different protein chains. These two structures are really interesting because it is possible to form them with the help of different crosslinking agents, giving a more structured framework to proteins (Cox and Nelson, 2000; McKee et al., 2003). The stabilization is obtained by the formation of the bonds previously described, but also by the surface charges which are present in the protein, due to the fact that they affect protein structuration and folding (and therefore their functionality) by the charge hindrance between the polypeptide chains. For this reason, techniques that involve solubility or Z-Potential measurements are very useful for the characterization of the protein.

The conformational changes of the protein chain that gives rise to the tertiary structure are mainly due to weak interactions, although sometimes it can also be due to covalent bonds such as: Hydrogen bonds, hydrophobic interactions, electrostatic interactions or disulphide bonds (Biesecker et al., 1977; Cox and Nelson, 2000). In addition, these conformational changes can be obtained by the crosslinking of the structure. The crosslinking method consists in the formation of additional bonds between polymer chains to reinforce the structure of the protein. In this sense, the content in glutamic acid or lysine allows planning a crosslinking modification using glutaraldehyde (among other alternatives).

Among the different protein concentrates, collagen is one of the most commonly used polymers for the fabrication of scaffolds polymers for obtaining scaffolds (Correia et al., 2013; Jose et al., 2009; Sionkowska

and Grabska, 2017). Collagen is the most abundant component of the skin and bones, covering 30% of the total protein mass in mammals. The basic structure of collagen is based on a triple helix of three polymeric chains of ca 1000 amino acids connected by peptide bonds (Jilek and Helmut, 1978; Lodish, 2013; Luparello and Sirchia, 2011; Merrett et al., 2012). Furthermore, it shows a typical amino acid profile, constituted mainly by glycine, proline and hydroxyproline (which represent 40% of the total). It is formed by two identical α1-chains and one α2(I)-chain (heterotrimers) (Allam et al., 2012).

However, there are more than sixteen types of collagen that differ from each other according to their origin and structure (Lodish, 2013), although collagen types I, II and III are the most abundant:

- Type I Collagen: It is found abundantly in the dermis, bones and tendons. It occurs in striated fibrils of 20 to 100 nm in diameter, grouping to form larger fibers. Its major subunits consist of α-chains of two types (called α1 and α2). Its main function is the stretch resistance.
- Type II Collagen: It is found mostly in cartilage, but also occurs in the embryonic cornea and vitreous humor of the eye. In cartilage, it forms fine fibrils of 10 to 20 nm, but in other microenvironments, it can form larger fibrils, indistinguishable from type I collagen. They consist of three α2 chains. Its main function is resistance to intermittent pressure.
- Type III Collagen: It is found in the connective tissue, in the walls of blood vessels, the dermis of the skin and the stroma of several glands. It seems an important constituent of 50 nm fibers that have traditionally been called "reticular fibers". It consists of a single class of α3 chain. Its function is the support of various organs.

Collagen, like most proteins, can lose its three-dimensional structure due to different factors (temperature, changes in pH, etc.) (Cox and Nelson, 2000). This process is called denaturation and leads to the formation of gelatin (the denatured form of collagen) (Figure 2.2). It is important to differentiate between collagen and gelatin proteins because the possible applications (Tissue Engineering, pharmaceutical and cosmetics applications) may be different (Kittiphattanabawon et al., 2005).

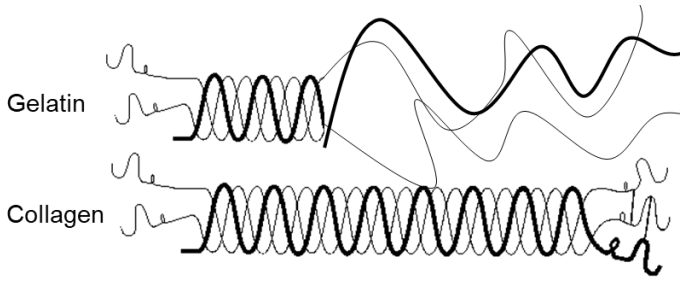

Figure 2.2. Collagen and gelatin protein structures

Collagen-based scaffolds may be constructed either in the native form or the denatured form (gelatin). Gelatin is generally obtained by denaturation of type I collagen from animal skin or fish scales. Like collagen, gelatin is mainly composed of three amino acids (glycine, proline and hydroxyproline). Furthermore, its chemical and physical properties are similar to those of collagen, but with even better biological responses (Echave et al., 2017). There are two types of gelatin (type A or type B), which differs by the method of production. Type A gelatin is obtained by an acidic treatment, whereas type B gelatin is achieved following a basic treatment. As a consequence, it leads to a different isoelectric point, in the range between 4.5-6 for the type B and between 7-9 for the type A (Aramwit et al., 2015; Mohiti-Asli and Loboa, 2016). Thereby, it is important to consider the properties of the raw material used in the scaffold fabrication and, specifically for collagen studies, its structure in order to evaluate their denaturation degree to analyse the

purity of collagen. The latter allows to analyze if the raw material used is collagen, gelatin or gelatinized collagen. Thus, a previous characterization of the raw material is advisable in order to make a good selection. The determination of the denaturation of proteins implies the study of their secondary structure. Thus, Circular Dichroism (CD) or Fourier Transform Infrared Spectroscopy (FTIR) are widely used techniques for this purpose (Goormaghtigh et al., 2009), but they are not the only ones because others like microthermal analyses or atomic force microscopy can be performed (Lin and Goh, 2002). However, the precise mechanism of collagen denaturation remains unknown due to its crosslinking and polymeric nature (Ravikumar and Hwang, 2008). CD measurements applied to biological systems give information about their conformational changes or the folding and unfolding of proteins (S M Kelly and Price, 2000). Advances in this field have allowed the analysis of the spectra obtained using specific software. K2D software, for example, gives an estimation of the percentages of secondary structure in proteins (Orrego Cardozo et al., 2015). FTIR, in turn, gives information about the chemical bonds present in the molecules studied. When analysing biological molecules (such as proteins), the carboxyl and amino bonds are the most interesting groups to consider, since the intensity of these peaks gives information about the denaturation of the protein studied (Muyonga et al., 2004a).

Furthermore, other possible techniques to be used are free and total sulfhydryls or Differential Scanning Calorimetry (DSC) measurements. The former allows the determination of S-S bonds, which could give an idea of the agglomeration of the protein and, for that matter, of its denaturation (Greensteik, 1938). On the other hand, DSC measurements study the thermal properties of the protein, which vary depending on its

denaturation (showing specific peaks depending on whether it is collagen or gelatin) (Badea et al., 2012; Beveridge et al., 1974).

Thus, the aim of this work is the physicochemical characterization and assessment of different protein concentrates, namely type I collagen and type B gelatin protein concentrates from different sources to analyze their properties and compare their denaturation degree using a combination of different techniques. Therefore, their chemical and amino acid composition, as well as their superficial and structural charge are determined. The information obtained in this study can be useful for the selection of suitable raw material for the fabrication of scaffolds.

2.2 Material and methods

2.2.1. Materials

Type I collagen protein concentrates (CG) from two different sources were evaluated: pork (HI95 and T95) and turkey. These three protein concentrates were supplied by Essentia Protein Solutions (Grasten, Denmark). In addition, gelatin protein (GE) from fish skin was also studied. It was supplied by Henan Boom Gelatin Co. Ltd (China). The main difference between the pork HI95 and pork T95 collagen proteins is that pork T95 is a cold-setting protein which is capable of gelling at low temperatures.

2.2.2. Physicochemical characterization of the protein concentrates

2.2.2.1. Chemical composition

Protein quantification: Protein content was determined using a LECO CHNS-932 microanalyzer (Leco Corporation, USA) (Figure 2.3) to measure the nitrogen content of the sample and multiplying this by 5.95 (Liang et al., 2014).

This analyzer allows knowing the content of C, N, H and S measured in percentage with respect to the total weight. The analysis technique is fully automated, and it is based on the combustion of the samples under optimal conditions (T = 950-1,100ºC, pure oxygen atmosphere) to convert the aforementioned elements into simple gases (CO_2, N_2, H_2O and SO_2) to obtain a quantitative result.

Sulfur content: Sulfur content was determined using a LECO CHNS-932 microanalyzer (Leco Corporation, USA).

Figure 2.3. LECO CHNS-932 nitrogen microanalyzer

Likewise, lipid, moisture and ash contents were determined according to A.O.A.C. (2005).

Lipid quantification: the Soxhlet extraction device, shown in Figure 2.4, was used to quantify lipid content. The method used in the present study consisted of heating and volatilizing a solvent (hexane) at 80ºC and, subsequently, condensing the solvent to bring it into contact with the CG or GE, allowing 4 h for the solvent to leach the lipids out of the sample. Lipid content was calculated using the following equation (Equation 2.1):

$$\%\ Lipids = \frac{Initial\ sample\ weight - Final\ sample\ weight}{Initial\ \ sample\ weight} \cdot 100 \quad (2.1)$$

Figure 2.4. Soxhlet extraction device

Ash quantification: First, 2 g of CG or GE was calcined at 550 ºC in a muffle furnace for 4-5 h (Hobersal HD-230, Spain). Then, it was kept in a desiccator, cooling at room temperature and weighed again. Ash content was calculated from the difference in weight of the protein isolate before and after the treatment.

Moisture quantification: The moisture in the CG or GE was determined by treating a 1.5-2.0 g sample in an oven (MEMMERT B216.1126, Germany) at 105 ºC for 24 h. The moisture percentage was obtained using Equation 2.2.

$$\%\, Moisture = \frac{Initial\ sample\ weight - Final\ sample\ weight}{Initial\ \ sample\ weight} \cdot 100 \quad (2.2)$$

2.2.2.2. Amino acid composition

The amino acid composition of each collagen protein concentrate was obtained using a method previously described by Felix et al. (2017). Collagen or gelatin samples were dissolved in 6 M hydrochloric acid and were incubated in an oven at 110 ºC for 24 h. After hydrolysis, pH was adjusted to 7 using 6 M NaOH and the samples were filtered through a Whatman glass microfiber filter (GF/C). Finally, the samples were diluted (1:500) by adding doubly distilled water. Reverse phase HPLC by precolumn fluorescence derivatization with o-phtaldialdehyde (SIL-9A Auto Injector, LC-9A Liquid Chromatograph (Figure 2.5), RF-530 Fluorescence HPLC Monitor, all parts from Shimadzu Corporation, Japan). It was performed using a NovaPak C18 cartridge (Waters, Milford, MA, USA), by the method of Lindroth and Mopper (1979).

Figure 2.5. LC-9A Liquid Chromatograph

2.2.2.3. Electrophoresis

Electrophoresis is one of the most common technique for the separation of proteins based on the migration of charged proteins in an electric field. Electrophoresis is especially useful as an analytical method. Its advantage is that proteins can be visualized as well as separated, allowing to estimate the number of different proteins in a mixture or the degree of purity of a particular protein preparation.

Electrophoresis assays were performed using polyacrylamide gels (10%) in the presence of sodium dodecyl sulfate (SDS-PAGE) according to the method of Laemmli (1970). The molecular weights of the fractions of extracted proteins have been determined in SDS-PAGE gels, considering the relationship between the logarithm of the Molecular Weight of the protein and the electrophoretic mobility, using as an analytical standard "Protein Plus Protein Standards" (Bio-Rad, Richmond, CA, USA). Figure 2.6 shows the device used to perform this technique.

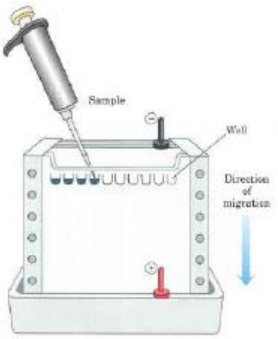

Figure 2.6. Electrophoresis device

2.2.2.4. Protein solubility and Z-Potential

Solubility: Protein solubility was determined at different pH values. Aqueous dispersions (ca. 1 g protein/40 mL) were prepared with buffers at different pH values (2.5, 3.5, 5, 6.5, 7, 8, 9 and 10). The samples were homogenized and subsequently centrifuged at 15,000 rpm and 10 ºC for 20 min. The supernatants were collected for protein content measurement by the Markwell method (Markwell et al., 1978). This method of analysis is an adaptation of Lowry's method, which consists in the formation of a complex between the soluble protein and the Folin-Ciocalteau reagent in an alkaline medium. The samples were transferred to a 3 mL cuvette where the absorbance is measured at a wavelength of 750 nm, taking as a target distilled water with the same amount of Folin-Ciocalteau and using a calibration curve for which Bovine Serum Albumin (BSA) is used (Mohammed et al., 2000) to determine the amount of protein.

A Genesys-20 spectrophotometer (Thermo Scientific, USA) is used to measure the absorbance (Figure 2.7). Solubility was expressed as a percentage (g soluble protein/100 g sample).

Figure 2.7. Spectrophotometer Genesys-20

Z-Potential: Surfaces of proteins have net charges due to their amino acid content depending on the pH of their environment. Z-Potential measures the net charge of the proteins as a function of electrophoretic mobility

measurements. This technique allows obtaining the isoelectric point, which is the point at which proteins have a net charge of 0. This technique was developed using a "Zetasizer 2000" (Malvern Instruments, U.K.) (Figure 2.8). Different samples were prepared at 1 wt.% with buffers at different pH values (2.5, 3.5, 5, 6.5, 8 and 10). Prior to analysis, the samples were stirred at 20 ºC and then centrifuged at 10,000*xg* for 10 min in an RC5C Sorvall centrifuge (Sorvall Instruments, Wilmington, DE, USA). After that, the samples were measured in triplicate at 20 ºC. The Z-Potential was calculated from electrophoretic mobility using the Henry equation and the Smoluchowski approximation. The isoelectric point corresponds to the point where the potential value is zero, at which all charges of particles are neutralized (Tan et al., 2008).

Figure 2.8. Zetasizer 2000

2.2.3. Assessment of the denaturation degree of the raw materials

The evaluation of the denaturation of the different collagen/gelatin proteins was performed in order to select the most suitable raw materials for the production of scaffolds. This evaluation has been carried out with FTIR measurements, the analysis of the free and total sulfhydryls content and DSC spectra. In addition, Circular Dichroism spectra were also obtained for the different protein concentrates.

2.2.3.1. Fourier Transform Infrared Spectroscopy (FTIR)

The FTIR spectrum was obtained for discs containing a 2 mg collagen sample using a FT/IR-4100 spectrophotometer (Jasco, Japan) (Figure 2.9). The spectra were obtained for a wavenumber range from 4,000 to 600 cm^{-1} and processed with Jasco Spectra Manager™ software. Furthermore, the deconvolution of the Amide I signal was performed for all the spectra obtained.

Figure 2.9. Spectrophotometer Jasco FTIR-4100

2.2.3.2. Free/Total Sulfhydryls

'Total sulfhydryls' are referred to as the total of S-groups in the protein, whereas 'free sulfhydryls' are referred to as the SH-groups which are not forming disulfide bonds. The determination of the concentrations of free and total sulfhydryl groups was performed using the method developed by Beveridge et al. (1974) and Thannhauser et al. (1984), respectively.

Briefly, the samples (1 mg/mL) were suspended in a buffer containing 0.086 mol/L Tris-HCl (pH 8.0), 0.09 mol/L glycine, 4 mmol/L EDTA, and 8 mol/L urea. Dispersions were stirred at 25 ºC for 10 min at 500 rpm in a thermomixer and then centrifuged at 12,000*xg* (10 min, 10 ºC). The supernatant was incubated in Ellman's reagent (5,5-dithiobis-2-nitrobenzoic acid in Tris-Gly buffer, 4 g DTNB L-1 methanol) for free sulfhydryl groups and in 1 mL 2-nitro 5-thio-sulfobenzoic acid for total sulfhydryls. Absorbance at 412 nm was measured in a Genesys-20 spectrophotometer (Thermo Scientific, Waltham, MA, USA) (Figure

2.7). For the calculations, the molar extinction coefficient of 3-thio-6-nitrobenzoate (13,600 $L \cdot mol^{-1} \cdot cm^{-1}$) was used. The protein concentration of the extracts was determined by the Bradford method (Bradford, 1976). This assay is based on the color change of Coomassie brilliant blue G-250 dye in response to various concentrations of protein - the dye binds to primarily basic (especially arginine) and aromatic amino acid residues. The color change is observed measuring the absorbance at 595 nm. A standard curve of BSA is used for protein quantification.

2.2.3.3. Differential Scanning Calorimetry (DSC)

A DSC measures the temperature difference (transcript into heat flux) between the sample and an inert reference as a function of time and temperature. It is a technique used to characterize polymers by endothermic and exothermic transitions, being able to detect thermal events such as glass transition temperature (Tg), fusion or crystallization temperatures, among others. DSC experiments were performed with a Q20 (TA Instruments, USA) (Figure 2.10), using 3 to 8 mg samples, in hermetic aluminum pans. A heating rate of 10 ºC/min was selected. The sample was purged with a nitrogen flow of 50 mL/min. A first run was performed until 80 ºC; then, the sample was cooled and heated again to 150 ºC (second run).

Figure 2.10. DSC Q20 calorimeter

2.2.3.4. Circular Dichroism (CD)

Electronic Circular Dichroism (CD) is a spectroscopic electronic absorption technique based on the change of molecular electronic configuration of a fundamental state to an excited state due to the absorption of electromagnetic radiation polarized Its signal is obtained as the difference between the absorbances of the circularly polarized light to the left and right. CD spectra were recorded in a Biologic Mos-450 spectropolarimeter (Figure 2.11).

Figure 2.11. Circular dichroism equipment (Biologic Mos-450 spectropolarimeter)

A standard quartz cell of 10 mm path length was used. Scans were taken from 190 to 240 nm under a nitrogen atmosphere. Spectra were performed at a fixed collagen concentration of 0.01 g/L for each type of protein concentrate in acetic acid (0.05 M). All CD spectra of collagen solution were solvent subtracted, and each spectrum was obtained from an average of 10 runs at a fixed temperature of 25.1 ± 0.1 ºC with a 10 min equilibration before each scan. The spectra obtained were expressed in terms of mean residue ellipticity (deg·cm^2·dmol^{-1}) (Orrego Cardozo et al., 2015). This term can be expressed as:

$$[\theta]_{\mathrm{mrw}} = \frac{MRW \cdot \theta}{10 \cdot d \cdot c} \qquad (2.3)$$

Where θ is the observed ellipticity (degrees), d is the path length (cm) and c is the concentration (g/L).

From the CD spectra, the 'positive-negative ratio' (*RPN*) was calculated, using Equation 2.4:

$$RPN = \frac{\theta_p}{\theta_n} \qquad (2.4)$$

Where θ_p and θ_n are the positive and negative peaks, respectively.

Furthermore, an estimation of the secondary structure content (α-helix and β-sheets) of these proteins was carried out using the deconvolution program K2D2, a re-implementation of the K2D program developed by Andrade et al. (1993).

2.2.4. Statistical analysis

At least three replicates were carried out for each measurement. Student´s t-test and one-way analysis of variance ($p<0.05$) were performed using PASW Statistics for Windows (Version 18: SPSS, Chicago, IL). Standard deviations were calculated for selected parameters.

2.3 Results and Discussion

2.3.1. Characterization of the protein concentrates

2.3.1.1. Chemical and amino acid composition

The chemical composition of the four protein concentrates is summarized in Table 2.1.

Table 2.1. Chemical composition of the different protein concentrates (Pork HI95, Pork T95, Turkey and Fish). Values with different letters/symbols are significantly different (p<0.05)

Raw Material	Composition			
Collagen	Protein (%)	Ash (%)	Lipids (%)	Moisture (%)
Pork HI95	94.2 ± 0.9^{a}	0.7 ± 0.1^{A}	$0.3 \pm 0.1^{\alpha}$	3.2 ± 0.8^{I}
Pork T95	90.4 ± 0.2^{b}	0.8 ± 0.2^{A}	$0.7 \pm 0.1^{\beta}$	7.4 ± 0.3^{II}
Turkey	80.3 ± 0.4^{c}	0.6 ± 0.1^{A}	$8.3 \pm 2.8^{\gamma}$	10.0 ± 0.9^{III}
Fish	97.9 ± 0.1^{d}	0.6 ± 0.3^{A}	$0.3 \pm 0.1^{\alpha}$	0.4 ± 0.1^{IV}

Interestingly, the four samples showed different protein contents; the sample from fish had 98%, whereas those from pork as raw material (HI95 and T95) had a protein content of ca. 95% and 90%, respectively. The protein contents of these three systems were over 90% (i.e. higher than 97%) on a dry basis, and thus they were considered protein isolates (Pearson, 1983). On the other hand, turkey collagen presented lower protein content (ca. 81%), and thus it was considered a protein concentrate. In addition, the microanalysis results reveal a sulfur content of 0.51±0.01 %, 0.54±0.03 %, 1.11±0.13 %, 0.46±0.01 % for pork HI95, pork T95, turkey and fish collagen, respectively.

The chemical composition of collagen obtained from pork raw material (pork HI95 and pork T95) was similar to the gelatin isolated from fish skin.

Furthermore, Table 2.2 shows the amino acid compositions of the four proteins. As may be observed, the values obtained for all the samples (pork HI95, pork T95, turkey and fish) show apparent similarities. All of

them were rich in glycine (21.0, 17.4, 14.0 and 30.9 g/100g, respectively), which is the most abundant amino acid, alanine (8.4, 8.6, 7.5 and 13.9 g/100g, respectively), arginine (7.9, 8.2, 7.0 and 6.6 g/100g, respectively) and glutamic acid (10.3, 10.1, 12.0 and 9.8 g/100g, respectively). Besides, the higher content in methionine and cysteine for turkey collagen can explain its higher amount of sulfur present.

Table 2.2. Amino acid composition of the four different protein concentrates (g/100g). * refers to the essential amino acids. Values with different letters/symbols are significantly different for each different response variable (p<0.05)

Amino Acid Composition				
Amino acid	**Pork HI95**	**Pork T95**	**Turkey**	**Fish**
Alanine	8.4 ± 0.1^{a}	8.6 ± 0.1^{a}	7.5 ± 0.1^{b}	13.9 ± 0.1^{c}
Arginine	7.9 ± 0.1^{A}	8.2 ± 0.1^{B}	7.0 ± 0.1^{C}	6.6 ± 0.1^{D}
Aspartic Acid	$6.3 \pm 0.1^{\alpha}$	$6.3 \pm 0.1^{\alpha}$	$7.8 \pm 0.1^{\beta}$	$5.5 \pm 0.1^{\gamma}$
Cystine/Cysteine	0.3 ± 0.1^{I}	0.7 ± 0.1^{II}	0.9 ± 0.1^{II}	0.1 ± 0.1^{I}
Glutamic Acid	10.3 ± 0.1^{a}	10.1 ± 0.1^{a}	12.0 ± 0.1^{b}	9.8 ± 0.1^{c}
Glycine	21.0 ± 0.1^{A}	17.4 ± 0.1^{B}	14.0 ± 0.1^{C}	30.9 ± 0.1^{D}
Histidine*	$1.0 \pm 0.1^{\alpha}$	$1.6 \pm 0.1^{\beta}$	$1.7 \pm 0.1^{\beta}$	$0.8 \pm 0.1^{\alpha}$
Isoleucine*	1.6 ± 0.1^{I}	1.8 ± 0.1^{I}	3.3 ± 0.1^{II}	1.2 ± 0.1^{III}
Leucine*	3.7 ± 0.1^{a}	3.9 ± 0.1^{a}	5.9 ± 0.1^{b}	2.9 ± 0.1^{c}
Lysine*	4.0 ± 0.1^{A}	4.3 ± 0.1^{B}	6.1 ± 0.1^{C}	3.7 ± 0.1^{D}
Methionine*	$0.9 \pm 0.1^{\alpha}$	$1.1 \pm 0.1^{\alpha}$	$1.8 \pm 0.1^{\beta}$	$1.4 \pm 0.1^{\gamma}$
Phenylalanine*	2.4 ± 0.1^{I}	3.4 ± 0.1^{II}	3.4 ± 0.1^{II}	1.8 ± 0.1^{III}
Serine	3.6 ± 0.1^{a}	3.6 ± 0.1^{a}	3.7 ± 0.1^{a}	5.0 ± 0.1^{b}
Threonine*	2.2 ± 0.1^{A}	2.2 ± 0.1^{A}	3.5 ± 0.1^{B}	3.4 ± 0.1^{B}
Tryptophan*	$0.2 \pm 0.1^{\alpha}$	$0.2 \pm 0.1^{\alpha}$	$0.6 \pm 0.1^{\beta}$	$0.1 \pm 0.1^{\alpha}$
Tyrosine	1.3 ± 0.1^{I}	1.8 ± 0.1^{II}	2.3 ± 0.1^{III}	0.6 ± 0.1^{IV}
Valine*	2.8 ± 0.1^{a}	2.8 ± 0.1^{a}	4.4 ± 0.1^{b}	2.5 ± 0.1^{c}

The amino acid profile obtained for all the collagen flours is typical of collagen (Li et al., 2009; Yousefi et al., 2017). Glycine is the one that causes the assembling of the triple helix structure, being present in every third position of the polypeptide chain (Lungu et al., 2013; Neurath, 1943). Therefore, it is the most abundant amino acid in collagen as can be seen in Table 2.2 (Gelse et al., 2003). Moreover, the relatively high content in glutamic acid is very interesting since this amino acid participates in crosslinking processes by adding glutaraldehyde

(allowing a better stabilization of the scaffolds produced). These results are in line with those reported by Gauza-Włodarczyk et al. (2017) and Qin et al. (2018) who presented the amino acid composition of collagen proteins highlighting their content in glycine, glutamic acid, and alanine. Proline and hydroxyproline are imino acids, which improve the stability of collagen (the structure is maintained by restrictions on changes in the secondary structure) (Nagai et al., 2008). The imino acid content for the different proteins revealed a proline and hydroxyproline content in the range of 11-12% and 7.5-9%, respectively, for all the collagen proteins. However, the gelatin protein presented a proline content of 7-8% and 4-5% of hydroxyproline. Therefore, the structure may have been more stabilized in the collagens obtained from pork. These values are in accordance with the values presented in the studies carried out by Eastoe (1955, 1957).

2.3.1.2. Electrophoresis

An SDS-PAGE Electrophoresis has been performed for the different protein concentrates with the objective of obtaining the different fractions which constitute the protein. Figure 2.12 shows the profile obtained as well as a standard pattern with different molecular weights. As may be observed, two different profiles can be clearly distinguished. On the one hand, Lanes 1 to 3 show the profiles for the Pork HI95, Pork T95 and Turkey, respectively.

The profiles obtained are very similar, mainly formed by two α-chains, corroborating their collagen nature because it has been proven that the major components of type I collagen are composed of two α-chains (α1- and α2-chains) (Chi et al., 2014). On the other hand, the profile shown in Lane 4 corresponds to fish protein. This profile is different to the one explained before. In this sample, α- and β-chains are its major

constituents. Comparing this profile with the ones obtained in other studies, as the ones carried out by Kittiphattanabawon et al. (2015), in which α-helix and β-sheets were found as the dominant constituents in gelatin protein, it can be confirmed that fish protein is pure gelatin protein.

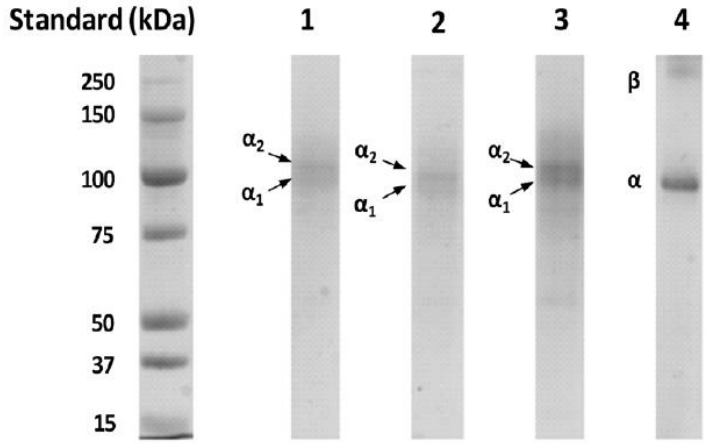

Figure 2.12. SDS-PAGE Electrophoresis of the different protein concentrates: Pork HI95 (Lane 1), Pork T95 (Lane 2), Turkey (Lane 3) and Fish (Lane 4). Standard molecular weight values have also been included

2.3.1.3. Protein solubility and Z-potential

The values of protein solubility and Z-potential for protein concentrates as a function of pH are shown in Figure 2.13.

Collagen solubility reached a maximum of ca. 80% for pork and turkey collagen proteins, presenting a higher solubility at basic pH value. The profiles obtained were similar, with a huge increase in solubility beyond pH 7 and a minimum in the pH range 5-7. However, fish gelatin presented the highest solubility in all the pH range, reaching the maximum values (ca. 95%) at basic pH as the other protein concentrates. On the other hand, the Z-potential measurements showed a shift in the electric potential from positive to negative values from acid to basic pH,

passing through a null value close to pH 5-6. In addition, extreme values were obtained at pH limits (in the range between 15-30 at pH 2 and 10). The combination between the solubility profile and Z-potential measurements of protein dispersions for different pH values provides information about the isoelectric point (there is a coincidence between the pH at which the minimum solubility is observed and the null value at which the electric potential takes place). The pH at which the electric potential becomes zero corresponds to the isoelectric point, being located in the pH range 5-6 (Cao et al., 2014). A low solubility can be observed around pH 8, which may be due to myofibrillar protein fractions of collagen protein (Lin and Liu, 2006). In addition, it is important to control the pH value for the processing of scaffolds, in order to obtain greater solubilization at acidic pH to facilitate the incorporation of protein into the scaffolding structure.

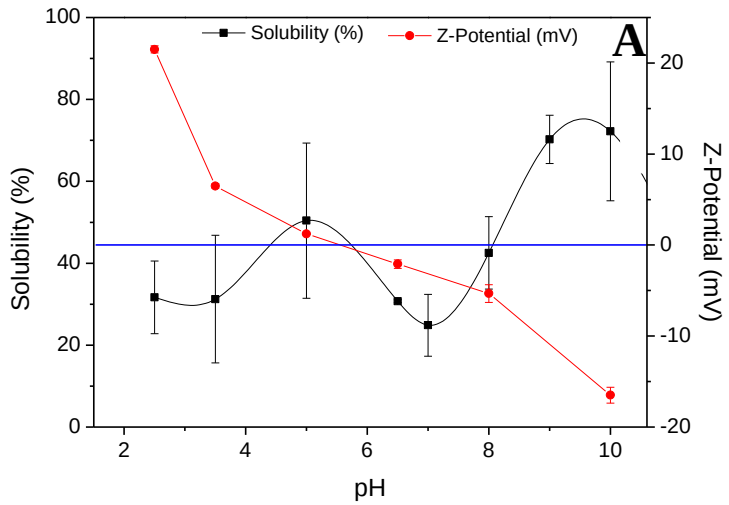

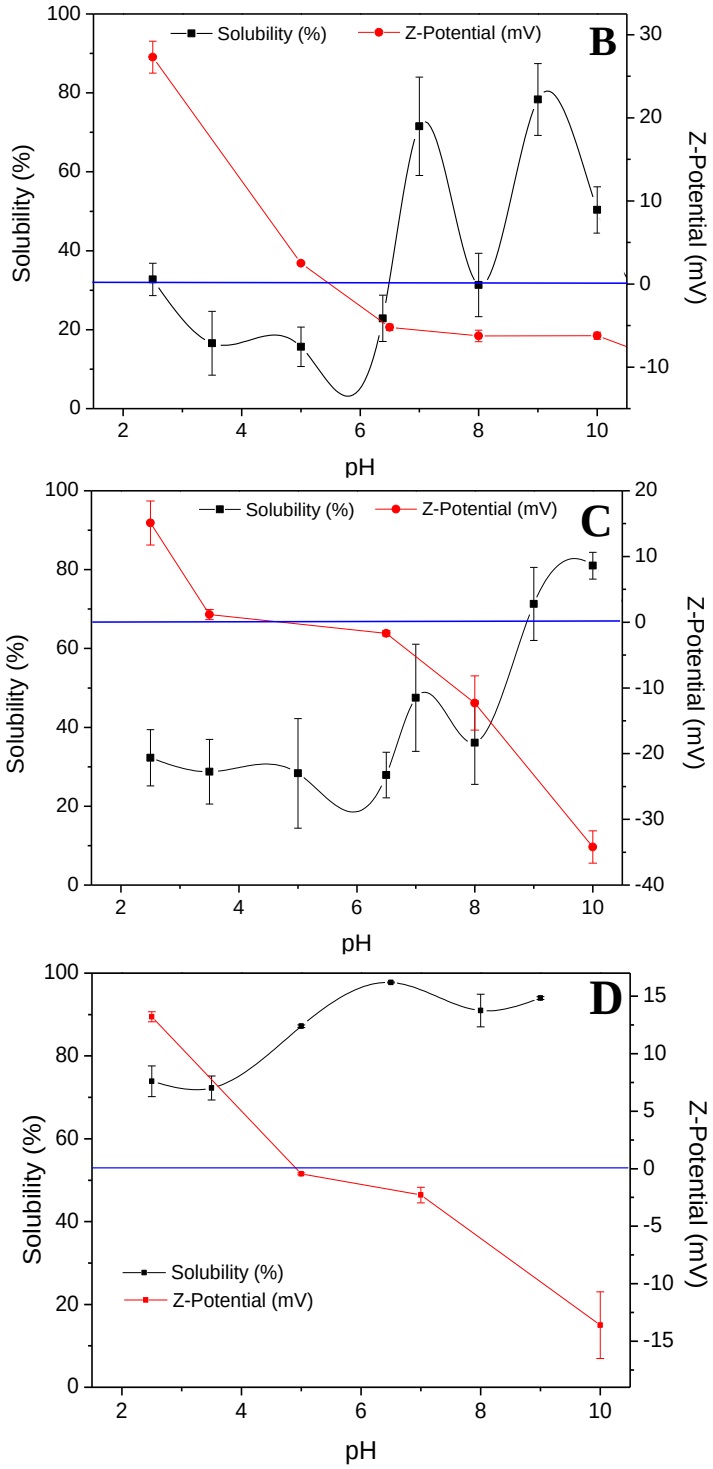

Figure 2.13. Protein solubility (%) and Z-Potential (mV) of the different collagen and gelatin protein concentrates as a function of pH values: (A) Pork HI95, (B) Pork T95, (C) Turkey and (D) Fish

2.3.2. Assessment of the denaturation degree

2.3.2.1. Fourier Transform Infrared Spectroscopy (FTIR)

The FTIR spectra of pork HI95, pork T95 and turkey collagen protein concentrates (Figures 2.14A, 2.14B and 2.14C, respectively), as well as the profile for fish gelatin protein (Figure 2.14D) are shown in Figure 2.14. Moreover, the main peaks and their assignments can be seen in Table 2.3.

Protein samples present characteristic FTIR peaks according to the stretching and bending of their different bonds. A band related to the N-H stretching (Amide A signal) occurs in the range 3300-3200 cm^{-1}, taking place at 3240 cm^{-1} for pure collagen. Another signal associated with the CH_2 symmetric stretching is presented between 2940 and 2850 cm^{-1} (Amide B signal, shown at 2927 cm^{-1} for collagen). In addition, the absorption of the amide I band produced by C=O stretching is between 1700-1600 cm^{-1}, being characteristic for collagen at 1640 cm^{-1}. Finally, the signals for the N-H bending (Amide II and III bands) occurs in the range 1550-1520 cm^{-1} and 1245-1235 cm^{-1}, respectively. Specifically, for pure collagen protein, these signals appear at 1530 and 1242 cm^{-1} (Qin et al., 2018).

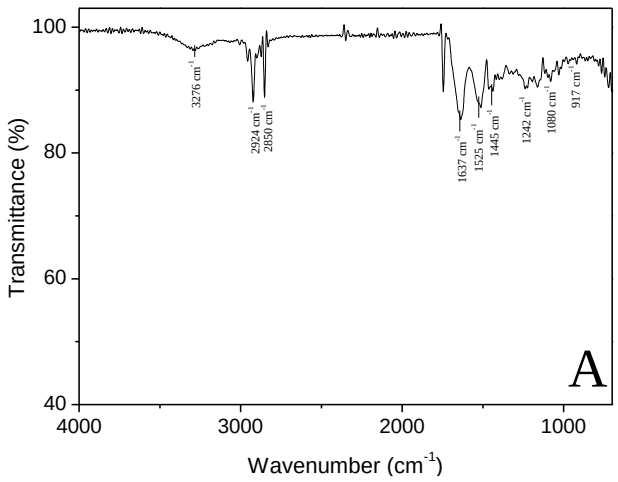

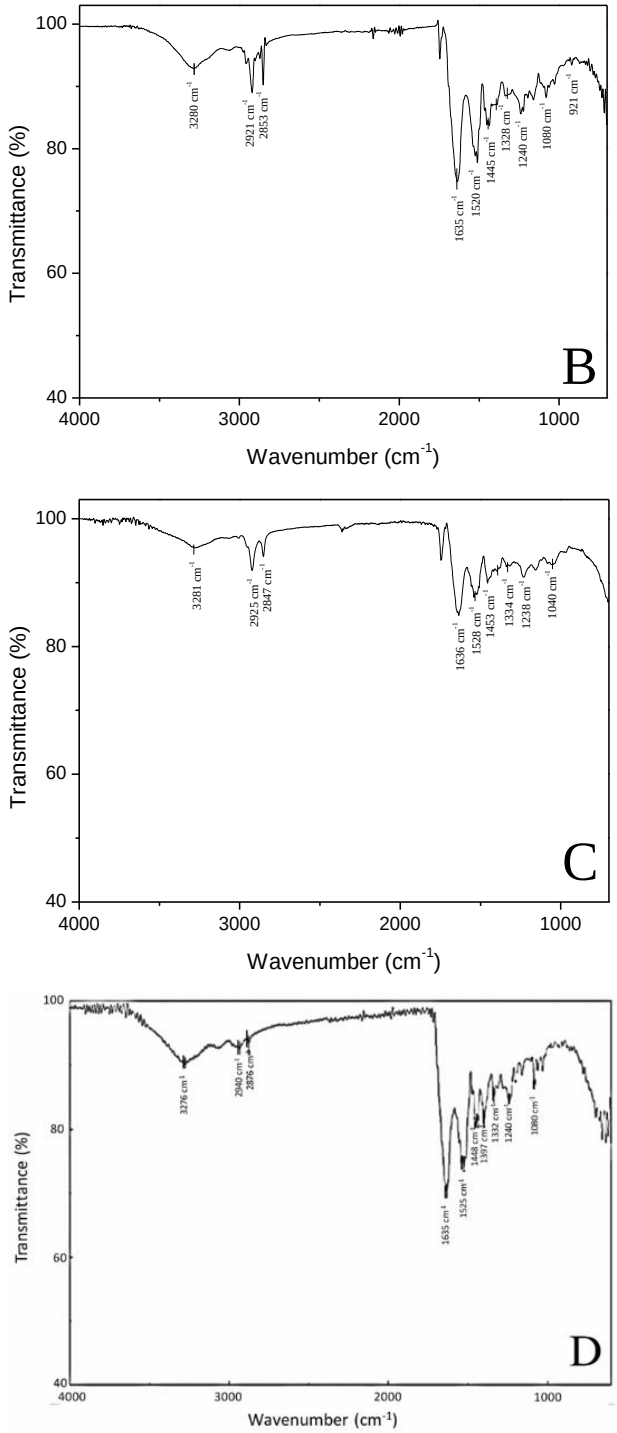

Figure 2.14. FTIR spectra of the four different protein concentrates: (A) Pork HI95, (B) Pork T95, (C) Turkey and (D) Fish

All of them present a similar profile, with the characteristic signals above mentioned. However, the four spectra present slight differences, indicating some variances in the structures of these proteins (Muyonga et al., 2004b). These differences are referred to the intensity of bands, a fact related to prominent absorption bands associated directly with the secondary structure of proteins found in gelatins (Cebi et al., 2016).

Table 2.3. FTIR spectra peak assignments for four different protein concentrates (pork HI95, Pork T95, Turkey and Fish)

SIGNAL/REGION		PEAK (cm^{-1})				ASSIGNMENTS	REFERENCE
		Pork HI95	**Pork T95**	**Turkey**	**Fish**		
A	Amide A	3276	3280	3281	3276	N-H Stretch	(Muyonga et al., 2004b)
B	Amide B	2924	2921	2925	2940	CH_2 asymmetrical stretch	
C		2850	2853	2847	2876	CH_2 symmetrical stretch	
D	Amide I	1637	1635	1636	1635	C=O Stretch	(Vidal and Mello, 2011)
E	Amide II	1525	1520	1528	1525	N-H Bend coupled with C-N Stretch	(Payne and Veis, 1988)
F		1445	1445	1453	1448	CH_2 Bend	(Jackson et al., 1995)
G		1380	1400, 1328	1393, 1334	1397, 1332	CH_2 wagging of Proline	
H	Amide III	1242	1240	1238	1240	N-H Bend	(Payne and Veis, 1988)
I		1080, 917	1080, 921	1040	1080, 920	Skeletal Stretch	(Abe and Krimm, 1972)

Apart from the intensity of the bands (sharper and stronger peaks), the study of the Amide I signal allows better differentiation between collagen and gelatin. This fact was reported by Payne and Veis (1988), showing that this peak is a combination of two marked peaks at ca 1650 and 1633 cm^{-1}, and depending on the peak with the highest intensity, the sample can be considered as collagen or gelatin.

Thus, a zoom in of this signal was included (Figure 2.15). As can be seen, the signal for the fish gelatin protein shows two marked peaks at 1633 and 1650 cm^{-1} (characteristic of gelatin proteins), whereas the other three

samples (pork T95, pork HI95 and turkey protein concentrates) do not show a discrete peak, but a broad peak as a combination of both.

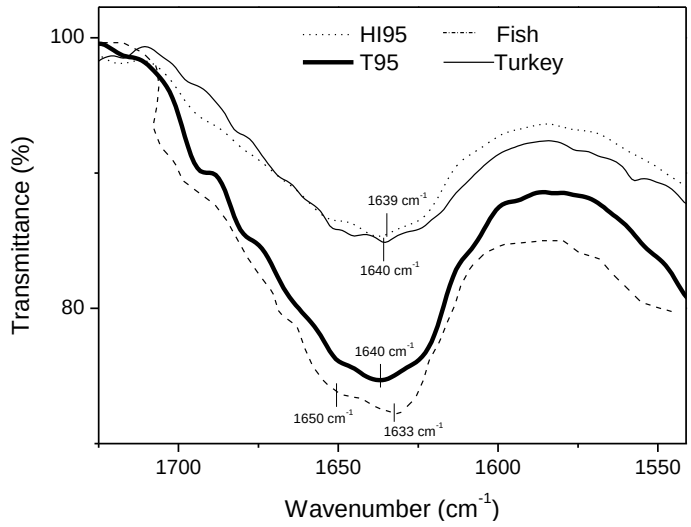

Figure 2.15. Zoom in of the Amide I band from the FTIR spectra of the four different protein concentrates: Pork HI95, Pork T95, Turkey and Fish

For that reason, it can be deduced that these three protein concentrates present a certain denaturation degree, so they are not either native collagen or gelatin, as the fish protein.

2.3.2.2. Free/Total Sulfhydryls

The values obtained for the total and free sulfhydryls for the four collagen protein concentrates are shown in Table 2.4. The values obtained from both free and total sulfhydryls provide information about those sulfhydryls forming disulfide bonds (S-S). Although it is true that the number of free sulfhydryl groups is not necessarily a measure of denaturation, it is a good indicator of the aggregation of a protein (Margaritis et al., 2011).

S-S groups play an important role in fibrous proteins. Considering pure native collagen, almost all the S-content is forming S-S bridges, so this protein consists of subunits joined by S-S bridges among others

(Torchinskii, 2013). Therefore, the ratio between free and total SH-groups is very low. This statement is corroborated with the values obtained for the four samples analyzed (Table 2.4).

Table 2.4. Free/total sulfhydryl values and ratio for the four different collagen protein concentrates (pork HI95, pork T95, turkey and fish). Values with different letters are significantly different (p<0.05)

Raw Material	Sulfhydryls (μmol/g)		
Protein System	Free	Total	Free/Total ratio
Pork HI95	45 ± 15[a]	1658 ± 343[a]	2.7%
Pork T95	155 ± 35[b]	2300 ± 450[a]	6.7%
Turkey	108 ± 30[b]	1819 ± 171[a]	5.9%
Fish	49 ± 6[a]	645 ± 186[b]	7.6%

Comparing the values obtained, the collagen protein from Pork HI95 presented the lower ratio and fish gelatin (used as reference) presented the higher free/total sulfhydryls ratio. Apart from that, these results connected with the ones obtained in Circular Dichroism spectra (data shown in section 3.2.4), stablishing the Pork HI95 collagen protein as the one with the lowest denaturation degree, followed by turkey and pork T95 collagen proteins.

It is also important to point out that the more free sulfhydryls present, the more disulfide bonds can be generated. However, according to the results shown, it can be asserted that the low presence of free sulfhydryls in all the protein concentrates studied (compared to the total sulfhydryls content) indicates that these proteins have some oxidation (probably due to the high temperatures reached during their production process).

2.3.2.3. Differential Scanning Calorimetry (DSC)

Heat flow patterns obtained from DSC measurements in a temperature range between -20 ºC and 140 ºC for the four studied protein concentrates are shown in Figure 2.16.

A first run (dash line) and a second run (straight line) were conducted to detect irreversible dips. On the one hand, pork (HI95 and T95) and turkey collagen concentrates exhibited a similar profile (Figures 2.16A, 2.16B and 2.16C, respectively). These profiles showed three min dips (T_1, T_2 and T_3) and an inflection point (T_4). A remarkable dip (T_1) was found at *ca* 0 ºC, related to ice melting (Kopp et al., 1990). The second dip (T_2) appeared in the range of 25 to 35 ºC (25, 33 and 35 ºC for turkey, pork HI95 and pork T95, respectively) is characteristic of partial gelatinized (denatured) collagen (Beveridge et al., 1974), which indicates that these three collagen concentrates present a certain denaturation degree.

Furthermore, the three samples showed an endothermic peak in the region between 60 and 63 ºC, which is reversible, since it did not appear in the re-scanning (second run). The intensity of this endothermic peak is low, and it is probably related to an enthalpic relaxation associated with the physical aging of these collagen concentrates (Farahnaky et al., 2008). In addition, the inflection point (T_4), observed in the range between 95-100 ºC, corresponds to the glass transition temperature, which is the temperature at which many changes in the properties (enthalpy, viscoelasticity, etc.) of materials take place (Urbaniak, 2011). On the other hand, the profile obtained for the fish protein concentrate (Figure 2.16D) only showed two important signals: a dip at 71 ºC (T_3) related to the physical aging of the protein concentrate and an inflection point at 88 ºC (T_4), which correspond to the glass transition of this protein. The Tg of the fish protein concentrate appears at 88 ºC in the second run because the gelatin molecules could undergo a better interaction after the first run, obtaining a stiffer matrix and a displacement of the Tg value (Tongnuanchan et al., 2016). In addition,

the peak related to ice melting did not appear due to the low moisture of this protein concentrate (below 1%).

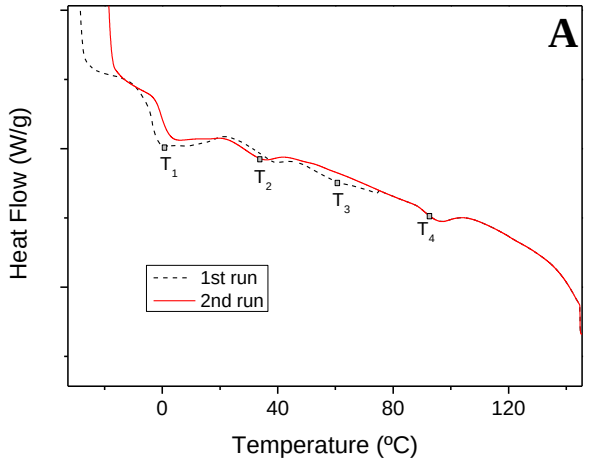

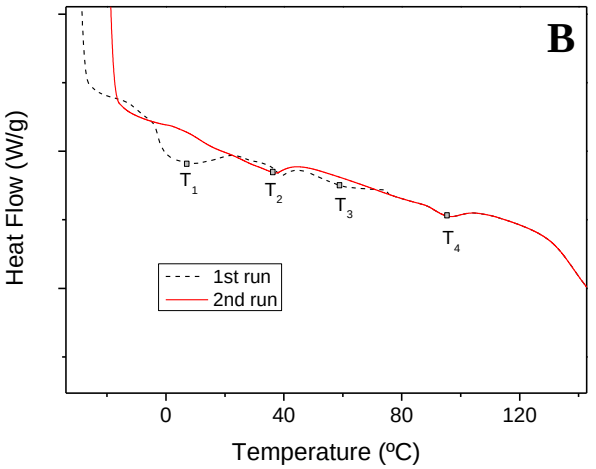

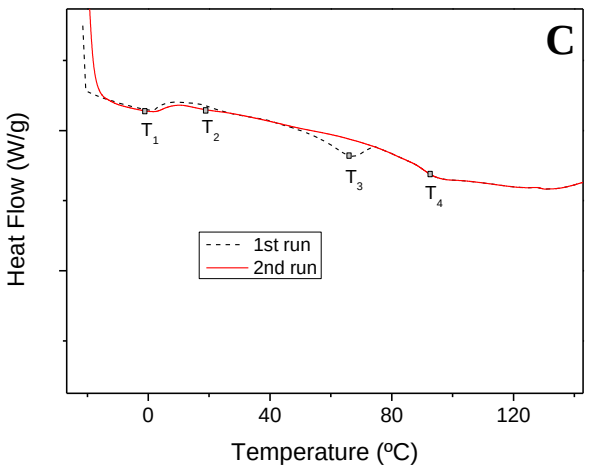

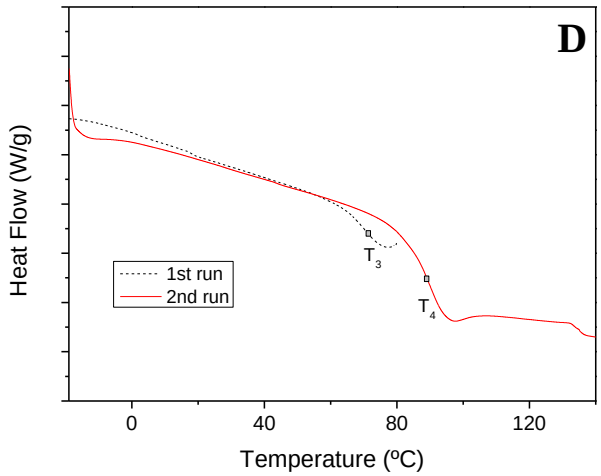

Figure 2.16. DSC profiles of the four different protein concentrates: (A) Pork HI95, (B) Pork T95, (C) Turkey and (D) Fish

2.3.2.4. Circular Dichroism

The Circular Dichroism spectroscopy (CD) of the four protein samples at the wavelength range of 190–240 nm is shown in Figure 2.17.

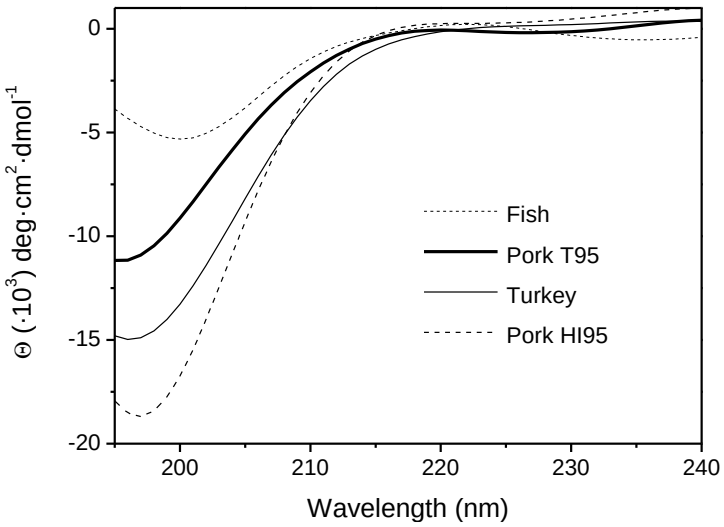

Figure 2.17. CD spectra of the four different protein concentrates: Pork HI95, Turkey, Pork T95 and Fish

The CD spectrum of collagen presents a positive peak at 222 nm, typical for the triple helical structure of collagen (Goo et al., 2003). On the other

hand, gelatin protein also presents a deep negative peak at 198-204 nm, typical for a random coil conformation (Gopal et al., 2012).

The CD spectra of the samples evaluated showed a combination of both spectra above described because they are formed by a negative peak at ca 200 nm and a maximum at 222 nm. Therefore, the samples can be considered as gelatinized collagen proteins. Looking at the CD profiles from Figure 2.17, they are similar although there are some important differences. The main difference is the intensity of the negative peak, being more intense for the fish gelatin sample. The intensity of this peak can be considered as an indicator of the denaturation of the protein according to previous studies (Gopal et al., 2012).

Two different studies could be assessed from the CD spectra obtained for the four protein concentrates studied. First, according to Gopinath et al. (2017), there is a relationship between the maximum (positive) and minimum (negative) peaks and the denaturation of the protein (RPN). According to the assumption that a higher ratio implies a more denatured protein and considering the CD profiles shown in Figure 2.17, the most denatured protein is the fish gelatin protein (in accordance with the FTIR measurements) and the lowest one is the pork HI95 protein concentrate.

In addition, an approximation to the denaturation degree can also be obtained from the CD spectra, since a higher RPN ratio implies a more denatured protein, so a more negative peak corresponds to a lower denaturation. The RPN value for native collagen structure (100% pure) is *ca* -0.10 (Gopinath et al., 2017) and the RPN value obtained for the fish gelatin can be associated to a 100% denatured collagen, so with these values it is possible to give a qualitative approximation of the denaturation degree of the other three protein concentrates studied (pork HI95, pork T95 and turkey) (Table 2.5), comparing the values obtained

with the values belonging to the pure and denatured collagen (shown above). The results illustrated that pork T95 had the highest RPN values, associated with a higher denaturation degree.

Considering the prediction of the secondary structure (Table 2.5), the pork HI95 protein concentrate presents the highest proportion of α-helix (8.8%) and the lowest of β-strand (27.1%), whereas the fish protein system presents the lowest proportion of α-helix (2.9%) and the highest of β-sheet (44.9%). However, in general, the four protein concentrates present a significantly lower proportion of α-helix in the structure, compared to the proportion of β-strand, which is related to an increase in the denaturation degree, in accordance to the results shown in the study (Kelly and Price, 2000).

Table 2.5. RPN (the 'positive-negative ratio') values, approximated denaturation degree and estimation of the secondary structure (α-helix and β-sheet) for the four different protein concentrates (pork HI95, pork T95, turkey and fish). Values with different letters are significantly different (p<0.05)

Raw Material	RPN	Denaturation Degree	Secondary Structure	
Protein System			α-helix	β-strand
Pork HI95	-0.028	~ 25%	8.8 ± 0.9^{a}	27.1 ± 4.2^{A}
Pork T95	0.015	~ 75%	5.5 ± 1.1^{b}	31.0 ± 2.0^{A}
Turkey	0.005	~ 65%	7.4 ± 1.0^{a}	30.5 ± 2.5^{A}
Fish	0.037	~ 100%	2.9 ± 0.3^{c}	44.9 ± 6.2^{B}

Furthermore, according to Echave et al. (2017), the use of denatured collagen protein (gelatin protein), instead of collagen, produces a better cell growth during the implantation of the scaffolds (developed using this protein as raw material). For that reason, an increase in the denaturation degree of collagen protein, used as raw material for the formation of scaffolds, favors the biological response of these scaffolds in tissue engineering applications.

2.4 Concluding remarks

As a general conclusion, the characterization of the different type I collagen proteins reveals high contents in protein, obtaining concentration values of 90% and higher for fish and pork proteins (HI95 and T95) on a dry basis. The amino acid profiles show a relatively narrow distribution of molecular weight. All of them, although with differences, are rich in glycine, alanine, proline, hydroxyproline and glutamic acid but low in cysteine, histidine and tryptophan. Furthermore, protein solubility reaches a maximum of 80% under basic conditions for the pork and turkey protein powders, whereas the fish collagen presents a maximum of ca. 100% observing a decrease at pH 8 due to the presence of myofibrillar proteins in the composition.

The study of the different collagen protein concentrates reveals that all of them showed a certain denaturation degree. In fact, sulfhydryl content and DSC measurements also evidence that aggregation and physical aging are present in protein concentrates although has different sulfur content. These effects, aggregation and physical aging, are a consequence of the production process and storage, respectively. On the other hand, specifically, all the samples presented the characteristic FTIR profile for proteins (N-H bending, N-H and C-N stretching, etc.), with fish and pork T95 standing out due to their sharper and broader bands (typical of gelatin-like proteins), which can be better seen in the deconvolution of the Amide I signal. In addition, the CD spectra showed that the denaturation degree of all these protein concentrates was over 40% (fish protein was almost 100% denatured). Furthermore, the higher the denaturation degree, the higher the amount of β-strand present in the structure of the proteins studied and the better biological response of the scaffolds produced.

Four different techniques have been used to analyze the denaturation degree with their advantages and drawbacks. Sulfhydryls content gives information about the aggregation of the protein rather than the denaturation, although a relation between both can be carried out. Respect the FTIR, the denaturation can be deduced based on the peaks at 1650 and 1633 cm^{-1} but it is difficult to quantify due to the overlapping of these peaks. Considering the DSC spectra, it is interesting to study thermal peaks which differ depending on the denaturation of the sample, although the heating process may induce additional denaturation. Finally, the CD measurements are the most suitable because it allows to estimate the secondary structure of the protein and quantify the denaturation degree with the RPN ratio.

In general, according to the characterization of the four raw materials, pork HI95 collagen protein was selected for further studies (concerning the development of scaffolds for Tissue Engineering applications) because it is the one that presents a higher purity (lower denaturation degree). In addition, fish gelatin protein was also selected to establish a comparison in the properties of gelatin-based scaffolds and collagen-based scaffolds. Moreover, it is important to mention that the protein content of both protein concentrates is higher than 95%.

Acknowledgements

The authors gratefully acknowledge the Characterization and Microanalysis Service (CITIUS-Universidad de Sevilla) for providing full access and assistance to the Q20 (TA Instruments) and to the LECO-CHNS-932 (Leco Corporation). The authors also thank the Physical Chemistry Department (Universidad de Sevilla) and especially to D. Pilar López Cornejo and Francisco José Ostos Marcos for their supervision, assistance and help with the Circular Dichroism measurements.

Finally, authors also acknowledge Essentia Protein Solutions and Henan Boom Gelatin Co. Ltd for supplying the three Type I collagen protein concentrates and gelatin protein isolate, respectively.

Related publications

- Perez-Puyana, Víctor Manuel; Jiménez Rosado, Mercedes; Romero García, Alberto; Guerrero Conejo, Antonio (2019). Highly porous protein-based 3D scaffolds with different collagen concentrates for potential application in Tissue Engineering, *Journal of Applied Polymer Science*, 136, 47954, DOI:10.1002/app.47954
- Perez-Puyana, Víctor Manuel; Ostos Marcos, Francisco José; Lopez Cornejo, María del Pilar; Romero García, Alberto; Guerrero Conejo, Antonio (2019). Assessment of the denaturation of collagen protein concentrates using different techniques, *Biological Chemistry*,
- DOI: 10.1515/hsz-2019-0206

References

Abe, Y., Krimm, S., 1972. Normal vibrations of crystalline polyglycine I. Biopolymers 11, 1817–1839.

Aldana, A.A., Abraham, G.A., 2017. Current advances in electrospun gelatin-based scaffolds for tissue engineering applications. Int. J. Pharm. 523, 441–453.

Allam, E., Bottino, M.C., Al-Shibani, N., Jack Windsor, L., 2012. Collagen scaffolds: Tissue engineering and repair, Type I Collagen: Biological Functions, Synthesis and Medicinal Applications.

Andrade, M.A., Chacon, P., Merelo, J.J., Moran, F., 1993. Evaluation of secondary structure of proteins from UV circular dichroism spectra using an unsupervised learning neural network. Protein Eng. 6, 383–390.

AOAC, I., 2005. Official Methods of Analysis of AOAC International. AOAC International.

Aramwit, P., Jaichawa, N., Ratanavaraporn, J., Srichana, T., 2015. A comparative study of type A and type B gelatin nanoparticles as the controlled release carriers for different model compounds. Mater. Express 5, 241–248.

Badea, E., Gatta, G. Della, Usacheva, T., 2012. Effects of temperature and relative humidity on fibrillar collagen in parchment: A micro differential scanning calorimetry (micro DSC) study. Polym. Degrad. Stab. 97, 346–353.

Beveridge, T., Toma, S.J., Nakai, S., 1974. Determination of SH- and SS-groups in some food proteins using Ellman's reagent. J. Food Sci. 39, 49–51.

Biesecker, G., Ieuan Harris, J., Thierry, J.C., Walker, J.E., Wonacott, A.J., 1977. Sequence and structure of D-glyceraldehyde 3-phosphate dehydrogenase from Bacillus stearothermophilus. Nature 266, 328–333.

Bradford, M.M., 1976. A rapid and sensitive method for the quantitation of microgram quantities of protein utilizing the principle of protein-dye

binding. Anal. Biochem. 72, 248–254.

Cao, S., Xia, S., Liu, L., Qi, X., 2014. Extraction and characterization of collagen from navodon septentrionalis skin. J. Chinese Inst. Food Sci. Technol. 14, 117–123.

Cebi, N., Durak, M.Z., Toker, O.S., Sagdic, O., Arici, M., 2016. An evaluation of Fourier transforms infrared spectroscopy method for the classification and discrimination of bovine, porcine and fish gelatins. Food Chem. 190, 1109–1115.

Chi, C., Cao, Z., Wang, B., Hu, F., Li, Z., Zhang, B., 2014. Antioxidant and Functional Properties of Collagen Hydrolysates from Spanish Mackerel Skin as Influenced by Average Molecular Weight. Molecules 19, 11211–11230.

Correia, D.M., Padrão, J., Rodrigues, L.R., Dourado, F., Lanceros-méndez, S., 2013. Thermal and hydrolytic degradation of electrospun fi sh gelatin membranes. Polym. Test. 32, 995–1000. https://doi.org/10.1016/j.polymertesting.2013.05.004

Cox, M., Nelson, D., 2000. Lehninger Principles of Biochemistry, Wh Freeman.

Deng, L., Zhang, X., Li, Y., Que, F., Kang, X., Liu, Y., Feng, F., 2018. Food Hydrocolloids Characterization of gelatin / zein nano fi bers by hybrid electrospinning. Food Hydrocoll. 75, 72–80.

Eastoe, J.E., 1957. The amino acid composition of fish collagen and gelatin. Biochem. J. 65, 363–368.

Eastoe, J.E., 1955. The amino acid composition of mammalian collagen and gelatin. Biochem. J. 61, 589–600.

Echave, M.C., Saenz del Burgo, L., Pedraz, J.L., Orive, G., 2017. Gelatin as Biomaterial for Tissue Engineering. Curr. Pharm. Des. 23, 3567–3584.

Farahnaky, A., Guerrero, A., Hill, S.E., Mitchell, J.R., 2008. Physical ageing of crayfish flour at low moisture contents. J. Therm. Anal. Calorim. 93, 595–598.

Felix, M., Romero, A., Rustad, T., Guerrero, A., 2017. Physicochemical,

microstructure and bioactive characterization of gels made from crayfish protein. Food Hydrocoll. 63, 429–436.

Gauza-Włodarczyk, M., Kubisz, L., Włodarczyk, D., 2017. Amino acid composition in determination of collagen origin and assessment of physical factors effects. Int. J. Biol. Macromol. 104, 987–991.

Gelse, K., Pöschl, E., Aigner, T., 2003. Collagens - Structure, function, and biosynthesis. Adv. Drug Deliv. Rev. 55, 1531–1546.

Goo, H.C., Hwang, Y.S., Choi, Y.R., Cho, H.N., Suh, H., 2003. Development of collagenase-resistant collagen and its interaction with adult human dermal fibroblasts. Biomaterials 24, 5099–5113.

Goormaghtigh, E., Gasper, R.R., Bénard, A., Goldsztein, A.A., Raussens, V., Benard, A., Goldsztein, A.A., Raussens, V., 2009. Protein secondary structure content in solution, films and tissues: Redundancy and complementarity of the information content in circular dichroism, transmission and ATR FTIR spectra. Biochim. Biophys. Acta - Proteins Proteomics 1794, 1332–1343.

Gopal, R., Park, J.S., Seo, C.H., Park, Y., 2012. Applications of circular dichroism for structural analysis of gelatin and antimicrobial peptides. Int. J. Mol. Sci. 13, 3229–3244.

Gopinath, A., Shanmugam, G., Madhan, B., Rao, J.R., 2017. Differential behavior of native and denatured collagen in the presence of alcoholic solvents: A gateway to instant structural analysis. Int. J. Biol. Macromol. 102, 1156–1165.

Greensteik, P., 1938. Sulfhydryl Groups in Proteins. J. Biol. Chem. 125, 501–513.

Jackson, M., Choo, L.-P., Watson, P.H., Halliday, W.C., Mantsch, H.H., 1995. Beware of connective tissue proteins: Assignment and implications of collagen absorptions in infrared spectra of human tissues. Biochim. Biophys. Acta - Mol. Basis Dis. 1270, 1–6.

Jilek, F., Helmut, H., 1978. Cold-Insoluble Globulin (Fibronectin), IV Affinity to Soluble Collagen of Various Types. Biol. Chem.

Jose, M. V, Thomas, V., Dean, D.R., Nyairo, E., 2009. Fabrication and characterization of aligned nanofibrous PLGA / Collagen blends as bone tissue scaffolds. Polymer (Guildf). 50, 3778–3785.

Kelly, S.M., Price, N.C., 2000. The use of circular dichroism in the investigation of protein structure and function. Curr. Protein Pept. Sci. 1, 349–384.

Kelly, S.M., Price, N.C., 2000. The use of circular dichroism in the investigation of protein structure and function. Curr. protein Pept. Sci. 1, 349–384.

Khajavi, R., Abbasipour, M., Bahador, A., 2016. Electrospun biodegradable nanofibers scaffolds for bone tissue engineering. J. Appl. Polym. Sci. 133, 42883.

Kittiphattanabawon, P., Benjakul, S., Sinthusamran, S., 2015. Gelatin from clown featherback skin LWT - Food Science and Technology Gelatin from clown featherback skin : Extraction conditions. LWT - Food Sci. Technol. 66, 186–192.

Kittiphattanabawon, P., Benjakul, S., Visessanguan, W., Nagai, T., Tanaka, M., 2005. Characterisation of acid-soluble collagen from skin and bone of bigeye snapper (Priacanthus tayenus). Food Chem. 89, 363–372.

Kopp, J., Bonnet, M., Renou, J.P., 1990. Effect of Collagen Crosslinking on Collagen-Water Interactions (A DSC Investigation). Matrix 9, 443–450.

Laemmli, U.K., 1970. Cleavage of Structural Proteins during the Assembly of the Head of Bacteriophage T4. Nature 227, 680–685.

Langer, R., Vacanti, J., 2016. Advances in tissue engineering. J. Pediatr. Surg. 51, 8–12.

Li, F., Jia, D., Yao, K., 2009. LWT - Food Science and Technology Amino acid composition and functional properties of collagen polypeptide from Yak (Bos grunniens) bone. LWT - Food Sci. Technol. 42, 945–949.

Liang, Q., Wang, L., Sun, W., Wang, Z., Xu, J., Ma, H., 2014. Isolation and characterization of collagen from the cartilage of Amur sturgeon (Acipenser schrenckii). Process Biochem. 49, 318–323.

Lin, A.C., Goh, M.C., 2002. Investigating the ultrastructure of fibrous long spacing collagen by parallel atomic force and transmission electron microscopy. Proteins Struct. Funct. Bioinforma. 49, 378–384.

Lin, Y.K., Liu, D.C., 2006. Comparison of physical-chemical properties of type I collagen from different species. Food Chem. 99, 244–251.

Lindroth, P., Mopper, K., 1979. High Performance Liquid Chromatographic Determination of Subpicomole Amounts of Amino Acids by Precolumn Fluorescence Derivatization with o-Phthaldialdehyde 51, 1667–1674.

Lodish, H.F., 2013. Molecular cell biology. W.H. Freeman and Co., New York.

Lungu, A., Albu, M.G., Stancu, I.C., Florea, N.M., Vasile, E., Iovu, H., 2013. Superporous collagen-sericin scaffolds. J. Appl. Polym. Sci. 127, 2269–2279.

Luparello, C., Sirchia, R., 2011. Type V collagen-induced upregulation of capn2 (large subunit of m-calpain) gene expression and DNA fragmentation in 8701-BC breast cancer cells. Biol. Chem. 392, 501–504.

Margaritis, A., Priora, R., Frosali, S., Di Giuseppe, D., Summa, D., Coppo, L., Di Stefano, A., Di Simplicio, P., 2011. The role of protein sulfhydryl groups and protein disulfides of the platelet surface in aggregation processes involving thiol exchange reactions. Pharmacol. Res. 63, 77–84.

Markwell, M.A.K., Haas, S.M., Bieber, L.L., Tolbert, N.E., 1978. A modification of the Lowry procedure to simplify protein determination in membrane and lipoprotein samples. Anal. Biochem. 87, 206–210.

McKee, T., McKee, J.R., de Buitrago, J.M.G., 2003. Bioquímica: la base molecular de la vida. McGraw-Hill, Interamericana.

Merrett, K., Ljunggren, M.K., Mondal, D., Griffith, M., Rafat, M., 2012. Collagen Type I: A promising scaffold material for Tissue Engineering and Regenerative Medicine, in: Type I Collagen. pp. 1–42.

Mohammed, Z.H., Hill, S.E., Mitchell, J.R., 2000. Covalent Crosslinking in Heated Protein Systems. Food Chem. Toxicol. 65, 221–225.

Mohiti-Asli, M., Loboa, E.G., 2016. 23 - Nanofibrous smart bandages for wound care, in: Ågren, M.S.B.T.-W.H.B. (Ed.), Wound Healing

Biomaterials. Woodhead Publishing, pp. 483–499.

Muyonga, J.H., Cole, C.G.B., Duodu, K.G., 2004a. Characterisation of acid soluble collagen from skins of young and adult Nile perch (Lates niloticus). Food Chem. 85, 81–89.

Muyonga, J.H., Cole, C.G.B., Duodu, K.G., 2004b. Fourier transform infrared (FTIR) spectroscopic study of acid soluble collagen and gelatin from skins and bones of young and adult Nile perch (Lates niloticus). Food Chem. 86, 325–332.

Nagai, T., Suzuki, N., Nagashima, T., 2008. Collagen from common minke whale (Balaenoptera acutorostrata) unesu. Food Chem. 111, 296–301.

Neurath, H., 1943. The Role of Glycine in Protein Structure. J. Am. Chem. Soc. 65, 2039–2041.

Orrego Cardozo, M., Ponte, I., Suau, P., 2015. Caracterización de la estructura secundaria de subtipos de la histona H1 por dicroísmo circular. Biosalud 14, 29–48.

Payne, K.J., Veis, A., 1988. Fourier transform IR spectroscopy of collagen and gelatin solutions: deconvolution of the amide I band for conformational studies. Biopolymers 27, 1749–1760.

Payne, K.J., Veis, A., 1988. Fourier transform ir spectroscopy of collagen and gelatin solutions: Deconvolution of the amide I band for conformational studies. Biopolymers 27, 1749–1760.

Pearson, A.M., 1983. Soy proteins, in: Hudson, B.J.F. (Ed.), Developments in Food Proteins, Developments in Food Proteins. Applied Science Publishers, London and Englewood, New Jersey, pp. 67–108.

Pok, S., Vitale, F., Eichmann, S.L., Benavides, O.M., Pasquali, M., Jacot, J.G., 2014. Terms of Use Biocompatible Carbon Nanotube À Chitosan Sca ff old Matching the Electrical Conductivity of the Heart. ACS Nano 9822–9832.

Qin, S., Liu, J., Qiao, Y., Wang, M., Wu, W., Li, J., Tian, Y., 2018. Extraction and characterization of type I collagen from skin of tilapia (Oreochromis niloticus) and its potential application in biomedical scaffold material for

tissue engineering. Process Biochem. 74, 156–163.

Ravikumar, K.M., Hwang, W., 2008. Region-specific role of water in collagen unwinding and assembly. Proteins Struct. Funct. Bioinforma. 72, 1320–1332.

Reeb, J., Rost, B., 2019. Secondary Structure Prediction. Encycl. Bioinforma. Comput. Biol. 488–496.

Sionkowska, A., Grabska, S., 2017. Preparation and characterization of 3D collagen materials with magnetic properties. Polym. Test. 62, 382–391.

Stratton, S., Manoukian, O.S., Patel, R., Wentworth, A., Rudraiah, S., Kumbar, S.G., 2018. Polymeric 3D printed structures for soft-tissue engineering. J. Appl. Polym. Sci. 135, 45569.

Tan, W.F., Koopal, L.K., Weng, L.P., van Riemsdijk, W.H., Norde, W., 2008. Humic acid protein complexation. Geochim. Cosmochim. Acta 72, 2090–2099.

Thannhauser, T.W., Konishi, Y., Scheraga, H.A., 1984. Sensitive quantitative analysis of disulfide bonds in polypeptides and proteins. Anal. Biochem. 138, 181–188.

Tongnuanchan, P., Benjakul, S., Prodpran, T., Pisuchpen, S., Osako, K., 2016. Mechanical, thermal and heat sealing properties of fish skin gelatin film containing palm oil and basil essential oil with different surfactants. Food Hydrocoll. 56, 93–107.

Torchinskii, Y.M., 2013. Sulfhydryl and Disulfide Groups of Proteins, Studies in Soviet Science. Springer US.

Urbaniak, M., 2011. A relationship between the glass transition temperature and the conversion degree in the curing reaction of the EPY® epoxy system. Polimery/Polymers 56, 240–243.

Vidal, B. de C., Mello, M.L.S., 2011. Collagen type I amide I band infrared spectroscopy. Micron 42, 283–289.

Yousefi, M., Ariffin, F., Huda, N., 2017. An alternative source of type I collagen based on by-product with higher thermal stability. Food Hydrocoll. 63, 372–382.

Zhang, X., Tang, K., Zheng, X., 2016. Electrospinning and Crosslinking of COL/PVA Nanofiber-microsphere Containing Salicylic Acid for Drug Delivery. J. Bionic Eng. 13, 143–149.

Chapter 3: Development of scaffolds via freeze-drying process

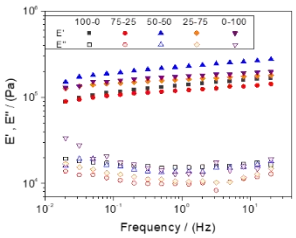

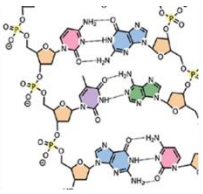

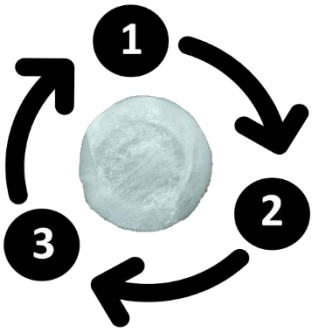

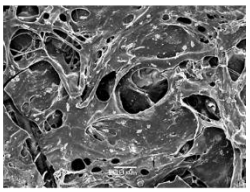

3.1 Introduction

Tissue Engineering (TE) is a multidisciplinary field where different branches of science interact, such as chemistry, physics, medicine, biology and engineering. In recent years, the most researched element of TE has been the scaffold, which is a structure that acts as an anchorage and adhesion platform for cells. In this way, these scaffolds must have well-designed mechanical and morphological properties to promote optimal growth of cells and their integration within the tissue (Sachlos and Czemuszka, 2003).

The properties of scaffolds are highly dependent on the type of polymer used and the processing method followed to develop these structures. Thus, the choice of the raw material must be in accordance with the type of function and structure of the growing tissue that will be later implanted. The most used raw materials for the elaboration of scaffolds are synthetic biopolymers since it is easier to control their characteristics, which allows high reproducibility (Geutjes et al., 2006). However, they show some features of post-implantation immunogenicity and inflammation. To solve these drawbacks, a new pathway is being investigated, which consists in the use of proteins and polysaccharides (biopolymers) (Jana et al., 2014). Biopolymers have beneficial properties, such as biocompatibility, biodegradability and functionalization capacity, which make them an attractive resource for the formation of scaffolds (Zhao et al., 2012). Among them, proteins as collagen (CG) or gelatin (GE) can adopt a large number of structures similar to biological ones, which contributes a high level of biocompatibility and biodegradability. They also lead to high tensile strength and contain cell adhesion sequences (Cristescu et al., 2014). In addition, Chitosan (CH) comes from chitin through a deacetylation

process, which is very common in nature, since it is part of the cell walls of fungi, the exoskeleton of arthropods and some organs of many other animals, such as annelids (Zhang and Neau, 2001). It has a large number of applications, since it is usually used as a flocculating agent in water treatment, wound disinfectant in medicine and thickener in the food industry (Rodríguez-Vázquez et al., 2015). One of these fields, in which chitosan is useful, is in Regenerative Medicine because it is a biocompatible and biodegradable substance (Mármol et al., 2012). An image of its chemical structure can be seen in Figure 3.1.

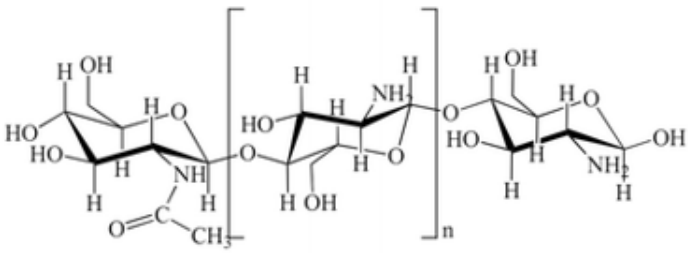

Figure 3.1. Chemical structure of chitosan. Image obtained from the studies of Islam et al. (2017)

For this reason, its use is very common in the elaboration of biodegradable sutures, contributing to avoid bleeding. Nevertheless, an interesting option is the combination of these two raw materials (CH and CG) could help to combine their qualities by creating a hybrid scaffold that has the characteristics of both, thus having a high porosity and biocompatibility. Moreover, they have a synergistic effect that improves their mechanical and microstructural properties (Martínez et al., 2015). For this reason, it has been studied previously by other authors. As examples, Kaczmarek et al. combined collagen and chitosan with other substances as glycosaminoglycans or hyaluronic acid to create composites for specific applications (Kaczmarek et al., 2017, 2018). Furthermore, Oliveira et al. (2019) recently evaluated the *in vivo*

degradation of collagen/chitosan blends by using bi-fluorescence imaging (Oliveira et al., 2019). Other studies prepared collagen/chitosan composites with the addition of different particles to enhance their properties. In this sense, Muthukumar et al. (2016) evaluated the influence of the incorporation of *Ginseng* compound K on collagen/chitosan scaffolds for the treatment of osteoporosis. Following the same trend, You et al. (2017) loaded silver nanoparticles to collagen/chitosan scaffolds to investigate its possible application on wound healing.

As for the preparation methods, several processing techniques have been used to develop three-dimensional scaffolds, such electrospinning, 3D printing, freeze-drying, etc. (Aguirre-Chagala et al., 2017; Correia et al., 2011; Fereshteh et al., 2016; Senatov et al., 2017; Varley et al., 2016; Zhong et al., 2006). Among them, the freeze-drying process is widely used to produce materials for TE applications. This technique consists in the formation of an aqueous polymer solution, which is frozen and lyophilized to eliminate the solvent by sublimation. This technique is very useful for natural polymers, since it allows the elimination of the solvent without degrading the polymer and, thus, without affecting its structure (Sachlos et al., 2003). Moreover, it is one of the few techniques that allows the formation of macropores in structures obtained from natural polymers (Maji et al., 2018; Mohammadi et al., 2016; O'Brien et al., 2004b; Perdivara et al., 2013; Shahbazarab et al., 2018; Teimouri and Azadi, 2016; Wu et al., 2010; Yannas and Burke, 1980). In addition to this, the structures obtained are considered as "sponge-like" materials because it allows the production of a high porous (porosity higher than 75%) three-dimensional latticework formed by interconnected pores of different sizes (Whang et al., 1995). However, in general, this method

makes the scaffolds showing limited mechanical properties due to the microstructural properties achieved such as the high porosity previously mentioned. Both properties, although opposed, are necessary for the optimal growth of the cells in the scaffolds (Vallet-Regi and Munuera, 2000), and therefore, it is necessary to strengthen them. Concerning the processing method followed, there are three main ways of modifying the properties of scaffolds. In this sense, the first way is to modify the processing variables involved (which vary depending on the process followed) (Horgnies, 2009), the second way is to include a crosslinking method to the global process (Martínez et al., 2015; Naghieh et al., 2018; Oryan et al., 2018); whereas the third way is the incorporation of an additional intermediate stage (i.e. heat treatment or agitation) to the process. All these ways mainly affect the latticework structure of scaffolds and, consequently, their mechanical properties change (Yin et al., 2009).

Regarding the modification of the processing variables, the different parameters to be considered in this process are the container used during the freeze-drying process, the freezing temperature, the pH value of the solution and the solvent used. Among these, freezing temperature is the most studied variable (Lin et al., 2013; O'Brien et al., 2004b; Reys et al., 2017; Rodríguez-Parra et al., 2012), obtaining better properties for those scaffolds fabricated at a lower temperature (Reys et al., 2017; Zamanian et al., 2014). As for the mold where the solution is added to remove the solvent, the use of a hydrophobic container has been reported to favour the elimination of aqueous solvents, improving the process (Schwarzenbach et al., 2002).

Concerning the crosslinking modification of the scaffold, there are three main crosslinking techniques: chemical, physical or enzymatic

crosslinking (Pinto et al., 2015). Some studies, as the one driven by Ma et al. (2003) used aldehydes (e.g., glutaraldehyde) as crosslinking agent of collagen/chitosan scaffolds for skin tissue engineering, being the most frequently used chemical crosslinking agent, although an excess thereof can be cytotoxic (Bae et al., 2013; Ruijgrok et al., 1994). The substitution of these crosslinking agents by other agents (e.g. genipin as a chemical crosslinking or transglutaminase as a enzymatic crosslinking) or with physical crosslinking (e.g. a thermal treatment) can solve the problems of toxicity, as they involve high specificity (O'Brien et al., 2004b; Teixeira et al., 2012). Finally, the incorporation of a heat treatment as an intermediate stage of the freeze-drying process may allow modifying the final properties of the scaffolds through a reorganization in their polymer chains, improving their solubilization and combination. That better reorganization allows a better interaction between the polymer chains improving the microstructure and, therefore, modifying the mechanical properties of the sponge-like scaffolds obtained.

On these grounds, the aim of this work was to develop hybrid (CH and CG) sponge-like scaffolds, starting with the complete assessment of all the different processing variables involved in the freeze-drying technique (type of container, processing conditions and solvent used). Combinations of collagen and chitosan were also studied to obtain the optimal ratio of collagen and chitosan that would provide good mechanical and microstructural properties. In addition, the crosslinking produced by glutaraldehyde, genipin, a thermal treatment or transglutaminase was evaluated and compared in order to find a non-toxic crosslinking to strengthen the scaffolds. Apart from that, an alternative to collagen-based scaffolds was studied by producing binary gelatin-chitosan structures and modifying the freeze-drying process

obtaining two new alternative methods. All these alternatives were assessed by measuring the mechanical and microstructural properties of the resulting scaffolds.

3.2 Material and methods

3.2.1. Materials

Protein isolates from two different sources were used: Type I collagen protein isolate (CG) from pork (HI95) and type B gelatin protein (GE) from fish skin (Bloom 80-120 g). The former was supplied by Essentia Protein Solutions (Grasten, Denmark), whereas the latter was provided by Henan Boom Gelatin Co. Ltd (China). The complete composition of both proteins is shown in Chapter 2. In addition, low molecular weight chitosan (CH, 50000-190000 Da/mol, 75-85% deacetylated) was used, provided by Sigma Aldrich (USA).

The following crosslinking agents were used: Glutaraldehyde (GA), in a water solution of 50%, provided by Panreac Química S.A. (Spain); genipin (GN) (purity greater than 98%, extracted from *Gardenia jasminoides* plant), supplied by Guangxi Shanyun Biochemical Science and Technology Co. (China); commercial enzyme transglutaminase ProbindTX (TG), with an enzymatic activity of 100 units/g, supplied by BDF Ingredients (Spain).

Finally, a 0.05 M solution of acetic acid was used as solvent, also supplied by Panreac Química S.A. (Spain).

3.2.2. Fabrication of sponge-like porous scaffolds

3.2.2.1 Freeze-Drying process

The scaffolds were prepared following a freeze-drying method, considered as the traditional process to produce sponge-like structures (O'Brien et al., 2004a), which consists of four stages (Figure 3.2): preparation of the biopolymer solution, centrifugation, freezing and freeze-drying of the solution.

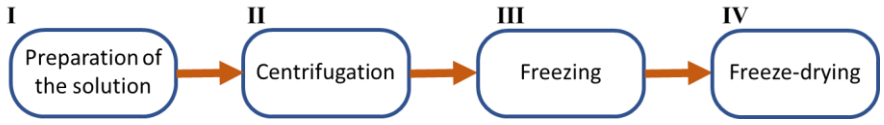

Figure 3.2. Stages of the freeze-drying process

The four stages, in which the process consists, were included in the phase diagram of water for a better comprehension of the process (Figure 3.3):

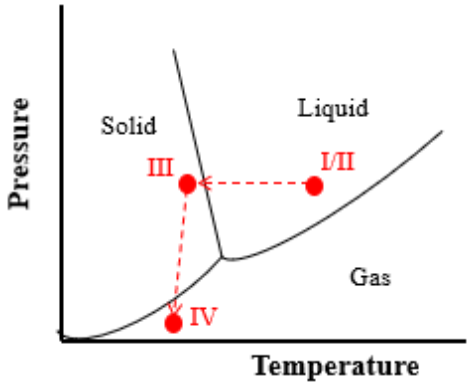

Figure 3.3. Phase diagram of water with the four stages of the Freeze-Drying process

<u>Preparation of biopolymer solutions (I) and centrifugation (II)</u>

First, polymeric solutions were prepared using 0.05 M acetic acid as solvent. Then, the non-soluble part was separated by centrifugation at a speed of 12,000*xg* for 10 min at a temperature of 4 ºC using a Sigma 3-18k centrifuge (SIGMA, UK) (Figure 3.4).

Figure 3.4. Sigma 3-18k centrifuge

Freezing (III) and freeze-drying (IV) of solutions

Once the solutions were prepared, they were frozen at -40 ºC for 2 h in an EQUITEC -40ºC Freezer (Equitec, Spain) (Figure 3.5).

Figure 3.5. EQUITEC -40ºC Freezer

Subsequently, the solvent (acetic acid) was sublimated by freeze-drying in a LyoQuest lyophilizer (Telstar, Spain) at low pressure (<15 Pa) and a temperature of -80 ºC for 24 h (Figure 3.6).

Figure 3.6. LyoQuest lyophilizer (Telstar)

3.2.2.2 Reinforcement stage

Three different types of crosslinking processes have been considered: Chemical crosslinking, physical crosslinking and enzymatic crosslinking. The different crosslinking methods were evaluated in the hybrid sponge-like scaffold CG-CH (ratio: 50-50).

Chemical crosslinking

Two different compounds were used to perform a chemical crosslinking of the selected systems. Glutaraldehyde has been extensively used to reinforce the properties of the scaffolds (Ma et al., 2003; Oryan et al., 2018; Perez-Puyana et al., 2016; Ruijgrok et al., 1994; Songchotikunpan et al., 2008). In this study, Glutaraldehyde (GA) was incorporated into the solution once prepared at different concentrations (0.03, 0.05 and 0.10% w/v with respect to the prepared solution), following the steps of the conventional processing of the scaffold without modifications. These concentrations were selected based on the optimal proportion of GA in CG scaffolds studied in the literature (O'Brien et al., 2004b; Perez-Puyana et al., 2016).

Apart from glutaraldehyde, a chemical crosslinking was also performed by using genipin (GN). Genipin is a natural substance which spontaneously crosslinks chitosan, gelatin or collagen and presents a much lower level of cytotoxicity than glutaraldehyde (Yoo et al., 2011). According to Dimida et al. (2017), the optimal concentration of genipin was found to be ca. 3 wt.% of the total biopolymer concentration. Thus, collagen-chitosan scaffolds with genipin incorporated (0.03 wt.%) were prepared following the reference method to evaluate the influence of this natural substance to the properties of the scaffolds produced.

Physical crosslinking

As an alternative to a chemical crosslinking, the scaffolds were exposed to a temperature of 105 ºC in a conventional oven for 24 h in order to cause covalent crosslinking between the collagen chains to improve the strength of the final structure of the scaffolds (Weadock et al., 1983).

Enzymatic crosslinking

Furthermore, aiming for testing the effect of an enzymatic crosslinking, transglutaminase (TG) was incorporated into the hybrid scaffolds. TG acted on the two biopolymers used (CG and CH) instead of only on CG, as GA did (Yang et al., 2016). Therefore, for comparison purposes (using as a reference the amount of crosslinking agent acting on CG), 0.10% w/v of TG was incorporated to the solution prepared with 0.5% w/v of TG acting on each biopolymer. In addition, since TG has an optimum operating temperature of 50 ºC (Jozami and Seselovsky, 2003), the scaffolds preparation process was modified. In this process, once TG was incorporated in the solution, it was heated in a bath at 50ºC for 2 h.

3.2.2.3 Optimization of the freeze-drying process

The optimization of the freeze-drying process was carried out by performing two alternatives to the traditional process (named as reference or P1), described in Section 2.2.1 (Figure 3.2).

Protocol 2 (P2)

The only difference between the reference protocol and protocol 2 was the inclusion of a heat treatment after the centrifugation and before freezing step (shown in Figure 3.7).

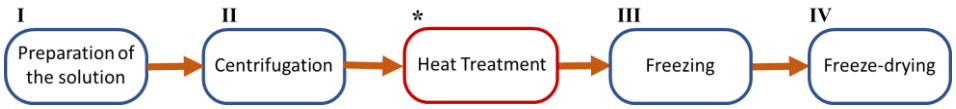

Figure 3.7. Alternative scaffolds preparation stages (P2)

Therefore, the sequence of steps was as follows: first, the solution was prepared, then centrifuged, heated, frozen and finally freeze-dried to eliminate the solvent and obtain the scaffold. The objective of this heat treatment was to give greater mobility to the chains of biopolymers present in the solution, in this way its interaction will be easier, being

able to achieve a greater chain organization that favours the mechanical properties of the scaffolds (Van Vlierberghe et al., 2011).

This heat treatment consisted of heating the biopolymers solution in a thermal bath with distilled water at approximately 50 ° C for 2 h with magnetic stirring. It is not advisable to use a higher temperature to avoid the degradation of collagen (Perez-Puyana et al., 2019).

Protocol 3 (P3)

Protocol 3 was similar to protocol 2 except for the alteration of the sequence of the centrifugation and heat treatment steps in order to find out in which is the most efficient (shown in Figure 3.8). In this case, the parameters of heat treatment were the same as in protocol 2.

Figure 3.8. Alternative scaffolds preparation stages (P3)

3.2.3. Studies performed

The different studies performed have been summarized in the following table (Table 3.1).

Table 3.1. Studies performed, systems involved and section in which the results have been included

Studies	Systems	Variables	Sections
Processing Conditions	GE 1 wt.%	Container, pH, solvent and temperature	3.3.1
Protein Concentration	GE and CG	0.5 and 1 wt.%	3.3.2
Addition of chitosan	CH-CG 1 wt.%	100-0, 75-25, 50-50, 25-75 and 0-100	3.3.3
Crosslinking methods (Chemical, physical and enzymatic)	CG-CH 50-50	GA (0.03, 0.05 and 0.10 %) GE (0.03%) HT TG (0.10 %)	3.3.4
Optimization of the process	GE-CH 50-50	Intermediate heat treatment (P2 and P3)	3.3.5

3.2.4. Characterization of sponge-like porous scaffolds

The evaluation of the properties of the scaffolds was carried out by performing a rheological and a microstructural analysis, as well as other additional techniques such as Circular Dichroism or Water Contact Angle measurements in specific studies. In addition, the degree of crosslinking was also evaluated when a crosslinking method was performed.

3.2.4.1. Rheological characterization

The rheological characterization of the scaffolds was carried out by means of a dynamic-mechanical analyzer (DMA), model RSA3 (TA Instruments, USA), with a plate-plate geometry (dia: 15 mm) (Figure 3.9). The RSA3 rheometer is a controlled strain equipment, in which the motor applies a deformation to the material while a transducer measures the force generated by its resistance to be deformed. In this type of transducer, a position sensor detects the movement and a linear motor measures the reaction force required to drive the support containing the scaffold to its initial position. The great advantage of this system is that it allows measuring within a wide range of stresses with a high sensitivity and low inertia.

Figure 3.9. RSA-3 rheometer (TA Instruments)

Two different types of dynamic compression measurements (oscillatory tests) were performed: Strain sweep tests and frequency sweep tests.

Strain sweep tests: Measurements were carried out at 1 Hz in a range of strain percentages between $2.5 \cdot 10^{-4}$ and 2.5% to determine the linear viscoelastic range and the critical strain of each system. The critical strain (γ_c) is the true strain value at the onset of the non-linear viscoelastic region at which proportionality between the stress and strain is not further maintained. This parameter is calculated plotting the data obtained in a stress-strain curve. The last values are discarded until the correlation coefficient (R^2) of the linear regression is greater than 0.999 (Figure 3.10). The last value in which the correlation fulfilled the linear regression is defined as the critical strain. Therefore, the linear viscoelastic range corresponds to strains lower than the critical strain.

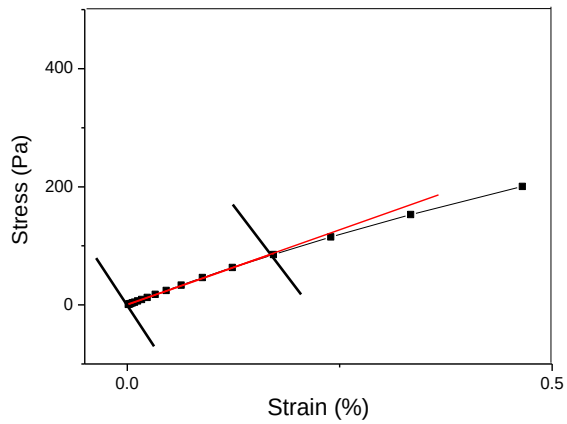

Figure 3.10. Example of a strain-stress curve to obtain the critical strain

Frequency sweep tests: The elastic and viscous moduli (E' and E'', respectively) were measured at constant compressional strain within the linear viscoelastic range (specific for each system analyzed) as a function of frequency (between 0.02 and 20 Hz). All measurements were performed at 25 ºC. E'_1 and tan (δ_1) (rate between E''_1 and E'_1) at 1 Hz

were selected as parameters for a better comparison between the systems in order to corroborate if there are significant differences between them. To compare the results obtained of the different protocols (Section 3.5.2), a new parameter has been defined, K_{i1}, which is defined as the ratio between the elastic modulus at 1 Hz obtained for the rheological measurements of the scaffolds obtained in the two alternative protocols developed (Pi) respect the E' at 1 Hz obtained for a system produced with the reference system (P1) (Eq. 3.1):

$$K_{i1} = \frac{E'1\ (Pi)}{E'1\ (P1)} \qquad (3.1)$$

3.2.4.2. Microstructural characterization

Scanning Electron Microscopy (SEM): This technique is based on the principle of optical microscopy in which the beam of light is replaced by an electron beam. A resolution of up to 100 Å can be achieved, much higher than that of any optical instrument. Its operation consists in having an electron beam scan on the sample. When the beam reaches the surface of the sample, mainly backscattered electrons and secondary electrons are generated. The microscope is internally equipped with detectors that collect energy and transform it into images and data, obtaining high resolution surfaces. An incident electron beam is scanned across the surface of the sample, and the resulting electrons emitted from the sample are attracted and picked up by a detector and translated into a signal. Imaging can be done using secondary electrons to obtain fine surface topographic features or with backscattered electrons that give contrast based on the atomic number. The sample (unless it is already conductive) is usually covered with a very thin layer of gold, which gives it conductive properties. The technique of preparation of the samples is called "sputtering".

The SEM imaging was performed by using a JEOL JSM 6460 LV (JEOL, Japan) scanning electron microscope with a secondary electron detector at an acceleration voltage of 20 kV (Figure 3.11).

Figure 3.11. JEOL JSM 6460 LV scanning electron microscope

Porosity: The porosity (ε) of the scaffolds was obtained using the method described previously by Al-Munajjed et al. (2008). Briefly, the porosity was obtained from the density of each scaffold (calculated with the weight and volume of each scaffold) and the theoretical density of the raw material used (Eq. 3.2):

$$\varepsilon\ (\%) = \left(1 - \frac{\rho_s}{\rho_m}\right) \cdot 100 \qquad (3.2)$$

Where ρ_s is the density of the scaffold and ρ_m is the density of the raw material used, which is 0.68 g·cm^{-3} for type I collagen and gelatin and 1.46 g·cm^{-3} for chitosan (Yang et al., 2009). These density values were corroborated using a Pentapyc 5200e gas pycnometer (Quantachrome Instruments, USA) (Figure 3.12). In addition, the density of the scaffold was obtained with mass and volume measures of different samples.

Figure 3.12. Pentapyc 5200e gas pycnometer

This analytical technique allows determining the approximated overall porosity of the system, although its main drawback is the lack of any data on pore size or distribution.

Pore size distribution: Low-pressure mercury porosimetry was performed to investigate pore size. This technique was performed using a PoreMaster-60 GT porosimeter (Quantachrome Instruments, USA) (Figure 3.13). It is a destructive and indirect technique for the characterization of the porous system of the materials, obtaining from it the distribution of the porosity based on the apparent size of access to the pores. It is based on the application of pressure, thus forcing the penetration of mercury into the porous framework of the solid. This technique is used in the study of materials that have macropores and mesopores; With this analysis the area, the volume of macro and mesopores are determined and the distribution of the porosity of the material is calculated. To do this, the volume is registered against the pressure using the equipment control software.

Figure 3.13. PoreMaster-60 GT porosimeter

3.2.4.3. Degree of crosslinking

Measurements of the degree of crosslinking of the different scaffolds were made to compare the crosslinking caused by the incorporation of GA, GE and TG or the heat application. To quantify this, the content of free and crosslinked amino groups was measured in the different systems, using the same protocol presented by Ofner and Bubnis (1996). In this sense, 0.5 mL of 4% w/v $NaHCO_3$ solution and 0.5 mL of a freshly prepared solution of 0.05% w/v TNBS (2,4,6-trinitro-benzene-sulfonic acid) was added to one part of the system (2-4 mg), keeping it at 40 ºC for 2 h. Thus, the reaction of the free amino groups of different scaffolds with the TNBS was promoted, with the free amino groups being transferred to the solution, which changed color with their presence. Then, 1.5 mL of 6 M HCl (hydrochloric acid) was added, hydrolyzing the systems at 60 ºC for 90 min and preventing the crosslinked amino groups from reacting with the TNBS. Finally, the solutions were diluted with 2.5 mL of distilled water and the absorbance at 325 nm of the different solutions was measured. A blank was made following the same protocol but without adding any system, and it was used as 100% crosslinked amino groups. In addition, a control system was prepared using a scaffold with no crosslinking agent incorporated, and it was used as 0% crosslinked amino groups.

$$\%\, Crosslinking = \frac{A_{325}(sample) - A_{325}(blank)}{A_{325}(blank)} \cdot 100 \qquad (3.3)$$

Where $A_{325}(sample)$ is the absorbance of each system evaluated and $A_{325}(blank)$ is the absorbance of the blank.

3.2.4.4. Swelling degree

Another important parameter in the scaffolds is their swelling ratio. This parameter gives information about the behavior of the scaffolds with the medium present in both the bioreactor and the human body (Rodríguez-Rodríguez et al., 2019). Thus, the swelling ratio was calculated as indicated in equation 3.4 by the relation between the weight of dry scaffolds after the freeze-drying step (w_0) and their weight after remaining in a known amount of water for 30 min (w_1). The measurements were performed using water as liquid at 25 ± 1 ºC and pH 7.0 ± 0.4.

$$Swelling\ ratio = \frac{w_1 - w_0}{w_0} \cdot 100 \qquad (3.4)$$

3.2.4.5. Circular Dichroism (CD)

Electronic Circular Dichroism (CD) spectra were recorded in a Biologic Mos-450 spectropolarimeter. A standard quartz cell of 10 mm path length was used. Scans were taken from 190 to 240 nm under a nitrogen atmosphere. Spectra were performed at a fixed collagen concentration of 0.01 g/L for each type of protein concentrate in acetic acid (0.05 M). All CD spectra of collagen solution were solvent subtracted and each spectrum was obtained from an average of 10 runs at a fixed temperature of 25.1 ± 0.1 ºC with a 10 min equilibration before each scan. The spectra obtained were expressed in terms of mean residue ellipticity (deg·cm^2·dmol^{-1}) (Orrego Cardozo et al., 2015). This term can be expressed as:

$$[\theta]_{mrw} = \frac{MRW \cdot \theta}{10 \cdot d \cdot c} \qquad (3.5)$$

Where θ is the observed ellipticity (degrees), d is the path length (cm) and c is the concentration (g/L).

From the CD spectra, the 'positive-negative ratio' (RPN) was calculated, using Equation 3.6:

$$RPN = \frac{\theta_p}{\theta_n} \qquad (3.6)$$

Where θ_p and θ_n are the positive and negative peaks, respectively.

3.2.4.6. Water Contact Angle (WCA)

Surface wettability and hydrophobicity were assessed by water contact angle (WCA) measurements using a Drop Shape Analyser (Krüss, Germany) (Figure 3.14).

Figure 3.14. Drop Shape Analyser (Krüss)

The WCA was measured using the sessile drop method (droplets with an approximate volume of 5 μL). Both WCA values of the right (defined as *y* in Figure 3.15) and left (defined as *x* in Figure 3.15) sides of the deionized water droplets were measured and the average value was calculated as it can be seen schematically in Figure 3.15.

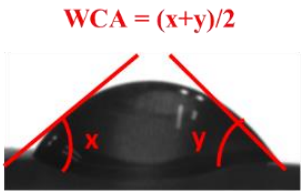

Figure 3.15. Illustration about the calculation of the water contact angle (WCA)

3.2.5. Statistical analysis

At least three replicates were carried out for each measurement. Student´s t-test and one-way analysis of variance ($p<0.05$) were performed using PASW Statistics for Windows (Version 18: SPSS, Chicago, IL). Standard deviations were calculated for selected parameters.

3.3 Results and Discussion

3.3.1. Evaluation of the freeze-drying processing parameters

This study is divided into three different sections according to the different variables considered: 3.3.1.1) effect of the container (type); 3.3.1.2) the processing conditions (pH and freezing temperature); and 3.3.1.3) solvent (type and concentration). Sponge-like scaffolds produced with gelatin (1 wt.%) were used to evaluate the different parameters obtaining them using the reference protocol (P1).

3.3.1.1. Effect of the type of container

Figure 3.16 shows the evolution of E' and E'' values with frequency obtained for the systems elaborated using two different containers (glass and plastic). Both systems show a similar profile with a slight increase of both E' and E'' with frequency. In all the systems studied (in this section and the following sections of this chapter), E' values are above E'' values highlighting the solid character of these systems.

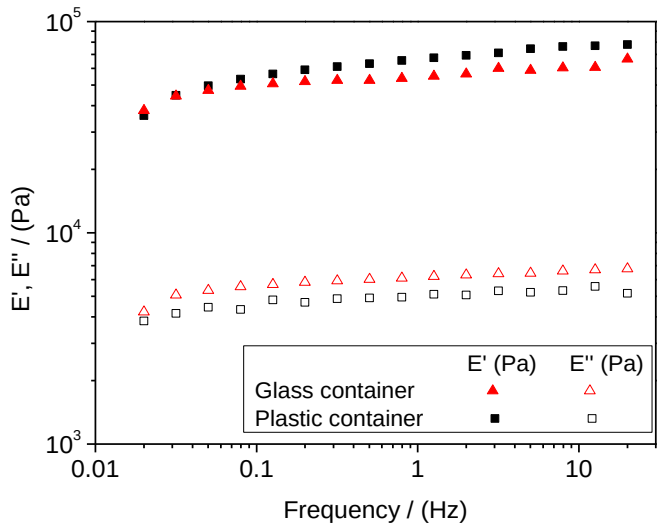

Figure 3.16. Frequency sweep tests of the scaffolds obtained with different containers (glass container and plastic container). An image of the drop formed is also included for each material

In addition, Table 3.2 shows the values of E'_1 and tan (δ_1) for both systems. Although the E'_1 values showed no significant differences ($p<0.05$), the mechanical properties obtained from the system produced with a plastic container can be highlighted, since these scaffolds presented much lower values of tan (δ), revealing a more structuring material than the one obtained with the glass container.

Table 3.2. Porosity (ε), E' and tan (δ) values at 1 Hz (E'_1 and tan (δ_1)) of gelatin scaffolds obtained with different containers (glass and plastic). Values with different letters are significantly different ($p<0.05$)

Scaffolds		E'_1 (kPa)	tan (δ_1)	ε (%)
Container	Glass	64.7 ^{a}	0.135 ^{A}	98.4 $^{\alpha}$
	Plastic	61.6 ^{a}	0.070 ^{B}	98.3 $^{\alpha}$

In addition to the elastic and viscous moduli, the influence of the container on the critical strain was also evaluated (shown in Figure 3.17), with the system made using a plastic container presenting the highest value. Eventually, the porosity of the samples was also studied. No significant differences were found ($p<0.05$) among them, which had in all cases a value above 98% (Table 3.2).

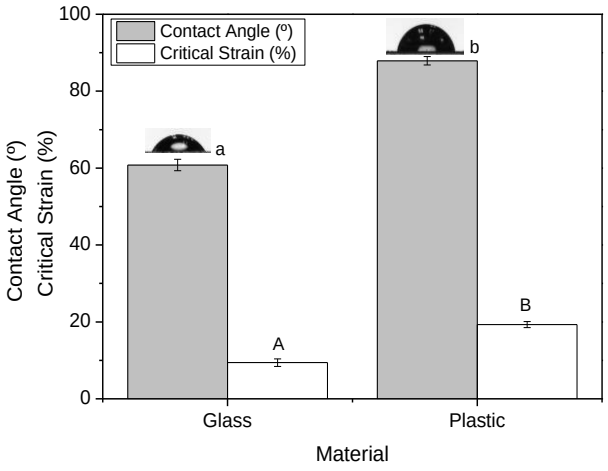

Figure 3.17. Water contact angle and critical strain of the scaffolds obtained with different containers (glass container and plastic container). An image of the drop formed is also included for each material

Furthermore, the hydrophobicity of the two study materials (glass and plastic) was analyzed. Figure 3.17 shows the analysis of the water contact angle, corroborating that the glass container is more hydrophilic since it presented a lower value of the contact angle. In view of these results, and according to Schwarzenbach et al. (2002), the freeze-drying process will be carried out with greater effectiveness in the plastic container, which has a lower affinity for the solvent (water) than the glass container.

3.3.1.2. Effect of the processing conditions: pH

The effect of pH on the mechanical properties of the scaffolds can also be observed in Figure 3.18, which shows the evolution of E' with frequency (Figure 3.18A) and the critical strain (Figure 3.18B). The pH traditionally used to make scaffolds by freeze-drying was 3.2 (O'Brien et al., 2004a), which is corroborated by these results, where the best properties were obtained for those systems elaborated at pH 3.0 and 3.2. This can be also deduced from the results shown in Table 3.3. All the values of tan (δ_1) correspond to an elastic gel network, ranging from 0.04 to 0.07, except for the system at pH 5.5 that shows a tan (δ_1) higher than 1. This system does not follow a gel behavior.

Table 3.3. Porosity (ε), E' and tan (δ) values at 1 Hz (E'$_1$ and tan (δ_1)) of gelatin scaffolds obtained with different pH values (2.5, 3.0, 3.2, 3.5, 4.0, 5.5). Values with different letters are significantly different ($p<0.05$)

Scaffolds		E'$_1$ (kPa)	tan (δ_1)	ε (%)
pH	2.5	34.8 ^{a}	0.036 ^{A}	96.2 $^{\alpha}$
	3.0	69.9 ^{b}	0.041 ^{A}	97.0 $^{\beta}$
	3.2	61.6 ^{b}	0.070 ^{B}	98.3 $^{\gamma}$
	3.5	41.0 ^{a}	0.056 ^{C}	97.2 $^{\beta}$
	4.0	36.2 ^{a}	0.039 ^{A}	96.4 $^{\alpha}$
	5.5	30.0 ^{a}	1.650 ^{D}	95.8 $^{\alpha}$

Interestingly, the further the pH values were from this optimal point, the lower the mechanical properties obtained were (E' values and critical strain). In addition to the mechanical properties, the structural properties (porosity) were also better for the system elaborated at pH 3.2, decreasing as moving away from that pH value.

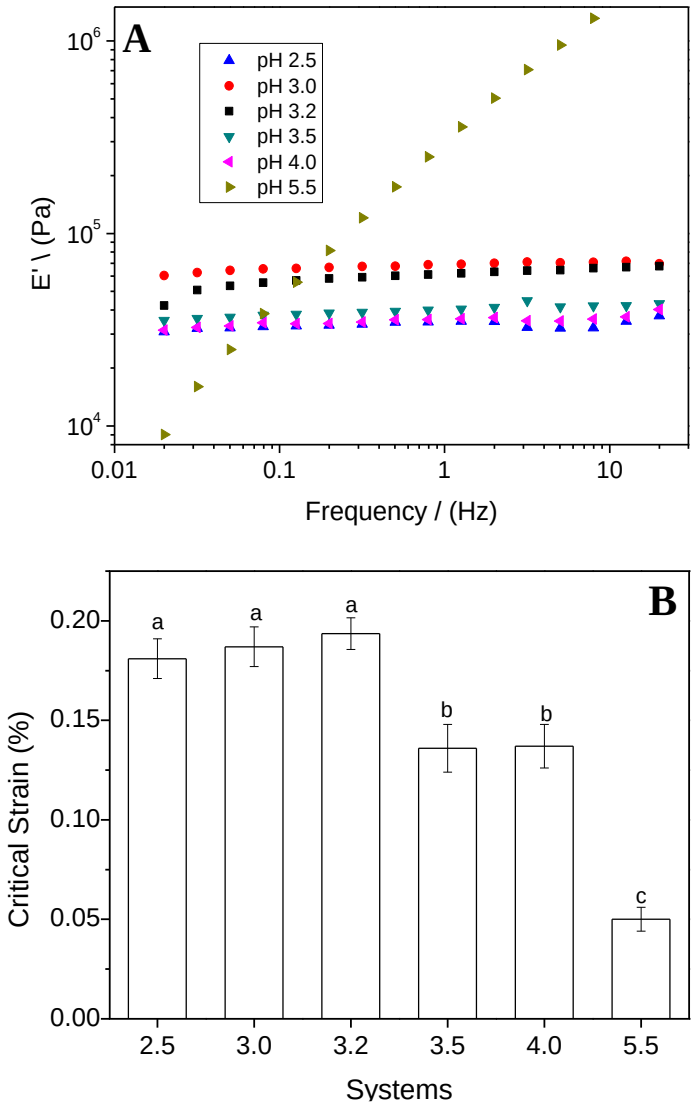

Figure 3.18. (A) Frequency sweep tests and (B) critical strain of the scaffolds obtained with different pH (2.5, 3.0, 3.2, 3.5, 4.0 and 5.5). Values with different letters are significantly different (p<0.05)

The use of a pH value that coincided with the isoelectric point of the protein produced its stabilization by the interaction of complementary charges; however, this caused the aggregation of the protein due to these complementary interactions when it is in its zwitterionic form (Ju and Kilara, 1998). In fact, this aggregation influenced the protein interaction with the solvent, thus worsening its processing. However, working at a pH value lower than its isoelectric point, the protein was positively charged, which provided an even greater stabilization by positive repulsion, according to the studies of Russell (Russell, 1974). This stabilization was especially noticeable when working with gelatin at a pH slightly lower than 3.5. On the other hand, working at a pH higher than the isoelectric point of the protein, found around pH 5.0 (Perez-Puyana et al., 2016), caused the protein to be negatively charged in solution, thus decreasing its stability and, therefore, worsening its processing and decreasing the properties of the obtained scaffolds.

3.3.1.3. Effect of the processing conditions: Freezing temperature

The freezing temperature and heat flow during the cooling prior to the freeze-drying is crucial for the protein matrix in order to obtain specific and suitable properties, such as a certain pore size, which is higher when the heat flow is lower (O'Brien et al., 2004a). For that reason, the scaffolds processed at four different freezing temperatures were also studied (-9, -20, -40 and -80 ºC).

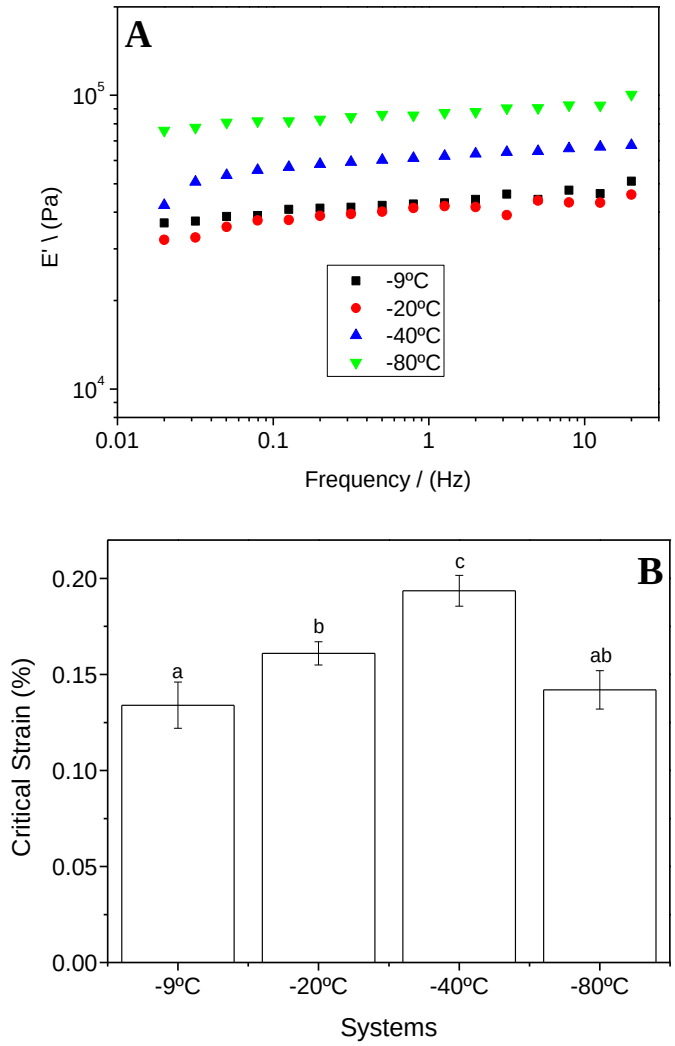

Figure 3.19. (A) Frequency sweep tests and (B) critical strain of the scaffolds obtained with different freezing temperatures (-9, -20, -40 and -80 ºC). Values with different letters are significantly different (p<0.05)

Furthermore, the selection of the freezing temperature affected the crystallinity of the material. In this sense, Ramkumar and Bhattacharya (1997) determined that a treatment at lower temperature increases the crystallinity of the material, decreasing the freedom of movement of the polymer chains and, thus, increasing the rigidity of the material. This behavior agreed with the values of E', shown both in Table 3.4, and in

the profiles of Figure 3.19 which reflect how the freezing treatment of the solutions at lower temperatures gave rise to a more structured system that presents better mechanical properties, according to the studies carried out by Reys et al. (2017).

Table 3.4. Porosity (ε), E' and tan (δ) values at 1 Hz (E'$_1$ and tan (δ$_1$)) of gelatin scaffolds obtained with different freezing temperatures (-9, -20, -40 and -80 ºC). Values with different letters are significantly different (p<0.05)

Scaffolds		E'$_1$ (kPa)	tan (δ$_1$)	ε (%)
Freezing Temperature	-9ºC	42.7 ^{a}	0.037 ^{A}	95.8 $^{\alpha}$
	-20ºC	41.7 ^{ab}	0.067 ^{B}	97.5 $^{\beta}$
	-40ºC	61.6 ^{b}	0.070 ^{B}	98.3 $^{\gamma}$
	-80ºC	86.6 ^{c}	0.050 ^{C}	94.8 $^{\delta}$

However, according to the results shown in Figure 3.19B, the critical strain increased with a decrease in the freezing temperature, with the system elaborated at -40 °C having the highest critical strain. A similar effect took place with the porosity, since although all the systems have a porosity higher than 95 %, the treatment at lower temperature produced systems with higher porosity (reaching the maximum for the system at -40 ºC).

3.3.1.4. Effect of the solvent

The protein solution which finally yielded the scaffold was prepared using an aqueous acidic solution at low concentration (0.05 M) and the pH value at which the best scaffolds were achieved in the previous section (pH 3.2). In order to determine the influence of the solvent in the freeze-drying process, three different acids were analyzed: a strong acid (hydrochloric acid, HCl), a weak monoprotic acid (acetic acid, CH_3COOH) and a weak polyprotic acid (ortho-phosphoric acid, H_3PO_4). It is important to take into account that strong acids are completely dissociated in solution, whereas in the case of weak acids it depends on

their pKa. Considering the three acids studied and the working pH, acetic acid was not dissociated (it has a pKa value of 4.8), while phosphoric acid was partially dissociated when it was found at a pH higher than one of its pKa values (2.1, 7.2 and 12.3) (Housecroft and Sharpe, 2008).

Figure 3.20 shows the mechanical properties measured for the scaffolds produced with the three different acids. Figure 3.20A illustrates the behaviour of E' as a function of frequency. As can be observed, the use of a weak monoprotic acid (acetic acid, CH_3COOH) produced a system with higher E' values and, therefore, better mechanical properties, followed by the system made with phosphoric acid (H_3PO_4) and finally the scaffold produced with hydrochloric acid (HCl). This sequence is also observed in Table 3.5 for E'_1, which also shows how the values of tan (δ_1) are always lower than 0.1.

Table 3.5. Porosity (ε), E' and tan (δ) values at 1 Hz (E'_1 and tan (δ_1)) of gelatin scaffolds obtained with different acids (hydrochloric acid, HCl; acetic acid, CH_3COOH; phosphoric acid, H_3PO_4). Values with different letters are significantly different ($p<0.05$)

Scaffolds		E'_1 (kPa)	tan (δ_1)	ε (%)
Solvent	$HCl_{(0.05M)}$	14.8 ^{a}	0.047 ^{A}	98.7 $^{\alpha}$
	$H_3PO_{4(0.05M)}$	36.7 ^{b}	0.116 ^{B}	98.2 $^{\alpha}$
	$CH_3COOH_{(0.05M)}$	61.6 ^{c}	0.070 ^{C}	98.3 $^{\alpha}$

A similar effect was observed with the critical strain (Figure 3.20B), whose highest value was obtained in the scaffold made with acetic acid. However, no significant differences were observed in porosity (over 98%), which was slightly higher for the system prepared with HCl. In view of these results, the dissociation of the acid caused an interaction with the protein that hindered the processing, thus generating scaffolds with worse properties.

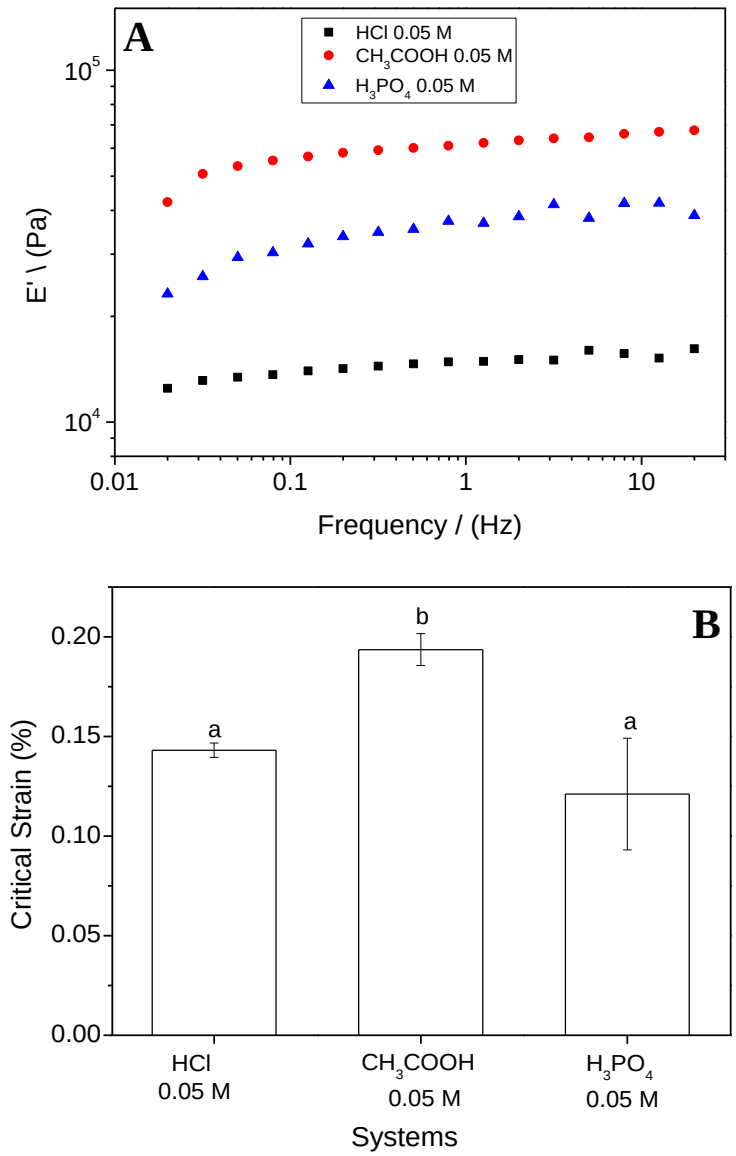

Figure 3.20. (A) Frequency sweep tests and (B) critical strain of the scaffolds obtained with different acids (hydrochloric acid, HCl; acetic acid, CH_3COOH; phosphoric acid, H_3PO_4). Values with different letters are significantly different ($p<0.05$)

In addition to the type of acid used in the preparation of protein solutions, the concentration of acid used could influence the protein structures. Therefore, taking CH_3COOH as a reference, three different concentrations were studied (0.05, 0.10 and 0.30 M) at pH 3.2. Figure

3.21A shows the evolution of E' with frequency, where all systems followed the same evolution, among which the system prepared at 0.05 M had significantly better mechanical properties with respect to the others (higher values of E' and critical strain) (Figures 3.21A and 3.21B).

Table 3.6. Porosity (ε), E' and tan (δ) values at 1 Hz (E'$_1$ and tan (δ_1)) of gelatin scaffolds obtained with solutions at different acetic acid (CH_3COOH) concentration (0.05, 0.10 and 0.30 M). Values with different letters are significantly different (p<0.05)

Scaffolds		$E'_{1Hz} \cdot 10^4$ (Pa)	tan (δ_1)	ε (%)
Solvent	$CH_3COOH_{(0.05M)}$	61.6 ^{a}	0.070 ^{A}	98.3 $^{\alpha}$
	$CH_3COOH_{(0.10M)}$	20.9 ^{b}	0.071 ^{AB}	98.4 $^{\alpha}$
	$CH_3COOH_{(0.30M)}$	19.7 ^{b}	0.056 ^{B}	98.4 $^{\alpha}$

However, no significant differences (p<0.05) in the porosity of these systems were observed. In addition, all systems had a tan (δ_1) value lower than 0.10 (Table 3.6), which demonstrated the marked elastic character of these scaffolds.

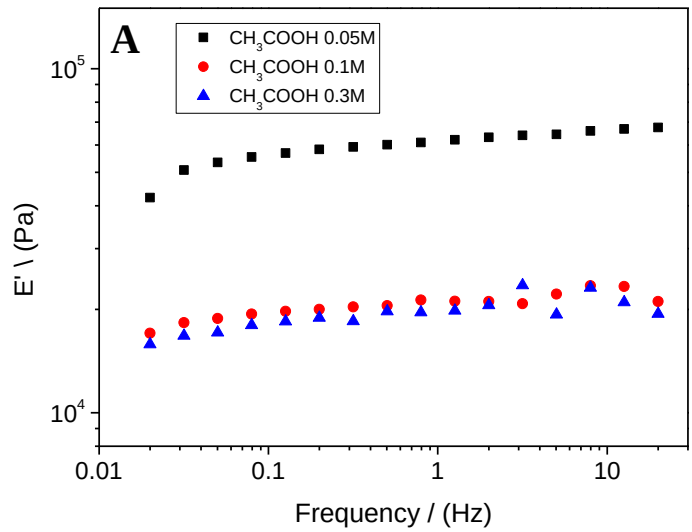

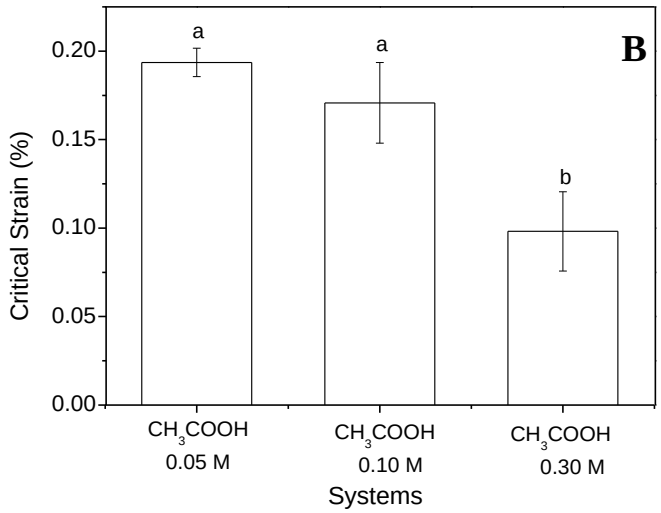

Figure 3.21. (A) Frequency sweep tests and (B) critical strain of the scaffolds obtained with solutions at different acetic acid (CH_3COOH) concentration (0.05, 0.10 and 0.30 M). Columns with different letters are significantly different ($p<0.05$)

The influence of the acid concentration in proteins during the preparation of the protein solutions was also determined by measuring circular dichroism (Figure 3.22).

According to Gopinath et al. (2017), there is a relationship between the maximum (positive) and minimum (negative) peaks with the denaturation of the protein (RPN). It should be noted that a higher ratio implies a more denatured protein, although the values obtained were similar for both concentrations (for the highest concentration, 0.30 M, it could not be measured). In that case, it is necessary to look at the profiles, since a less pronounced negative peak also corresponds to a higher denaturation (Gopinath et al., 2017).

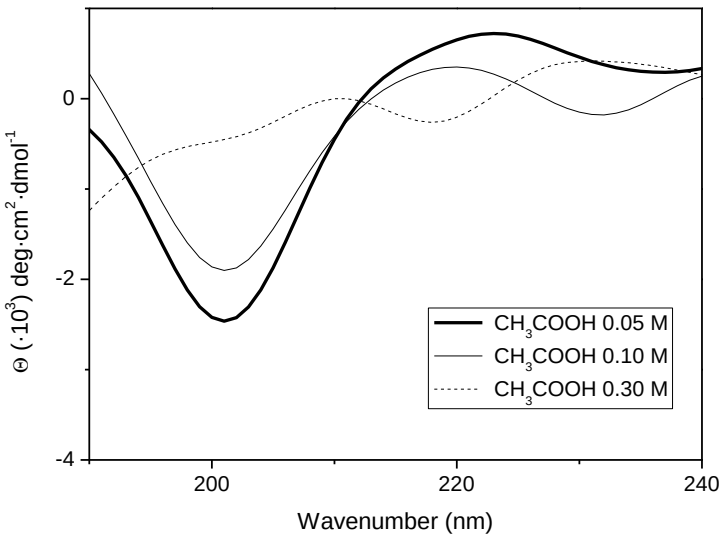

Figure 3.22. CD spectra of the gelatin solutions at different acetic acid concentration (0.05, 0.10 and 0.30 M)

In our case, denaturation implied aggregation, thus a concentration of 0.05 M caused a lower protein aggregation when presenting a more negative peak (more pronounced) and, therefore, improving the processing of scaffolds. Furthermore, and according to Yang et al. (2016), the acetic acid concentration influenced the conformation of collagen, which was more significant at 0.30 M; at this concentration, the typical profile for collagen/gelatin was lost.

3.3.1.5. Processing conditions selected

The following studies were carried out by producing scaffolds using the parameters chosen as references since they were those with which the best properties were obtained (plastic, -40ºC, pH 3.2 and acetic acid 0.05 M).

3.3.2. Study of the effect of the protein concentration

On previous studies, it has been shown that producing scaffolds with a protein (either CG or GE) concentration higher than 1 wt.% led to structures with a significant decrease in both critical strain and porosity, which could drive to a worse neovascularization (Perez-Puyana et al., 2016). Thus, scaffolds with 0.5 and 1.0 wt.% were processed and compared to select the most suitable polymer concentration.

Rheological characterization

Figure 3.23 shows the mechanical parameters of the systems with different concentration of collagen and gelatin.

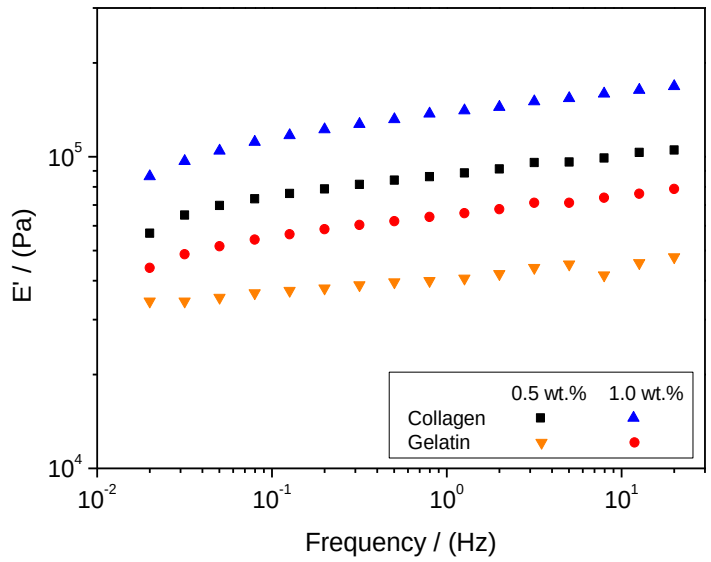

Figure 3.23. Frequency sweep tests carried out for gelatin and collagen-based scaffolds at different protein concentrations (0.5 and 1.0 wt.%)

Figure 3.23 shows the values of the elastic component (E') of the collagen- and gelatin-based systems in a frequency range. Both systems show a similar trend: an increase in protein concentration led to an improvement of the mechanical (higher E' values) properties.

Comparing the different proteins, the structures produced with collagen exhibited higher values compared to the ones obtained with gelatin, regardless of the concentration used.

Table 3.7. E' and tan (δ) values at 1 (E'$_1$ and tan (δ_1)) and porosity (ε) of gelatin and collagen-based scaffolds with different protein concentrations (0.5 and 1.0 wt.%). Values with different letters are significantly different (p<0.05)

SYSTEMS		E'$_1$ (kPa)	tan (δ_1)	ε (%)
Gelatin scaffolds	0.5 wt.%	41.2 ^{a}	0.06 ^{A}	99.5 $^{\alpha}$
	1.0 wt.%	65.2 ^{b}	0.09 ^{B}	98.5 $^{\beta}$
Collagen scaffolds	0.5 wt.%	88.3 ^{c}	0.09 ^{B}	99.3 $^{\alpha}$
	1.0 wt.%	134.1 ^{d}	0.11 ^{B}	98.8 $^{\beta}$

In addition, the E' and tan (δ) values of the previous tests at 1 Hz (E'$_1$ and tan (δ_1)), shown in Table 3.7, allowed comparing the systems to determine whether there were significant differences between them. Interestingly, the values of tan (δ_1) were less than or equal to 0.1 for all the systems studied, which means that the elastic values (E') were much higher than the viscous values (E''), highlighting their elastic behavior. Comparing the data exhibited by the different systems in Table 3.7, the E'$_1$ values increased with the polymer content, whereas the tan (δ_1) values showed no significant differences ($p<0.05$). As it was demonstrated in Table 3.7, the collagen-based systems have greater E'$_1$ values than those with gelatin.

The study of the critical strain of the protein-based sponges is very interesting, since it is related to an increase in the elastomeric character and, considering a possible biomedical application, a better working performance in the bioreactor, where the samples are subjected to a continuous strain along time to favor cell growth (Lin, Hsu, Huang, Cheng, & Su, 2009). The critical strain of the different systems can also be seen in Figure 3.24.

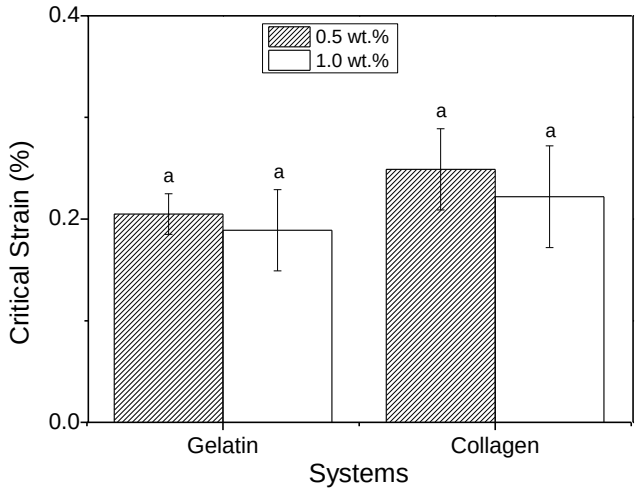

Figure 3.24. Critical strain values for gelatin and collagen-based scaffolds at different protein concentrations (0.5 and 1.0 wt.%). Columns with different letters are significantly different (p<0.05)

There were no significant differences ($p<0.05$) between the systems presenting values in the range of ca. 0.2 % although the critical strain was slightly lower when the protein content was higher.

Microstructural characterization

Table 3.7 also shows the porosity values (ε) obtained for the different systems studied (gelatin or collagen-based scaffolds at 0.5 and 1.0 wt.%). As can be observed, an increase in protein concentration led to a decrease in the porosity values, reaching its maximum with the system produced at 0.5 wt.% gelatin. In general, the porosity values are in the range between 95 and 99 %, similar than the ones obtained in other studies (Lv and Feng, 2006). It is worth mentioning that the values shown in Table 3.7 are around the upper limit of this range.

Figure 3.25 shows the macroscopic images of the systems produced. It can be seen how all the systems present white sponge-like scaffolds with a well-defined and compacted shape when the concentration of

biopolymer is 1% (Figures 3.25B and 3.25D), compared to the systems obtained at 0.5% (Figures 3.25A and 3.25C).

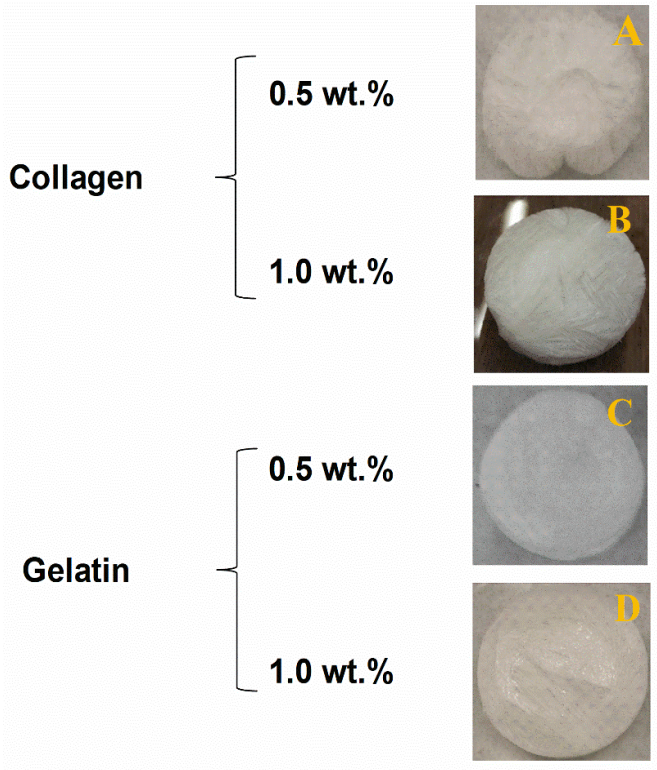

Figure 3.25. Macroscopic images of the scaffolds obtained from collagen and gelatin with different protein composition (wt. %): (A) 0.5 % Collagen, (B) 1.0 % Collagen, (C) 0.5% Gelatin and (D) 1.0% Gelatin

On the other hand, Figure 3.26 shows the SEM images of these sponge-like materials produced. As can be noted, an increase in protein concentration led to a more compacted structure. Considering the SEM images, although the porosity is similar for all the systems, a decrease in the protein concentration produced structures with a latticework with a more marked porosity.

On these grounds, the collagen-based system with a 1% of total biopolymer content can be highlighted taking into account the different properties obtained for the four systems analyzed. Particular attention

has been paid to the elastic properties of the scaffolds since the porosity is, in any case, at the upper limit suggested in the literature. Therefore, this system was selected for the further studies carried out.

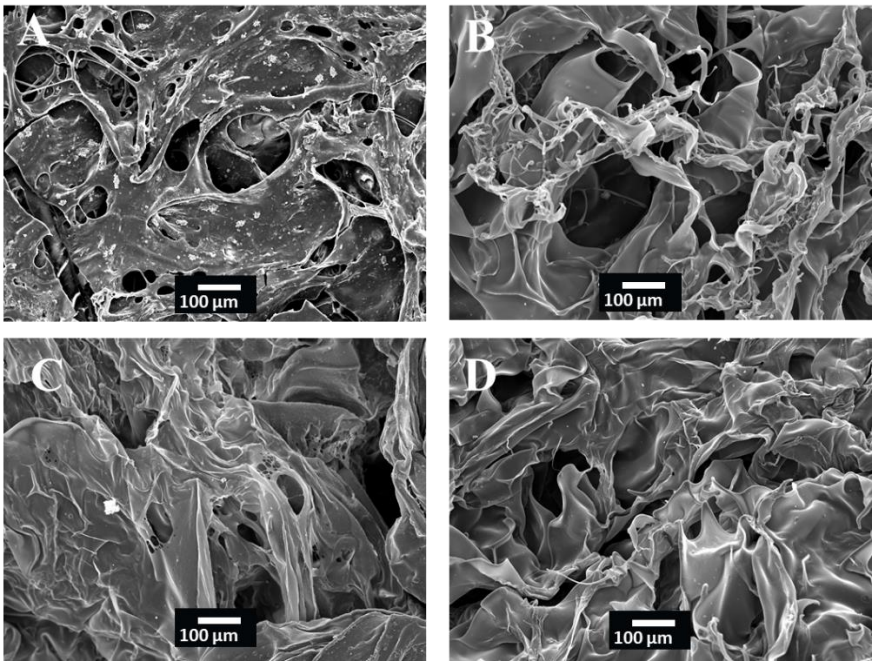

Figure 3.26. SEM images of the microstructure of the scaffolds obtained from collagen and gelatin with different protein composition (wt. %): (A) 0.5 % Collagen, (B) 1.0 % Collagen, (C) 0.5% Gelatin and (D) 1.0% Gelatin

3.3.3. Influence of the addition of chitosan

The properties of materials can be tuned with the combination of different polymers. In this way, mixtures of collagen with chitosan were studied by producing and comparing binary scaffolds. For this study, different ratios (100-0; 75-25; 50-50; 25-75; 0-100) of collagen and chitosan were used at 1% (weight/volume) of the biopolymer material content in the solution, studying the rheological and microstructural properties of the different scaffolds obtained.

Rheological characterization

Figure 3.27 shows the rheological properties of the scaffolds processed with different ratios of CG-CH (100-0; 75-25; 50-50; 25-75; 0-100). Figure 3.27A shows the values of the elastic (E') moduli against the frequency range studied. As can be seen, E' values have a slight dependence on the frequency used, which is related to very stable gel structures over time. This behavior has already been observed in sponge-like scaffolds made only from either collagen or gelatin studied in the previous section. It is interesting to start mentioning that CH provides higher strength to the scaffold than CG, as may be inferred from Figure 3.27.

Figure 3.27B shows the elastic modulus and the loss tangent at a frequency of 1 Hz (E'_1 and tan (δ_1), respectively) in order to compare the different binary systems between them. As may be observed, adding CH to CG scaffolds does not initially improve E' but improves tan (δ). On the other hand, adding CG to CH scaffolds does not improve significantly either E' or tan (δ).

However, the system that contained a 50-50 ratio of CG-CH, presented a significant maximum in E'_1, which made it the system with the best mechanical properties of this study, and it requires the creation of a

synergistic structure with this CG-CH ratio. This behavior may be due to the different typology of the fibers used (CG and CH), which allows introducing one of them in the holes left by the other structure, thus favoring their rheological characteristics.

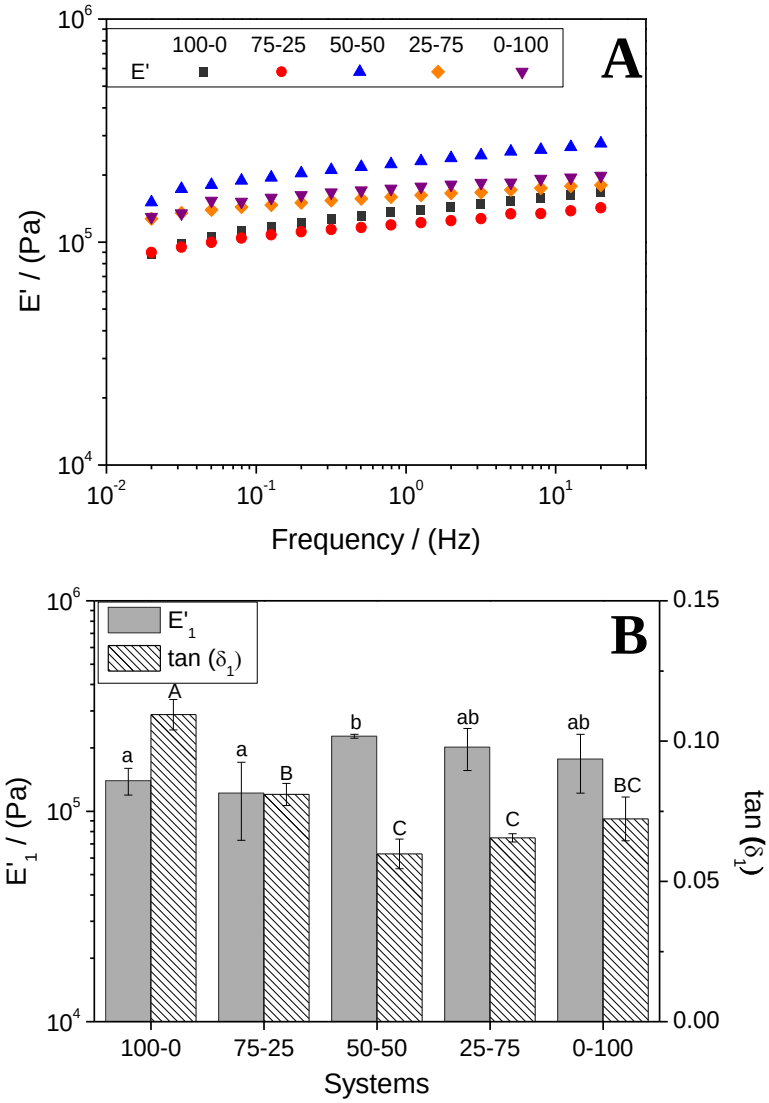

Figure 3.27. (A) Frequency sweep tests and (B) E'₁ and tan (δ₁) values for scaffolds produced with a different collagen-chitosan ratio (100-0, 75-25, 50-50, 25-75 and 0-100). Columns with different letters are significantly different (p<0.05)

Regarding the loss tangent, tan (δ_1), observed in Figure 3.27B, all the values obtained are lower than 0.15, which highlights the predominantly solid character of the systems, as mentioned above.

On the other hand, critical strain values have been summarized in Table 3.8. Considering the values obtained for the collagen-chitosan binary systems, it can be concluded that the elaboration of binary systems, where one of the fibers is predominant, produces higher critical strain values compared to those obtained for the unitary systems. However, when both fibers were in equal proportion, there were no significant differences in critical strain with the unitary systems.

Table 3.8. Critical strain values of scaffolds produced with collagen (CG) and chitosan (CH) with different ratios (100-0, 75-25, 50-50, 25-75, 0-100). Values with different letters are significantly different (p<0.05)

SYSTEMS		Critical Strain (%)
CG-CH scaffolds	100-0	0.22 [a]
	75-25	0.47 [b]
	50-50	0.21 [a]
	25-75	0.34 [c]
	0-100	0.16 [d]

Microstructural characterization

Apart from the mechanical properties, the microstructure of the scaffolds was also characterized. Figure 3.28 shows the microstructural properties of the different scaffolds studied. Figures 3.28A, 3.28A' and 3.28A'' show that the incorporation of CH confers a yellowish color to the scaffolds.

Concerning the images shown (Figures 3.28B, 3.28B' and 3.28B''), the unitary systems (CG-CH 100-0 and 0-100, Figures 3.28B and 3.28B'', respectively) had a laminated structure, in which the pores seemed to be mainly formed by the spaces between its various sheets or piles.

However, the binary system CG-CH 50-50 (Figure 3.28B') showed greater pore formation, which was evident even in the sheets. This fact may contribute to explain the formation of a synergistic structure in the CG-CH 50-50 scaffold, thus explaining the best mechanical properties observed in Figure 3.27.

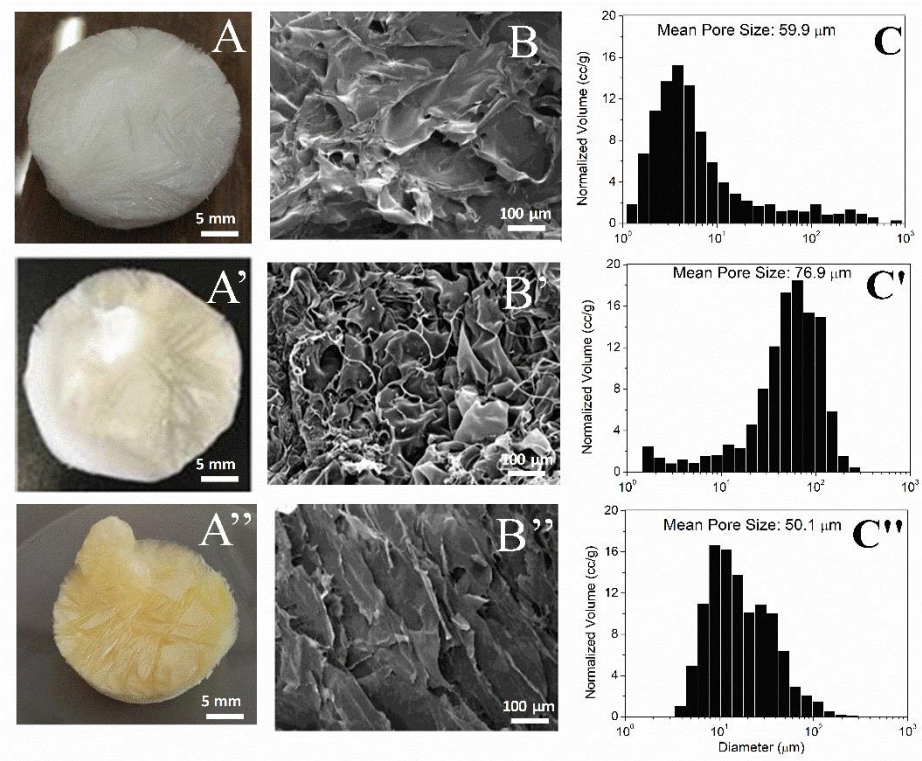

Figure 3.28. Macroscopic, microscopic and pore size distribution of scaffolds produced with a different collagen-chitosan ratio: 100-0 (A, B and C), 50-50 (A', B' and C') and 0-100 (A'', B'' and C''). The mean pore size of the systems was also included

On the other hand, Figure 3.28C, 3.28C' and 3.28C'' show the pore distribution obtained in the porosimetry measurements. All the systems had a roughly unimodal distribution; however, the CG-based scaffold shows larger pore size than the CH-based one. Nevertheless, the CG-CH 50-50 system showed a clear shift in the maximum toward larger pore size values, possibly due to the greater number of large pores found with

respect to the unitary systems, with this being the most heterogeneous system. Thus, the mean pore size was greater in the case of CG-CH 50-50 (87.1 µm) than in the unit systems (CG-CH 100-0: 59.9 µm and 0-100: 50.1 µm). These pores with heterogeneous distribution would be positive for cell incorporation adhesion and growth. These results reinforce the idea of selecting the 50-50 system as the most promising combination for producing hybrid CG-CH scaffolds.

3.3.4. Influence of the addition of a reinforcement stage

First, the influence of the addition of glutaraldehyde on the selected system from the previous section (1 wt.% CG-CH 50-50) was carried out. Then, three possible methods have been evaluated to look for suitable alternatives. The same system without any crosslinking method has been considered as reference (Ref.).

3.3.4.1. Traditional chemical crosslinking: Addition of Glutaraldehyde (GA)

Figure 3.29 shows the mechanical properties for the CG-CH 50-50 systems with different percentages of GA (0.03, 0.05 and 0.10% w/v with respect to the solution prepared).

Figure 3.29A presents the evolution of the elastic (E') moduli in the frequency range studied. As can be observed, all the systems showed only a slight dependence on frequency, a trend that was already observed in the systems without the crosslinking. Moreover, the incorporation of the crosslinking agent reduces the values of E', which can also be observed in the values of the elastic modulus at 1 Hz (E'_1) in Figure 3.29B, with a remarkably significant difference between the systems with and without the crosslinking agent.

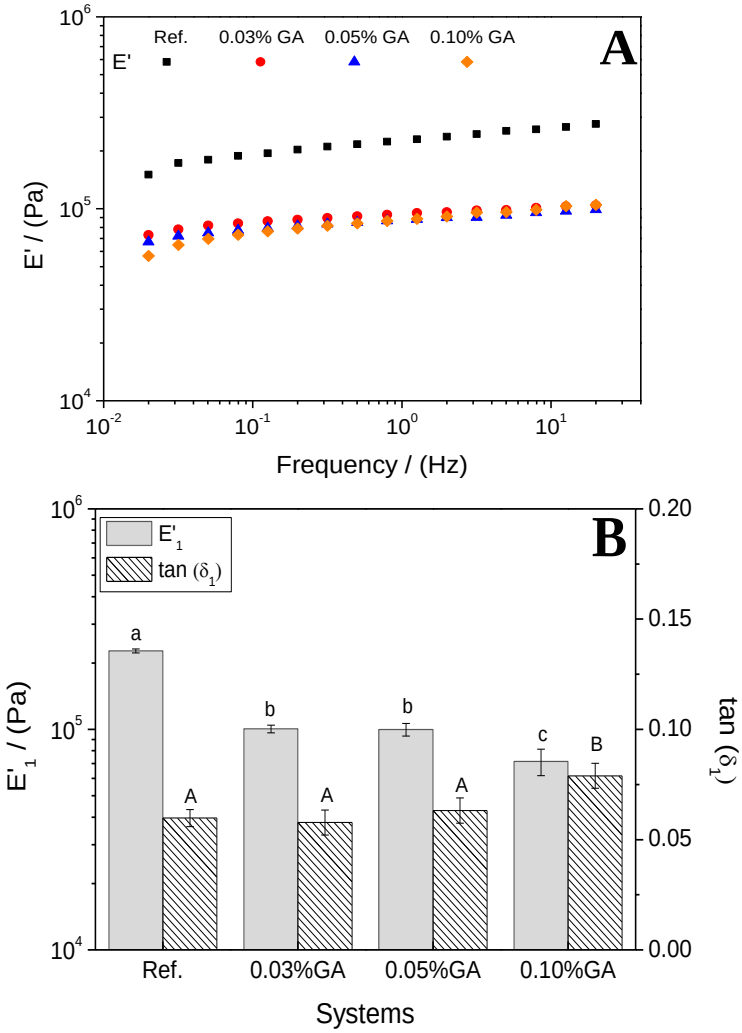

Figure 3.29. (A) Frequency sweep tests and (B) E'₁ and tan (δ₁) values for hybrid CG-CH 50-50 scaffolds produced with GA crosslinking at different concentrations (0.03, 0.05 and 0.10 % w/v). The CG-CH 50-50 system without crosslinking has also been included as reference (Ref.). Values with different letters are significantly different (p<0.05)

Regarding the critical strain of these systems (Table 3.9), the incorporation of a crosslinking agent increased it, being more noticeable at low concentrations of GA (0.03 and 0.05% w/v), which made these scaffolds more deformable. Interestingly, the addition of glutaraldehyde in a higher concentration (0.10% w/v) produced a decrease in the critical strain, which indicates that the use of crosslinking agent in a certain

concentration (higher than the optimal value) is not advisable to improve the properties of the scaffolds.

Table 3.9. Critical strain values for hybrid CG-CH 50-50 scaffolds produced with GA crosslinking at different concentrations (0.03, 0.05 and 0.10 % w/v). The CG-CH 50-50 system without crosslinking has also been included as reference (Ref.). Values with different letters are significantly different (p<0.05)

SYSTEMS	Critical Strain (%)
Reference	0.22 [a]
0.03% GA	0.64 [b]
0.05% GA	0.61 [b]
0.10% GA	0.35 [c]

3.3.4.2. Alternative crosslinking methods: Genipin, heat treatment and transglutaminase

From the studies shown in Section 3.3.4.1, a glutaraldehyde concentration of 0.05 % w/v has been selected as the most suitable for the CG-CH 50-50 system. However, due to the toxicity of glutaraldehyde, other possible alternatives have been considered. Therefore, three different alternatives have been studied: a chemical crosslinking with the addition of genipin, a physical crosslinking with a heating treatment of the scaffolds and an enzymatic crosslinking with the addition of transglutaminase to the initial formulation. The properties of the scaffolds after performing these three crosslinking methods were compared to the glutaraldehyde selected in the previous section. Furthermore, a CG-CH 50-50 sponge-like scaffold without any crosslinking was also included as reference (Ref.).

It is important to take into account that the concentrations for genipin (0.03 wt.%) and transglutaminase (0.10% w/v) have been selected according to previous studies (Dimida et al., 2017; Orban et al., 2004).

Rheological characterization

Figure 3.30 shows the mechanical properties of the different scaffolds studied with crosslinking (GA, GN, heat treatment and TG). Figure 3.30A presents the evolution of the elastic (E') moduli in the frequency range studied for the CG-CH 50-50 systems after performing different crosslinking methods: addition of GA (0.05 % w/v), GN (0.03 % w/v), TG (0.10 % w/v) or the inclusion of a heat treatment (HT, at 50 ºC for 2 h).

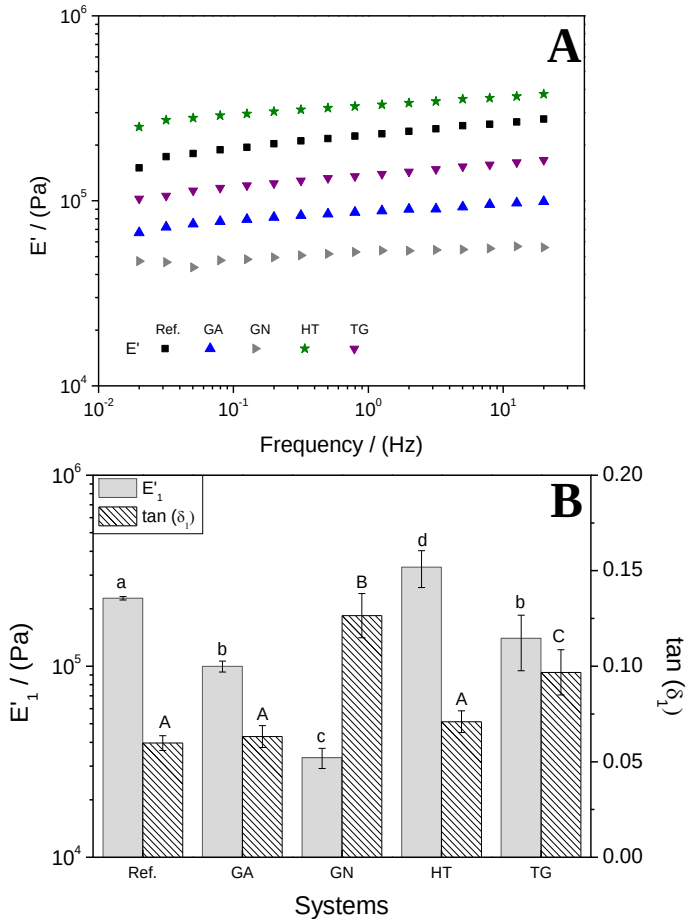

Figure 3.30. (A) Frequency sweep tests and (B) values of E'₁ and tan (δ₁) of hybrid CG-CH 50-50 scaffolds crosslinked by different methods: Glutaraldehyde [GA] addition, genipin [GN] addition, heat treatment [HT] and transglutaminase [TG] addition. The CG-CH 50-50 system without crosslinking has also been included as reference (Ref.). Values with different letters are significantly different (p<0.05)

Once again, all the systems showed only a slight dependence on frequency, a trend that was already observed in the systems without the crosslinking (Ref). Moreover, the incorporation of the crosslinking agents reduces the values of E', which can also be observed in the values of the elastic modulus at 1 Hz (E'_1) in Figure 3.30B, with a remarkably significant difference between the systems with and without any of the crosslinking agent used. However, the application of a heat treatment as a crosslinking method increases significantly the values of E', which can be seen in both Figure 3.30A and 3.30B. On the other hand, there are no great significant differences in the values of the loss tangent at 1 Hz [tan (δ_1)] of the studied systems, which indicates that the relationship between the elastic and viscous moduli was not lost by the application of a crosslinking to the scaffolds.

Table 3.10. Critical Strain (%) of scaffolds prepared with different crosslinking (GA: glutaraldehyde, GN: genipin, HT: heat treatment and TG: transglutaminase). The CG-CH 50-50 system without crosslinking has also been included as reference. Values with different letters are significantly different (p<0.05)

SYSTEMS	Critical Strain (%)
CG-CH (reference)	0.22 ^{a}
GA	0.61 ^{b}
GN	0.51 ^{bc}
HT	0.20 ^{a}
TG	0.47 ^{c}

Regarding the critical strain of these systems (Table 3.10), the incorporation of TG or GN produced a decrease in the critical strain compared to the GA, although they were still larger than the reference system. This fact made these scaffolds more deformable and, consequently, more viable for the growth of cells in them as they better stood the periodic strains caused by this growth. On the other hand, the

application of a heat treatment caused the critical strain to decrease below the reference value, although without significant differences.

Comparing the crosslinking methods, the scaffolds produced using GA and TG had values of elastic modulus and loss tangent similar to each other, with no significant differences between them. However, the scaffolds produced with GN presented lower E' values and higher tan (δ) respect to the others. On the other hand, critical strain values found in the systems with GA were greater than those obtained with TG, but no significantly different to the critical strain obtained for the system with GN. In addition, the heat treatment although increases the elastic modulus (E') of the scaffolds does not improve its capacity of deformation, making its values not suitable for its later implantation in the bioreactor.

Microstructural properties

Figure 3.31 shows the microstructural properties of the scaffolds obtained with different crosslinking (GA, GN, heat treatment and TG). The scaffold with the same proportion of biopolymer, but without the addition of a crosslinking agent, was used as reference.

At the macroscopic level (Figures 3.31A', 3.31A*, 3.31A**, 3.31A*** and 3.31A****), the scaffolds present a slight change in its color, becoming more yellow when the crosslinking occurs. Particularly interesting is the bluish color of the system with GN.

Respecting the micrographs (Figures 3.31B', 3.31B*, 3.31B**, 3.31B*** and 3.31B****), they show that the addition of GA or GN (Figures 3.31B' and 3.31B*, respectively) led to the formation of more heterogeneous scaffolds with smaller pores. Moreover, the incorporation of TG (Figure 3.31B****) seems to have led to systems with smaller and longer pores of very heterogeneous. On the other hand, the application

of a heat treatment (Figure 3.31B***) led to the formation of a less laminated structure than when using crosslinking agents (GA or TG), also presenting larger pores.

Finally, the pore size distributions (Figures 3.31C', 3.31C*, 3.31C**, 3.31C*** and 3.31C****) show that the application of any crosslinking method created a more heterogeneous system. This heterogeneity is more significant in the case of the incorporation of GA. In addition, the porosity of the scaffolds, all the systems present a porosity value in the range between 95 and 99 %.

However, the mean pore size is lower in the case of the incorporation of TG or GN, since a large number of small pores and few large pores were found in its structure. The incorporation of any of the crosslinking agents improved the functionality of the scaffold for the growth of cells by improving the heterogeneity of the system, by providing adhesion for the proliferation of the cells, and by providing it with an optimum mean pore size for its increase (Netti, 2014). However, the application of the heat treatment, although it improves the functionality of the scaffolds due to the heterogeneity of its microstructure, has a mean pore size that is too high (even higher than the reference system), leaving the optimum range (Netti, 2014).

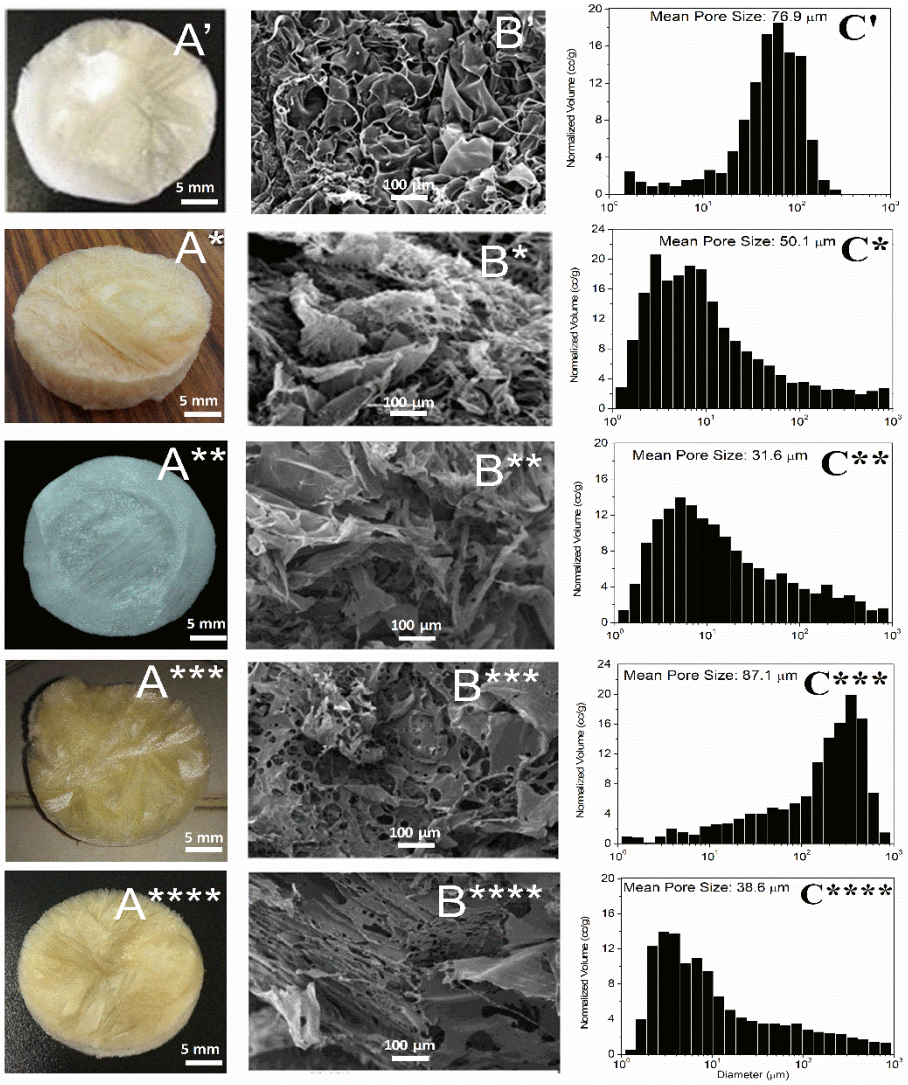

Figure 3.31. Macroscopic, microscopic and pore size distribution of scaffolds produced with a 50-50 collagen/chitosan ratio with a different crosslinking method: Glutaraldehyde addition [GA] (A*, B* and C*), genipin addition [GN] (A**, B** and C**), heat treatment [HT] (A, B*** and C***) and transglutaminase addition [TG] (A****, B**** and C****). The 50-50 collagen/chitosan system without crosslinking has also been included as reference (A', B' and C'). The mean pore size of the systems was also included***

Degree of crosslinking

To make a complete comparison, the degree of crosslinking was measured in the scaffolds with the addition of crosslinking agent (GA, GN or TG) with respect to the prepared solution and the scaffold after

the heat treatment. Table 3.11 shows the degree of crosslinking for the systems with the different crosslinking methods (GA, GN, heat treatment and TG). The system with GA presented greater crosslinking than the systems with GN, TG or heat treatment. Interestingly, the degree of crosslinking obtained for genipin and transglutaminase is not significantly different, presenting intermediate values (31 and 34 %, respectively).

This greater crosslinking possibly provided better critical strain to the system and a pore distribution with a tendency to smaller sizes. However, it is necessary to consider the range of sustainable values of the necessary properties for the optimal growth of cells in scaffolds. Therefore, the study of the mechanical and structural properties of these scaffolds is necessary.

Table 3.11. Degree of crosslinking and swelling ratio of scaffolds prepared with different crosslinking methods (CG: Collagen 1%; CH: Chitosan 1%; CG-CH: CG-CH 50-50 (reference); GA: CG-CH 50-50 + 0.05% of glutaraldehyde; GN: CG-CH 50-50 + 0.03% genipin, HT: CG-CH 50-50 + heat treatment and TG: CG-CH 50-50 + 0.10% of transglutaminase). Values with different letters are significantly different (p < 0.05)

SYSTEMS	Crosslinking (%)	Swelling (%)
CG	4 ^{A}	113 ^{a}
CH	5 ^{A}	131 ^{a}
CG-CH (reference)	3 ^{A}	135 ^{a}
GA	82 ^{B}	14 ^{b}
GN	31 ^{C}	54 ^{c}
HT	9 ^{D}	33 ^{bc}
TG	34 ^{C}	27 ^{bc}

Swelling ratio

The swelling ratio of the systems with different crosslinking is also shown in Table 3.11. It was observed that the crosslinking interferes in this parameter, decreasing the swelling ratio when the degree of crosslinking increases, although without significant differences. Thus,

the scaffold with the lowest swelling ratio was that containing GA, followed by the one containing TG and finally the scaffold treated with temperature and containing GN. However, all the crosslinked scaffolds showed great differences with respect to the scaffold without any crosslinking treatment. These results indicate that a higher degree of crosslinking leads to a minor modification of the systems when they are incorporated into the aqueous medium, making these systems more predictable and presenting fewer problems in the bioreactor and human body. Interestingly, the swelling ratio obtained are in the same range as the ones obtained in other studies as the ones carried out by Nazemi et al. (2014); Neira-Carrillo et al. (2011); or Stoyneva et al., (2014).

3.3.5. Optimization of the production of sponge-like scaffolds

As shown in previous sections, the properties of sponge-like materials can be enhanced considering different reinforcement methods. However, the high price of collagen with respect to other potential raw materials, such as gelatin, means that the development of new scaffolds with a more affordable price is still being investigated (Pandey et al., 2017; Shen et al., 2000; Shi et al., 2018). For this reason, a recent promising alternative of these scaffolds is the replacement of collagen with gelatin (denatured collagen), which could induce similar effects at a lower price, making it a field of research of great interest (Shen et al., 2000). In general, as shown, collagen-based structures present better properties than gelatin ones. However, our hypothesis is that improved gelatin-based structures can be obtained modifying its initial formulation or the processing technique.

Specifically, the production of gelatin-based systems with chitosan was analyzed, and their properties were compared. It is important to mention that 1.0 wt.% of total biopolymer concentration was used due to the better properties found for this concentration in the previous sections. Furthermore, the process was also optimized with the analysis of the inclusion of a heating stage for the polymer solution before the freeze-drying stage.

3.3.5.1. Modification of the raw material

Apart from using of additives, which can cause toxicity, this hypothesis is based on the modification of the properties of materials with the combination of different polymers. Thus, mixtures of gelatin with chitosan were studied by producing and comparing these binary structures with the collagen ones previously obtained. In this line, a gelatin-chitosan 50-50 ratio was used to simulate the collagen-chitosan

system which exhibited the best properties in the previous section (Section 3.3.3).

Rheological characterization

Figure 3.32A shows the profiles obtained for the frequency sweep tests of the different sponge-like scaffolds fabricated, comparing them with the unitary systems selected as reference. The evolution is similar for all the cases and, once again, E' values were improved, although in this case by the addition of chitosan.

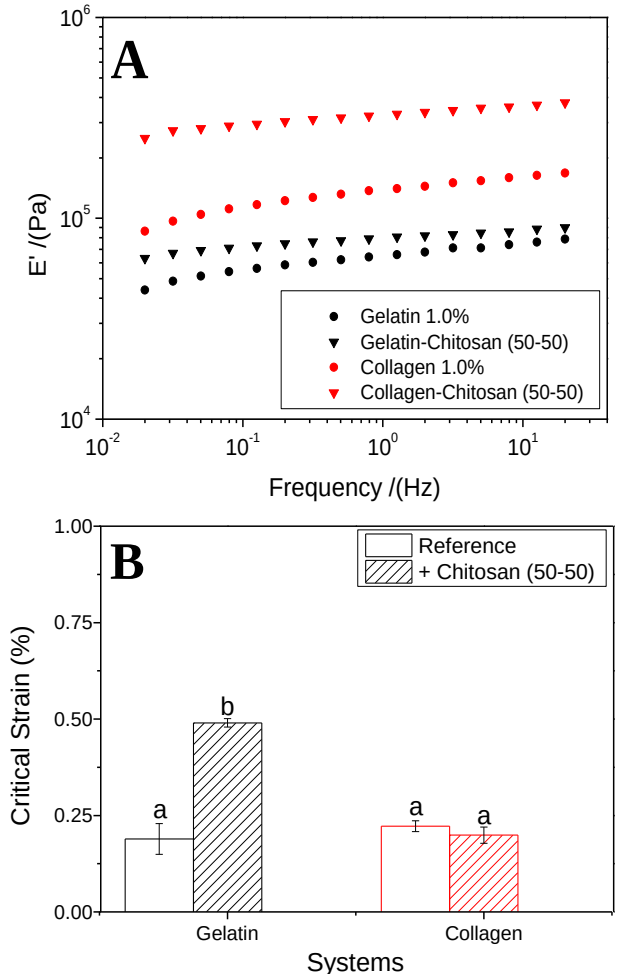

Figure 3.32. (A) Frequency sweep tests and (B) critical strain values of the protein-chitosan sponge-like scaffolds studied: GE-CH 50-50 and CG-CH 50-50. The unitary structures of 1 wt.% collagen and gelatin were also included as reference. Values with different letters are significantly different (p<0.05)

Interestingly, the addition of chitosan to the collagen-based sponge produced a marked increase in E' values, whereas the combination gelatin-chitosan produced no significant changes in E' values respect the collagen unitary system (Table 3.12).

Table 3.12. Critical Strain (%) of the protein-chitosan sponge-like scaffolds studied: GE-CH 50-50 and CG-CH 50-50. The unitary structures of 1 wt.% collagen and gelatin were also included as reference. Values with different letters are significantly different (p<0.05)

Systems		$E'_1 \cdot 10^5$ (Pa)
Collagen	1.0% Collagen	1.34 ± 0.02 [a]
	1.0% Collagen-Chitosan (50-50 ratio)	3.30 ± 0.62 [b]
Gelatin	1.0% Gelatin	0.65 ± 0.11 [c]
	1.0% Gelatin-Chitosan (50-50 ratio)	1.18 ± 0.16 [a]

On the other hand, the synergic effect of chitosan on gelatin-based structures gives rise to different results when studying the critical strain (Figure 3.32B). In this case, the mixture collagen-chitosan produced no significant differences ($p<0.05$) in the critical strain compared to the unitary collagen-based structure. Nevertheless, the addition of chitosan to gelatin produced an increase in the critical strain of the final structure formed.

Microstructural characterization

Considering the SEM images shown in Figure 3.33, mixtures of protein-chitosan (either collagen or gelatin, Figures 3.33B and 3.33B') produced structures with a similar framework, favoring the formation of micropores in the inner structure. In addition, the structures produced presented a much higher porosity than the values obtained in other studies involving polysaccharide-based porous structures (Autissier et al., 2010).

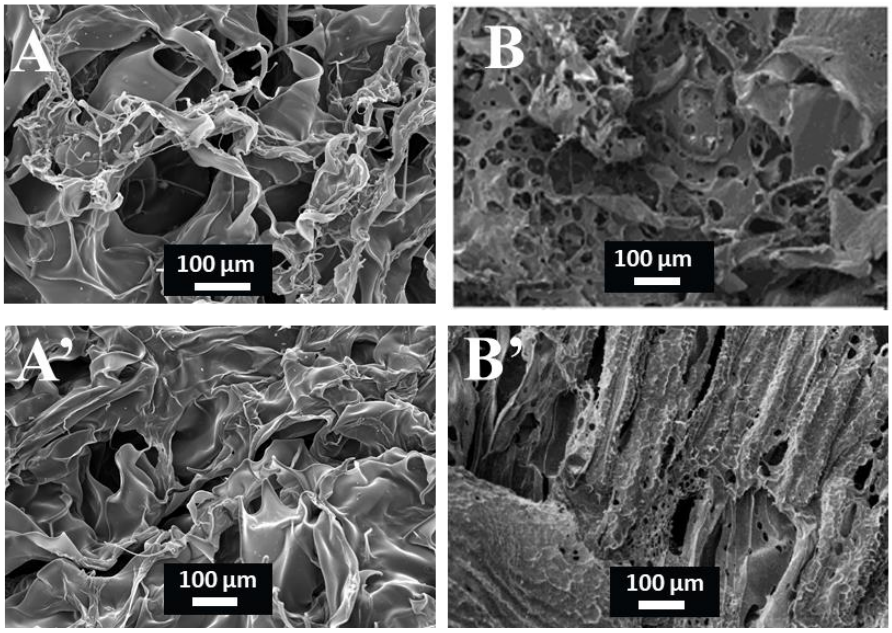

Figure 3.33. SEM images of the microstructure of the sponge-like materials obtained from collagen and gelatin at 1 wt.% with the addition of chitosan: (B) CG-CH 50-50 and (B') GE-CH 50-50. The unitary systems collagen (A) and gelatin (A') at 1 wt.% were also included as reference

3.3.5.2. Modification of the processing technique

In this study, the production of scaffolds encompassed three different protocols. In all cases, a GE-CH 50-50 ratio with a 1 wt.% of total biopolymer was used. It is worth mentioning that all protocols had in common the traditional steps used to develop the scaffolds by phase separation technique: preparation of the solution, centrifugation, freezing and freeze-drying, following the same operating conditions in order to carry out comparisons between the different protocols (P1 considered as reference, P2 and P3). The different protocols studied were described in the 'Materials and Methods' section (Section 3.2.2.3).

Rheological characterization

Figure 3.34 shows the values of the elastic modulus (E') as a function of frequency for the different scaffolds produced from protocols 1, 2 and 3 (P1, P2 and P3, respectively).

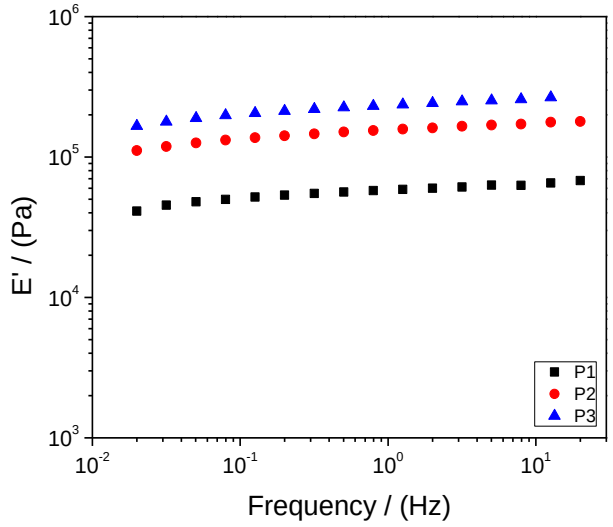

Figure 3.34. E' values of the scaffolds with a GE-CH 50-50 ratio obtained by the different protocols (P1, P2 and P3)

It can be observed that there is a slight variation of E' values with frequency, showing enough stability and solid character, such as the scaffolds studied in previous sections. Furthermore, the different critical strain (γ_c) values obtained are shown in Table 3.13, evidencing the improvement of both alternatives (P2 and P3) respect the reference system, with an increase of 0.12 and 0.22 %, respectively.

Table 3.13. Critical Strain (γ_c, %) and K_{i1} values of the scaffolds with a GE-CH 50-50 ratio obtained by the different protocols (P1, P2 and P3). Values with different letters are significantly different ($p<0.05$)

SYSTEM	Protocol	γ_c (%)	K_{i1}
50-50 Gelatin-Chitosan	P1 (reference)	0.46^a	-
	P2	0.58^b	1.29
	P3	0.68^c	1.57

Focusing on the results obtained in the different protocols and comparing them, protocol 3 stands out against the others, obtaining the best mechanical properties, which are reflected in the greatest critical strains (γ_c) and E' values. However, protocols 2 also obtained better properties than protocol 1, although without reaching the values obtained in protocol 3. This comparison between the protocols can be better evaluated by observing Table 3.13, which shows the K_{i1} values of the different systems calculated, which is the ratio of the elastic modulus of the systems produced by the different protocols respect the reference one (P1), as explained in the 'Materials and Methods' section (Eq. 3.1). As can be seen, the values obtained with protocol 2 are 1.3 times higher than the reference, whereas protocol 3 shows an increase of 1.6 respect to the reference protocol.

Therefore, it is deduced that the increases that are reflected in protocols 2 and 3 with respect to the reference one are due mainly to the improvement in the synergy between chitosan (CH) and gelatin (GE). In addition, protocol 3 improves significantly more than protocol 2. This improvement may be due to the reorganization of the polymer chain with the heating process after the homogenization of the solution with the centrifugation. That better reorganization allows a better interaction between the polymer chains of collagen and chitosan improving the microstructure and, for that reason, the mechanical properties of the sponge-like scaffolds obtained.

Microstructural characterization

Figure 3.35 shows the average pore size distributions of the reference composition (GE-CH 50-50), for the three processing methods (P1, P2 and P3). In Figure 3.35A (P1, reference), it can be seen a profile that shows a bimodal distribution with two peaks with a size of about 15 and

45 μm. This fact supposes that the polydispersion of sizes is high (low uniformity) also presenting high percentages of pores at high sizes. This may mean that, although there are not many large pores, their presence may affect the mechanical properties. In any case, the average pore size is 35.6 μm. The mean pore size of the scaffolds fabricated with protocol 2 is 28.7 μm. However, this system (Figure 3.35B) is the most polydispersed system without any unimodal distribution. Finally, in Figure 3.35C belonging to protocol 3, there is a unimodal distribution with a peak around 50 μm. Although the distribution is less polydispersed, this system has a larger mean pore size than the others (51.2 μm).

In any case, this larger pore size does not imply any inconvenience since it will facilitate the entry of cells and the neovascularization of the scaffolds once implanted. In general, it is established that for the development of soft tissue scaffolds, a pore size range between 20 and 200 μm is required (Tu, 2017). Therefore, the pore sizes are higher than the lower limit of those necessary to lead to a good regeneration of the tissues. Specifically, Klawitter and Hulbert (1971) showed that scaffolds produced with a pore size between 30 and 100 μm presented bone and fibrous tissue ingrowth during the cell studies. In this sense, these scaffolds could be useful for bone regeneration according to their mean pore size.

On the other hand, Figure 3.36 shows the micrographs for the GE-CH 50-50 scaffolds obtained by the three protocols (Protocol 1: 3.36A, protocol 2: 3.36B and protocol 3: 3.36C). In Figure 3.36A, it can be observed how there is a high porosity throughout the scaffold. It is also seen how the pores are distributed heterogeneously throughout the scaffold processed by protocol 1, observing: a small distribution of large

pores (in the form of holes) and mostly a small pore distribution; which reaffirms what was discussed in the previous section (Figure 3.35).

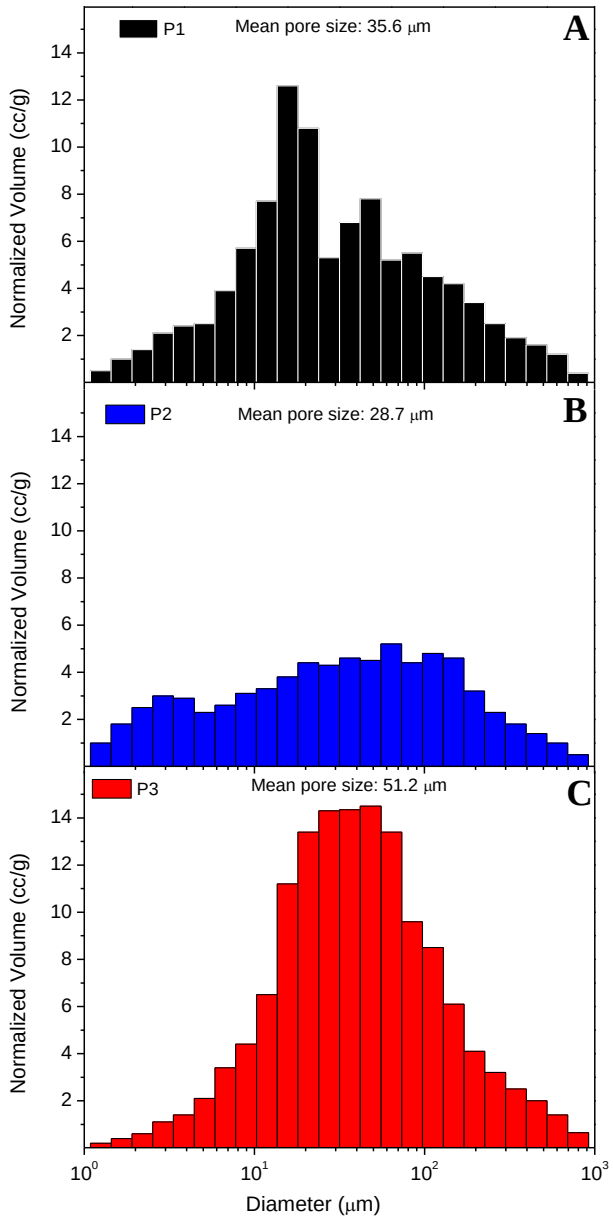

Figure 3.35. Pore size distribution of the scaffolds with a GE-CH 50-50 ratio obtained by the different protocols (P1, P2 and P3). The mean pore size of the systems was also included

However, Figure 3.36B shows that the scaffold obtained by the protocol 2 has a great heterogeneity as it was obtained in the measurements of porosimetry (with respect to the pore size). Finally, Figure 3.36C shows the porosity presented though the scaffold processed by protocol 3. In this case, a more homogeneous distribution is more closely observed.

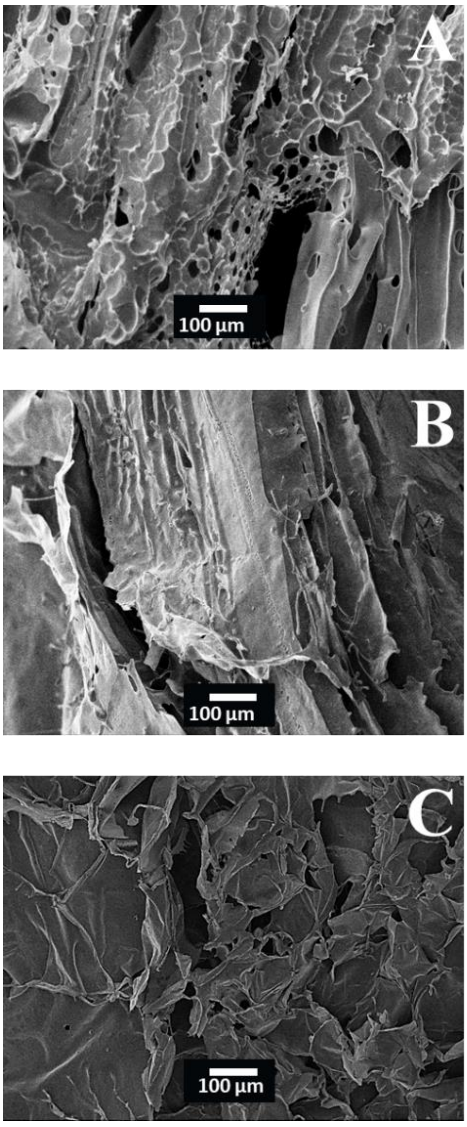

Figure 3.36. SEM images of the scaffolds with a GE-CH 50-50 ratio obtained by the different protocols (P1, P2 and P3)

3.4 Concluding remarks

As a general conclusion, it is evident that a porous protein-based matrix (scaffold) was achieved through a process consisting of two main stages: preparation of a polymer solution and a freeze-drying step. Different systems were studied by analyzing their rheological and microstructural properties. Regardless of the composition and fabrication method used, the scaffolds obtained in the present chapter constitute biopolymer matrices with porosity greater than 95 % and pore sizes and interconnectivity suitable for application in tissue engineering.

The tailoring of their mechanical and structural properties can be produced by modifying the different processing conditions involved in the process. Considering the container used, the freeze-drying process is carried out more effectively when using a hydrophobic mold, since it allows better removal of the solvent. Moreover, protein-based scaffolds with better properties are achieved by working at a pH below the isoelectric point of the protein, which causes its stabilization during processing. A pH value of 3.2 has been confirmed to lead to scaffolds showing optimal properties. Furthermore, although lower temperatures lead to more rigid scaffolds, using a freezing temperature of -40 ºC results in scaffolds with greater critical strain and more suitable porosity for their use in the bioreactor. Furthermore, the properties of the scaffolds will depend on the acid used for its preparation, more specifically on the dissociation of the acid. Scaffolds with better properties will be obtained using an acid that is not dissociated at the working pH value. In addition, the increase in the concentration of the acid used as solvent has a negative effect on the properties of the scaffolds.

The increase in protein content increased both the elastic moduli and the porosity of the sponges fabricated, with the system with 1.0 wt.% collagen reaching the maximum values. The increase in protein concentration produced a more compacted structure.

The combination of collagen with another polymer like chitosan produce binary systems which present better properties than their unitary systems separately, although there is an optimal ratio of biopolymers (50-50 CG-CH), in which there is synergy between them.

The study of the different crosslinking methods shows different results. Physically induced crosslinking with a heat treatment did not result in a high degree of crosslinking, not improving the properties of the scaffolds. In this way, this method of crosslinking is not effective for this type of application. On the other hand, the addition of a crosslinking agent has provided better qualities to the scaffolds regardless of their nature, giving the greater critical strain and optimal pore heterogeneity. In any case, although glutaraldehyde is the most used crosslinking agent at present, it has been shown that transglutaminase or genipin could be a clear substitute for it. In this sense, considering the range of sustainable values of the necessary properties for the optimal growth of cells in scaffolds, although both crosslinking agents provided a lower degree of crosslinking, gave the scaffolds the appropriate properties, with lower toxicity problems, as compared to GA.

The substitution of collagen by gelatin revealed that the addition of chitosan produces a significant increase in the critical strain of gelatin-based structures, which allows using higher strain values in the bioreactor.

The optimization of the freeze-drying process stated that applying a heat treatment (protocol 2 and 3) produces a considerable increase in

mechanical properties, possibly due to some improvement in solubility and, above all, to the chain structuring that occurs in the biopolymer matrix when applied to it.

Acknowledgements

The authors gratefully acknowledge the Characterization and Microscopy Service (CITIUS-Universidad de Sevilla) for providing full access and assistance to the PoreMaster-60 GT porosimeter (Quantachrome Instruments) and to the JEOL 6460-LV (JEOL).

Related publications

- Perez-Puyana, Víctor Manuel; Romero García, Alberto; Guerrero Conejo, Antonio (2016). Influence of collagen concentration and glutaraldehyde on collagen-based scaffold properties, *Journal of Biomedical Materials Research. Part A*, 104, 1462-1468
- Perez-Puyana, Víctor Manuel; Félix Ángel, Manuel; Romero García, Alberto; Guerrero Conejo, Antonio (2019). Influence of the processing variables on the microstructure and properties of gelatin-based scaffolds by freeze-drying, *Journal of Applied Polymer Science*, 136, 47671, DOI: 10.1002/APP.47671
- Perez-Puyana, Víctor Manuel; Jiménez Rosado, Mercedes; Rubio Valle, José Fernando; Guerrero Conejo, Antonio; Romero García, Alberto (2019). Gelatin vs collagen-based sponges: Evaluation of concentration, additives and biocomposites, *Journal of Polymer Research*, 26, DOI: 10.1007/s10965-019-1863-9
- Perez-Puyana, Víctor Manuel; Jiménez Rosado, Mercedes; Romero García, Alberto; Guerrero Conejo, Antonio (2019).

Crosslinking of hybrid scaffolds produced from collagen and chitosan, *International Journal of Biological Macromolecules*, 139, 262-269.

- Perez-Puyana, Víctor Manuel; Rubio Valle, José Fernando; Jiménez Rosado, Mercedes; Guerrero Conejo, Antonio; Romero García, Alberto (2020). Alternative processing methods of hybrid porous scaffolds based on gelatin and chitosan, *Journal of the mechanical behavior of biomedical materials*, 102, 103472.
- Perez-Puyana, Víctor Manuel; Rubio Valle, José Fernando; Jiménez Rosado, Mercedes; Guerrero Conejo, Antonio; Romero García, Alberto. Chitosan as a potential alternative to collagen for the development of genipin-crosslinked scaffolds, Under Review in *Reactive and Functional Polymers* (October 2019)

References

Aguirre-Chagala, Y.E., Altuzar, V., León-Sarabia, E., Tinoco-Magaña, J.C., Yañez-Limón, J.M., Mendoza-Barrera, C., 2017. Physicochemical properties of polycaprolactone/collagen/elastin nanofibers fabricated by electrospinning. Mater. Sci. Eng. C 76, 897–907.

Al-Munajjed, A.A., Hien, M., Kujat, R., Gleeson, J.P., Hammer, J., 2008. Influence of pore size on tensile strength, permeability and porosity of hyaluronan-collagen scaffolds. J. Mater. Sci. Mater. Med. 19, 2859–2864.

Autissier, A., Le Visage, C., Pouzet, C., Chaubet, F., Letourneur, D., 2010. Fabrication of porous polysaccharide-based scaffolds using a combined freeze-drying/cross-linking process. Acta Biomater. 6, 3640–3648.

Bae, K.H., Wang, L.-S., Kurisawa, M., 2013. Injectable biodegradable hydrogels: progress and challenges. J. Mater. Chem. B 1, 5371–5388.

Correia, C.R., Moreira-Teixeira, L.S., Moroni, L., Reis, R.L., van Blitterswijk, C.A., Karperien, M., Mano, J.F., 2011. Chitosan scaffolds containing hyaluronic acid for cartilage tissue engineering. Tissue Eng. Part C Methods 17, 717–730.

Cristescu, I., Zamfirescu, D., Vilcioiu, D., Marina, L., Safta, F., 2014. Experimental Evaluation on Rat Model of Different Bioresorbable Materials Potentially Used as Orthopedic Biomaterials, in: Bioceramics 25: Supplement, Key Engineering Materials. Trans Tech Publications, pp. 196–199.

Dimida, S., Barca, A., Cancelli, N., De Benedictis, V., Raucci, M.G., Demitri, C., 2017. Effects of Genipin Concentration on Cross-Linked Chitosan Scaffolds for Bone Tissue Engineering: Structural Characterization and Evidence of Biocompatibility Features. Int. J. Polym. Sci. 2017, 1–8.

Fereshteh, Z., Fathi, M., Bagri, A., Boccaccini, A.R., 2016. Preparation and characterization of aligned porous PCL/zein scaffolds as drug delivery systems via improved unidirectional freeze-drying method. Mater. Sci. Eng. C 68, 613–622.

Geutjes, P.J., Daamen, W.F., Buma, P., Feitz, W.F., Faraj, K.A., Van Kuppevelt, T.H., 2006. From Molecules to Matrix: Construction and Evaluation of Molecularly Defined Bioscaffolds, in: Tissue Engineering. Springer, Boston, pp. 279–295.

Gopinath, A., Shanmugam, G., Madhan, B., Rao, J.R., 2017. Differential behavior of native and denatured collagen in the presence of alcoholic solvents: A gateway to instant structural analysis. Int. J. Biol. Macromol. 102, 1156–1165.

Horgnies, M., 2009. Influences of freeze-drying and UV-irradiation on the microstructured morphology and on the wetting properties of PS41–PAA271 coating. J. Mater. Process. Technol. 209, 2338–2348.

Housecroft, C., Sharpe, A., 2008. Chapter 6: Acids, Bases and Ions in Aqueous Solution, in: Inorganic Chemistry. Prentice Hall.

Islam, S., Bhuiyan, M.A.R., Islam, M.N., 2017. Chitin and Chitosan: Structure, Properties and Applications in Biomedical Engineering. J. Polym. Environ. 25, 854–866.

Jana, S., Tefft, B.J., Spoon, D.B., Simari, R.D., 2014. Scaffolds for tissue engineering of cardiac valves. Acta Biomater. 10, 2877–2893.

Jozami, F., Seselovsky, R., 2003. Usos de la transglutaminasa en la industria alimentaria. Elaboración de carne reconstruida. Invenio 6, 157–164.

Ju, Z.Y., Kilara, A., 1998. Gelation of pH-aggregated whey protein isolate solution induced by heat, protease, calcium salt, and acidulant. J. Agric. Food Chem. 46, 1830–1835.

Kaczmarek, B., Sionkowska, A., Osyczka, A.M., 2018. Scaffolds based on chitosan and collagen with glycosaminoglycans cross-linked by tannic acid. Polym. Test. 65, 163–168.

Kaczmarek, B., Sionkowska, A., Osyczka, A.M., 2017. The comparison of physic-chemical properties of chitosan/collagen/hyaluronic acid composites with nano-hydroxyapatite cross-linked by dialdehyde starch and tannic acid. Polym. Test. 62, 171–176.

Klawitter, J.J., Hulbert, S.F., 1971. Application of porous ceramics for the attachment of load bearing internal orthopedic applications. J. Biomed. Mater. Res. 5, 161–229.

Lin, L., Wang, Z., Zhou, L., Hu, Q., Fang, M., 2013. The influence of prefreezing temperature on pore structure in freeze-dried beta-TCP scaffolds. Proc. Inst. Mech. Eng. H. 227, 50–57.

Lv, Q., Feng, Q., 2006. Preparation of 3-D regenerated fibroin scaffolds with freeze drying method and freeze drying/foaming technique. J. Mater. Sci. Mater. Med. 17, 1349–1356.

Ma, L., Gao, C., Mao, Z., Zhou, J., Shen, J., Hu, X., Han, C., 2003. Collagen/chitosan porous scaffolds with improved biostability for skin tissue engineering. Biomaterials 24, 4833–4841.

Maji, S., Agarwal, T., Das, J., Maiti, T.K., 2018. Development of gelatin/carboxymethyl chitosan/nano-hydroxyapatite composite 3D macroporous scaffold for bone tissue engineering applications. Carbohydr. Polym. 189, 115–125.

Mármol, Z., Páez, G., Rincón, M., Araujo, K., Aiello-Mazzarri, C., Chandler, C., Gutierrez, E., 2012. Quitina y Quitosano, polímeros amigables. Una revisión de sus aplicaciones. Rev. Tecnocientífica URU 1, 53–58.

Martínez, A., Blanco, M.D., Davidenko, N., Cameron, R.E., 2015. Tailoring chitosan/collagen scaffolds for tissue engineering: Effect of composition and different crosslinking agents on scaffold properties. Carbohydr. Polym. 132, 606–619.

Mohammadi, Z., Mesgar, A.S.-M., Rasouli-Disfani, F., 2016. Reinforcement of freeze-dried chitosan scaffolds with multiphasic calcium phosphate short fibers. J. Mech. Behav. Biomed. Mater. 61, 590–599.

Muthukumar, T., Aravinthan, A., Sharmila, J., Kim, N.S., Kim, J.H., 2016. Collagen/chitosan porous bone tissue engineering composite scaffold incorporated with Ginseng compound K. Carbohydr. Polym. 152, 566–574.

Naghieh, S., Karamooz-Ravari, M.R., Sarker, M.D., Karki, E., Chen, X., 2018. Influence of crosslinking on the mechanical behavior of 3D printed alginate scaffolds: Experimental and numerical approaches. J. Mech. Behav. Biomed. Mater. 80, 111–118.

Nazemi, K., Moztarzadeh, F., Jalali, N., Asgari, S., Mozafari, M., 2014. Synthesis and Characterization of Poly(lactic-co-glycolic) Acid Nanoparticles-Loaded Chitosan/Bioactive Glass Scaffolds as a Localized Delivery System in the Bone Defects, BioMed research international. DOI: 10.1155/2014/898930

Neira-Carrillo, A., S. Fernández, M., L. Arias, J., Navarrete G, S., Paz Díaz, M., Yazdani-Pedram, M., 2011. Preparation of a porous scaffold based on polypropylene grafted with monomethylitaconate as potential bone graft, Macromolecular Research 19, 1105-1113.

Netti, P., 2014. Biomedical Foams for Tissue Engineering Applications. Woodhead Publishing, Italy.

O'Brien, F.J., Harley, B.A., Yannas, I. V., Gibson, L., 2004a. Influence of freezing rate on pore structure in freeze-dried collagen-GAG scaffolds. Biomaterials 25, 1077–1086.

O'Brien, F.J., Harley, B.A., Yannas, I. V., Gibson, L.J., 2004b. Influence of freezing rate on pore structure in freeze-dried collagen-GAG scaffolds. Biomaterials 25, 1077–1086.

Ofner III, C.M., Bubnis, W.A., 1996. Chemical and swelling evaluations of amino group crosslinking in gelatin and modified gelatin matrices. Pharm. Res. 13, 1821–1827.

Oliveira, P.N., Montembault, A., Sudre, G., Alcouffe, P., Marcon, L., Gehan, H., Lux, F., Albespy, K., Centis, V., Campos, D., Roques, S., Meulle, M., Renard, M., Durand, M., Denost, Q., Bordenave, L., Vandamme, M., Chereul, E., Vandesteene, M., Boucard, N., David, L., 2019. Self-crosslinked fibrous collagen/chitosan blends: Processing, properties evaluation and monitoring of degradation by bi-fluorescence imaging. Int. J. Biol. Macromol. 131, 353–367.

Orban, J.M., Wilson, L.B., Kofroth, J.A., El-Kurdi, M.S., Maul, T.M., Vorp, D.A., 2004. Crosslinking of collagen gels by transglutaminase. J. Biomed. Mater. Res. A 68, 756–762.

Orrego Cardozo, M., Ponte, I., Suau, P., 2015. Caracterización de la estructura secundaria de subtipos de la histona H1 por dicroísmo circular. Biosalud 14, 29–48.

Oryan, A., Kamali, A., Moshiri, A., Baharvand, H., Daemi, H., 2018. Chemical crosslinking of biopolymeric scaffolds: Current knowledge and future directions of crosslinked engineered bone scaffolds. Int. J. Biol. Macromol. 107, 678–688.

Pandey, A.R., Singh, U.S., Momin, M., Bhavsar, C., 2017. Chitosan: Application in tissue engineering and skin grafting. J. Polym. Res. 24, 125.

Perdivara, I., Yamauchi, M., Tomer, K.B., 2013. Molecular Characterization of Collagen Hydroxylysine *O*-Glycosylation by Mass Spectrometry: Current Status. Aust. J. Chem. 66, 760–769.

Perez-Puyana, V., Ostos, F.J., Lopez-Cornejo, P., Romero, A., Guerrero, A., 2019. Assessment of the denaturation of collagen protein concentrates using different techniques. Biol. Chem.
DOI: 10.1515/hsz-2019-0206

Perez-Puyana, V., Romero, A., Guerrero, A., 2016. Influence of collagen concentration and glutaraldehyde on collagen-based scaffold properties. J. Biomed. Mater. Res. Part A 104, 1462–1468.

Pinto, C.F., Berger, S.B., Cavalli, V., Bedran-Russo, A.K., Giannini, M., 2015. Influence of chemical and natural cross-linkers on dentin bond strength of self-etching adhesives. Int. J. Adhes. Adhes. 60, 117–122.

Ramkumar, D.H.S., Bhattacharya, M., 1997. Effect of crystallinity on the mechanical properties of starch/synthetic polymer blends. J. Mater. Sci. 32, 2565–2572.

Reys, L.L., Silva, S.S., Pirraco, R.P., Marques, A.P., Mano, J.F., Silva, T.H.,

Reis, R.L., 2017. Influence of freezing temperature and deacetylation degree on the performance of freeze-dried chitosan sca ff olds towards cartilage tissue engineering. Eur. Polym. J. 95, 232–240.

Rodríguez-Parra, J.M., Moreno, R., Nieto, M.I., 2012. Effect of cooling rate on the microstructure and porosity of alumina produced by freeze casting. J. Serbian Chem. Soc. 77, 1775–1785.

Rodríguez-Rodríguez, R., Espinosa-Andrews, H., Velasquillo-Martínez, C., García-Carvajal, Z.Y., 2019. Composite hydrogels based on gelatin, chitosan and polyvinyl alcohol to biomedical applications: a review. Int. J. Polym. Mater. Polym. Biomater. 1–20.

Rodríguez-Vázquez, M., Vega-Ruiz, B., Ramos-Zúñiga, R., Saldaña-Koppel, D.A., Quiñones-Olvera, L.F., 2015. Chitosan and its potential use as scaffold for Tissue Engineering in Regenerative Medicine. Biomed Res. Int. 2015, 121–143.

Ruijgrok, J.M., de Wijn, J.R., Boon, M.E., 1994. Glutaraldehyde crosslinking of collagen: Effects of time, temperature, concentration and presoaking as measured by shrinkage temperature. Clin. Mater. 17, 23–27.

Russell, A.E., 1974. Effect of pH on thermal stability of collagen in the dispersed and aggregated states. Biochem. J. 139, 277.

Sachlos, E., Czemuszka, J.T., 2003. Making tissue engineering scaffolds work. Review: the application of solid freeform fabrication technology to the production of tissue engineering scaffolds. Eur. Cells Mater. 5, 29–40.

Sachlos, E., Czernuszka, J.T., others, 2003. Making tissue engineering scaffolds work. Review: the application of solid freeform fabrication technology to the production of tissue engineering scaffolds. Eur Cell Mater 5, 39–40.

Schwarzenbach, M.S., Reimann, P., Thommen, V., Hegner, M., Mumenthaler, M., Schwob, J., Güntherodt, H.-J., 2002. Interferon α-2a interactions on glass vial surfaces measured by atomic force microscopy. PDA J. Pharm. Sci. Technol. 56, 78–89.

Senatov, F.S., Zadorozhnyy, M.Y., Niaza, K. V, Medvedev, V. V, Kaloshkin,

S.D., Anisimova, N.Y., Kiselevskiy, M. V, Yang, K.-C., 2017. Shape memory effect in 3D-printed scaffolds for self-fitting implants. Eur. Polym. J. 93, 222–231.

Shahbazarab, Z., Teimouri, A., Chermahini, A.N., Azadi, M., 2018. Fabrication and characterization of nanobiocomposite scaffold of zein/chitosan/nanohydroxyapatite prepared by freeze-drying method for bone tissue engineering. Int. J. Biol. Macromol. 108, 1017–1027.

Shen, F., Cui, Y., Yang, L., Yao, K., Dong, X., Jia, W., Shi, H., 2000. A study on the fabrication of porous chitosan/gelatin network scaffold for tissue engineering. Polym. Int. 49, 1596–1599.

Shi, L., Xiong, L., Hu, Y., Li, W., Chen, Z., Liu, K., Zhang, X., 2018. Three-dimensional printing alginate/gelatin scaffolds as dermal substitutes for skin tissue engineering. Polym. Eng. Sci. 58, 1782–1790.

Songchotikunpan, P., Tattiyakul, J., Supaphol, P., 2008. Extraction and electrospinning of gelatin from fish skin. Int. J. Biol. Macromol. 42, 247–255.

Stoyneva, V., Momekova, D., Kostova, B., Petrov, P., 2014. Stimuli sensitive super-macroporous cryogels based on photo-crosslinked 2-hydroxyethylcellulose and chitosan. Carbohydr. Polym. 99, 825–830.

Teimouri, A., Azadi, M., 2016. Preparation and characterization of novel chitosan/nanodiopside/nanohydroxyapatite composite scaffolds for tissue engineering applications. Int. J. Polym. Mater. Polym. Biomater. 65, 917–927.

Teixeira, L.S.M., Feijen, J., van Blitterswijk, C.A., Dijkstra, P.J., Karperien, M., 2012. Enzyme-catalyzed crosslinkable hydrogels: Emerging strategies for tissue engineering. Biomaterials 33, 1281–1290.

Tu, X., 2017. Fabrication et étude de scaffolds multidimensionnels pour l'ingénierie cellulaire et tissulaire. Paris Sciences et Lettre.

Vallet-Regi, M., Munuera, L., 2000. Biomateriales: Aquí y Ahora. Editorial Dykinson.

Van Vlierberghe, S., Dubruel, P., Schacht, E., 2011. Biopolymer-Based

Hydrogels As Scaffolds for Tissue Engineering Applications : A Review. Biomacromolecules 12, 1387–1408.

Varley, M.C., Neelakantan, S., Clyne, T.W., Dean, J., Brooks, R.A., Markaki, A.E., 2016. Cell structure, stiffness and permeability of freeze-dried collagen scaffolds in dry and hydrated states. Acta Biomater. 33, 166–175.

Weadock, K., Olson, R.M., Silver, F.H., 1983. Evaluation of Collagen Crosslinking Techniques. Biomater. Med. Devices. Artif. Organs 11, 293–318.

Whang, K., Thomas, C.H., Healy, K.E., Nuber, G., 1995. A novel method to fabricate bioabsorbable scaffolds. Polymer (Guildf). 36, 837–842.

Wu, X., Liu, Y., Li, X., Wen, P., Zhang, Y., Long, Y., Wang, X., Guo, Y., Xing, F., Gao, J., 2010. Preparation of aligned porous gelatin scaffolds by unidirectional freeze-drying method. Acta Biomater. 6, 1167–1177.

Yang, G., Xiao, Z., Ren, X., Long, H., Qian, H., Ma, K., Guo, Y., 2016. Enzymatically crosslinked gelatin hydrogel promotes the proliferation of adipose tissue-derived stromal cells. PeerJ 4, e2497.

Yang, H., Xu, S., Shen, L., Liu, W., Li, G., 2016. Changes in aggregation behavior of collagen molecules in solution with varying concentrations of acetic acid. Int. J. Biol. Macromol. 92, 581–586.

Yang, Y., Zhu, X., Cui, W., Li, X., Jin, Y., 2009. Electrospun Composite Mats of Poly[(D,L-lactide)-co-glycolide] and Collagen with High Porosity as Potential Scaffolds for Skin Tissue Engineering. Macromol. Mater. Eng. 294, 611–619.

Yannas, I.V., Burke, J.F., 1980. Design of an artificial skin. I. Basic design principles. J. Biomed. Mater. Res. 14, 65–81.

Yin, L., Venkatesan, S., Kalyanasundaram, S., Qin, Q.-H., 2009. Effect of microstructure on micromechanical performance of dry cortical bone tissues. Mater. Charact. 60, 1424–1431.

Yoo, J.S., Kim, Y.J., Kim, S.H., Choi, S.H., 2011. Study on genipin: A new alternative natural crosslinking agent for fixing heterograft tissue. Korean

J. Thorac. Cardiovasc. Surg. 44, 197–207.

You, C., Li, Q., Wang, X., Wu, P., Ho, J.K., Jin, R., Zhang, L., Shao, H., Han, C., 2017. Silver nanoparticle loaded collagen/chitosan scaffolds promote wound healing via regulating fibroblast migration and macrophage activation. Sci. Rep. 7, 1–11.

Zamanian, A., Ghorbani, F., Nojehdehian, H., 2014. Morphological comparison of PLGA/gelatin scaffolds produced by freeze casting and freeze drying methods, in: Applied Mechanics and Materials. pp. 108–111.

Zhang, H., Neau, S.H., 2001. In vitro degradation of chitosan by a commercial enzyme preparation: effect of molecular weight and degree of deacetylation. Biomaterials 22, 1653–1658.

Zhao, Y., Gao, S., Zhao, S., Li, Y., Cheng, L., Li, J., Yin, Y., 2012. Synthesis and characterization of disulfide-crosslinked alginate hydrogel scaffolds. Mater. Sci. Eng. C 32, 2153–2162.

Zhong, S.P., Teo, W.E., Zhu, X., Beuerman, R.W., Ramakrishna, S., Yung, L.Y.L., 2006. An aligned nanofibrous collagen scaffold by electrospinning and its effects on in vitro fibroblast culture. J. Biomed. Mater. Res. Part A 79A, 456–463.

Chapter 4: Development of scaffolds *via* electrospinning

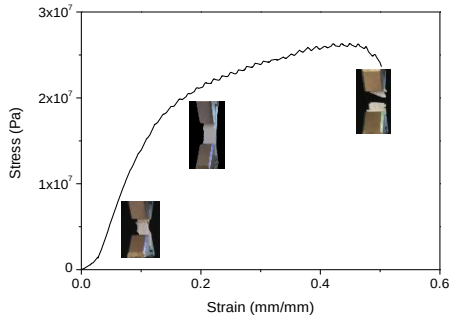

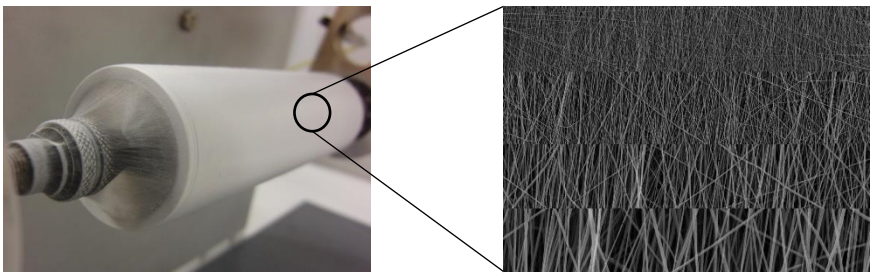

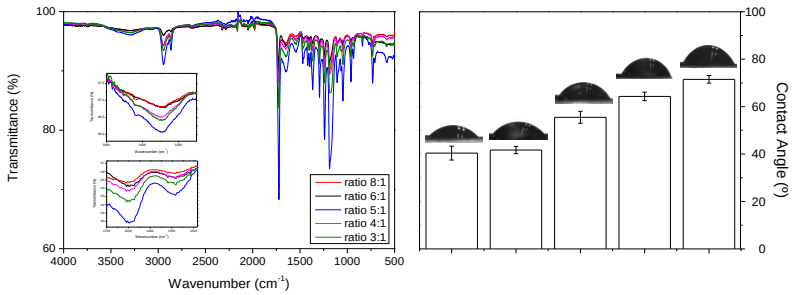

4.1 Introduction

The field of electrospinning has been constantly growing and evolving over the past 20 years (Liu et al., 2018). This technique allows the formation of nanofibrous membranes by the application of an electric field between the syringe, where the polymer solution is placed, and the collector. While the process is working, the jet experiences a whipping instability that allows enough time for the solvent to evaporate, resulting in the formation of fibers (Duque Sánchez et al., 2014).

A schematic overview of the electrospinning process can be seen in Figure 4.1. This process is based on the extremely fast uniaxial elongation of a drop of the viscoelastic polymer solution to form an ultra-thin filament when a high voltage electric field is applied. Unlike mechanical spinning, the filament is formed by electrostatic repulsions between charged surfaces induced by the application of the electric field. Therefore, the charges accumulate, and the formation of a drop is promoted at the tip of the capillary. The intensity of the electric field is increased until reaching the equilibrium between the electrostatic forces, which causes a value of the surface tension in the liquid that causes the drop to lengthen. When the electric field strength exceeds the cohesive forces of the solution, the drop takes a conical shape (Taylor cone) and it is projected from the needle, fitted to a syringe, to the collector, which remains connected to ground and to a power supply (Duque Sánchez et al., 2014). A membrane composed of fibers of varying diameters between 10 nm and a few micrometers is formed on the surface of the collector.

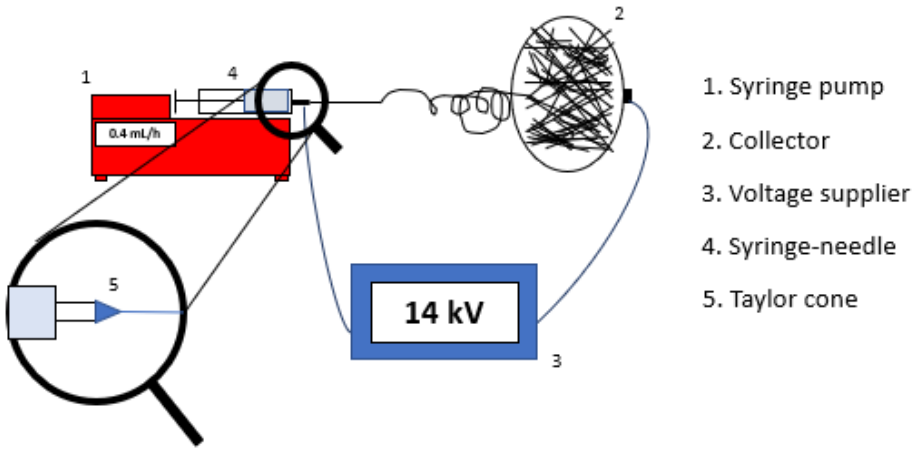

Figure 4.1. Schematic overview of the electrospinning process with the main elements involved

There are currently two standard electrospinning configurations concerning the direction of the jet, vertical and horizontal setup. In the horizontal assembly, contamination of the sample is avoided by dripping the solution on the collector, while in the vertical assembly gravity, in turn, is a force that helps the electric field in advancing the solution. However, independently on the assembly used, the formation of the Taylor cone is indispensable for the formation of nanofibers. Taylor cone is formed due to electrostatic interactions (Taylor, 1964). The charged drop will have an electrostatic repulsion, which together with the surface tension of the solution; will cause the drop to stretch, generating a conical geometry (Taylor Cone). Subsequently, a thin jet is formed which, together with solvent evaporation, leads to the solidification of the filament into fibers, which are finally deposited on the collector usually forming a randomly oriented fiber mat (Agrahari et al., 2017; Lagaron et al., 2017)

A characteristic feature of the electrospinning process is the extremely quick formation of the nanofibrous membranes. These membranes present a very high surface area, making these structures a suitable

candidate for many different applications in a variety of fields, such as catalysis or biotechnology, among others (Agarwal et al., 2013), and even in medicine, where they can be used as scaffolds for Tissue Engineering (Gautam et al., 2013). More specifically, polymeric electrospun scaffolds provide a suitable three-dimensional support for cell adhesion, proliferation and differentiation, which is essential to guide tissue formation (de la Portilla et al., 2016; Jin et al., 2018).

The formation of fibers and the final properties exhibited by the membranes depend on the correct development of the electrospinning process. If the process is not carried out continuously and efficiently, a process called electrospraying takes place, where the initial droplets formed at the exit of the needle are continuously broken up as a result of the coulombic interactions until reaching the collector (Ebrahimgol et al., 2014). The concentration and type of polymer are key parameters for the development of electrospinning since they affect both the surface tension and the viscosity, two fundamental aspects for the success of the electrospinning process. Ghafoor et al. (2018) showed a comparison of the properties of the structures obtained using different polymers. The selection of the polymer is important since the properties of the scaffolds can be modulated depending on the polymer used. The use of synthetic polymers allows obtaining structures with better mechanical properties, although most of them present problems related to the lack of biocompatibility (Perez-Puyana et al., 2018). This can be corrected by the combination of these polymers with biopolymers, that is, natural polymers such as proteins or polysaccharides that improve the biocompatibility of the system (Merrett et al., 2012; Zhang et al., 2014). The most used synthetic polymers are polyethylene oxide (POE), polylactic acid (PLA) or polycaprolactone (PCL) (Agarwal et al., 2013;

Cui et al., 2015; Gautam et al., 2013). Among them, the latter stands out due to its biocompatibility, biodegradability, suitable mechanical properties and easy processing ability (Gümüşderelioğlu et al., 2011). PCL with an average molecular weight of 45,000 or 80,000, has been extensively used for electrospinning studies (Aguirre-Chagala et al., 2017; Dulnik et al., 2016; Fereshteh et al., 2016; Gümüşderelioğlu et al., 2011; Srinivasa Reddy et al., 2014). These molecular weights are seen as a more efficient raw material to low molecular weight polycaprolactone (LMW PCL, Mw=14,000 g/mol), for which the electrospinning process is much more complex, thus no electrospinning studies were found to be carried out with this polymer. This may be caused by the formation of beads, which do not allow complex structures to appear, possibly due to PCL's low surface tension or low molecular weight, which would prevent the electrospinning process from taking place continuously. In addition, although low molecular weight PCL indeed showed lower bulk material stiffness, some authors have revealed its good biological activity since, for example, they presented a stronger tendency of cells for chondrogenic differentiation compared to high molecular weight PCL (Guarino et al., 2017; Hendrikson et al., 2015).

On the other hand, among the most used natural polymers, gelatin and collagen stand out for their high compatibility, bioresorbability, non-immunogenicity, and their favorable functional properties, which make them very useful in tissue engineering applications (Aldana and Abraham, 2017; Chen et al., 2016). The combination of these natural polymers with synthetic polymers produce more hydrophilic systems in order to improve cell attachment and growth. For example, gelatin has been combined with PVA to produce systems with a lower contact angle and, therefore, more hydrophilic (Perez-Puyana et al., 2018; Yang et al.,

2007). In this line, both collagen and gelatin have been used with other polymers as PLA (Naghieh et al., 2017) or PCL (Aguirre-Chagala et al., 2017; Gautam et al., 2013; Khajavi et al., 2016) to improve their biological properties for cardiac or bone regeneration applications.

Some authors have reported that the concentration of the polymer is a key factor which influences the formation of a homogeneous fiber mat or circular spheroids interconnected by small fibers (Hekmati et al., 2013; Hossain et al., 2016). As an example, if the solution is highly diluted, the Taylor's cone is broken into droplets as a consequence of an unappropriated balance of forces. Under such conditions, droplets usually reach the collector in a liquid form (Tiwari and Venkatraman, 2012). However, electrospinning does not depend only on the concentration of the polymer solution. Previous studies revealed that there are other important properties, as its surface tension or its conductivity, which also can influence the electrospinning process (Perez-Puyana et al., 2018). However, among them, the viscosity can be highlighted since it depends on the intermolecular interactions in these polymer solutions (Lee et al., 2003). The intermolecular interactions of binary polymer solutions are based on the interactions between the molecules of both polymers, affecting their entanglement. Therefore, the limiting concentration from which homogeneous fibers are obtained may differ depending on the polymer or the solvent used to form the polymeric solution. In general, higher concentrations cause an increase in viscosity (Klossner et al., 2008). Apart from the polymer concentration, the viscosity of the polymeric solution is influenced by the molecular weight since it affects the molecular entanglement. The entanglement concentration (commonly known as Ce) is defined as the point at which the overlap between the polymer chains constrains the

chains' motion and, thus, produces entanglement couplings (Graessley, 1980). In practice, this concentration is the boundary between two of the four different concentration regimes reported by Colby et al. (1991): (i) dilute regime, (ii) semidilute unentangled regime, (iii) semidilute entangled regime and (iv) concentrated regime. More specifically, the entanglement concentration delimits the boundary between regimes (ii) and (iii). Figure 4.2 illustrates the SEM images than can be obtained after applying a high-voltage field to a polymer solution leaving from a syringe pump, as a function of the concentration regime. Although the entanglement concentration is different depending on the working system, McKee et al. (2004) found that a concentration between 2 and 2.5 times the entanglement concentration is necessary to achieve defect-free nanofibrous mats (McKee et al., 2004). This statement has been generally accepted and followed by the electrospinning research community.

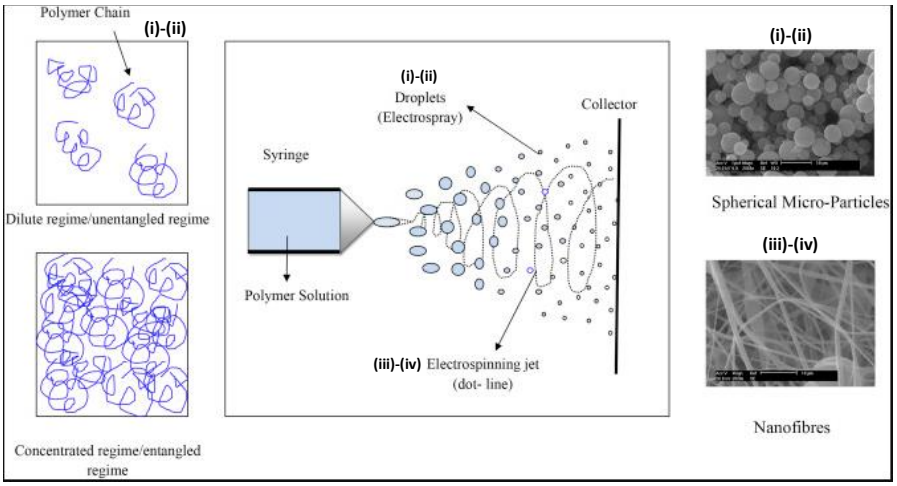

Figure 4.2. Schematic representation of the molecular entanglement and its influence on the electrospinning process. Image obtained from Ghorani and Tucker (2015)

On the other hand, apart from the initial formulation, the properties of the scaffolds can also be tuned by selecting the suitable processing

parameters. Environmental (temperature or humidity) or processing parameters (voltage, working distance, etc.) influence the size of the fibers obtained (Badea et al., 2012; Hossain et al., 2016; Sencadas et al., 2012). Nevertheless, there is a processing variable that affects both the size and the orientation of the fibers, which is the rotational speed of the collector. This results in aligned fiber membranes that allow modifying the mechanical and structural properties of these membranes. This allows encouraging the oriented growth of the cells in the mentioned structures. Despite this, these aligned structures may drive to the formation of non-homogeneous systems. This causes their properties to change depending on the region studied or the direction of application; thus, they have similarities with anisotropic materials.

Thus, the main objective of this chapter is the development of polymeric membranes based on PCL and proteins (gelatin and collagen) by electrospinning with the objective of modeling and evaluating their influence on the physicochemical, microstructural and mechanical properties of the obtained fibers. The influence of the different processing parameters will also be evaluated, paying special attention to the alignment of the fibers and its influence on the properties of the anisotropic scaffolds obtained. Thereby, once the scaffolds were fabricated, a comprehensive characterization was carried out, including physicochemical properties (Water Contact Angle, Energy Dispersive Analysis and Fourier Transform Infrared Spectroscopy), morphological properties (Scanning Electron Microscopy and the analysis of the mean fiber diameter, fiber size distribution, fiber alignment, porosity and mean pore area) and mechanical properties (uniaxial tension tests).

4.2. Materials and methods

4.2.1. Materials

Gelatin protein (GE) is a fish gelatin type B (80-120g Bloom) and it was supplied by Henan Boom Gelatin Co. Ltd (China). On the other hand, type I pork collagen protein HI95 (CG) was supplied by Essentia Protein Solutions (Grasten, Denmark). The use of these polymers was selected according to the initial characterization carried out in Chapter 2. Their complete compositions are also shown in Chapter 2 (Table 2.1). Furthermore, a hydrophobic polymer as Poly(ε-caprolactone) [$(C_6H_{10}O_2)n$] (PCL), was selected as synthetic polymer and purchased from Sigma Aldrich (Germany). Three molecular weights were studied: 14,000 [PCL_{14}]; 45,000 [PCL_{45}] and 80,000 g/mol [PCL_{80}].

In addition, other reagents as 1,1,1,3,3,3-hexafluoro-2-propanol (HFIP), used as solvent, were also purchased from Sigma Aldrich (Germany).

4.2.2. Electrospinning process

During the electrospinning process, a nanofibrous membrane is obtained which can act as a scaffold with potential application in Tissue Engineering. The electrospinning technique requires a previous solution of the polymeric material to be passed into a syringe to carry out the electrospinning process.

An optimal electrospinning process depends on both the properties of the solution and the processing conditions. On the one hand, the properties of the polymer solution, such as viscosity, surface tension, conductivity, etc. may exert a strong influence on the electrospinning process. Unfortunately, all the polymer solutions were prepared with HFIP, which presents the drawback of being highly volatile, which makes it more difficult to measure all these properties. On the other hand, the control

of the processing parameters is indispensable since there are certain parameters (voltage, flow, etc.) that are intimately related to the properties and characteristics of the fibers obtained by electrospinning. For this reason, different processing conditions were studied by analyzing each parameter which can affect the electrospinning process: Humidity (30-50%), flow rate (0.2-0.8 mL/h), working distance (11-17 cm) and voltage (10-18 kV). The temperature was fixed at 25 ºC and a 10 mL syringe with an 18G stainless steel needle (inner diameter 0.5 mm) was used.

Preliminary studies were performed using a NE-300 Pump System (New Era Pump Systems, USA) as the syringe pump and an HV-Power Supply 0-25kV (PHYWE, Germany) as the voltage supplier. On the other hand, the main studies concerning PCL were carried out with a Fluidnatek LE-100 equipment (Bioinicia).

4.2.3. Characterization of nanofibrous scaffolds

FTIR measurements were carried out to evaluate the presence of proteins in the scaffolds by measuring the chemical bonds present. This analysis was carried out using an iS50 ATR-FTIR spectrophotometer (Nicolet, Thermo Scientific, USA) (Figure 4.3). The different spectra were collected in the range of 4000-500 cm^{-1}.

Figure 4.3. iS50 ATR-FTIR spectrophotometer (Nicolet)

4.2.3.2 Water Contact Angle (WCA)

Scaffolds wettability and hydrophobicity were assessed by water contact angle (WCA) measurements using a Drop Shape Analyzer (Krüss, Germany) (Figure 4.4).

Figure 4.4. Drop Shape Analyzer (Krüss)

The WCA was measured using the sessile drop method (droplets with an approximate volume of 5 μL). Both WCA values of the right and left sides of the deionized water droplets were measured and the average value was calculated as it can be seen schematically in Figure 4.5.

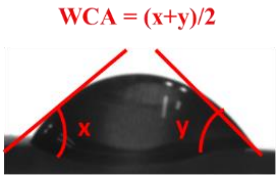

Figure 4.5. Illustration about the calculation of the water contact angle (WCA)

4.2.3.3. Viscosity

The polymer chain entanglement was determined by measuring the viscosity of the solutions. Viscosity measurements of unitary solutions of PCL and Gelatin as well as binary systems produced with the combination of both polymers were measured with an Ubbelohde glass capillary viscometer (VWR, Avantor, The Netherlands) (Figure 4.6).

Figure 4.6. Ubbelohde glass capillary viscometer (VWR, Avantor)

All the measurements were carried out at 20±2 ºC. The specific viscosity (η_{sp}) was obtained using the following equation (Rey et al., 1996):

$$\eta_{sp} = \frac{\eta - \eta_0}{\eta_0} \cdot 100 \qquad (4.1)$$

Where η is the viscosity of the solution (Pa·s) and η_0 is the viscosity of the solvent used (1.65 mPa·s at 20 °C for HFIP).

4.2.3.4 Microscopy evaluation

Scanning Electron Microscopy (SEM): Microscopy examination of scaffolds was assessed with an XL 30 Microscope (Philips XL Series, The Netherlands) at an acceleration voltage of 15 kV (Figure 4.7).

Figure 4.7. XL 30 Microscope (Philips XL Series)

The samples were covered with a film of gold in a high-resolution sputter coater. A digital processing software, ImageJ, was used to determine the mean fiber size (mean diameter of the fibers), fiber size distribution

(diameter distribution of the nanofibrous scaffolds), scaffolds porosity and mean pore area (space left between the fibers). Furthermore, the uniformity of the systems was also evaluated as (Eq. 4.2):

$$Uniformity = (1 - \frac{Standard\ deviation}{Mean\ value}) \cdot 100 \qquad (4.2)$$

Apart from that, the orientation/alignment is measured with ImageJ by the coherency of the fibers, taking values from 0 to 1, where 0 corresponds to a random distribution and 1 is referred to a complete alignment.

Energy Dispersive X-ray Spectroscopy (EDAX): The atomic compositions of the membrane were examined with the energy dispersive spectroscopy capability of the SEM equipment using an EDAX Si(Li) detector and an acceleration voltage of 5 kV. The samples were covered with a film of gold in a high-resolution sputter coater. This technique allows determining the presence of atomic nitrogen in the sample, as a direct measure of the protein content in the electrospun systems.

4.2.3.5 Mechanical characterization

Tensile tests were performed using an ElectroForce 3200 (TA Instruments, USA) (Figure 4.8A), evaluating the evolution of the tensile load with the strain. The extensional rate was 0.1 mm·s^{-1} at 20 ºC.

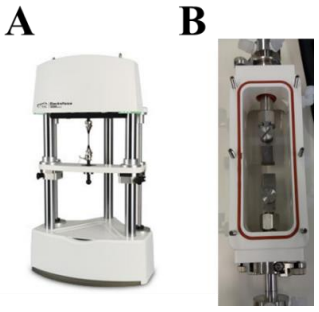

Figure 4.8. Electroforce 3200 and wet chamber used

From the different measurements, three parameters were obtained: Young's modulus, maximum stress and strain at break. An example curve has been included in which the parameters have been remarked (Figure 4.9): Young's modulus (E), maximum stress (τ_m) and strain at break (ε_m).

The mechanical characterization was performed in both dry and wet conditions using a wet chamber (Figure 4.8B) to carry out the experiments in PBS medium simulating the conditions of the scaffolds in a bioreactor. PBS (phosphate-buffered saline) is a buffer solution based on a water-based salt solution containing disodium hydrogen phosphate or sodium chloride among other salts.

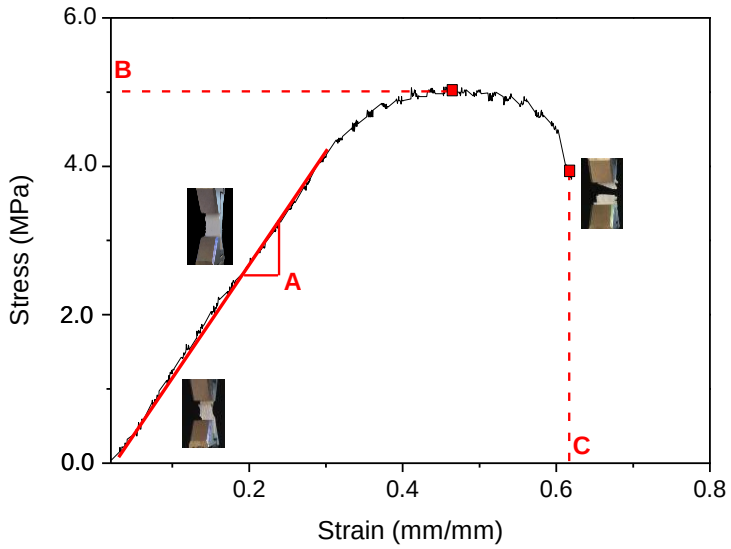

Figure 4.9. Example of the strain-stress curve obtained, and the parameters evaluated: Young's modulus (E), maximum stress (τ_m) and strain at break (ε_m)

Furthermore, a cyclic loading test was also performed for some selected systems. The cyclic loading tests allow proving if the structure of the material remains unalterable by measuring the stress over the cycles. In addition, the coupling between the stress and the elongation also allows

determining if the measurements have been performed in the viscoelastic region on the sample. Specifically, a total of 500 cycles were performed at a constant strain of 10 %. Subsequently, a tensile test was carried out to evaluate the variation suffered in the properties of the scaffolds when a cyclic loading test is previously performed.

4.2.4. Statistical analysis

At least three replicates were carried out for each measurement. Student´s t-test and one-way analysis of variance ($p<0.05$) were performed using PASW Statistics for Windows (Version 18: SPSS, Chicago, IL). Standard deviations were calculated for selected parameters.

4.3. Results and Discussion

4.3.1. Effect of the molecular weight of PCL

The molecular weight of a polymer is one of the intrinsic parameters which influence the electrospinning process to a larger extent. Polymers require a certain molecular weight to ensure the molecular entanglement which enables electrospinning to be conducted properly and continuously. As a matter of fact, a first approach in this technique has been produced by studying the influence of the molecular weight of PCL. Thus, three commercial PCL polymers with different molecular weights (14, 45 and 80 kDa), denoted respectively as PCL_{14}, PCL_{45} and PCL_{80}, were used at a total polymer concentration of 16% to produce and characterize electrospun scaffolds.

The electrospinning process was carried out using the following processing conditions: 14 kV of voltage, 0.4 mL/h of flow rate and 14 cm as the needle-collector distance.

4.3.1.1. Functional evaluation

Figure 4.10 shows the evolution of the contact angle of PCL-based membranes generated with PCL of different molecular weights.

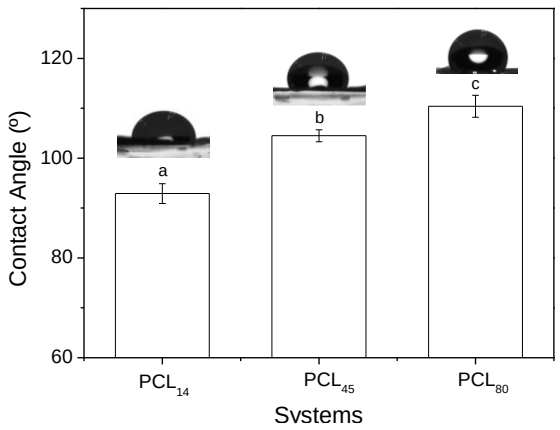

Figure 4.10. Contact Angle of PCL-based scaffolds with different molecular weights (14, 45 and 80 kDa)

The results evidence that the increase in the molecular weight produces an increase in the contact angle and, for that matter, in the hydrophobicity of the scaffolds, since a higher molecular weight implies a longer polymer chain and, therefore, an increase of the hydrophobic character of the polymer.

4.3.1.2. Microstructural evaluation

The SEM images of the different systems are shown in Figure 4.11.

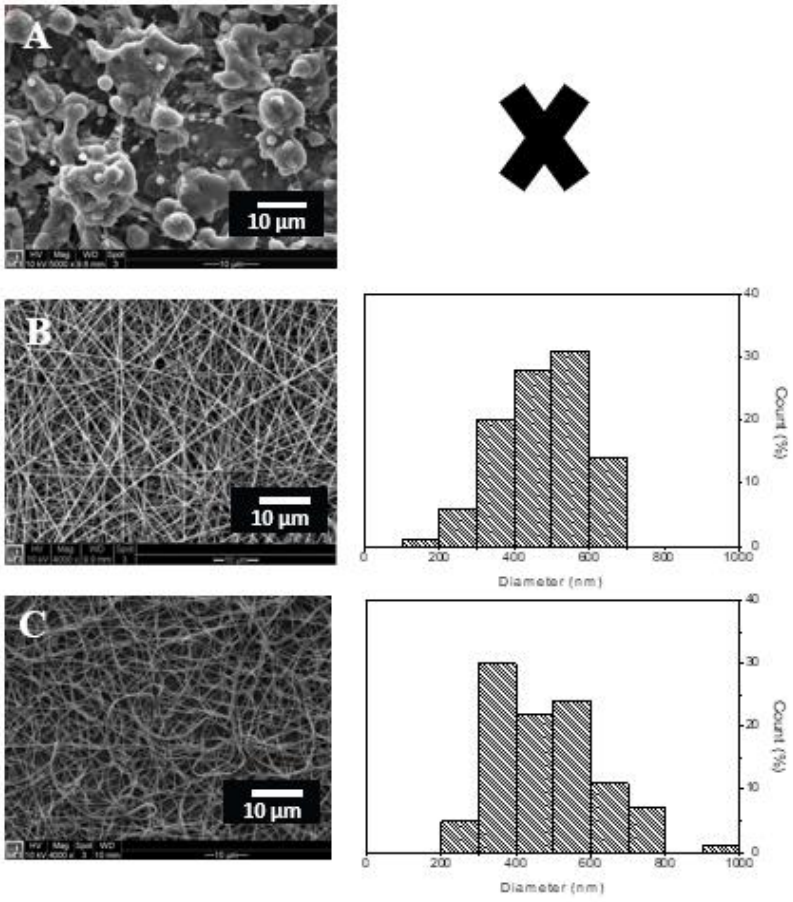

Figure 4.11. SEM images and fiber size distribution of the scaffolds processed with PCL of different molecular weights: (A) PCL_{14}; (B) PCL_{45}; (C) PCL_{80})

The electrospinning was not properly fulfilled for the system with the lowest molecular weight, improving the process by increasing the molecular weight of PCL, which results in mats constituted by

homogeneous fibers. Besides, the fiber analysis carried out with ImageJ software allows obtaining the fiber size distribution of the three samples (shown in Figure 4.11). The images observed in the figure showed the impossibility to obtain homogeneous fibers using PCL_{14}. Nevertheless, a more homogeneous distribution is found for the PCL_{45} since its profile is unimodal towards 400 nm, whereas the system obtained with PCL_{80} presented a bimodal profile with a higher heterogeneity. In addition, the mean fiber diameter, as well as the mean pore area and porosity, of the scaffolds were also calculated (results shown in Table 4.1).

Table 4.1. Mean fiber diameter, mean pore area and porosity values obtained of PCL-based scaffolds with different molecular weights (14,000; 45,000; 80,000). *means that no suitable scaffolds could be obtained

SYSTEM	**Mean fiber diameter (nm)**	**Mean Pore area (nm^2)·10^6**	**Porosity (%)**
PCL_{14}	*	*	*
PCL_{45}	451 ± 112^{a}	3.0 ± 1.3^{A}	$60.9 \pm 1.8^{\alpha}$
PCL_{80}	513 ± 159^{a}	2.1 ± 1.1^{A}	$51.3 \pm 0.9^{\beta}$

As can be seen, although there are no significant differences due to the high dispersion of sizes, mats of fibers with a trend towards higher size are obtained when the molecular weight is higher. Consequently, scaffolds with lower mean pore size and porosity are obtained when using PCL with a higher molecular weight.

4.3.1.3. Mechanical evaluation

Strain-stress curves of PCL-based scaffolds with different molecular weights (45 and 80 kDa) are shown in Figure 4.12. Both systems had a first elastic zone (more pronounced for the PCL_{80} system), where the strain could be recovered over time. In this zone, a linear relationship was maintained between strain and stress, thus making it possible to obtain the Young's modulus of the different scaffolds. Then, a

smothering of the slope leads to a plastic region, which remained until the breakage of the scaffold.

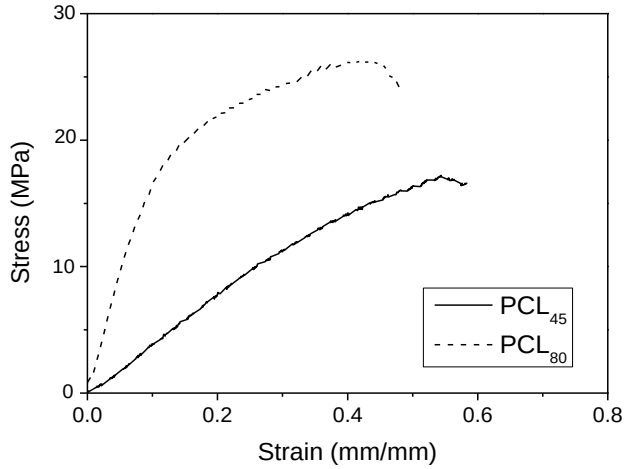

Figure 4.12. Strain-stress curves obtained from the mechanical testing performed to PCL-based scaffolds with different molecular weights (45 and 80 kDa)

The parameters (Young's modulus, strain at break and maximum stress) obtained from the mechanical testing of the PCL-based scaffolds are summarized in Table 4.2. As can be seen, there is an increase in Young's modulus and maximum stress with the increase in the molecular weight, although the strain at break is lower.

Table 4.2. Young's modulus, strain at break and maximum stress values obtained of PCL-based scaffolds with different molecular weights (14,000; 45,000; 80,000). *means that no suitable scaffolds could be obtained. Values with different letters are significantly different ($p<0.05$)

SYSTEM	Young's modulus (MPa)	Strain at break (%)	Maximum stress (MPa)
PCL_{14}	*	*	*
PCL_{45}	36.1 ± 5.1^{A}	56.9 ± 5.3^{a}	$12.9 \pm 1.8^{\alpha}$
PCL_{80}	170.8 ± 23.8^{B}	51.7 ± 9.2^{a}	$21.9 \pm 6.5^{\beta}$

In conclusion, stiffer and less deformable scaffolds are obtained when the molecular weight of the polymer is higher.

4.3.2. Influence of the combination of 2 polymers: PCL_{14} and gelatin

As shown in the previous section, the polymer molecular weight plays a role in the development of electrospun fibers. However, if the desired polymer is combined with another polymer the electrospinning process might be improved and, as a result, the properties of the scaffolds could be enhanced. As an example, in the previous section was observed the impossibility to obtain homogeneous fibers using PCL_{14}. In this sense, a further study was carried out using PCL with the lowest molecular weight (PCL_{14}) by its combination with gelatin to improve the electrospinning process. It has to be born in mind that the scaffolds based only on gelatin could not be either obtained. Therefore, scaffolds with combinations of PCL_{14} and gelatin in different ratios were performed. The different systems processed are shown in Table 4.3:

Table 4.3. PCL_{14}, gelatin and total polymer concentration for the different PCL/Gelatin ratios and concentrations studied

System	PCL/GE Ratio	PCL concentration (w/v%)	Gelatin concentration (w/v%)	Total Polymer concentration (w/v%)
12/4	3:1	12	4	16
16/4	4:1	16		20
20/4	5:1	20		24
24/4	6:1	24		28
32/4	8:1	32		36
32/6	6:1*		6	36
32/6	5:1*		6.4	38.4
32/8	4:1*		8	40
32/10	3:1*		10.7	42.7

Two different studies were performed, based on the polymer whose concentration was increased in order to obtain different PCL/GE ratios. The first study was carried out at constant GE concentration (12/4; 16/4;20/4; 24/4 and 32/4) and the second one at constant PCL content (32/4; 32/6 and 32/10).

All the electrospun systems were processed using the following processing conditions: 14 kV of voltage, 0.4 mL/h of flow rate and 14 cm as the needle-collector distance.

4.3.2.1. Functional evaluation

In addition to the microstructural characterization of the membranes, water contact angle (WCA) and EDAX measurements of the PCL/GE systems were also evaluated.

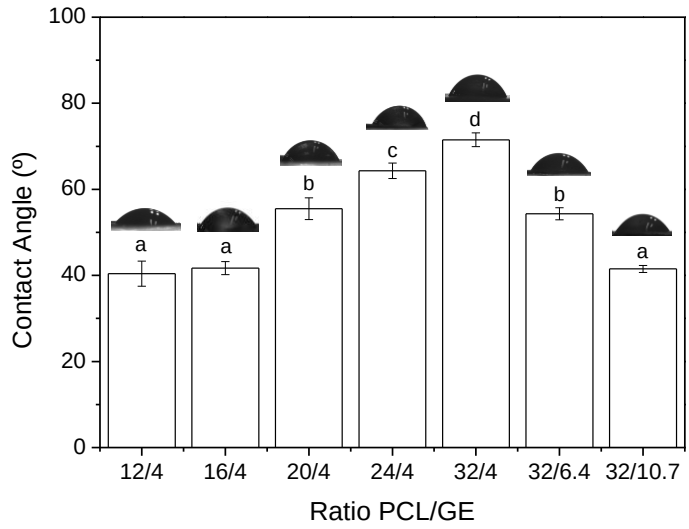

Figure 4.13. Water Contact Angle values of the structures processed with different PCL/GE ratio: 12/4 (3:1), 16/4 (4:1), 20/4 (5:1), 24/4 (6:1) and 32/4 (8:1), 32/6.4 (5:1*) and 32/10.7 (3:1*)

Figure 4.13 shows how the value of the contact angle increased when the ratio between the polymers was higher, due to the presence of the hydrophobic polymer (PCL) in a higher concentration compared to the concentration of gelatin, which is the hydrophilic polymer of the mixture.

For that reason, the contact angle varied (almost doubled) comparing the values obtained for the systems with the lowest (ca 40º, ratio 3:1) and the highest (ca 75º, ratio 8:1) ratio between PCL and gelatin. Moreover, an evolution towards a more hydrophilic system took place when the concentration of gelatin was increased, switching from ca 70º (8:1 system) to ca 40º (3:1* system). Furthermore, similar contact angle values were obtained for the systems processed with a similar PCL/GE ratio. Perhaps the increase in protein concentration would have produced more hydrophilic membranes with suitable contact angle values to improve muscle cell adhesion (Quigley et al., 2013).

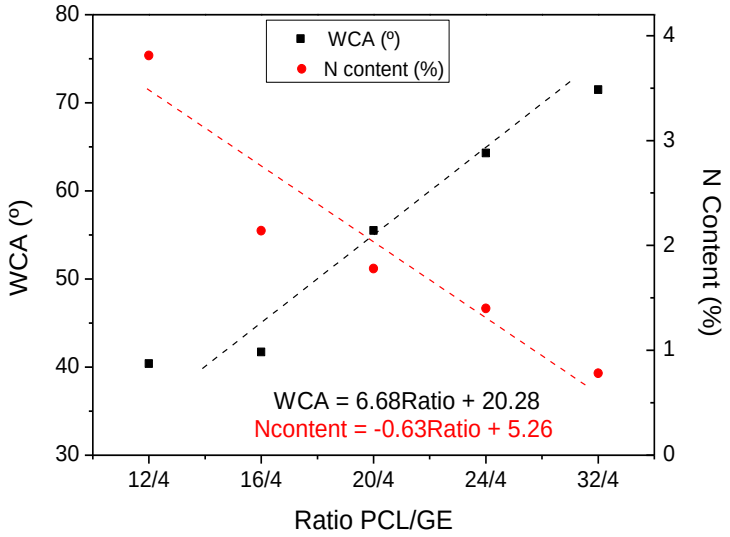

Figure 4.14. Correlation between the WCA and N content of the membranes processed with different PCL/GE ratio: 12/4 (3:1), 16/4 (4:1), 20/4 (5:1), 24/4 (6:1) and 32/4 (8:1)

Figure 4.14 shows the evolution of the Nitrogen content (N content) and Water Contact Angle (WCA) as a function of the PCL/GE ratio. Considering the contact angle values obtained for the systems elaborated with PCL/GE ratios from 3:1 to 8:1, it was possible to establish a

correlation between the ratio used and the contact angle achieved (Figure 4.14), obtaining the following equation (Eq. 4.3):

$$WCA = 6.68 \cdot (PCL/GE) + 20.28 \qquad (4.3)$$

Eq. 3 shows how an increase in the ratio between PCL and gelatin produces an increase in the contact angle since the system obtained is more hydrophobic due to the greater presence of PCL. In addition, a linear trend is followed which justified that the protein was homogeneously distributed regardless of the PCL/GE ratio.

On the other hand, the relation between PCL and gelatin can be identified by the presence of nitrogen in it. Thus, an EDAX analysis was conducted to confirm that the electrospun fibers contained proteins in their structure. The nitrogen present in the surface obtained from the EDAX profiles was shown in Figure 4.14, with an obvious decrease in N when the ratio between the two polymers is higher. The results shown in Figure 4.14 conclude that there is a decreasing linear trend (Eq. 4.4):

$$Ncontent = -0.63 \cdot (PCL/GE) + 5.26 \qquad (4.4)$$

which shows that by increasing the PCL/GE ratio used, the amount of nitrogen is lower compared to the PCL present.

4.3.2.2. Microstructural evaluation

Figure 4.15 shows the evolution of the PCL-based membranes generated with a constant amount of gelatin (4 %) and increasing concentrations of PCL_{14} (12/4 [ratio 3:1], 16/4 [ratio 4:1], 20/4 [ratio 5:1], 24/4 [ratio 6:1] and 32/4 [ratio 8:1]). SEM images in Figure 4.12 show how the increase in the PCL/GE ratio led to an improved electrospinning process, with the formation of a homogeneous fiber-based mat, until a specific polymer/protein ratio. Interestingly, the process was optimal when a specific ratio was used. In fact, the process improved up to the 6:1 ratio

(PCL 24% and gelatin 4%), from which the formation of fibers started to be heterogeneous again for the processing conditions used in this study. This homogeneity found for the systems with ratio 5:1 is also observed in the fiber size distribution (Figure 4.14), in which a narrower distribution is observed towards a central value (0.5 µm).

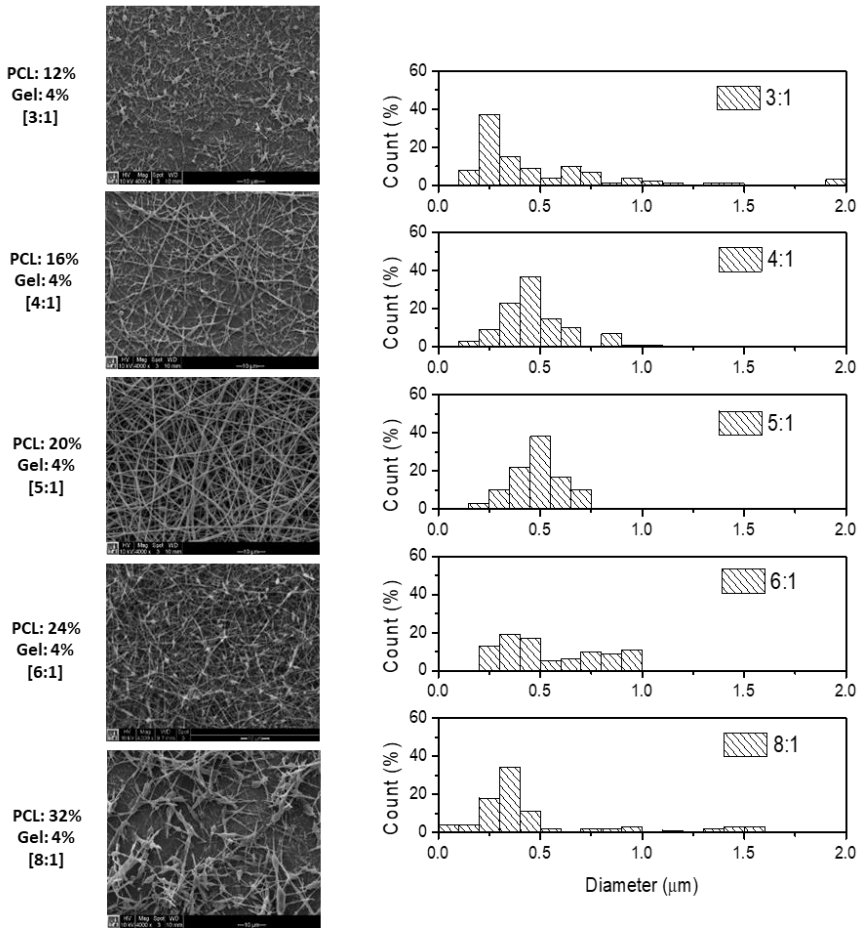

Figure 4.15. SEM images and fiber size distributions of the membranes generated with mixed PCL/GE systems with different ratios: 12/4 (3:1), 16/4 (4:1), 20/4 (5:1), 24/4 (6:1) and 32/4 (8:1)

On the other hand, when the ratio is higher than 5:1 (6:1 and 8:1), the distribution widens, giving rise to a system with more heterogeneous fiber sizes that encourage the formation of new spheroids among them.

A similar study was carried out, this time increasing the concentration of the natural polymer (gelatin) and maintaining a constant amount of PCL (32 %), obtaining the same ratios studied previously. The 32 % PCL system is also included to compare and analyze the influence of gelatin.

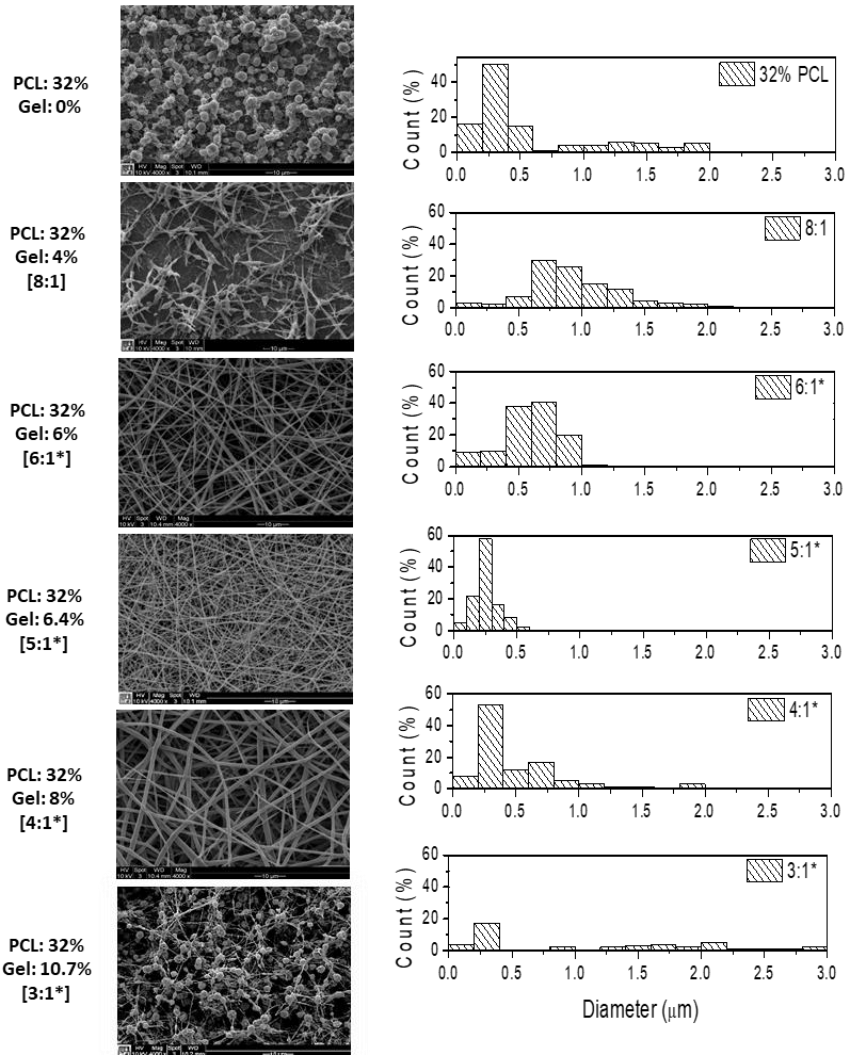

Figure 4.16. SEM images and fiber size distributions of the membranes generated with mixed PCL/GE systems with different synthetic/natural polymer ratios: 32/4 (8:1), 32/6 (6:1*), 32/6.4 (5:1*), 32/8 (4:1*) and 32/10.7 (3:1*)

The SEM images and fiber size distributions of these systems are shown in Figure 4.16. The systems containing only PCL presented a structure

formed mainly by spheroids. However, the addition of gelatin to a constant concentration of PCL (32 %) tended to evolve from membranes with heterogeneous fibers (system 8:1) to membranes formed by spheroids and small fibers (system 3:1*), moving through intermediate systems (6:1*, 5:1* and 4:1*) in which homogeneous fibers were obtained. The improvement exhibited by the electrospinning process can also be observed in the fiber size distributions.

In addition, the systems processed with a similar ratio can also be compared between them. A similar Gaussian distribution was found for the systems obtained by adding different gelatin concentrations (ratios 4:1*, 5:1* and 6:1*), although the Gaussian curve widens towards higher diameters for the 3:1* systems due to the presence of spheroids in the structure.

Furthermore, the effect of the PCL/GE ratio can also be seen by evaluating the size of both the fibers and the beads. These sizes were measured in the mixed PCL/GE systems (Table 4.4). Two complementary effects took place: the increase of the PCL/GE ratio produced an increase in the mean fiber diameter (reaching the maximum at the 4:1 ratio) in addition to avoiding the formation of beads for the 4:1 and 5:1 PCL/GE systems. However, increasing the PCL/GE ratio over 5:1 allows the reappearance of the beads (together with a trend to decrease the mean fiber diameter). This is most likely due to the transformation of the spheroids into homogeneous fibers, which explains the increase in size observed for the 4:1 and 5:1 systems, in which the formation of these spheroids was not observed. Remarkably, in the systems with the highest ratios (6:1 and 8:1) the formation of spheroids was again observed. These were larger for the 8:1 ratio, which is combined with the new decrease in the size of the fibers generated.

Table 4.4. Mean fiber diameter and mean bead size of membranes processed with different PCL and gelatin percentages and PCL/GE ratios: 12/4 (3:1), 16/4 (4:1), 20/4 (5:1), 24/4 (6:1) and 32/4 (8:1), 32/6 (6:1*), 32/6.4 (5:1*), 32/8 (4:1*) and 32/10.7 (3:1*)

Systems	Ratio	Mean fiber diameter (nm)	Mean bead size (nm)
PCL (12%) Gelatin (4%)	3:1	288 ± 86	807 ± 223
PCL (16%) Gelatin (4%)	4:1	485 ± 170	-
PCL (20%) Gelatin (4%)	5:1	445 ± 91	-
PCL (24%) Gelatin (4%)	6:1	343 ± 95	874 ± 176
PCL (32%) Gelatin (4%)	8:1	308 ± 100	1.460 ± 450
PCL (32%) Gelatin (6%)	6:1*	590 ± 218	-
PCL (32%) Gelatin (6.4%)	5:1*	357 ± 93	-
PCL (32%) Gelatin (8%)	4:1*	724 ± 376	-
PCL (32%) Gelatin (10.7%)	3:1*	290 ± 107	1.299 ± 328

Furthermore, the homogeneity of the fibers obtained was analyzed with the calculation of the uniformity (Figure 4.17). A Gaussian tendency is shown, reaching the maximum values for the 5:1 and 5:1* ratios (445 and 357 nm, respectively). It should be noted that systems with intermediate ratios have a tendency towards smaller fiber sizes and more homogeneous distribution (higher uniformity value). Therefore, using a PCL/GE ratio other than 5:1 would result in a fiber mat with larger fiber sizes and greater heterogeneity. Interestingly, the systems produced with 3:1 and 8:1 PCL/GE ratios led to less than 40 % uniformity and mean fiber sizes higher than 550 nm. This is most likely due to the emergence

of spheroids, which increased the mean fiber size and decrease the homogeneity of the system.

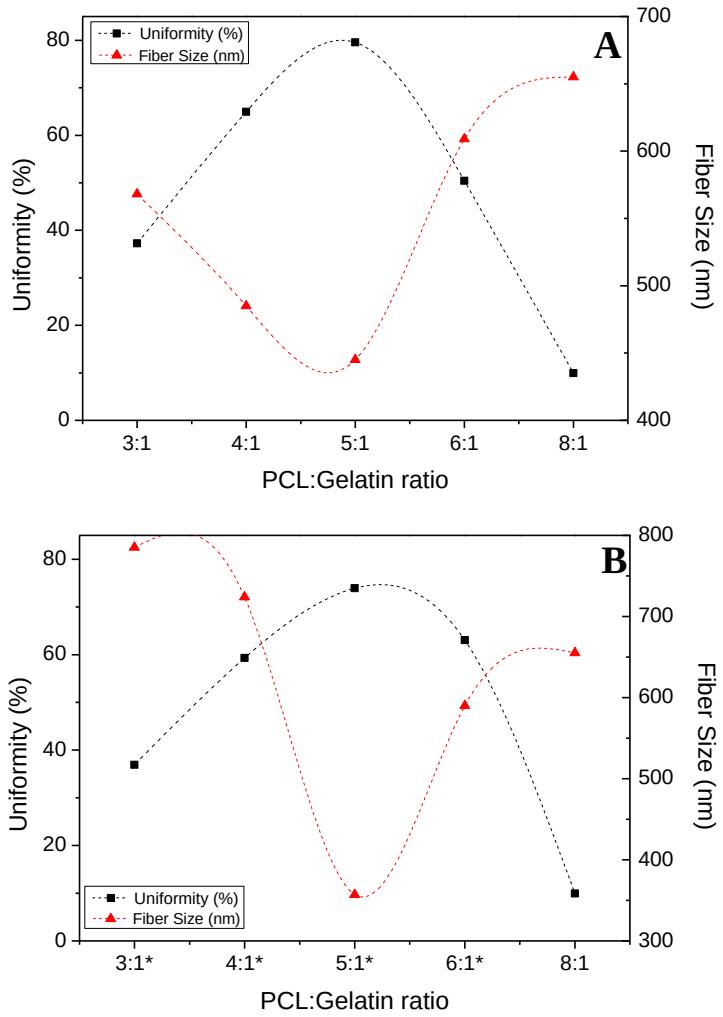

Figure 4.17. Relation between the uniformity (%) and mean fiber size (nm) of the membranes processed with different PCL/GE ratio by increasing the (A) PCL content: 12/4 (3:1), 16/4 (4:1), 20/4 (5:1), 24/4 (6:1) and 32/4 (8:1) and (B) Gelatin content: 32/6 (6:1*), 32/6.4 (5:1*), 32/8 (4:1*) and 32/10.7 (3:1*)

4.3.2.3. Viscosity measurements

As mentioned above, some authors have defined the electrospinning process as a function of the properties of the previous solutions prepared. In this way, two parameters can be highlighted: polymer concentration

and solution viscosity. Both parameters are interconnected, giving rise to a correlation with the minimum concentration needed to achieve a suitable solution viscosity in order to carry out the electrospinning process properly. Therefore, the viscosity of the polymer solutions at different concentrations was measured, and the results obtained are shown in Figure 4.18.

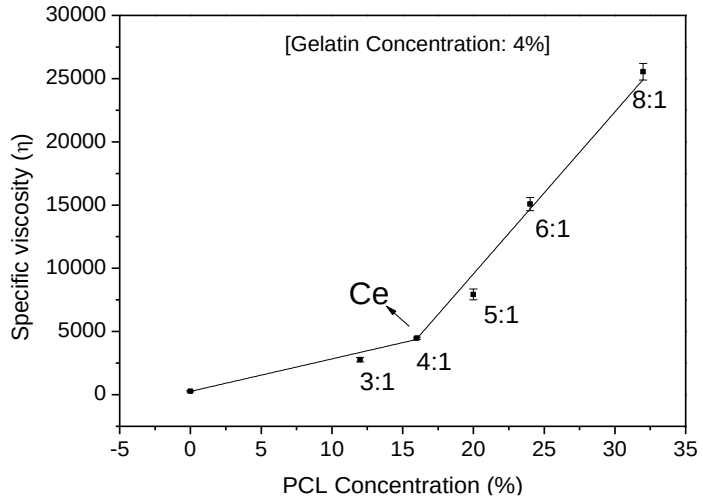

Figure 4.18. Evolution of the specific viscosity of binary systems PCL/GE as a function of the PCL concentration at a constant gelatin concentration of 4%.

Figure 4.18 shows the evolution of the specific viscosity of the systems produced with 4% of gelatin and increasing concentrations of PCL (from 12 to 32 %). A shift in the slope can be observed at a concentration value of 16 %, obtaining two well-differentiated regions. Considering the study conducted by Colby et al., (1991), these regions can be correlated with the regimes found for unitary systems formed by linear polymers. The first region corresponds to the semidilute unentangled regime (region ii) until the concentration of PCL is 16 %, at which the chains started to entangle. As a consequence, the viscosity of the solutions exponentially increases, obtaining a second region called the semidilute entangled

regime (region iii) in which the electrospinning process should be properly carried out. Therefore, the combination of 4% of gelatin and 16% of PCL can be considered as the entanglement concentration (Ce, 20% of total polymer concentration).

For a better comprehension of the results obtained for the binary systems, the viscosity of unitary solutions of PCL and Gelatin (with the same concentrations as the binary systems previously studied) was also measured to evaluate the different regimes for these polymers (Figures 4.19 and 4.20, respectively).

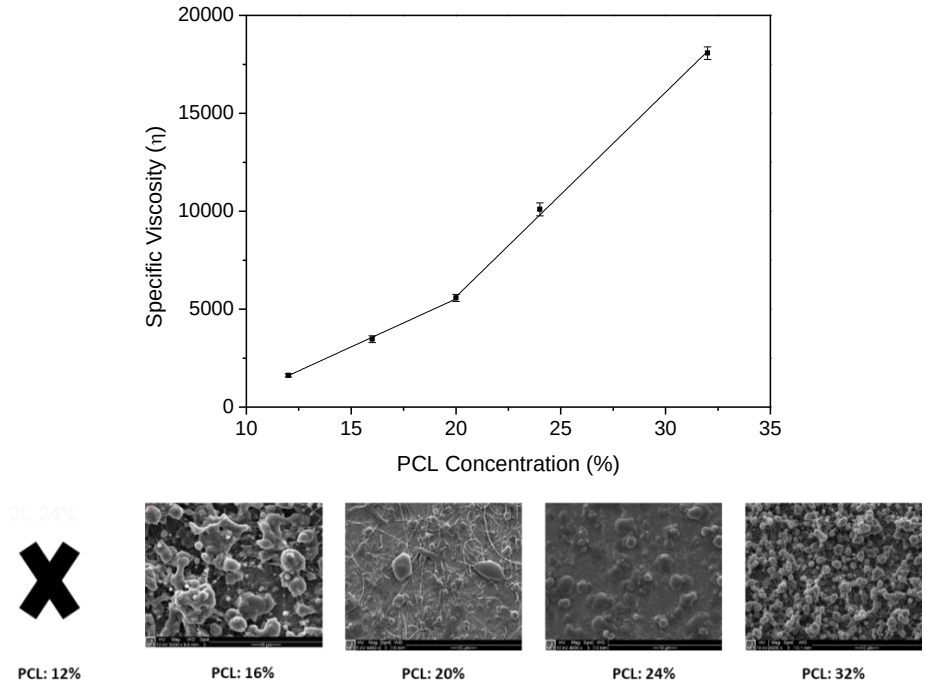

Figure 4.19. Evolution of the specific viscosity and SEM images of unitary PCL systems at different concentrations

Figure 4.19 shows the results obtained for unitary PCL systems. Once again, a shift in the slope is observed at 20 % PCL concentration, showing the same two regions as the ones shown in Figure 4.18 for the binary system PCL/GE. From the viscosity results obtained, the

homogeneity found in SEM images for the systems 5:1 and 6:1 can be explained because the total polymer concentration is 1.25 and 1.50 times the entanglement concentration, both values in the suitable electrospinning range found by Kong and Ziegler, (2014), who determined that to spin good fibers the concentration had to be 1.2-2.0 times the entanglement concentration.

On the other hand, the viscosity of unitary solutions of gelatin was plotted in Figure 4.20. The results show an initial linear region up to a concentration of 8 %, from which the viscosity increases sharply.

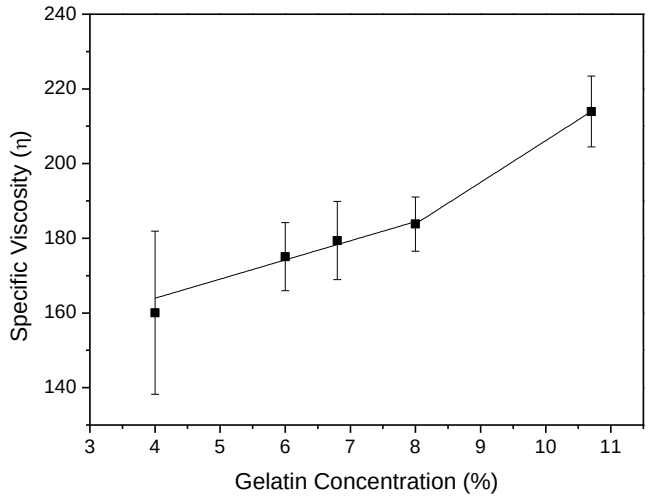

Figure 4.20. Evolution of the specific viscosity of unitary gelatin systems at different concentrations

These results may explain the SEM images shown in Figure 4.16, in which different concentrations of gelatin (4, 6, 6.4, 8 and 10.7 %) were added to a constant concentration of PCL (32 %). The electrospinning process was not properly obtained for the systems with a gelatin concentration up to 4%, from which homogeneous fibers with no beads could be obtained (using gelatin concentrations from 6 to 8%). However, from this concentration on, homogeneity is lost again, and beaded

membranes are obtained, with the subsequent decrease in uniformity. These beads may be formed since gelatin molecules start to interact with each other. This could be linked to the increase found in the viscosity of the gelatin solution when the concentration was higher than 8 %.

Since this study has been produced with a binary system (PCL and gelatin), it has been proved how the total polymer concentration affects the homogeneity of the fiber formation, but also the ratio between the polymers when using a binary system has been demonstrated to be a key factor since the 4:1 and 5:1 ratios are found to be the most suitable. These ratios can be highlighted because the use of a higher ratio increases the viscosity of the solution, increasing the heterogeneity of the system and worsening the fiber formation.

4.3.3. Influence of the processing conditions

It is generally admitted that the selection of suitable processing conditions is a key stage in the electrospinning process because they could exert a strong influence on the properties of the obtained fibers (Duque Sánchez et al., 2014). Hence, the influence of the different processing conditions on the properties of hybrid PCL/GE electrospun fibrous mats was assessed in this section. Taking into account the results obtained in previous sections, the polymers selected for this study were PCL_{45} and Gelatin at the ratio 16/4 (4:1). The different parameters were evaluated by analyzing the fiber properties of the membranes. Thus, scaffolds were produced varying the humidity, flow rate, working distance and voltage during the electrospinning process. As a summary, all the properties of the systems produced varying the processing conditions have been included in Table 4.5.

Table 4.5. Summary of properties of PCL_{45}/GE (16/4) scaffolds obtained with different processing conditions: Relative Humidity, Flow rate, Working distance and Voltage. Values with different letters are significantly different ($p<0.05$)

Processing Parameter		**Mean fiber diameter (nm)**	**Porosity (%)**	**Pore Area (nm^2)**	**Contact Angle (º)**
Relative Humidity (%)	30	326 ± 73 ^{a}	51.0 ± 1.2 $^{\beta}$	737 ± 387 ^{A}	44.6 ± 0.3 ^{c}
	40	307 ± 89 ^{a}	50.1 ± 0.2 $^{\beta}$	780 ± 420 ^{A}	51.7 ± 1.5 ^{f}
	50	476 ± 107 ^{a}	49.9 ± 0.1 $^{\alpha\beta}$	776 ± 432 ^{A}	34.1 ± 0.5 ^{a}
Flow Rate (mL/h)	0.2	267 ± 76 ^{a}	54.4 ± 0.3 $^{\gamma}$	805 ± 266 ^{A}	55.6 ± 0.2 ^{g}
	0.4	307 ± 89 ^{a}	50.1 ± 0.2 $^{\beta}$	780 ± 420 ^{A}	51.7 ± 1.5 ^{f}
	0.8	352 ± 129 ^{a}	49.1 ± 0.6 $^{\alpha}$	916 ± 463 ^{A}	36.6 ± 0.8 ^{b}
Working Distance (cm)	11	338 ± 121 ^{a}	49.7 ± 0.4 $^{\alpha\beta}$	819 ± 341 ^{A}	35.6 ± 0.5 ^{b}
	14	307 ± 89 ^{a}	50.1 ± 0.2 $^{\beta}$	780 ± 420 ^{A}	51.7 ± 1.5 ^{f}
	17	291 ± 94 ^{a}	54.0 ± 1.8 $^{\gamma}$	598 ± 378 ^{A}	58.0 ± 1.2 ^{h}
Voltage (kV)	10	373 ± 147 ^{a}	50.2 ± 0.4 $^{\beta}$	1620 ± 690 ^{A}	48.7 ± 0.4 ^{e}
	14	307 ± 104 ^{a}	50.1 ± 0.2 $^{\beta}$	780 ± 420 ^{A}	51.7 ± 1.5 ^{f}
	18	384 ± 135 ^{a}	49.8 ± 0.9 $^{\alpha\beta}$	942 ± 501 ^{A}	45.5 ± 0.3 ^{d}

No significant differences have been found for the size of the electrospun fibers with any of the processing variables studied (a similar effect takes place on the pore area). In the first place because extreme experimental conditions were avoided and secondly because the dispersion of the fiber diameters is generally very broad. However, some tendencies may be distinguished that coincide with the typical behavior reported in the literature.

Considering the effect of the humidity on the scaffolds, it can be highlighted how the increase in the humidity showed a tendency to increase in the fiber diameter (although the differences are not significant, $p<0.05$) because the evaporation rate of the solvent is higher when working at a reduced humidity (Pham et al., 2006). It is important to mention that the electrospinning process could not be properly achieved at humidity values higher than 50 % (data not shown). In addition, the decrease observed in the contact angle values with the increase in the humidity may be because a higher humidity induced the formation of more hydrophilic systems which, therefore, presented a lower water contact angle.

On the other hand, a similar effect took place by decreasing the working distance or increasing the flow rate related to the solvent evaporation. The increase in the flow rate, or the decrease in the working distance, caused that the solvent does not have enough time to evaporate during the electrospinning process, which translated into larger fibers with a greater hydrophilic character. Interestingly, the formation of larger fibers results in systems with lower porosity.

In addition to these parameters, the voltage plays an important role during the electrospinning process and still today generates controversy in the scientific community. Some authors claim that the application of

a high voltage produces fibers with a higher diameter because more fluid is ejected during the process (Huang et al., 2003), although others suggest that an increase in voltage decreases the diameter of the nanofibers (Sencadas et al., 2012). The results shown in Table 1 highlight that in the range between 10 and 18 kV, there were no significant differences neither in the fiber size nor the porosity ($p<0.05$). However, the use of higher voltages (14-18 kV) produced structures with a lower pore area (from ca 1600 to ca 800-950 nm^2).

According to Dowling et al. (2011), a suitable contact angle should be in the range between 40-65º to improve cell adhesion and proliferation; whereas Kitsara et al. (2017) and Quigley et al. (2013) showed suitable results with muscle cells using fibers with a diameter between 250-300 nm. Considering these properties and the ones obtained with the different processing conditions studied, the most suitable processing conditions to select were the following:

14 kV of voltage, with a flow rate of 0.4 mL/h and a needle-collector distance of 14 cm. The humidity was set at 40 %.

4.3.4. Influence of the addition of gelatin and collagen

As commented before, the combination of different polymers may enhance the properties of the scaffolds produced, even more, when combining synthetic and natural polymers in order to produce hybrid scaffolds with a mixture of properties from both sides. In addition, as observed in section 4.3.2, the addition of protein to the initial formulation can improve the electrospinning process in order to obtain homogeneous nanofibrous scaffolds. Thus, systems with PCL_{45} and gelatin or collagen were prepared in order to study the influence of gelatin (denoted as PCL/GE) and collagen (denoted as PCL/CG) on PCL scaffolds. Scaffolds with a constant concentration of PCL (16 w/v%) and different protein content (2 and 4 w/v%) were prepared and characterized. The electrospinning process was carried out using the processing conditions selected in the study shown in Section 4.3.3.

4.3.4.1. Functional evaluation

Fourier Transform Infrared Spectroscopy (FTIR)

Figure 4.21A shows the FTIR profiles for the systems with PCL and PCL/GE (16/2 and 16/4), whereas Figure 4.21B shows the FTIR profiles for the systems with PCL and PCL/CG (16/2 and 16/4). In addition, the main peaks are summarized in Table 4.6.

The spectrum of the PCL system shows two important areas: bands at 2950 and 2860 cm^{-1} related to the CH_2 symmetrical and asymmetrical stretching, and bands in the range of 1450-1000 cm^{-1} (C-H bending and wagging). The main one is the sharp band that appears at 1725 cm^{-1}, associated with carbonyl stretching (characteristic of PCL).

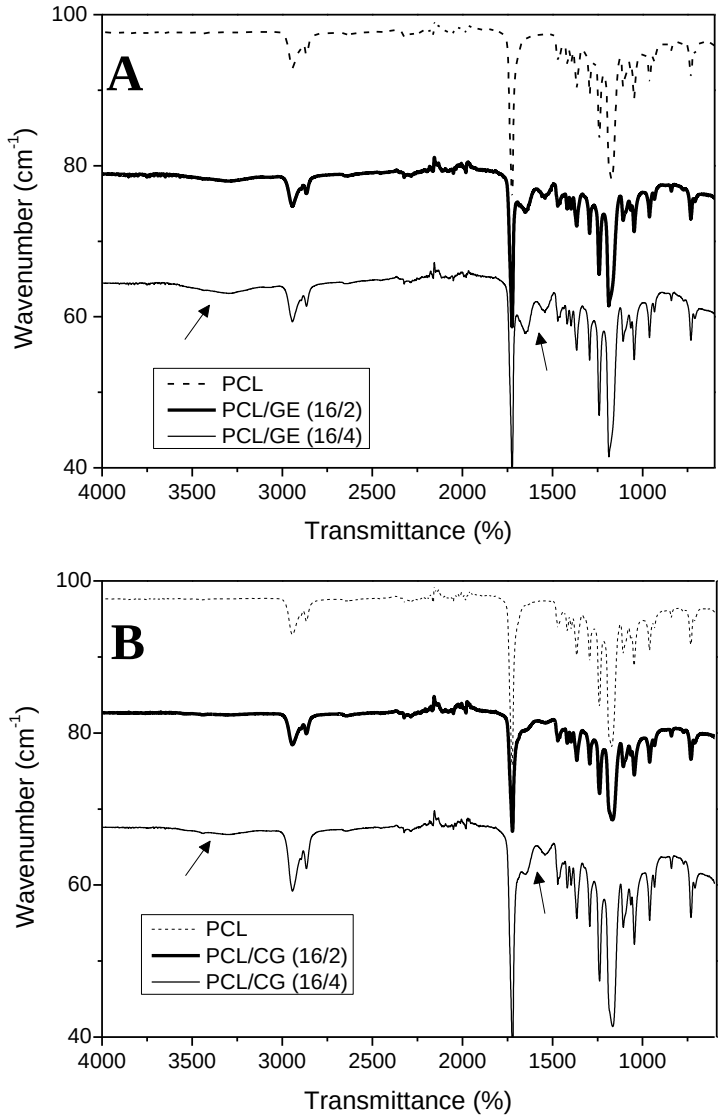

Figure 4.21. FTIR profiles of PCL-based scaffolds with different protein concentrations (2 and 4 %): (A) gelatin (GE) and (B) collagen (CG)

However, the other systems (combination of PCL and gelatin or collagen) presented a different profile, due to the presence of additional peaks which corresponded to the typical bands of proteins: a broad area at ca. 3280 cm^{-1} associated with N-H stretching (Amide A signal), and bands at 1635 and 1525 cm^{-1} related to carbonyl stretching and C-N stretching of amides, respectively (Muyonga et al., 2004). Interestingly,

the intensity of these signals increased when the protein used (either gelatin or collagen) was present in a higher concentration. However, the characteristic band for N-H bending (at ca. 1240 cm^{-1}) is overlapped with the bands related to the CH_2 symmetrical and asymmetrical stretching in the 1450-1000 cm^{-1} range (C-H bending and wagging) (Abe and Krimm, 1972; Jackson et al., 1995; Payne and Veis, 1988). These values obtained are in the same range as the ones obtained by the raw materials (described in Chapter 2), which evidenced the presence of both gelatin and collagen in the electrospun scaffolds produced.

Table 4.6. FTIR Spectra Peak Assignments for the systems with PCL, PCL/GE and PCL/CG

Region	**Peak (cm^{-1})**		**Assignments**
	PCL/GE	**PCL/CG**	
Amide A	3285	3280	N-H Stretch
	2943, 2859	2948, 2864	C-H Stretch (CH_2)
PCL peak	1741	1746	C=O Stretch (PCL)
Amide I	1646	1641	C=O Stretch (Protein)
Amide II	1551	1540	N-H Bending
	1450-1000		C-H bending and wagging

Water Contact Angle (WCA)

On the other hand, the wettability of the scaffolds produced was also measured in order to study the effect of gelatin and collagen on the hydrophobicity of the scaffold. The evolution of the contact angle with the addition of gelatin or collagen is shown in Figure 4.22 (Figure 4.22A and 4.22B, respectively).

PCL scaffolds are quite hydrophobic, presenting a contact angle of ca 105º. However, the addition of gelatin produced a drastic decrease of the contact angle, which resulted in more hydrophilic scaffolds obtained when the amount of gelatin was higher.

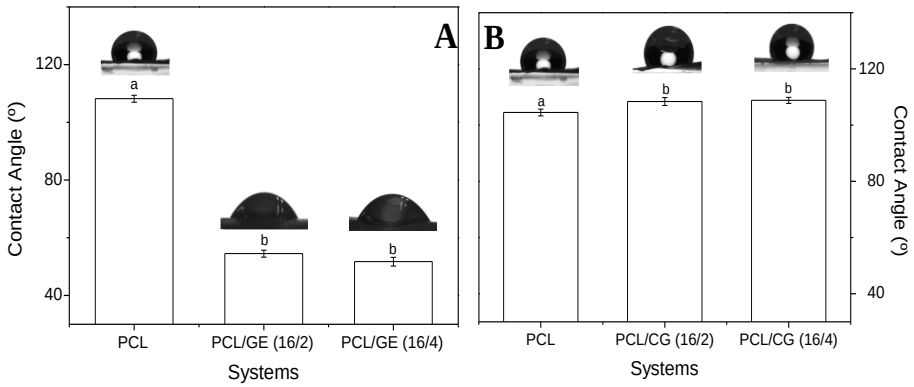

Figure 4.22. Contact Angle of PCL-based scaffolds with different protein concentrations (2 and 4%): (A) gelatin (GE) and (B) collagen (CG)

Nevertheless, an interesting effect occurred when the protein used was collagen instead of gelatin: the addition of collagen did not produce a decrease in the contact angle of scaffolds. In fact, a slight increase was observed, as shown in Figure 4.22B, in accordance to Dulnik et al. (2016). This effect may be due to two different aspects: On the one hand, gelatin has a higher content in glycine, valine and alanine amino acids, which allows the reorganization of the hydrophobic groups of proteins giving rise to a more hydrophilic structure, thus lowering the contact angle (Southall et al., 2002). On the other hand, collagen is not so homogeneously located on the surface, which explains the low variation of the contact angle.

Quigley et al. (2013) reported that hydrophilic surfaces are more suitable for cell adhesion (with contact angle values in the range of 40-65º). Comparing the different systems evaluated, those obtained with a gelatin concentration of 2% and 4% are the ones that presented the best contact angle values (55±2º and 52±1º, respectively).

Energy Dispersive X-ray Spectroscopy (EDAX)

The presence of protein in the network of the fibrous membrane can be identified by the presence of Nitrogen (N) in it. Thus, an EDAX analysis was performed to confirm that the electrospun fibers contained proteins in their structure. The Nitrogen present in the surface obtained from the EDAX profiles is shown in Table 4.7. In general, the results evidenced an increase in N content when the concentration of the ~~used~~ protein was higher (being either gelatin or collagen). The increase in N content was more remarkable for the scaffolds with gelatin, thus confirming the preferential tendency of GE to located at the surface as compared to CG.

Table 4.7. Nitrogen (N) content, mean fiber diameter and porosity of scaffolds obtained with PCL and different gelatin (GE) and collagen (CG) concentration (2 and 4%)

SYSTEM		N content (%)	Mean fiber diameter (nm)	Porosity (%)
PCL (16%)		0 ± 0.01 [a]	451 ± 112 [a]	60.91 ± 0.77 [a]
PCL (16%)	Gelatin (2%)	1.86 ± 0.12 [b]	347 ± 81 [ab]	50.67 ± 1.60 [b]
	Gelatin (4%)	3.31 ± 0.37 [c]	298 ± 89 [ab]	56.08 ± 0.17 [c]
	Collagen (2%)	0.76 ± 0.21 [d]	259 ± 80 [b]	56.47 ± 1.39 [c]
	Collagen (4%)	1.31 ± 0.11 [e]	294 ± 123 [ab]	57.28 ± 0.90 [c]

4.3.4.2. Microstructural evaluation

Figure 4.23 shows the SEM images of electrospun mats obtained as a function of gelatin (Figures 4.23B and 4.23C for the 2 and 4 %, respectively) and collagen (Figures 4.23D and 4.23E for the 2 and 4 %, respectively) content. The PCL-system (16 %) (Figure 4.23A) was also included to show the variations found in the fiber morphology with the addition of protein to the initial formulation. From the images analyzed, the porosity, the mean fiber size and the fiber size distribution were calculated and shown in Table 4.7 and Figure 4.24.

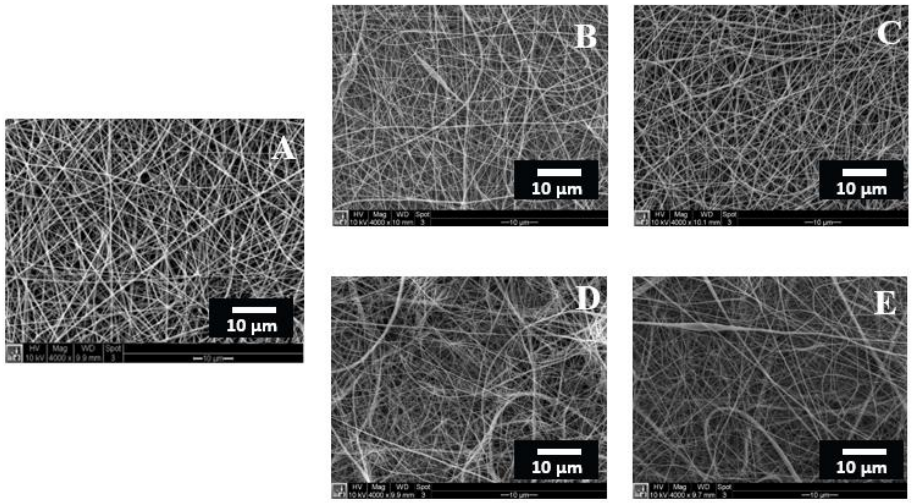

Figure 4.23. SEM images of PCL-based scaffolds with different protein concentration: (A) PCL (16%), (B) PCL/GE 16/2, (C) PCL/GE 16/4, (D) PCL/CG 16/2 and (E) PCL/CG 16/4

Fiber diameter decreased with the addition of a protein, which is more remarkable for the collagen-based scaffolds. However, there were no significant differences in the diameter of the fibers when comparing independently the results of the scaffolds obtained from PCL and gelatin or PCL and collagen. However, the comparison between the gelatin-based and collagen-based scaffolds established that the use of collagen produced, in general, fibers with lower mean fiber size but showing greater variability. Moreover, Chen et al. (2013) obtained a better cell behavior with electrospun scaffolds with fiber diameter in the range of 300-340 nm, which corresponded to the scaffolds processed with the combination of PCL and protein (either collagen or gelatin).

In addition, to mean fiber size, Figure 4.24 shows the fiber size distribution of the different systems studied. All scaffolds present a Gaussian distribution with respect to a central value (ranging between 0.3 and 0.5 µm). In general, the addition of a protein causes a widening of the distribution due to the presence of a greater number of fibers with different diameters, that is a greater heterogeneity in the size of the fibers.

The scaffolds produced with 4% of gelatin can be highlighted from the others as they show a much more homogeneous distribution.

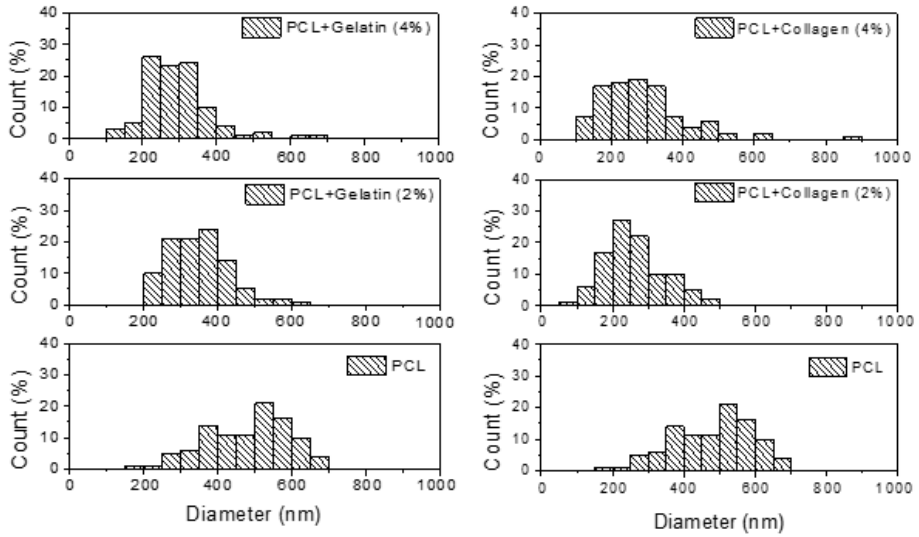

Figure 4.24. Fiber size distribution of the scaffolds processed with PCL and PCL with different protein concentrations (gelatin (GE) or collagen (CG) at 2 or 4%)

The porosity of the scaffolds was also evaluated (Table 4.7). All the systems presented porosity values between 50% and 60%, a suitable porosity range according to Vannozzi et al. (2017) for skeletal muscle cells. Although the addition of protein to the system indeed produced a decrease in the porosity of the scaffold, an increase in protein concentration tended to increase the porosity. In addition, comparing the PCL/GE-based scaffolds with those produced with PCL and collagen, the porosities obtained were slightly higher for the collagen-based scaffolds.

4.3.4.3. Mechanical evaluation

Figure 4.25 shows the strain-stress curves obtained for the systems processed with PCL (16 %) with different concentrations of gelatin and collagen (2 and 4 %).

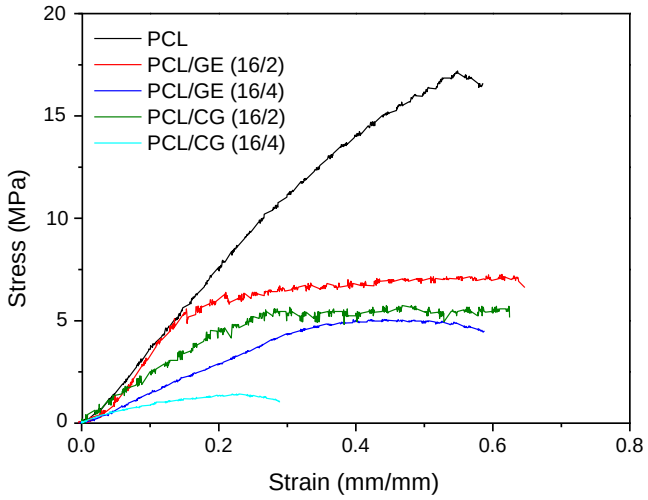

Figure 4.25. Strain-stress curves obtained from the mechanical testing performed to PCL-based scaffolds with different protein concentrations (gelatin (GE) or collagen (CG) at 2 and 4%)

All the systems showed a similar profile, with an initial region with a high constant stress-strain slope, which corresponds to the elastic region. This was followed by, a long plastic region with a continuous decrease in the stress-strain slope towards a constant value. After reaching the maximum stress and strain at break, the samples broke with a sudden decrease in stress.

Furthermore, the different parameters measured from the mechanical testing are shown in Figure 4.26 (4.26A, 4.26B and 4.26C). The analysis of the different parameters obtained from the strain-stress curves showed that the addition of a protein produced a decrease in both Young's Modulus and maximum stress, compared to the values obtained for pure PCL scaffolds. This effect was more pronounced when the protein concentration was 4%. Interestingly, the same decrease of 56% and 85% for the gelatin and collagen systems, respectively, occurred in both parameters (Young's Modulus and maximum stress). However, the effect on the strain at break differed depending on the protein used.

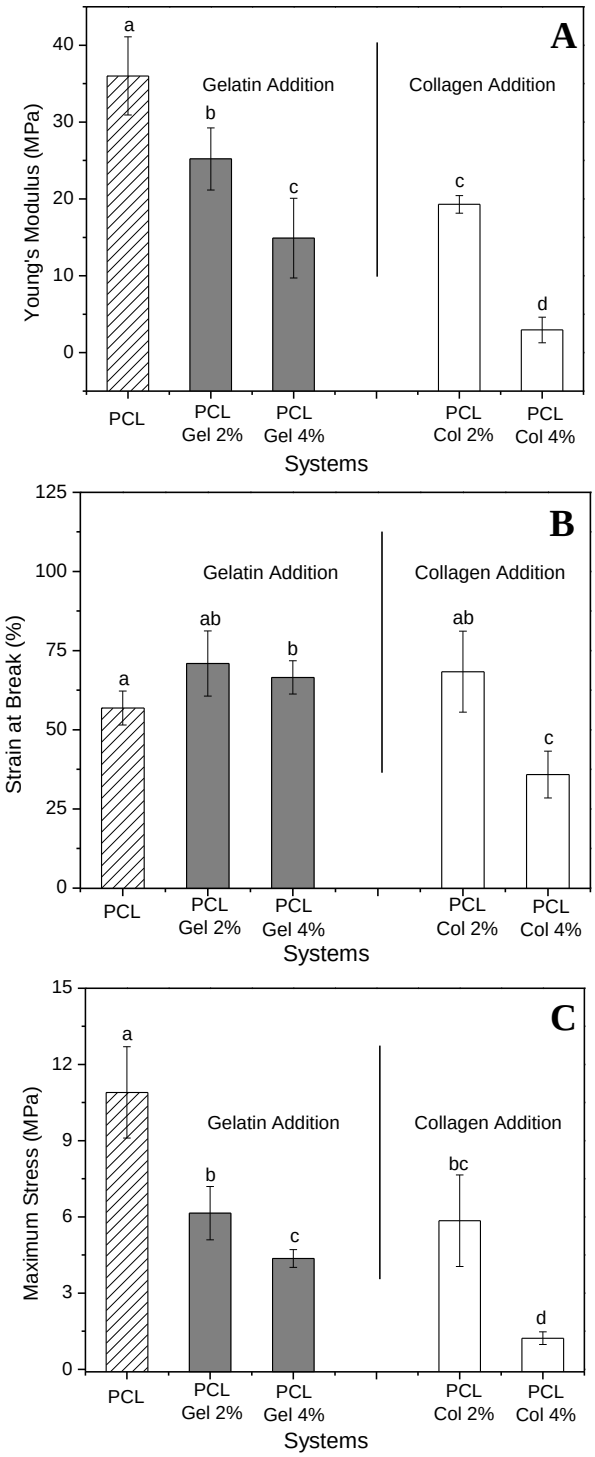

Figure 4.26. (A) Young's Modulus, (B) Strain at break and (C) Maximum stress obtained from the mechanical testing performed to PCL-based scaffolds with different protein concentrations (gelatin (GE) or collagen (CG) at 2 or 4%)

According to the result shown, the addition of a protein produced a tendency to increase the strain at break that would lead to higher deformability and, therefore, a better response of the scaffold in the bioreactor. In fact, the Young's Modulus of the PCL/GE (16/4) system is similar to the value obtained by Du et al. (2018) in their study with skeletal muscle cells.

For that reason, a further mechanical analysis was carried, with the PCL/GE (16/4) system, performing the uniaxial tests in PBS (using a wet chamber to place the scaffolds) to PCL and combinations of PCL with either gelatin or collagen at 4%. The results are shown in Figure 4.27.

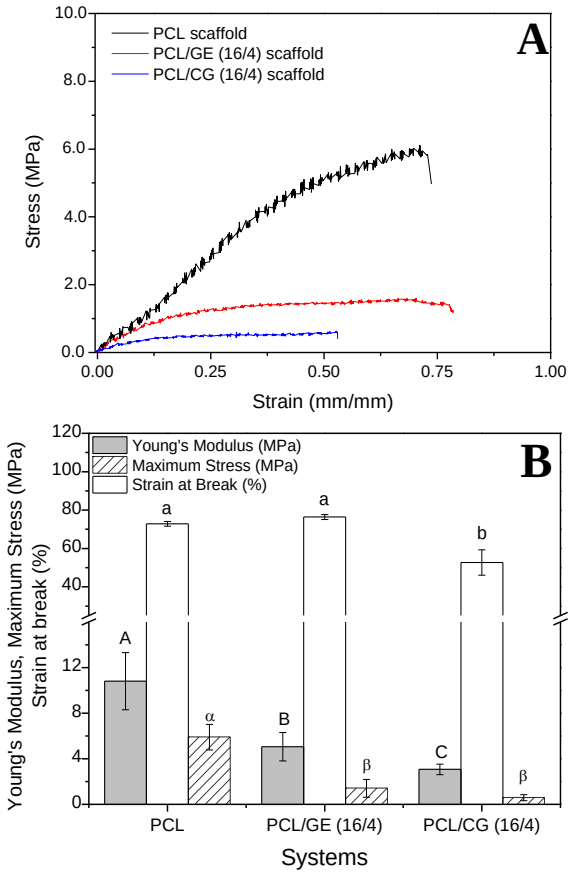

Figure 4.27. (A) Strain-stress curves and (B) parameters of the uniaxial tensile strength measurements (Young's modulus, strain at break and maximum stress) obtained for the PCL (16%) scaffolds and the PCL-based scaffolds with Gelatin or Collagen at 4%

In addition, the different parameters obtained have been summarized in Table 4.8 in order to compare the results obtained by the scaffolds produced with PCL (16%) and combinations of PCL and gelatin or collagen in different concentrations (2 and 4%) by performing the uniaxial tensile strength tests in dry and wet conditions.

Table 4.8. Parameters of the uniaxial tensile strength measurements (Young's modulus, strain at break and maximum stress) obtained for scaffolds produced with PCL (16%) and different Gelatin or Collagen concentrations (2 and 4%) in both dry (d) and wet (w) conditions. Values with different letters are significantly different ($p<0.05$)

SYSTEM		Young's modulus (MPa)	Strain at break (%)	Maximum stress (MPa)
PCL (16%)$_d$		35.8 ± 5.1 ^{A}	56.9 ± 5.4 ^{a}	10.9 ± 1.8 $^{\alpha}$
PCL (16%)$_w$		10.8 ± 2.6 ^{B}	72.9 ± 2.2 ^{b}	5.9 ± 1.1 $^{\beta}$
PCL (16%)	Gelatin (2%)$_d$	25.2 ± 4.0 ^{C}	70.9 ± 10.3 ^{ab}	6.2 ± 1.0 $^{\beta}$
	Gelatin (4%)$_d$	14.9 ± 5.2 ^{B}	66.3 ± 5.3 ^{a}	4.4 ± 0.6 $^{\beta}$
	Gelatin (4%)$_w$	5.1 ± 1.8 ^{D}	76.4 ± 2.3 ^{b}	1.4 ± 0.7 $^{\gamma}$
	Collagen (2%)$_d$	19.3 ± 1.2 ^{C}	68.3 ± 7.8 ^{ab}	5.9 ± 1.8 $^{\beta}$
	Collagen (4%)$_d$	3.0 ± 1.7 ^{D}	35.8 ± 6.1 ^{c}	1.2 ± 0.2 $^{\gamma}$
	Collagen (4%)$_w$	2.8 ± 0.5 ^{D}	52.2 ± 6.7 ^{a}	0.6 ± 0.2 $^{\gamma}$

Two opposite effects on the properties can be highlighted. On the one hand, the scaffolds get softer in a liquid environment, as it can be seen by the decrease observed in the Young's modulus and maximum stress. However, on the other hand, the increase in the strain at break evidenced that the scaffolds are more deformable in a wet environment.

4.3.5. Influence of the alignment of electrospun scaffolds

Apart from the above mentioned and described processing parameters (section 3.3), there is another processing parameter that may cause major changes in the morphological and structural disposition of a scaffold produced *via* electrospinning. This parameter is the rotational speed, which induces the alignment of the fibers produced depending on both the polymer and speed used. In this sense, the system produced with PCL_{45} (16 %) and Gelatin (4 %) [named as PCL/GE 16/4] was selected to perform a study with three different rotational speeds (0, 300 and 600 rpm), obtaining nanofibrous scaffolds with different alignment: random (at 0 rpm); semi-aligned (at 300 rpm); and aligned (at 600 rpm).

The electrospinning process was carried out using the processing conditions selected in the study shown in Section 4.3.3.

4.3.5.1. Functional evaluation

Water Contact Angle (WCA) was measured for the PCL/GE 16/4 scaffolds obtained with different alignments and plotted in Figure 4.28.

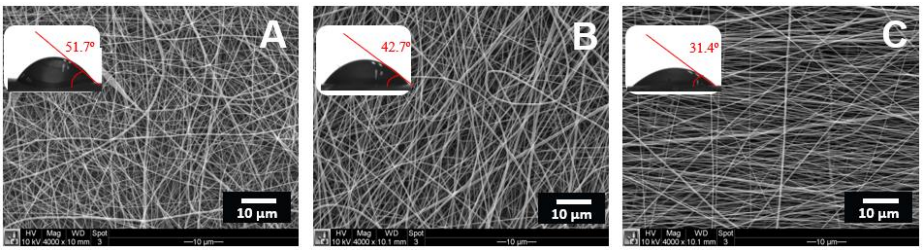

Figure 4.28. Water Contact Angle and SEM images of PCL/GE 16/4 scaffolds with different fiber alignment: (A) random, (B) semi-aligned and (C) aligned

The results showed that the scaffolds produced with PCL and gelatin presented a high hydrophilic character, showing a lower contact angle value (ca 50º). Comparing the values of the PCL/GE scaffolds with different alignments, there is a decrease in the contact angle values by

increasing the alignment of the scaffolds. Thus, a way to tune the wettability of the nanofibrous scaffolds is by using a suitable alignment.

4.3.5.2. Microstructural evaluation

The shape and structure of the scaffolds were analyzed with the SEM images (Figure 4.28). Besides, the alignment, mean fiber diameter, uniformity, porosity, and pore area were evaluated and summarized in Table 4.9.

Table 4.9. Fiber alignment, mean fiber diameter, uniformity values, porosity and mean pore area of PCL/GE 16/4 scaffolds with different alignment: Random, semi-aligned and aligned

SYSTEM	Alignment	Mean fiber diameter (nm)	Uniformity (%)	Porosity (%)	Mean Pore Area (nm^2)
PCL/GE 16/4 Random	0.13	307 ± 89^{a}	71	$50.1\pm0.5^{\alpha}$	780 ± 420^{A}
PCL/GE 16/4 Semi-aligned	0.40	265 ± 35^{a}	87	$51.2\pm1.8^{\alpha\beta}$	1856 ± 994^{A}
PCL/GE 16/4 Aligned	0.75	235 ± 68^{a}	71	$52.6\pm1.4^{\beta}$	913 ± 571^{A}

As can be seen in Figure 4.28 and deduced from the values shown in Table 4.9, homogeneous fibers with different alignment (0.13, 0.40 and 0.75) were obtained when the rotational speed was modified in the electrospinning process (the uniformity is higher than 70% for all the systems studied). Initially, the fibers were randomly oriented but when the rotational speed was higher than 300 rpm (semi-aligned) as well as a more organized latticework was obtained with more aligned fibers. In general, the increase in the rotational speed produces a slight decrease in the size of the fibers although the differences between them are not significant ($p<0.05$).

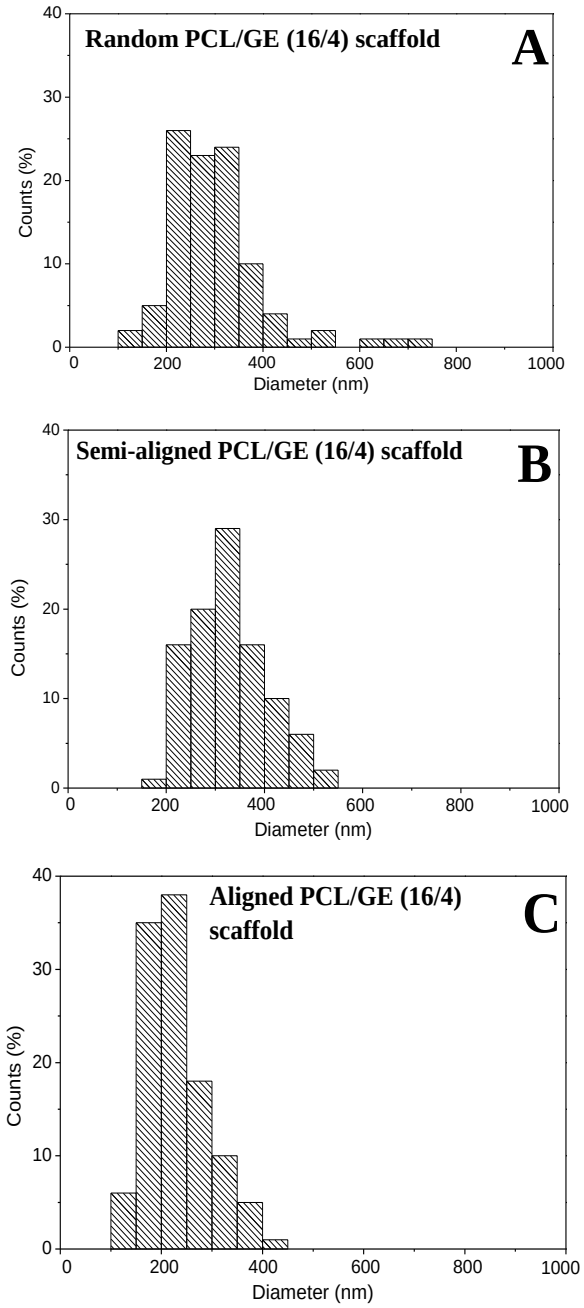

Figure 4.29. Fiber size distribution of PCL/GE 16/4 scaffolds with different alignment: (A) random, (B) semi-aligned and (C) aligned

In addition to the alignment and mean fiber size, fiber size distribution in Figure 4.29 showed how all systems presented a Gaussian distribution

with respect to a central value (ranging between 200 and 400 nm). Apart from obtaining thinner fibers, the increase in the alignment led to scaffolds formed by more homogeneous fibers, as it can be seen by the narrowing of the Gaussian bell curve shown in the fiber size distribution graphs. Interestingly, the uniformity of the systems is higher than 70%, highlighting the semi-aligned scaffold with a uniformity higher than 85%.

On the other hand, the porosity of the scaffolds was also evaluated (Table 4.9). All the systems presented porosity values in the range between 50 and 53%, showing a significant increase when the alignment of the fibers becomes higher.

4.3.5.3. Mechanical evaluation

The mechanical properties were also measured in both dry and wet conditions (simulating the incorporation of the scaffolds in a bioreactor with a wet chamber which contains a buffer solution, PBS) to compare their evolution of the scaffolds' properties. Nevertheless, generally, scaffolds in Tissue Engineering are placed in a bioreactor in which cells are included to grow within the structure, favored by a mechanical stimulus. Following the same idea, the mechanical properties of the scaffolds were measured before and after a cyclic loading test to study the influence of the cyclic loading on them. Thus, uniaxial tensile tests were carried out before and after a cyclic loading test for each system (random, semi-aligned and aligned).

First, the evolution of the stress was followed all over the cycle (Figure 4.30). It can be seen how the decrease observed in the stress for the three systems is lower than 5%: Random 4.9% (from 3.05 to 2.92 MPa), Semi-aligned 2.3% (from 1.77 to 1.73 MPa) and Aligned 3.9% (from 1.30 to 1.25 MPa). These results may indicate that the cyclic loading was

performed in the elastic region, where the stress was progressively decreased with increasing alignment.

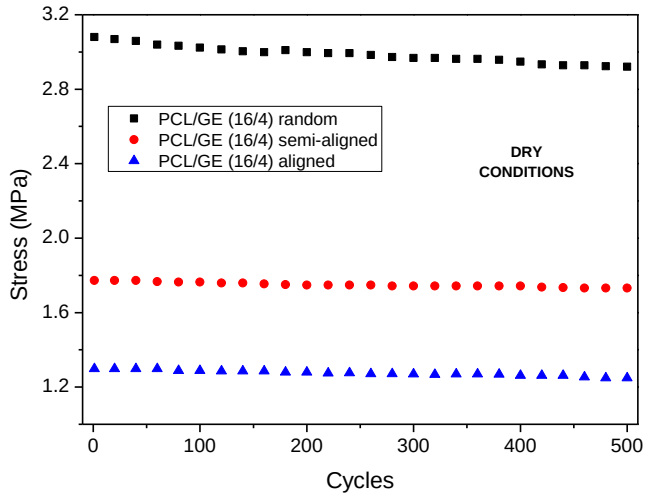

Figure 4.30. Evolution of the stress of PCL/GE (16/4) scaffolds fabricated with different alignments (random, semi-aligned and aligned) during a cyclic loading test of 500 cycles at a constant strain (10%) and frequency (1 Hz) in dry conditions

Apart from the cyclic loading, the different results obtained for the uniaxial tensile tests in dry conditions were plotted in Figure 4.30. Figure 4.30A and 4.30C show the strain-stress curves of the PCL/GE 16/4 scaffolds with different alignments. The profiles exhibited were similar, with an initial region with a high constant stress-strain slope (which corresponds to the elastic region). Then, there was a plastic region with a continuous decrease in the stress-strain slope towards a constant value and, after reaching the maximum stress and maximum strain, the break of the sample with a sudden decrease in stress.

Furthermore, the different parameters obtained from the mechanical tests before and after the cyclic loading were plotted in Figures 4.31B and 4.31D. Analyzing the parameters obtained, both experiments showed the same trend, a general decrease of the values with the alignment of the fibers, being more marked for the strain at break. In addition, two

different trends can be observed when comparing the results obtained before and after the cyclic loading. Both the Young's modulus and maximum stress suffer a slight decrease after performing the cyclic loading, whereas the strain at break does not change significantly.

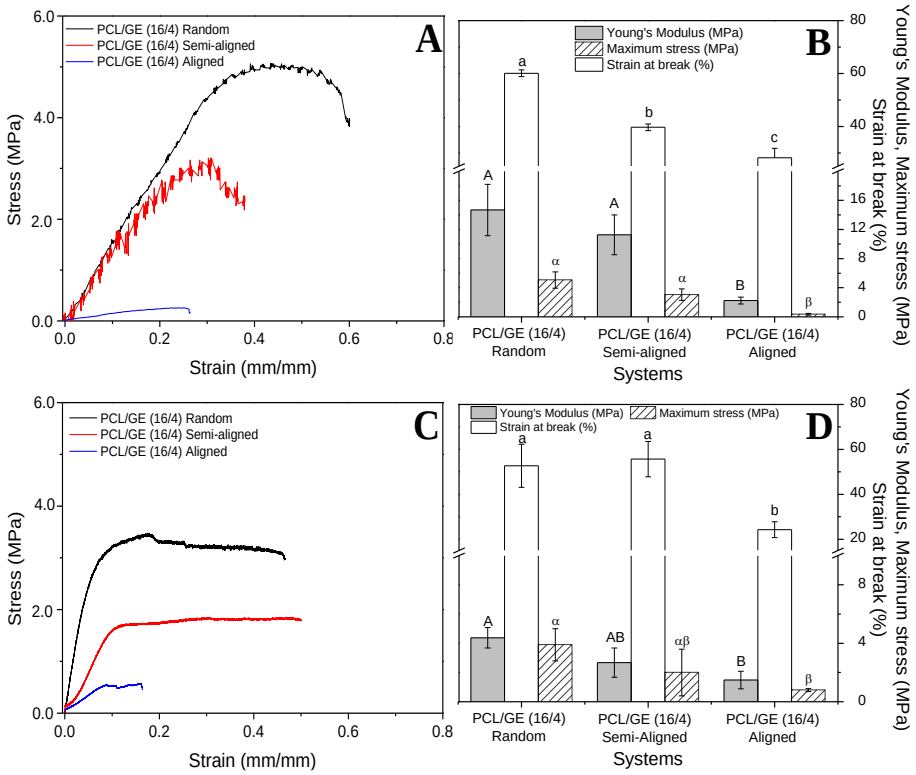

Figure 4.31. (A and C) Strain-Stress curves and (B and D) parameters (Young's Moduli, Strain at break and Maximum Stress) obtained from the mechanical testing carried out under dry conditions for PCL/GE 16/4 scaffolds produced with different alignments (random, semi-aligned and aligned) (A and B) before and (C and D) after a cyclic loading test of 500 cycles at a constant strain (10%) and frequency (1 Hz)

On the other hand, to improve the simulation of the behavior of the scaffolds in the bioreactor, the same experiments have been performed under wet conditions using a wet chamber coupled to the mechanical testing equipment. Once again, a cyclic loading test was performed to

evaluate the evolution of the stress with cycles and the results are shown in Figure 4.32.

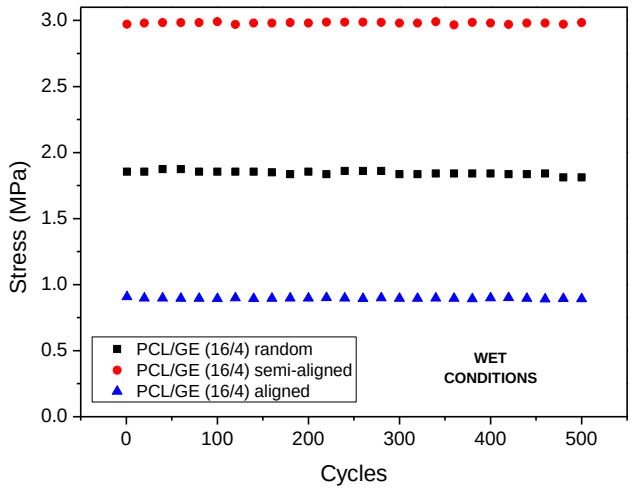

Figure 4.32. Evolution of the stress of PCL/GE (16/4) scaffolds produced with different alignments (random, semi-aligned and aligned) during a cyclic loading test of 500 cycles at a constant strain (10%) and frequency (1 Hz) in wet conditions

Interestingly, the evolution of the stress suffers a different trend compared to the cyclic loading performed under dry conditions. In this case, the system which suffered the greatest variation in the stress was the PCL/GE 16/4 aligned, being the random one the system with the lowest variation. However, the decrease observed cannot be considered significant as the maximum decrease obtained is lower than 2.5 % (0.4, 1.6 and 2.2 % for the random, semi-aligned and aligned system, respectively). Therefore, the cyclic loading was performed in the elastic region for the three systems.

Once again, a comparison between the uniaxial tensile strength experiments carried out under wet conditions before and after the cyclic loading was plotted in Figure 4.33. A similar tendency can be seen in the evolution of the parameters since Young's modulus and maximum stress presented maximum values for the semi-aligned system, whereas the

strain at break decreased with the increase of the alignment. Analyzing the evolution of the parameters after submitting the cyclic loading, a general decrease of the properties can be observed, specially marked for the Young's modulus and the strain at break.

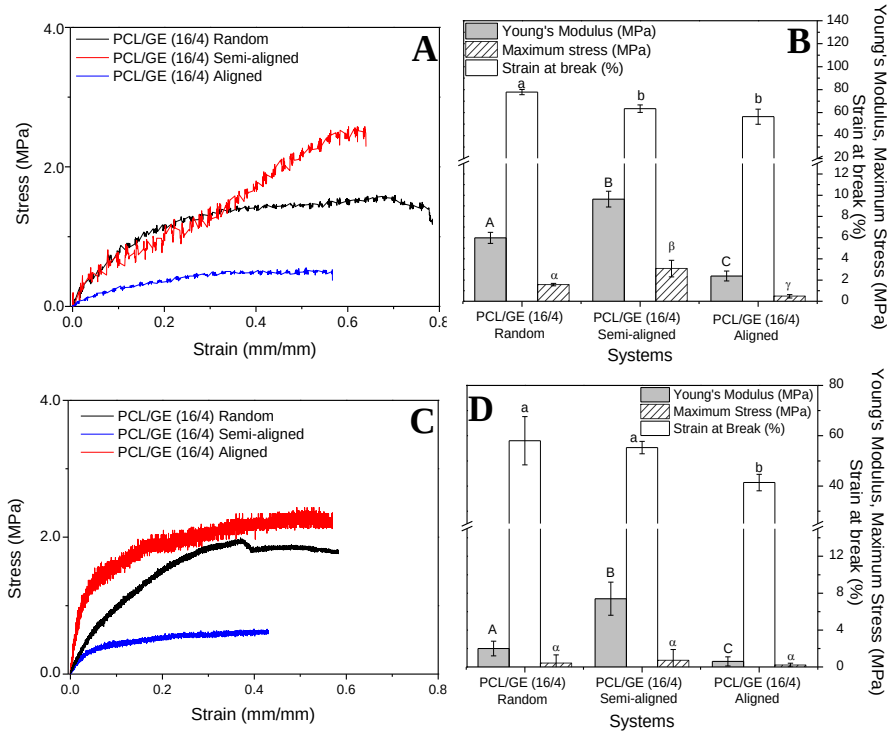

Figure 4.33. (A and C) Strain-Stress curves and (B and D) parameters (Young's Moduli, Strain at break and Maximum Stress) obtained from the mechanical testing carried out under wet conditions for PCL/GE (16/4) scaffolds produced with different alignments (random, semi-aligned and aligned) (A and B) before and (C and D) after a cyclic loading test of 500 cycles at a constant strain (10%) and frequency (1 Hz)

Furthermore, the parameters obtained are summarized in Table 4.10 to compare the values under dry and wet conditions. Comparing the values under dry and wet conditions, different effects can be observed depending on the parameter studied.

First, it may be seen an increase in the strain at break of the samples when performing the mechanical tests in wet conditions. This increase is more

pronounced with the alignment of the fibers, with an average ratio of an increase of 1.75 for the aligned system, compared to the values reached increase of 1.45 and 1.15 for the semi-aligned and random systems, respectively. Nevertheless, all the systems suffer a decrease in the maximum stress under wet conditions. In this case, the effect is more marked when the fibers are randomly distributed (average ratio of decrease of 6.5, much higher than the values around 1.5-2.0 for the semi-aligned and aligned systems). Finally, Young's modulus presents a decrease under wet conditions for all the samples with an average ratio of decrease between 1.0 and 3.0, except the semi-aligned system after the cyclic loading, which increases its Young's modulus.

Table 4.10. Comparison of the Young's modulus, strain at break and maximum stress of PCL/GE 16/4 scaffolds produced with different alignments (random, semi-aligned and aligned) before and after the cyclic loading under both dry and wet conditions. Values with different letters are significantly different (p<0.05)

PCL/GE 16/4 SYSTEMS	Young's modulus (MPa)		Strain at break (%)		Maximum stress (MPa)	
	Before	**After**	**Before**	**After**	**Before**	**After**
Random Dry	14.9 ^{a}	4.4 ^{b}	66.3 ^{A}	52.7 ^{A}	4.4 $^{\alpha}$	3.9 $^{\alpha}$
Random Wet	5.1 ^{b}	2.0 ^{c}	77.9 ^{B}	58.0 ^{AD}	1.4 $^{\beta}$	0.4 $^{\beta}$
Semi-Aligned Dry	11.3 ^{ad}	2.7 ^{c}	39.7 ^{C}	50.7 ^{AD}	3.0 $^{\alpha}$	1.9 $^{\beta}$
Semi-Aligned Wet	9.6 ^{d}	7.4 ^{e}	63.5 ^{A}	55.3 ^{D}	3.2 $^{\alpha}$	0.7 $^{\beta}$
Aligned Dry	2.2 ^{c}	1.7 ^{c}	28.2 ^{E}	24.3 ^{E}	0.4 $^{\beta}$	0.8 $^{\beta}$
Aligned Wet	2.4 ^{c}	0.6 ^{f}	56.5 ^{D}	36.9 ^{C}	0.5 $^{\beta}$	0.2 $^{\beta\gamma}$

These results suggest that nanofibrous scaffolds present higher deformability and a lower rigidity in a wet environment, compared to their behavior in dry conditions.

In conclusion, considering the results obtained, a certain alignment of the fibers induced an increase in the mechanical properties. In fact, parameters (Young's modulus, maximum stress and strain at break) values reached their maximum values for the scaffold formed by nanofibers with an intermediate alignment (semi-aligned scaffolds). An excessive alignment would drive to an anisotropic material showing a tendency to break in specific sites, which should be taken into account for the further biological studies carried out.

4.3.6. Anisotropy in aligned electrospun scaffolds

Although the properties of aligned nanofibrous structures have been extensively investigated in the literature (i.e. Jose et al., 2009; Kai et al., 2011; Wu et al., 2010), few attention has been paid so far to the anisotropic character of these structures and their response to the application of forces in different directions (anisotropy). We hypothesize that the properties of the scaffolds obtained are different depending on the measuring direction, considering that the alignment of the fibers exerts an influence on the variation of the properties. Therefore, random and aligned scaffolds were characterized through the evaluation of the contact angle, SEM imaging and mechanical analyses in two different directions: parallel and perpendicular to the fiber formation in order to analyze the anisotropy of the structures.

The electrospinning process was carried out using the processing conditions selected in the study shown in Section 4.3.3 for the PCL/GE 16/4 system, using PCL_{45}.

4.3.6.1. Morphological evaluation

Table 4.11 shows the values obtained for the contact angle measurements of the scaffolds in the two directions mentioned above. First, all the values were below 65°, concluding that all the systems presented a hydrophilic character (Law, 2014).

Table 4.11. Mean fiber diameter, Contact Angle, Young's modulus, strain at break and maximum stress values of electrospun PCL/GE 16/4 scaffolds with two different alignments: random and aligned

	Mean fiber diameter (nm)	**Direction of measurement**	**Contact Angle (º)**	**Young's modulus (MPa)**	**Strain at break (%)**	**Maximum stress (kPa)**
PCL/GE random	307 ± 89^{a}	Parallel	50.5^{a}	6.3^{A}	63.0^{α}	3854^{I}
		Perpendicular	52.7^{a}	7.2^{A}	66.5^{α}	4022^{I}
PCL/GE aligned	235 ± 68^{a}	Parallel	31.4^{b}	2.3^{B}	31.1^{β}	279^{II}
		Perpendicular	62.7^{c}	0.8^{C}	65.5^{α}	98^{III}

In addition, comparing the values obtained for each system, there were no significant differences in the contact angle obtained for the two directions measured in the randomly oriented scaffold. However, the contact angle values obtained in the direction parallel to the orientation of the nanofibers were significantly lower than those obtained by the system in its perpendicular direction.

These results are in line with those obtained by Kubiak and Mathia, (2014) and Wang et al. (2018), who concluded that the wettability of the systems is better in the direction of the fiber orientation, and, therefore, the value of the contact angle is lower. Therefore, during adhesion and cell proliferation, the cells grow in the direction of fiber orientation, as shown in Pandey et al. (2018).

Furthermore, the analysis of the SEM images shown in Figures 4.34 and 4.35 demonstrates that the alignment of the fibers does not cause significant changes in their mean size, obtaining fibers with an average size of 250-350 nm.

4.3.6.2. Mechanical evaluation

In addition to the morphological characterization, the scaffolds were mechanically characterized in both directions (parallel and perpendicular). Stress-strain curves are shown in Figure 4.33.

All the curves exhibit similar behavior, consisting of an initial linear region, which corresponds to the elastic deformation, followed by a plastic deformation region, characterized by a continuous decrease in the stress–strain slope, passing through a maximum value. Finally, each system broke down at a different elongation.

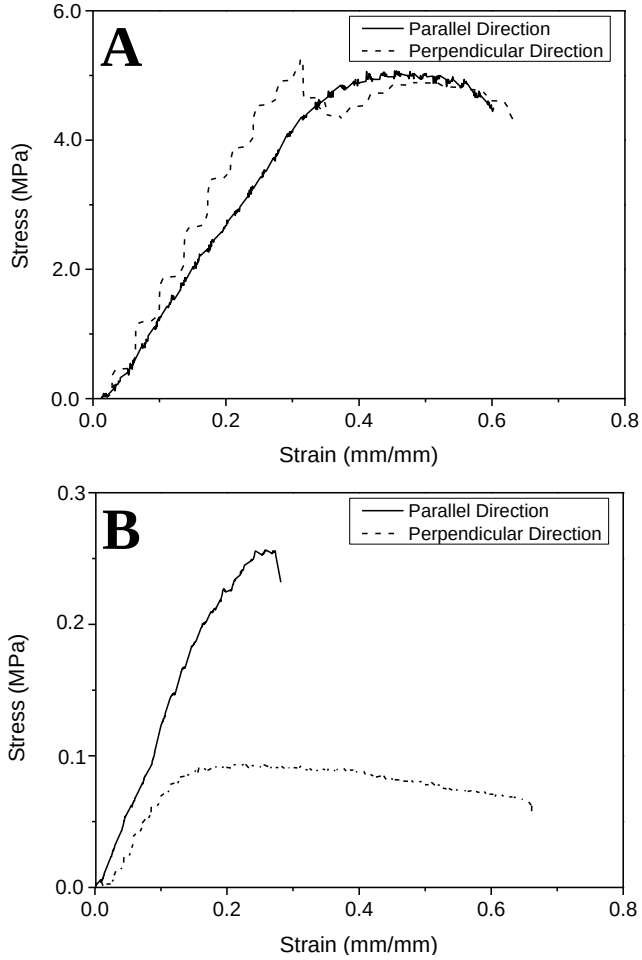

Figure 4.33. Stress-strain curves through a perpendicular and parallel analysis of electrospun PCL/GE 16/14 scaffolds with two different alignments: (A) random and (B) aligned

The parameters evaluated (Young's modulus, strain at break and maximum stress) are summarized in Table 4.11. First, comparing the effect of the direction on each scaffold, it can be observed that all the parameters present significant differences depending on the direction of the measurement for the system formed by aligned fibers, whereas for the system with randomly distributed fibers none of the evaluated parameters presents significant differences.

On the other hand, comparing the systems independently, the Young's modulus values are considerably higher for the random fiber system (6.3-7.2 MPa compared to 0.8-2.3 MPa for the aligned system). Something similar took place with the maximum stress, with values around 4000 kPa for the random system, well above the 200 kPa obtained for the aligned system. However, the values of strain at break are similar when comparing the perpendicular direction of the system aligned with the random system (ca 65%), which is, again, considerably higher than the value obtained for the direction parallel to the fiber orientation (30%), demonstrating the low deformability of the fibers when they are aligned parallel to the direction of the applied stress. These differences can be due to the propagation of tensions that take place between the fibers when they are arranged randomly, with respect to those oriented in the same direction, allowing the scaffold to withstand greater stress, as can be seen when comparing the values obtained by both systems (Table 4.11) (Wisnom and Green, 1995).

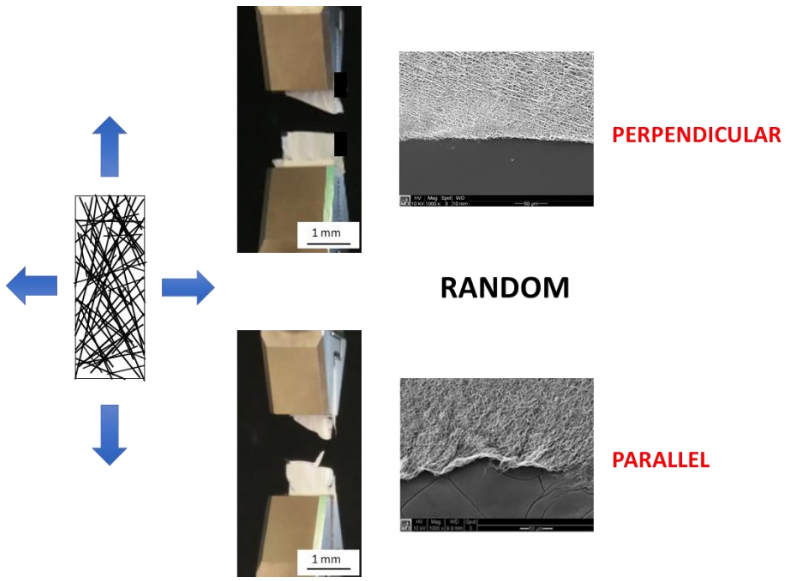

Figure 4.34. Macroscopic and SEM images of electrospun PCL/GE 16/4 random scaffolds after a mechanical break in perpendicular or parallel test

It is worth highlighting the breakage produced in the scaffold after performing the mechanical test (Figures 4.34 and 4.35). Two types of fracture can be observed depending on the direction of the applied stress and the sample on which it is applied. For the random system, the breakage observed was similar to the measuring direction (Figure 4.34). It was a fragile breakage favored by high deformations.

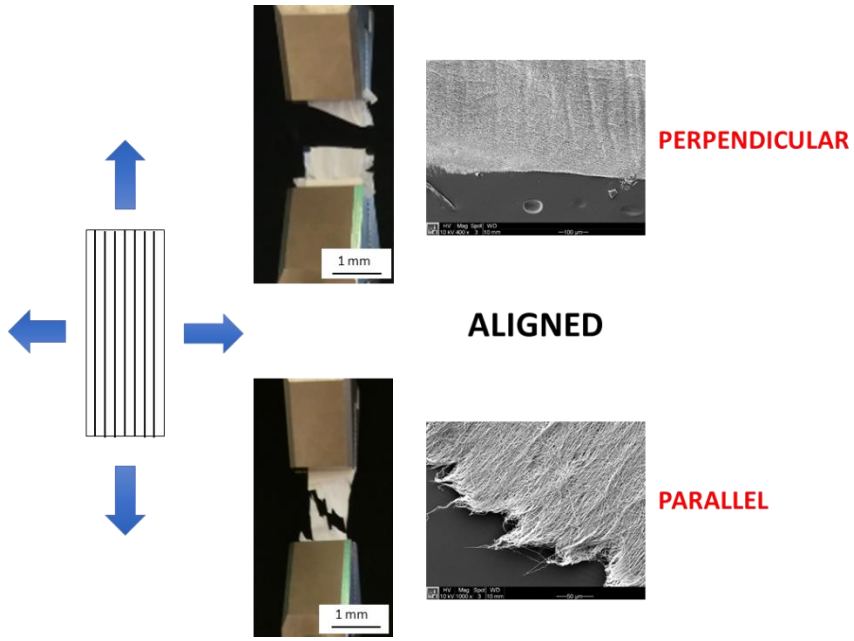

Figure 4.35. Macroscopic and SEM images of electrospun PCL/GE (16/4) aligned scaffolds after a mechanical break in perpendicular or parallel test

On the other hand, Figure 4.35 shows the two rupture types that took place in the aligned system. The images evidence how the breakage was much more uniform and homogeneous when the test was performed in the perpendicular direction to the orientation of the fibers. The application of a certain stress in the parallel direction to the fiber orientation breaks the fibers, which occurs as a result of the formation of a neck and cavities within the strangling area; this is called a moderately

ductile fracture. However, if the stress is applied perpendicular to the fiber orientation, then the global matrix breaks down, resulting in a fragile fracture (similar to that obtained for the random system).

In addition, the difference between the isotropy and anisotropy found in the systems studied can be explained by the combination of continuum-based descriptions and models for nanoporous materials (Gurtin and Ian Murdoch, 1978; Wang et al., 2011). The structure formed by randomly oriented fibers is induced by an imperfect homogeneous network, causing the applied stresses to be distributed over the entire surface with certain homogeneity, regardless of the direction of the stress. However, the aligned system behaves in a different way since the fibers are aligned, obtaining no connection points between them. Thus, this system favors the appearance of discontinuities, giving rise to fracture points (grains) and, consequently, inducing the sample to break down (Mikata, 2019; Wisnom and Green, 1995).

4.4 Conclusions

As a general conclusion, hybrid PCL/protein scaffolds formed by nanofibers with different concentrations and types of protein (collagen and gelatin) have been obtained by electrospinning.

More hydrophobic and stiffer scaffolds were obtained when using PCL with a higher molecular weight. It was observed that 14 kDa was a too low molecular weight for PCL to produce suitable nanofibrous scaffolds. However, the incorporation of gelatin to the initial formulation improved the electrospinning process (in a specific proportion), allowing it to obtain homogeneous nanofibrous scaffolds.

The most suitable conditions to produce scaffolds have been selected according to a processing parameter characterization. On the other hand, an increase in the rotational speed produced an increase in the alignment of the fibers which induced a better wettability as deduced by the decrease observed in the contact angle of the systems. As for the morphology of the fibers, the fiber alignment produced a slight decrease of the fiber size, and greater pore area and uniformity when the fibers are semi-aligned. In addition, the alignment of the fibers also produced scaffolds with better mechanical properties in wet conditions when the fibers are semi-aligned.

Higher protein content was observed in the gelatin-based scaffolds compared to the collagen ones, as a consequence of a better performance of the electrospinning process. Therefore, the hydrophilicity of PCL scaffolds can be enhanced with the addition of gelatin to their initial formulation, due to the hydrophilic character of this protein. In addition, hybrid PCL/protein scaffolds presented lower fiber size and, consequently, lower porosity. Consequently, there was a general reduction of the mechanical properties of PCL-based scaffolds,

dominated by the presence of protein (either gelatin or collagen) in the fibers, obtaining scaffolds with a Young's modulus or maximum stress up to four times lower than that of pure PCL scaffolds. In fact, the addition of gelatin produces more deformable scaffolds with lower stiffness.

Different correlations between the PCL/GE ratio and the different properties measured (N content and contact angle) were established. Linear correlations were obtained, although with opposite slopes, since WCA increases with the PCL/GE ratio whereas the N content decreases as the ratio increases. Furthermore, the uniformity of the systems was measured by analyzing the homogeneity of the nanofibrous membranes. A maximum was found for the ratio with the lowest mean fiber diameter (20/4, ratio 5:1), although there are variations in the concentration of each of the polymers. In fact, higher mean sizes lead to an increase in the heterogeneity of the systems. It has been proved how the total polymer concentration affects the fiber formation, but also the ratio between the two polymers when using a binary system. The studies revealed that for combinations of PCL and gelatin, the most suitable ratios have been found to be 4:1 and 5:1 (16/4 and 20/4 systems).

Hybrid PCL/protein scaffolds presented lower fiber diameter and, consequently, lower porosity. Lower fiber sizes are more suitable to obtain a larger surface for cell adhesion. Consequently, there was a general reduction of the mechanical properties of PCL-based scaffolds, dominated by the presence of protein (either gelatin or collagen) in the fibers, obtaining scaffolds with a Young's modulus or maximum stress up to four times lower than that of pure PCL scaffolds. In fact, the addition of gelatin produces more deformable scaffolds with lower stiffness. In addition, the hydrophilicity of PCL scaffolds can be

enhanced with the addition of gelatin to their initial formulation, due to the high hydrophilic character of this protein. Specifically, according to our results, PCL/GE 16/4 scaffolds seems to be the most appealing mixture.

Working in dry conditions, makes the scaffolds less stiff and more deformable due to a softening of their properties, being reflected by a decrease in both Young's modulus and maximum stress, but with an increase in the strain at break. In addition, the cyclic loading performed to the systems in both dry and wet conditions gives rise to a decrease in the Young's modulus, whereas the maximum stress and strain at break do not show significant differences (except the semi-aligned system which exhibits a slight increase in the strain at break at dry conditions).

It has been proved how the electrospinning technique allows creating anisotropic materials, which exhibited different properties depending on the measuring direction. The randomly oriented system [PCL/GE 16/4 random] showed no significant differences when measuring its properties in the parallel and perpendicular directions with respect to the fiber formation. However, the aligned system [PCL/GE 16/4 aligned] presented significant differences in all the properties when measuring them in these two directions. Young's modulus and maximum stress showed lower values in the perpendicular direction, whereas the contact angle and strain at break were lower when measuring them in the parallel direction of the fiber formation.

Acknowledgements

The authors gratefully acknowledge Complex Tissue Regeneration Department and especially to Dr. Lorenzo Moroni and Dr. Paul Wieringa (Maastricht University) for their supervision, assistance and help during the research stay in which most of these studies have been developed.

Related publications

- Perez-Puyana, Víctor Manuel; Jiménez Rosado, Mercedes; Romero García, Alberto; Guerrero Conejo, Antonio (2018). Development of PVA/gelatin nanofibrous scaffolds for Tissue Engineering via electrospinning, *Materials Research Express*, 5, DOI:10.1088/2053-1591/aab164

References

Abe, Y., Krimm, S., 1972. Normal vibrations of crystalline polyglycine I. Biopolymers 11, 1817–1839.

Agarwal, R., Alam, M.S., Gupta, B., 2013. Polyvinyl alcohol-polyethylene oxide-carboxymethyl cellulose membranes for drug delivery. J. Appl. Polym. Sci. 129, 3728–3736.

Agrahari, V., Agrahari, V., Meng, J., Mitra, A.K., 2017. Chapter 9 - Electrospun Nanofibers in Drug Delivery: Fabrication, Advances, and Biomedical Applications, in: Mitra, A.K., Cholkar, K., Mandal Drug Delivery and Medical Devices, A.B.T.-E.N. for D. (Eds.), Micro and Nano Technologies. Elsevier, Boston, pp. 189–215.

Aguirre-Chagala, Y.E., Altuzar, V., León-Sarabia, E., Tinoco-Magaña, J.C., Yañez-Limón, J.M., Mendoza-Barrera, C., 2017. Physicochemical properties of polycaprolactone/collagen/elastin nanofibers fabricated by electrospinning. Mater. Sci. Eng. C 76, 897–907.

Aldana, A.A., Abraham, G.A., 2017. Current advances in electrospun gelatin-based scaffolds for tissue engineering applications. Int. J. Pharm. 523, 441–453.

Badea, E., Gatta, G. Della, Usacheva, T., 2012. Effects of temperature and relative humidity on fibrillar collagen in parchment: A micro differential scanning calorimetry (micro DSC) study. Polym. Degrad. Stab. 97, 346–353.

Chen, M.C., Sun, Y.C., Chen, Y.H., 2013. Electrically conductive nanofibers with highly oriented structures and their potential application in skeletal muscle tissue engineering. Acta Biomater. 9, 5562–5572.

Chen, S., Zhang, Q., Nakamoto, T., Kawazoe, N., Chen, G., 2016. Gelatin Scaffolds with Controlled Pore Structure and Mechanical Property for Cartilage Tissue Engineering. Tissue Eng. Part C. Methods 22, 189–198.

Colby, R.H., Fetters, L.J., Funk, W.G., Graessley, W.W., 1991. Effects of concentration and thermodynamic interaction on the viscoelastic

properties of polymer solutions. Macromolecules 24, 3873–3882.

Cui, M., Liu, L., Guo, N., Su, R., Ma, F., 2015. Preparation, cell compatibility and degradability of collagen-modified poly(lactic acid). Molecules 20, 595–607.

de la Portilla, F., Pereira, S., Molero, M., De Marco, F., Perez-Puyana, V., Guerrero, A., Romero, A., 2016. Microstructural, mechanical, and histological evaluation of modified alginate-based scaffolds. J. Biomed. Mater. Res. - Part A 104, 3107–3114.

Dowling, D.P., Miller, I.S., Ardhaoui, M., Gallagher, W.M., 2011. Effect of surface wettability and topography on the adhesion of osteosarcoma cells on plasma-modified polystyrene. J. Biomater. Appl. 26, 327–347.

Du, Y., Ge, J., Li, Y., Ma, P.X., Lei, B., 2018. Biomimetic elastomeric, conductive and biodegradable polycitrate-based nanocomposites for guiding myogenic differentiation and skeletal muscle regeneration. Biomaterials 157, 40–50.

Dulnik, J., Denis, P., Sajkiewicz, P., Kołbuk, D., Choińska, E., 2016. Biodegradation of bicomponent PCL/gelatin and PCL/collagen nanofibers electrospun from alternative solvent system. Polym. Degrad. Stab. 130, 10–21.

Duque Sánchez, L.M., Rodriguez, L., López, M., 2014. Electrospinning: The Nanofibers Age. Rev. Iberoam. Polímeros Vol. Iber. Polímeros 14, 10–27.

Ebrahimgol, F., Tavanai, H., Alihosseini, F., Khayamian, T., 2014. Electrosprayed recovered wool keratin nanoparticles. Polym. Adv. Technol. 25, 1001–1007.

Fereshteh, Z., Fathi, M., Bagri, A., Boccaccini, A.R., 2016. Preparation and characterization of aligned porous PCL/zein scaffolds as drug delivery systems via improved unidirectional freeze-drying method. Mater. Sci. Eng. C 68, 613–622.

Gautam, S., Dinda, A.K., Mishra, N.C., 2013. Fabrication and characterization of PCL/gelatin composite nanofibrous scaffold for tissue engineering

applications by electrospinning method. Mater. Sci. Eng. C 33, 1228–1235.

Ghafoor, B., Aleem, A., Najabat Ali, M., Mir, M., 2018. Review of the fabrication techniques and applications of polymeric electrospun nanofibers for drug delivery systems. J. Drug Deliv. Sci. Technol. 48, 82–87.

Ghorani, B., Tucker, N., 2015. Fundamentals of electrospinning as a novel delivery vehicle for bioactive compounds in food nanotechnology. Food Hydrocoll. 51, 227–240.

Graessley, W.W., 1980. Polymer chain dimensions and the dependence of viscoelastic properties on concentration, molecular weight and solvent power. Polymer (Guildf). 21, 258–262.

Guarino, V., Gentile, G., Sorrentino, L., Ambrosio, L., 2017. Polycaprolactone: Synthesis, Properties, and Applications, in: Encyclopedia of Polymer Science and Technology. American Cancer Society, pp. 1–36.

Gümüşderelioğlu, M., Dalkıranoğlu, S., Aydın, R.S.T., Çakmak, S., 2011. A novel dermal substitute based on biofunctionalized electrospun PCL nanofibrous matrix. J. Biomed. Mater. Res. Part A 98A, 461–472.

Gurtin, M.E., Ian Murdoch, A., 1978. Surface stress in solids. Int. J. Solids Struct. 14, 431–440.

Hekmati, A.H., Rashidi, A., Ghazisaeidi, R., Drean, J.Y., 2013. Effect of needle length, electrospinning distance, and solution concentration on morphological properties of polyamide-6 electrospun nanowebs. Text. Res. J. 83, 1452–1466.

Hendrikson, W.J., Rouwkema, J., Van Blitterswijk, C.A., Moroni, L., 2015. Influence of PCL molecular weight on mesenchymal stromal cell differentiation. RSC Adv. 5, 54510–54516.

Hossain, M.F., Gong, R.H., Rigout, M., 2016. Effect of polymer concentration on electrospinning of hydroxypropyl-β-cyclodextrins/PEO nanofibres. J. Text. Inst. 107, 1511–1518.

Huang, Z.-M., Zhang, Y.-Z., Kotaki, M., Ramakrishna, S., 2003. A review on polymer nanofibers by electrospinning and their applications in nanocomposites. Compos. Sci. Technol. 63, 2223–2253.

Jackson, M., Choo, L.-P., Watson, P.H., Halliday, W.C., Mantsch, H.H., 1995. Beware of connective tissue proteins: Assignment and implications of collagen absorptions in infrared spectra of human tissues. Biochim. Biophys. Acta - Mol. Basis Dis. 1270, 1–6.

Jin, G., He, R., Sha, B., Li, W., Qing, H., Teng, R., Xu, F., 2018. Electrospun three-dimensional aligned nanofibrous scaffolds for tissue engineering. Mater. Sci. Eng. C 92, 995–1005.

Jose, M. V, Thomas, V., Dean, D.R., Nyairo, E., 2009. Fabrication and characterization of aligned nanofibrous PLGA / Collagen blends as bone tissue scaffolds. Polymer (Guildf). 50, 3778–3785.

Kai, D., Prabhakaran, M.P., Jin, G., Ramakrishna, S., 2011. Guided orientation of cardiomyocytes on electrospun aligned nanofibers for cardiac tissue engineering. J. Biomed. Mater. Res. - Part B Appl. Biomater. 98 B, 379–386.

Khajavi, R., Abbasipour, M., Bahador, A., 2016. Electrospun biodegradable nanofibers scaffolds for bone tissue engineering. J. Appl. Polym. Sci. 133, 42883.

Kitsara, M., Agbulut, O., Kontziampasis, D., Chen, Y., Menasche, P., 2017. Fibers for hearts: A critical review on electrospinning for cardiac tissue engineering. Acta Biomater. 48, 20–40.

Klossner, R.R., Queen, H.A., Coughlin, A.J., Krause, W.E., 2008. Correlation of chitosan's rheological properties and its ability to electrospin. Biomacromolecules 9, 2947–2953.

Kong, L., Ziegler, G.R., 2014. Molecular entanglement and electrospinnability of biopolymers. J. Vis. Exp. e51933–e51933.

Kubiak, K.J., Mathia, T.G., 2014. Anisotropic Wetting of Hydrophobic and Hydrophilic Surfaces–Modelling by Lattice Boltzmann Method. Procedia Eng. 79, 45–48.

Lagaron, J.M., Solouk, A., Castro, S., Echegoyen, Y., 2017. 3 - Biomedical applications of electrospinning, innovations, and products, in: Uyar, T., Kny, E.B.T.-E.M. for T.E. and B.A. (Eds.), . Woodhead Publishing, pp. 57–72.

Law, K.Y., 2014. Definitions for hydrophilicity, hydrophobicity, and superhydrophobicity: Getting the basics right. J. Phys. Chem. Lett. 5, 686–688.

Lee, K.-H., Kim, hy, Bang, H.J., Jung, Y.H., Lee, S., 2003. The change of bead morphology formed on electrospun polystyrene fibers, Polymer 44, 4029-4034.

Liu, Q., Zhu, J., Zhang, L., Qiu, Y., 2018. Recent advances in energy materials by electrospinning. Renew. Sustain. Energy Rev. 81, 1825–1858.

McKee, M.G., Wilkes, G.L., Colby, R.H., Long, T.E., 2004. Correlations of Solution Rheology with Electrospun Fiber Formation of Linear and Branched Polyesters. Macromolecules 37, 1760–1767.

Merrett, K., Ljunggren, M.K., Mondal, D., Griffith, M., Rafat, M., 2012. Collagen Type I: A promising scaffold material for Tissue Engineering and Regenerative Medicine, in: Type I Collagen. pp. 1–42.

Mikata, Y., 2019. Linear peridynamics for isotropic and anisotropic materials. Int. J. Solids Struct. 158, 116–127.

Muyonga, J.H., Cole, C.G.B., Duodu, K.G., 2004. Fourier transform infrared (FTIR) spectroscopic study of acid soluble collagen and gelatin from skins and bones of young and adult Nile perch (Lates niloticus). Food Chem. 86, 325–332.

Naghieh, S., Foroozmehr, E., Badrossamay, M., Kharaziha, M., 2017. Combinational processing of 3D printing and electrospinning of hierarchical poly(lactic acid)/gelatin-forsterite scaffolds as a biocomposite: Mechanical and biological assessment. Mater. Des. 133, 128–135.

Pandey, S., Rathore, K., Johnson, J., Cekanova, M., 2018. Aligned nanofiber material supports cell growth and increases osteogenesis in canine

adipose-derived mesenchymal stem cells in vitro. J. Biomed. Mater. Res. A 106, 1780–1788.

Payne, K.J., Veis, A., 1988. Fourier transform ir spectroscopy of collagen and gelatin solutions: Deconvolution of the amide I band for conformational studies. Biopolymers 27, 1749–1760.

Perez-Puyana, V., Jiménez-Rosado, M., Romero, A., Guerrero, A., 2018. Development of PVA/gelatin nanofibrous scaffolds for Tissue Engineering via electrospinning. Mater. Res. Express 5. DOI: 10.1088/2053-1591/aab164

Pham, Q.P., Sharma, U., Mikos, A.G., 2006. Electrospinning of polymeric nanofibers for tissue engineering applications: a review. Tissue Eng. 12, 1197–1211.

Quigley, A.F., Wagner, K., Kita, M., Gilmore, K.J., Higgins, M.J., Breukers, R.D., Moulton, S.E., Clark, G.M., Penington, A.J., Wallace, G.G., Officer, D.L., Kapsa, R.M.I., 2013. In vitro growth and differentiation of primary myoblasts on thiophene based conducting polymers. Biomater. Sci. 1, 983–995.

Rey, F., Ferreira, M.A., Facal, P., Machado, A.A.S.C., 1996. Effect of concentration , pH , and ionic strength on the viscosity of solutions of a soil fulvic acid 299, 295–299.

Sencadas, V., Correia, D.M., Areias, A., Botelho, G., Fonseca, A.M., Neves, I.C., Gomez Ribelles, J.L., Lanceros Mendez, S., 2012. Determination of the parameters affecting electrospun chitosan fiber size distribution and morphology. Carbohydr. Polym. 87, 1295–1301.

Southall, N.T., Dill, K.A., Haymet, A.D.J., 2002. A view of the hydrophobic effect. J. Phys. Chem. B 106, 521–533.

Srinivasa Reddy, C., Reddy Venugopal, J., Ramakrishna, S., Zussman, E., 2014. Polycaprolactone/oligomer compound scaffolds for cardiac tissue engineering. J. Biomed. Mater. Res. - Part A 102, 3713–3725.

Taylor, G.I., 1964. Disintegration of water drops in an electric field. Proc. R. Soc. London A 280, 383–398.

Tiwari, S.K., Venkatraman, S.S., 2012. Importance of viscosity parameters in electrospinning: Of monolithic and core–shell fibers. Mater. Sci. Eng. C 32, 1037–1042.

Vannozzi, L., Ricotti, L., Santaniello, T., Terencio, T., Oropesa-Nunez, R., Canale, C., Borghi, F., Menciassi, A., Lenardi, C., Gerges, I., 2017. 3D porous polyurethanes featured by different mechanical properties: Characterization and interaction with skeletal muscle cells. J. Mech. Behav. Biomed. Mater. 75, 147–159.

Wang, J., Huang, Z., Duan, H., Yu, S., Feng, X., Wang, G., Zhang, W., Wang, T., 2011. Surface stress effect in mechanics of nanostructured materials. Acta Mech. Solida Sin. 24, 52–82.

Wang, Z., Chen, E., Zhao, Y., 2018. The effect of surface anisotropy on contact angles and the characterization of elliptical cap droplets. Sci. China Technol. Sci. 61, 309–316. https://doi.org/10.1007/s11431-017-9149-1

Wisnom, M.R., Green, D., 1995. Tensile failure due to interaction between fibre breaks. Composites 26, 499–508.

Wu, X., Liu, Y., Li, X., Wen, P., Zhang, Y., Long, Y., Wang, X., Guo, Y., Xing, F., Gao, J., 2010. Preparation of aligned porous gelatin scaffolds by unidirectional freeze-drying method. Acta Biomater. 6, 1167–1177.

Yang, D., Li, Y., Nie, J., 2007. Preparation of gelatin/PVA nanofibers and their potential application in controlled release of drugs. Carbohydr. Polym. 69, 538–543.

Zhang, Q., Lu, H., Kawazoe, N., Chen, G., 2014. Pore size effect of collagen scaffolds on cartilage regeneration. Acta Biomater. 10, 2005–2013.

Chapter 5: (Macro)Molecular Imprinting

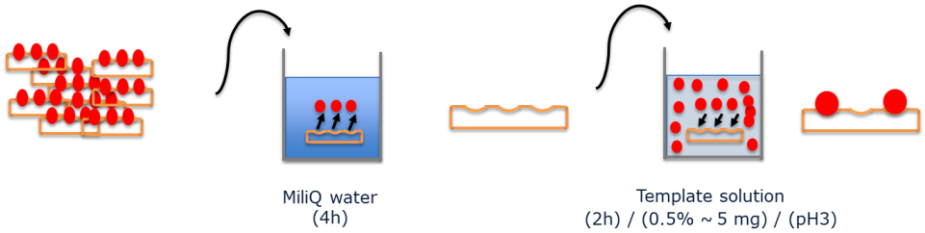

5.1 Introduction

Molecular Imprinting (MI) is a technique that allows the production of structures with desired properties by adding specific polymers which can modulate the structure of the system. This technique is based on the construction of ligand selective recognition sites in synthetic polymers where a template (atom, ion, molecule, complex, etc.) is employed as a recognition site shaper during the polymerization process. The subsequent removal of the template allows the formation of vacancies with selective recognition (Whitcombe et al., 2014; Ye et al., 2000).

The molecular imprinting technique is often described as a method to make a molecular lock match a molecular key based on the formation of sites with specific molecular recognition (Chen et al., 2016; Kadhirvel et al., 2015). Molecular recognition is a fundamental process in the natural world for the rapid recognition of enzymes and nucleic acids. Molecular imprinting technologies, such as processes for the preparation of synthetic polymers with binding sites for specific molecules, are the next development in the practical application of molecular recognition (Braunschweig et al., 2009; Chen et al., 2011).

A typical MI process contains a solvent, a target molecule and a template (Figure 5.1).

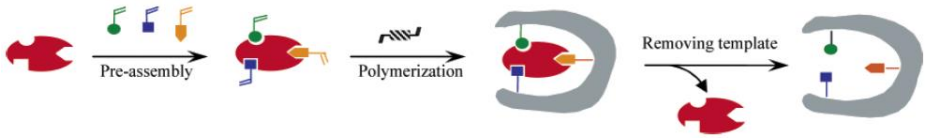

Figure 5.1. Schematic overview of a Molecular Imprinting process. Figure obtained from Chronakis et al. (2006)

The solvent is generally used as a dispersion media and recognition sites forming agent. On the other hand, the second element of the MI process

is the target. Its main role is to form a complex with the template, thus it is necessary to select a suitable target and process to form the previous target-template complex. Depending on the target used, the MI process can be divided into two different groups: conventional and alternative molecular imprinting. Traditionally, the molecular imprinting process has been carried out with monomers and crosslinkers through a pre-polymerization stage. In this case, the process is called conventional molecular imprinting. However, molecular imprinting can be obtained directly from polymers instead of combining monomers and crosslinkers. This new concept is called alternative molecular imprinting and was proposed by Yoshikawa in the late 90s (Yoshikawa, 2001; Yoshikawa et al., 1995). Basically, it is similar to conventional molecular imprinting, with the only difference being that the starting materials are polymers instead of monomers.

Finally, the template is the main element of the MI process. The process has been traditionally performed using small molecules as templates (Chen et al., 2011; Fasihi et al., 2011; Zhang et al., 2014). In addition, large species, such as drugs and viruses, have also been used for MI (Cai et al., 2010; Hayden and Dickert, 2001), whereas the use of proteins and other biomacromolecules still poses an important challenge. Removal of the template leaves a cavity, matching the physical and chemical characteristics of the template species. Any variation from the structure of the desired species to a structurally similar but non-identical entity may result in loss of selectivity. Template removal can be carried out in two different ways depending on the method used for the elimination of the template molecule in this stage. On the one hand, the template can be removed with simple solvent extraction. On the other hand, a chemical

cleavage is needed when a covalent process takes place (Ghorani et al., 2015).

There are different types of Molecular Imprinting techniques (Ertürk and Mattiasson, 2017). Thus, four different types of MI can be distinguished depending on the interaction between the template and the target. The most commonly used are the covalent and the non-covalent, produced through a covalent bond or hydrogen bonding, respectively. However, there are other types based on electrostatic or ionic interactions, and ligand-metal coordination, which are called ionic and metal centre coordination molecular imprinting, respectively (Chen et al., 2016).

In covalent imprinting, all the recognition sites have theoretically the same affinity and selectivity due to the identical depths and shapes of the binding cavities. However, covalent imprinting is seen as a less flexible method, since only a few molecules can be used with a chemical condensation reaction (Turiel et al., 2001). On the other hand, although the non-covalent approach is characterized by a more heterogeneous binding, leading to a significant decrease in overall recognition performance, the removal of the template is straightforward. This fact, combined with the different possibilities to be performed (ionic interactions, hydrogen bonding, etc.), has made this process become more popular, as it is easy to carry out and also due to its binding and removal rate (Wulff and Schauhoff, 1991).

Our approach is based on the use of systems produced by electrospinning. The electrospinning technique has been already studied in Chapter 4 and involves the formation of extremely long ultra-thin polymeric fibers. The combination of MI together with electrospinning was first developed by Chronakis et al., (2006), where poly(ethylene terephthalate) (PET) was used as the target and the drug 2,4-

dichlorophenoxyacetic acid as the template. In this sense, other approaches were produced (Frenot and Chronakis, 2003; Ghorani et al., 2015; Yoshikawa et al., 2011) by making use of the combination of electrospun nanofibers and the molecular imprinting technique. However, these studies were performed using a chemical cleavage, hindering the overall process due to the presence of additional steps involving chemical reactions.

Our hypothesis proposes the combination of the electrospinning process together with a solvent extraction step to induce the formation of specific sites in the target for the desired polymer. A combination of a synthetic and a natural polymer was considered when performing the electrospinning stage. More specifically, the selection of the systems was based on the study carried out in Chapter 4. Poly(ε-caprolactone) (PCL) was selected as the synthetic polymer due to its biocompatibility and easy processing, among other characteristics (Gümüşderelioğlu et al., 2011; Woodruff and Hutmacher, 2010). Gelatin, which is the denatured form of collagen, was selected as the natural protein due to its advantages (biomechanical and biocompatibility properties) in Tissue Engineering applications (Allam et al., 2012). Thus, the main goal is the development of a molecular imprinting technique to modify electrospun scaffolds in order to modulate their structure and properties by using macromolecules (more specifically proteins) as the template (MacroMolecular Imprinting). A schematic view of the overall process carried out is shown in Figure 5.2:

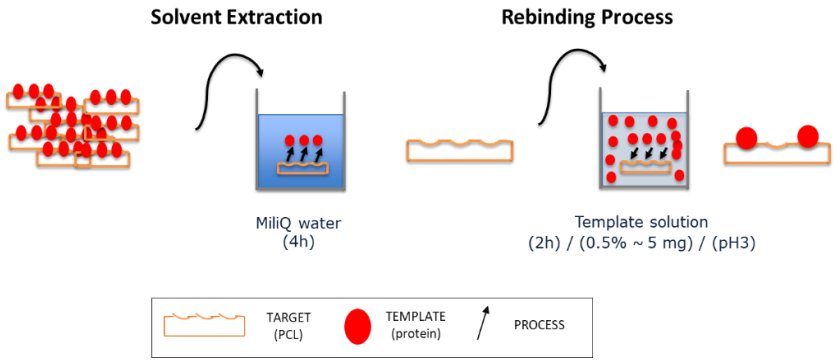

Figure 5.2. Schematic overview of the Molecular Imprinting process carried out

The systems were characterized after each stage of the process. The characterization encompasses the study of the template-target interaction through infrared spectroscopy (FTIR) and the analysis of the variations of the surface hydrophobicity with contact angle measurements. Moreover, the protein rebinding was evaluated with Energy Dispersive X-ray Spectroscopy (EDAX) and BCA protein quantification.

5.2 Material and methods

5.2.1. Materials

Gelatin protein (gelatin type B, 80-120g Bloom) was supplied by Henan Boom Gelatin Co. Ltd (China). Its protein content is higher than 90 wt.%. On the other hand, type I pork collagen protein (Pork HI95) was supplied by Essentia Protein Solutions (Grasten, Denmark). Their complete compositions can be seen in Chapter 2.

Poly(ε-caprolactone) (PCL, Mw = 45,000 g/mol), Bovine Serum Albumin (BSA, Mw = 66,000 g/mol), 1,1,1,3,3,3-hexafluoro-2-propanol (HFIP), Sodium Dodecyl Sulphate (SDS) and Dimethylsulfoxide (DMSO) were purchased from Sigma Aldrich (Germany).

5.2.2. Molecular Imprinting process (MI)

The overall process of the molecular imprinting process is mapped in the following figure (Figure 5.3):

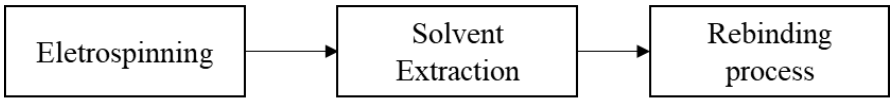

Figure 5.3. Stages of the Molecular Imprinting process

Electrospinning

The electrospinning process was carried out with the same processing conditions as the studies performed in Chapter 4. As a summary, the processing conditions used are: 14 kV of voltage, 0.4 mL/h of flow rate and 14 cm as the needle-collector distance.

Two different systems were produced using a Fluidnatek LE-100 (Bioinicia). On the one hand, PCL/GE 16/4 scaffolds were produced with the most promising concentration (16 % PCL and 4 % gelatin). On the

other hand, PCL neat scaffolds (16 %) were also produced and evaluated as a control.

Solvent Extraction

As commented before, the scaffolds were produced with PCL and gelatin, two molecules with different solubility character. Thus, the second stage consisted of a solvent extraction process by immersion of the scaffolds in MiliQ water for 4 h to allow the gelatin to dissolve. After that, the samples were dried overnight.

Rebinding process

The second stage consisted of the immersion of the membranes in a template solution (0.5 wt.%) at pH 3 for 2 h. This stage was carried out to study the possible rebinding of template molecules (gelatin) on the surface of the nanofibrous membrane.

5.2.3. Studies performed

The different studies performed have been summarised in the following table (Table 5.1).

Table 5.1. Studies performed: Systems used (PCL and PCL/GE), variables analyzed, and parameters involved

Systems	Variables studied	Parameters	Sections
PCL/GE **PCL**	Initial Study	-	5.3.1
	Template used (selectivity)	Gelatin/collagen/BSA	5.3.2
	Immersion time (reaction kinetics)	1/2/4 h	5.3.3
	Template solution concentration (efficiency)	0.5/0.05/0.005/0.0005 %	5.3.4.1
	Number Cycles (efficiency with time)	1/2/3 cycles	5.3.4.2
	pH	3/6/9	5.3.5.1
	Salting in/out	$MgCl_2$ (in) / KPO_3 (out) SDS / DMSO	5.3.5.2
	Target used	$PCL_{14,}$ PCL_{45}, PCL_{80}	5.3.5.3

All the studies were performed with a binary scaffold formed by PCL_{45} (16%) and gelatin (4%) [named as PCL/GE], while using a PCL_{45} (16%) scaffold [named as PCL] as a reference control. The operating conditions selected as reference are summarized in Table 5.2:

Table 5.2. Reference operating conditions selected to perform the MI process

Molecular Imprinting Reference Conditions	
Template	Gelatin
Target	PCL_{45}
Immersion Time	2 h
Template Solution Concentration	0.5 %
pH	3

5.2.4. Characterization of scaffolds

The membranes were characterized initially and after each stage to follow the evolution of the membranes within the process. The characterization techniques are described in detail in Chapter 4. A brief description is given below:

Fourier Transform Infrared Spectroscopy (FTIR)

The chemical bonds were analysed by ATR-FTIR method using an iS50 ATR-FTIR spectrophotometer (Nicolet, Thermo Fisher Scientific, USA). The different spectra were collected in the range of 4000-1500 cm^{-1}.

Water contact angle (WCA)

Scaffolds wettability and hydrophobicity were assessed by water contact angle (WCA) measurements using the sessile drop method (droplets with an approximate volume of 5 μL). Both WCA values of the right and left sides of the deionized water droplets were measured and the average

value was calculated. The equipment used was a Drop Shape Analyzer (Krüss, Germany).

Energy Dispersive X-ray Spectroscopy (EDAX)

The atomic compositions of the membrane were examined with the energy dispersive spectroscopy capability of the SEM equipment using an EDAX Si(Li) detector and an acceleration voltage of 5 kV. The samples were covered with a film of Au in a high-resolution sputter coater. Microscopy examination of the scaffolds was previously performed with an XL 30 (Philips XL Series, USA) at an acceleration voltage of 15 kV. This technique allows us to determine the presence of Nitrogen (N) in the sample, as a direct measure of the protein content in the systems.

Template Binding

The analysis of the template binding was performed using a BCA protein quantification using a BCA kit. The BCA Protein Assay Kit (Pierce, Germany) was used following the manufacturer's instructions: microplate procedure (10µL sample/200 µL BCA working reagent; incubate at 37°C for 30 min; measure the absorbance at 562 nm). For every microplate prepared, a BSA-dilution curve consisting of 8 points up to 2000 µg/mL BSA was included as standard to check for consistency between different experiments.

- Ligand Binding A: The result obtained corresponded to the total template content (in µg) in the membrane after the rebinding process.
- Ligand Binding B: Specifically, for the "template solution concentration study", the template content in the membrane was compared to the total amount of template in the rebinding solution using Equation 5.1:

$$\%\, Binding = \frac{Template\ content}{Template\ solution} \cdot 100 \qquad (5.1)$$

5.2.5. Statistical analysis

At least three replicates were carried out for each measurement. Student´s t-test and one-way analysis of variance ($p < 0.05$) were performed using PASW Statistics for Windows (Version 18: SPSS, Chicago, IL). Standard deviations were calculated for selected parameters.

5.3 Results and Discussion

Molecular Imprinting (MI) is an innovative technique used to place small molecules on surfaces with specific sites. However, carrying out the molecular imprinting process with larger molecules (i.e. proteins) is still challenging. Therefore, initially, to corroborate that the process was successfully performed, an initial study was performed with the designed reference conditions, comparing the results obtained for PCL/GE and PCL neat scaffolds.

5.3.1. Initial study

An evaluation of the process was performed through the analysis of both types of scaffolds in each different stage of the process. Thus, a characterization of the process was performed under different points of view and the results were shown in Figure 5.4 and Table 5.3.

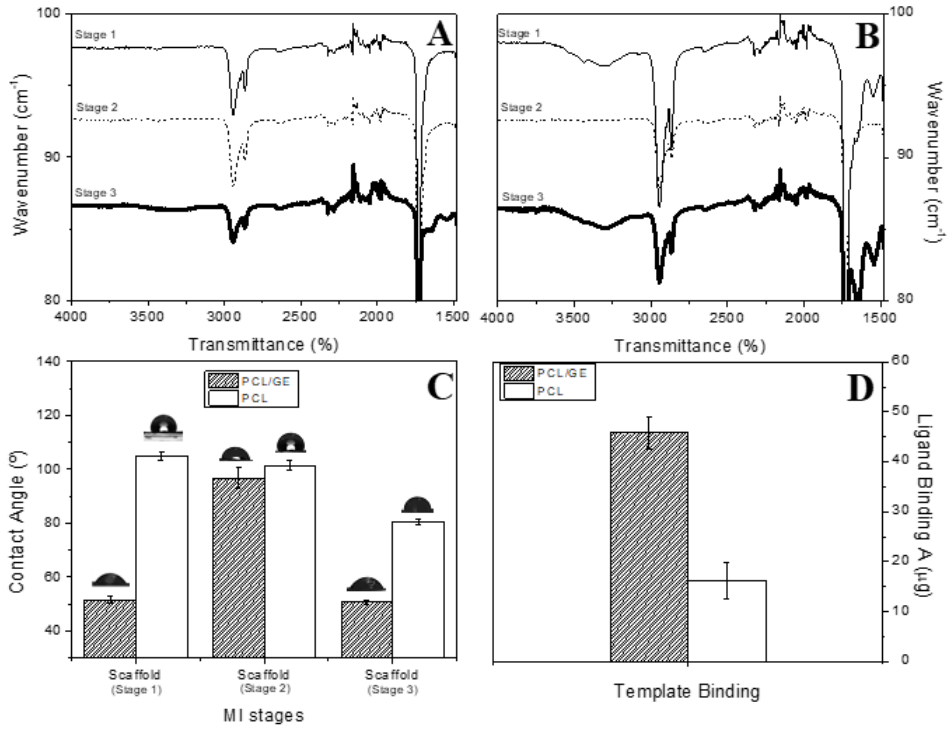

Figure 5.4. FTIR, water contact angle measurements and template binding results obtained for PCL and PCL/GE scaffolds after performing each stage of the MI process

Stage 1

This stage consisted in the fabrication of scaffolds via electrospinning. The main difference between the samples is the presence of proteins in the initial formulation for the PCL/GE system compared to the PCL neat sample.

Figures 5.4A and 5.4B show the FTIR profiles of both scaffolds. Considering the PCL neat scaffold (Figure 5.4A), a characteristic sharp band is observed at 1725 cm^{-1} (Cebi et al., 2016), associated with carbonyl stretching (characteristic for PCL). However, the PCL/GE system (Figure 5.4B) presented, apart from the peak at 1700 cm^{-1} previously mentioned, a broad area at 3276 cm^{-1} associated with N-H stretching (traditionally called Amide A signal) and two small bands at 1635 and 1525 cm^{-1}, related to carbonyl stretching and C-N stretching of amides, respectively. These peaks are characteristic of proteins (Muyonga et al., 2004). These peaks match with the ones obtained for fish gelatin in Chapter 2 (Section 2.3.2).

In addition, Figure 5.4C shows the contact angle values for these systems. PCL is a hydrophobic molecule, which explains the high value observed for WCA (ca. 105º), in contrast with gelatin, which presents a hydrophilic character and, thus, the resulting scaffold presented a WCA lower than 60º.

Table 5.3. EDAX values (%) obtained for the PCL/GE 16/4 and PCL systems after performing each stage of the molecular imprinting process. Values with different letters are significantly different ($p<0.05$)

EDAX Results (%)			
SYSTEMS	Stage 1	Stage 2	Stage 3
PCL/GE	3.31^{a}	-	2.83^{b}
PCL	-	-	1.34^{c}

Furthermore, Table 5.3 shows the EDAX results for both structures. The analysis of the PCL neat sample revealed no Nitrogen in its structure, whereas the PCL/GE presented 3.31 % of N in it.

Stage 2

In this stage, both systems were then submitted to solvent extraction using MiliQ water. PCL is insoluble in water, thus the properties found for the PCL neat scaffold were the same as before. However, gelatin is water-soluble, thus gelatin was released into the solution from the scaffold. This effect is corroborated by the different techniques performed. Figure 5.4B (dash line) exhibits the loss of the characteristic peaks for proteins in the FTIR profile, showing a profile similar to the one obtained for the PCL-neat system (Figure 5.4A). The alteration of the composition of the scaffold is also noticeable by the variation of WCA (Figure 5.4C). The WCA values of PCL/GE scaffolds go from 54º to 100º, obtaining a high hydrophobic system that was not significantly different ($p<0.05$) from the PCL neat sample. Moreover, the EDAX analysis is in line with the one observed in the other techniques, revealing the absence of N in the PCL/GE structure.

In conclusion, all the gelatin present in the structure (and observed in the previous section) is lost during this stage, giving rise to a scaffold similar to the one formed with only PCL.

Stage 3

The final stage of the process consisted of the immersion of the scaffolds from Stage 2 in a template (gelatin) solution. While one might think that the deposition of gelatin in both structures should be similar, the results revealed different behaviors.

Figures 5.4A and 5.4B show the FTIR spectra of both scaffolds after Stage 3 (black bold line). The characteristic peak of PCL at 1700 cm^{-1} is

observed again, together with the representative peaks for proteins (described in Stage 1). However, the intensity of the peaks is much higher for the PCL/GE system compared to the PCL neat scaffold. This result is linked to the WCA values obtained and shown in Figure 5.4C. In both systems, there was a decrease in the contact angle values as a consequence of the increase in their hydrophilicity due to the presence of protein on the surface of the fibers. However, the PCL/GE system presented a WCA of 50º, similar to the one obtained in Stage 1, whereas the PCL scaffold gave a value close to 80º.

These results reinforced the idea of the presence of a higher concentration of protein on the surface of the PCL/GE scaffold compared to the PCL neat scaffold after Stage 3. However, to estimate this, the template binding was measured in both systems after the sequence of stages and the results were plotted in Figure 5.4D. Ligand Binding A results enable the quantification of the total protein deposited over the surface, doubling the value obtained for the PCL/GE system compared to the PCL neat one.

In conclusion, the deposition of the protein on the surface of the scaffolds was different for the two cases studied, which was more remarkable for the PCL/GE system. This fact may be explained considering the third stage as a rebinding process in which gelatin molecules (from the template solution) are inserted in some of the specific sites left by the initial gelatin after coming out during Stage 2. That effect can be considered as a molecular imprinting process in which there are specific sites for gelatin binding. However, since this process is relatively new and innovative, a complete characterization is necessary in order to evaluate the influence of different parameters on the overall process.

5.3.2. Evaluation of the selectivity

The selectivity of the process was evaluated by repeating the same process with different template solutions. For this reason, the process was followed using other proteins instead of gelatin: collagen and BSA. Collagen was selected due to its structural similarity with gelatin, and BSA was selected in order to use a molecule from the same family as gelatin but with a different structure. The results of the characterization performed using different templates are shown in Figure 5.5.

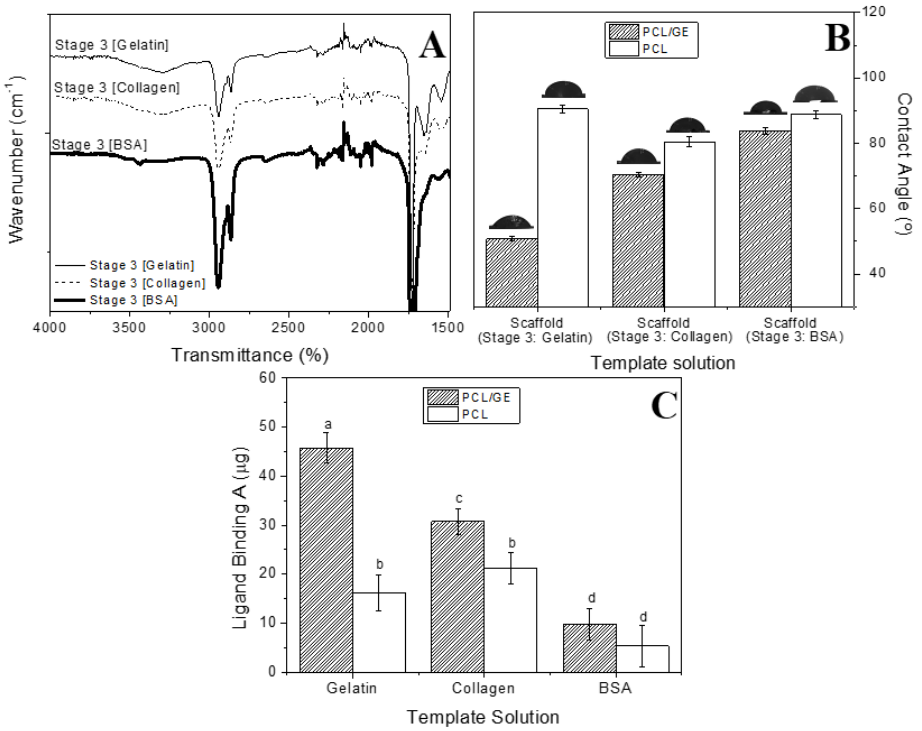

Figure 5.5. FTIR, water contact angle measurements and template binding results obtained for PCL and PCL/GE scaffolds after performing the MI process varying the template solution used (gelatin, collagen or BSA)

The FTIR profiles shown in Figure 5.5A correspond to PCL/GE scaffolds after performing the complete cycle using different template solutions. It can be observed that the characteristic peaks of proteins

appear in the three profiles (N-H, C=O and C-N stretching at 3276, 1635 and 1525 cm^{-1}, respectively). However, the intensity of the bands varied depending on the protein because, when the process was fulfilled using BSA (bold line), the peaks were softer and of lesser intensity than the ones obtained with collagen (dash line). The bands for the latter are closer to the ones obtained for the reference (gelatin, straight line).

Apart from the FTIR profiles, the contact angle values of the final systems after conducting the process with different template solutions are also shown in Figure 5.5 (Figure 5.5B). The results follow two different trends depending on the scaffold studied. PCL/GE scaffolds show increasing contact angle values following the sequence Gelatin>Collagen>BSA, which means that the surface presented a higher amount of protein when the process was carried out with gelatin or collagen rather than with BSA. On the other hand, the outcomes of the PCL neat-based system indicate that the process was better fulfilled with collagen compared to gelatin or BSA, giving rise to a lower contact angle value. For this system, the efficient sequence of deposition is Collagen>Gelatin>BSA.

Table 5.4. EDAX values (%) obtained for the PCL/GE and PCL systems after performing the molecular imprinting process with different template solutions (gelatin, collagen or BSA). Values with different letters are significantly different ($p<0.05$)

EDAX Results (%)			
SYSTEMS	Stage 3 [Gelatin]	Stage 3 [Collagen]	Stage 3 [BSA]
PCL/GE	2.83^{a}	1.78^{c}	0.73^{d}
PCL	1.34^{b}	1.50^{bc}	0.49^{d}

The EDAX results observed in Table 5.4 show the nitrogen concentration (%) of the membranes after performing the overall process with different template solutions, which can be associated with the

amount of protein rebound in the membranes. The results follow an inversely proportional trend as the contact angle values since the PCL/GE system show a decrease in the nitrogen content when using a template solution produced with collagen or BSA compared to the one produced with gelatin. On the other hand, the PCL neat-based scaffold presented the maximum value for collagen, followed by gelatin and BSA.

In addition, Figure 5.5C shows the results of the template binding calculations. These results are in accordance with the previous data shown (FTIR, contact angle and EDAX values). A decreasing stream is observed for the PCL/GE scaffold, with a protein rebinding four times higher for gelatin compared to BSA (45 and 10 µg, respectively). An intermediate value was obtained when the process was followed using collagen (10 µg).

Once again, these results correlate the effectivity of the MI process with the amount of protein presented over the surface of the scaffold. In this sense, the selectivity of the process is affected by the type of protein used. The specific sites generated by gelatin allow a better rebinding process of proteins with a similar shape, especially if it is the same protein as initially. This fact is verified by the better results obtained for the gelatin and collagen proteins with respect to BSA. However, relatively good results were obtained for collagen as a substitute for gelatin, demonstrating the possibility of using this technique to obtain scaffolds with expensive molecules from raw materials in a low concentration, using a dummy template (which is gelatin in our study).

5.3.3. Evaluation of the reaction kinetics

Apart from the binding capacity, reaction kinetics for a given molecularly imprinted material is a significant aspect of the MI process. Thus, the immersion time of the scaffolds in the template solution in Stage 3 was modified in order to study the evolution of the protein binding with time. The reference time was set at 2 h and a lower and higher time were evaluated (1 and 4 h, respectively). The results for the characterization of the systems are shown in Figure 5.6.

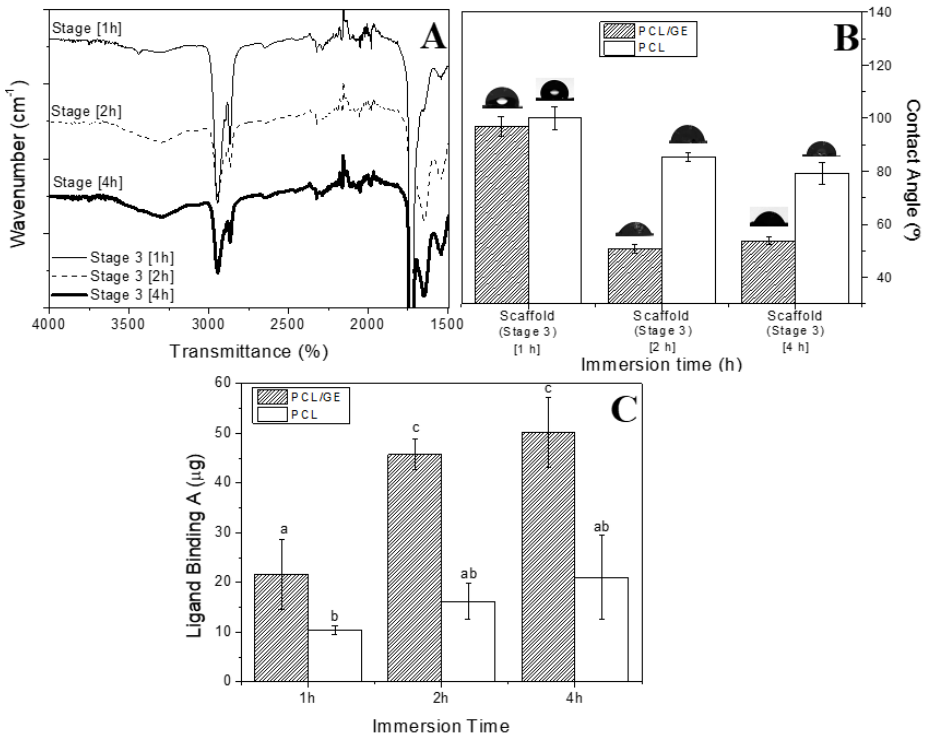

Figure 5.6. FTIR profiles, water contact angle measurements and template binding results obtained for PCL and PCL/GE scaffolds after performing the MI process varying the immersion time in the template solution (1, 2 or 4 h)

Figure 5.6A shows the evolution of the FTIR profile of the PCL/GE system with the immersion time. The characteristic peak of PCL remains constant at 1700 cm^{-1}, whereas the corresponding peaks of proteins

exhibit an increase with the immersion time, highlighting the peaks at 1635 and 1525 cm^{-1}. These results are in accordance with the contact angle values shown in Figure 5.6B, where the system PCL/GE shows a decrease in the WCA, reaching a plateau at ca. 50º when the immersion time is at least 2 h. In addition, the contact angle of the PCL/GE system at 1 h was not significantly different from the one obtained by the PCL neat system (97 and 102º, respectively).

Table 5.5. EDAX values (%) obtained for the PCL/GE and PCL systems after performing the molecular imprinting process with different immersion times (1, 2 and 4 h). Values with different letters are significantly different (p<0.05)

EDAX Results (%)			
SYSTEMS	Stage 3 [1 h]	Stage 3 [2 h]	Stage 3 [4 h]
PCL/GE	1.91^{a}	2.83^{b}	3.44^{b}
PCL	0.29^{c}	1.34^{d}	1.29^{d}

Comparing the EDAX results from both systems, they are significantly higher for the PCL/GE-based scaffolds with respect to the PCL neat scaffolds. However, both systems showed the same tendency, which is an increase in the nitrogen content until reaching a plateau as of 2 h immersion, presenting no significant differences with the 4 h immersion. Furthermore, the protein binding results plotted in Figure 5.6C show two different profiles. On the one hand, the PCL/GE system exhibits a marked increase in the template binding as of two hours of immersion in the template solution. On the other hand, the PCL system shows a slight increase in the protein binding with the immersion time but with no significant differences in the results ($p<0.05$). In any case, the protein binding was between 2 and 4 times higher for the PCL/GE compared to the pure PCL system.

5.3.4. Evaluation of the efficiency

The efficiency of the process can be evaluated from two completely different points of view. On the one hand, it can be considered as the minimum amount of protein (template) in the solution necessary to achieve proper rebinding. On the other hand, it can be also considered as the number of cycles necessary to be performed to achieve proper rebinding. Therefore, both types of studies were performed and are shown below.

5.3.4.1. Template solution concentration

Different template solution concentrations (0.5, 0.05, 0.005 and 0.0005 wt.%) were used to evaluate the minimum amount of protein (template) in the solution necessary to achieve proper rebinding. A summary of the results obtained was plotted and compared in Figure 5.7.

Figure 5.7A shows the evolution of the FTIR profile of the PCL/GE scaffold with the different concentrations of the template solution. As can be observed, the intensity of the peaks shown at 3276, 1635 and 1525 cm^{-1} decrease when the solution concentration is lower than 0.05 %; they even tend to disappear at the lowest concentration measured. Together with the FTIR results, the contact angle values show the same trend: scaffolds with higher contact angles are obtained when they are immersed in template solutions with lower concentrations (Figure 5.7B).

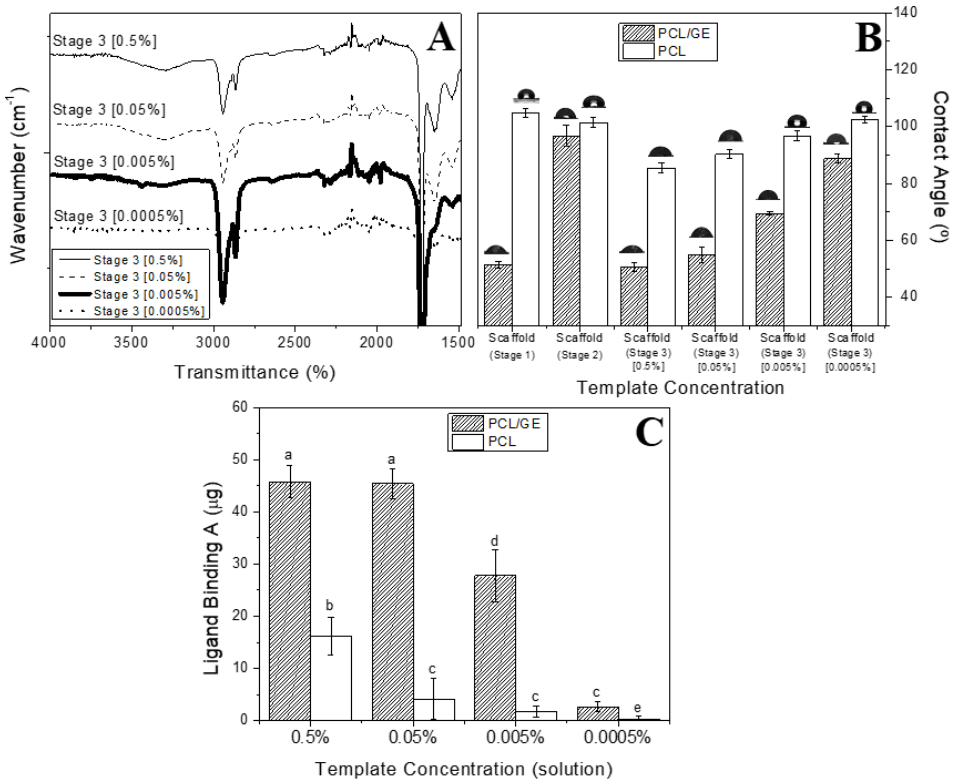

Figure 5.7. FTIR profiles, water contact angle measurements and template binding results obtained for PCL and PCL/GE scaffolds after performing the MI process varying the concentration template solution used (0.5, 0.05, 0.005 and 0.0005 %)

In the same line as the results plotted in Figures 5.7A and 5.7B, Table 5.6 shows the EDAX results of the final scaffolds obtained varying the template solution concentration.

Table 5.6. EDAX values obtained for the PCL/GE and PCL systems after performing the MI process varying the concentration template solution used (0.5, 0.05, 0.005 and 0.0005 %). Values with different letters are significantly different (p<0.05)

EDAX Results (%)				
SYSTEMS	Stage 3 [0.5 %]	Stage 3 [0.05 %]	Stage 3 [0.005 %]	Stage 3 [0.0005 %]
PCL/GE	2.83^{A}	2.47^{A}	1.38^{B}	0.44^{CD}
PCL	1.34^{B}	0.62^{C}	0.23^{D}	0.11^{D}

Two different trends are observed, as the PCL neat system shows a linear decrease with the decrease in the template solution, whereas the PCL/GE system shows a constant value, which decreases when the solution concentration is lower than 0.05 %.

The ligand binding results also reflect the influence of the solution concentration on the MI process. Interestingly, two different tendencies are observed depending on whether the process is carried out with the system formed by PCL/GE or just by PCL. The first case shows a plateau region up to 0.05 %, from which the rebinding decreases, going from 40 µg to ca. 10 µg (Figure 5.7C). However, the system formed by PCL neat shows a progressive decrease in protein deposition as the concentration of the solution used decreases.

Moreover, in order to relate the total amount of protein initially present in the solution with the amount of protein rebound after stage 3, Figure 5.8 was plotted, in which the *'Ligand Binding B'* results are shown.

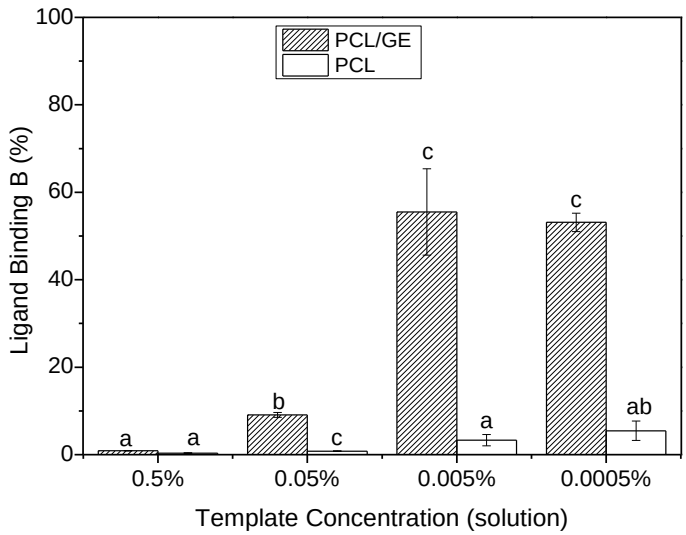

Figure 5.8. Template binding results (Ligand Binding B) obtained for PCL and PCL/GE scaffolds after performing the MI process varying the concentration template solution used (0.5, 0.05, 0.005 and 0.0005 %)

The efficiency of the process underwent a polynomial growth by decreasing the used concentration since, although the amount of rebound protein decreases, its ratio over with the amount of total protein in solution leads achieving an efficiency of more than 50%. However, as it is verified when comparing Figures 5.7C and 5.8, while it is true that an increase in efficiency takes place, it is at the expense of the amount of rebound protein. Therefore, it would be necessary to select an intermediate situation in which the efficiency is acceptable without affecting the amount of protein linked on the surface of the PCL (0.05%).

5.3.4.2. Number of cycles performed

The process was performed in successive cycles to evaluate whether there is a continuous growth of the protein rebinding or the process reaches a plateau. Thus, the MI process was studied after performing 1, 2 and 3 consecutive cycles (Figure 5.9).

The FTIR profiles shown in Figure 5.9A present a similar peak intensity, with a slight increase when the process was repeated 3 times (C3, bold line). In addition, Figure 5.9B shows the contact angle values of the PCL/GE system after performing the successive cycles. Interestingly, the contact angle values for the PCL/GE scaffolds did not show significant variations, with values of ca. 50º. These results are in accordance with the template binding observed in Figure 5.9C, with values in the range of 45 µg for the PCL/GE system, regardless of the number of cycles performed.

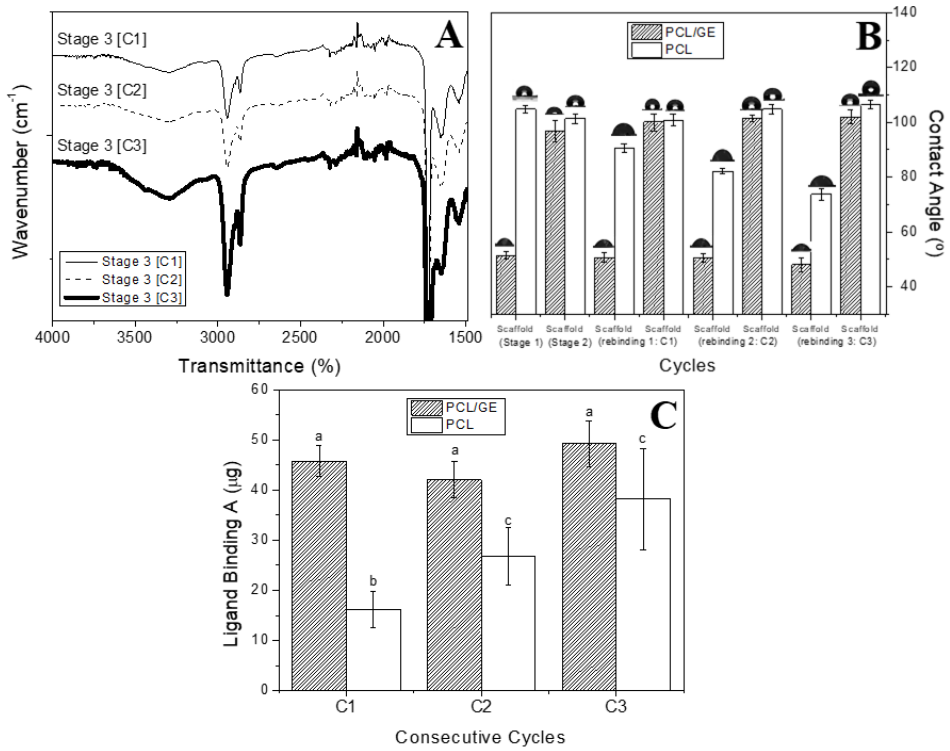

Figure 5.9. FTIR profiles, water contact angle measurements and template binding results obtained for PCL and PCL/GE scaffolds after performing the MI process varying the number of consecutive cycles performed: 1 cycle (C1), 2 cycles (C2) or 3 cycles (C3)

However, PCL scaffolds show different behavior. Contact angle values show a progressive decrease when the samples were subjected to a greater number of successive cycles. This fact, together with the increase in the template binding observed in Figure 5.9C evidenced the increase in the protein binding when the sample was immersed in the template solution for more cycles. Gelatin binding increased from 15 µg to ca. 35 µg when the cycle was performed 3 times. This increase is also observed in the EDAX results shown in Table 5.7 with an increase in the Nitrogen content (%).

Table 5.7. EDAX values obtained for the PCL/GE and PCL systems after performing the MI process varying the number of consecutive cycles performed: One cycle (C1), two cycles (C2) or three cycles (C3). Values with different letters are significantly different (p<0.05)

EDAX Results (%)			
SYSTEMS	Stage 3 [C1]	Stage 3 [C2]	Stage 3 [C3]
PCL/GE	2.83^{a}	3.05^{a}	4.05^{d}
PCL	1.34^{b}	1.93^{c}	2.12^{c}

On the other hand, WCA was also measured after performing a new solvent extraction process after the rebinding process and the results were also plotted in Figure 5.9B. Interestingly, the contact angle values reached values in the range between 95 and 105º, evidencing a marked hydrophobic character for both the PCL and PCL/GE systems after performing the new solvent extraction stage. Consequently, it seems that protein binding is lost after performing again solvent extraction (like the one carried out in Stage 2), as a proof of the reversibility of the process.

5.3.5. Evaluation of the environmental conditions

This study is divided into three different sections according to the different variables considered: 5.3.5.1) effect of the pH; 5.3.5.2) the addition of salts; and 5.3.5.3) the target used.

5.3.5.1. pH

An interesting parameter to evaluate is the pH of the template solution, as it may alter the structure of the template in solution. Three different pH values were analyzed (3, 6 and 9). Considering that the isoelectric point (Ip) of the gelatin protein is at pH 4.5 according to the characterization shown in Chapter 2, pH values lower and higher were studied to evaluate the shift that takes place in the structure and its consequence on the process. At pH 3, the protein is positively charged due to the fact that the pH of the solution is lower than its Ip. On the other hand, working at pH 6 and 9 allowed us to evaluate the process when the protein was negatively charged in an acidic and basic environment.

Figure 5.10A shows the evolution of the FTIR profile of the PCL/GE scaffold with the different pH values of the solution studied. Although it is true that the intensity of the broad peak at 3276 cm^{-1} did not vary, the intensity of the two peaks at 1635 and 1525 cm^{-1} decreased with the pH, which was more remarkable at pH 6 and 9. In this sense, contact angle values in Figure 5.10B show a similar trend, with a lower contact angle found at pH 3 compared to the ones obtained at pH 6 and 9, as a consequence of a lower protein deposition when the pH is higher than the Ip of the protein.

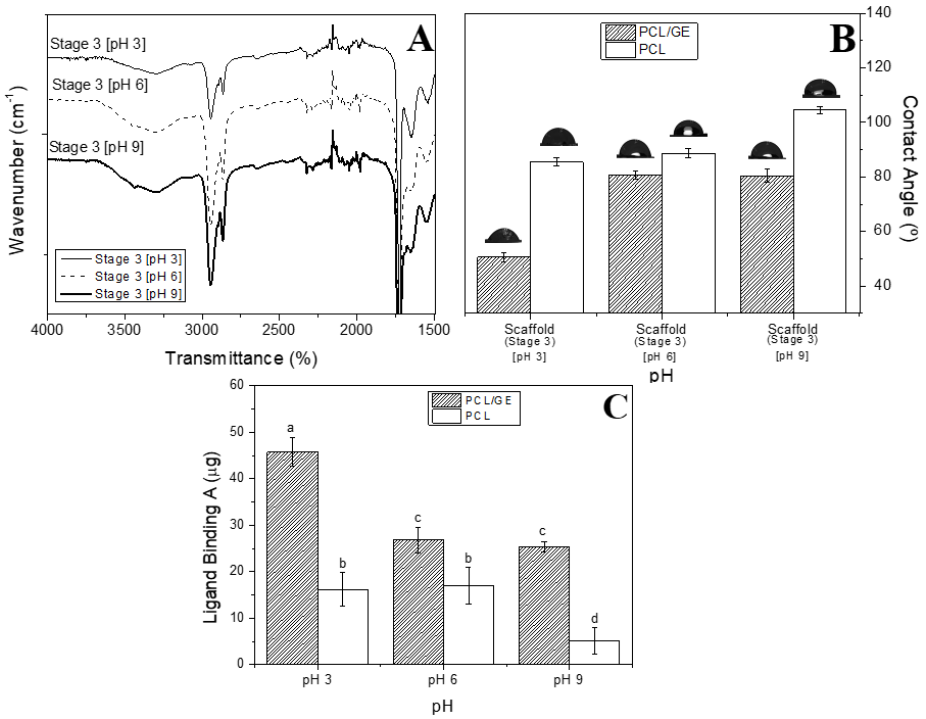

Figure 5.10. FTIR profiles, water contact angle measurements and template binding results obtained for PCL and PCL/GE scaffolds after performing the MI process varying the pH of the template solution (3, 6 or 9)

These results are in accordance with the EDAX and template binding results shown in Table 5.8 and Figure 5.10C, respectively. The EDAX results show an N content of 2.8 % for the system obtained at pH 3, higher than the ca. 1.6 % for the system obtained at pH 6 and 9. Besides, protein binding is almost double after performing the cycle at pH 3 compared to the system conducted at pH 6 and 9.

Table 5.8. EDAX values obtained for the PCL/GE and PCL systems after the MI process varying the pH of the template solution (3, 6 or 9). Values with different letters are significantly different ($p<0.05$)

EDAX Results (%)			
SYSTEMS	Stage 3 [pH 3]	Stage 3 [pH 6]	Stage 3 [pH 9]
PCL/GE	2.83^{a}	1.64^{b}	1.54^{b}
PCL	1.34^{b}	0.80^{c}	0.26^{d}

PCL in solution is negatively charged. These results show a better interaction between PCL and the protein at pH 3, reinforcing the idea of ionic binding between the specific sites formed in PCL and the protein (gelatin), which is positively charged at pH 3.

5.3.5.2. Salting in/out

The Hofmeister series are formed by different salts with different behaviors in solution (Table 5.9). On the one hand, there are salts that promote the salting in effect, which is related to the stabilization of a solute in solution (i.e. protein molecules) by decreasing the electrostatic energy between its molecules. On the other hand, there are salts that promote the salting out effect, which consists of the precipitation of a molecule (i.e. protein) due to its favourable protein-protein interaction, leading to the formation of an aggregate which is no longer soluble.

Table 5.9. Cationic and anionic Hofmeister series **(Arakawa and Timasheff, 1984; Hardy et al., 2008)**

Salting out						**Salting in**
NH_4^+	K^+	Na^+	Li^+	Mg^{+2}	Ca^{+2}	Gdn^+
SO_4^{-2}	PO_3^-	$Acetate^-$	Cl^-	NO_3^-	I^-	SCN^-

The influence of the *salting in/out* effect on the MI process was analysed with the addition of different salts (10 mg/mL) in the template solution ($MgCl_2$, KPO_3, SDS and DMSO). $MgCl_2$ was used to promote the *salting in* effect, whereas KPO_3 was used to promote the *salting out* effect (as shown in Table 5.9). In addition, SDS and DMSO were used to study the influence of the protein folding and unfolding on the MI process. The results obtained when no salts were added, were included as a reference (initial study, section 5.1).

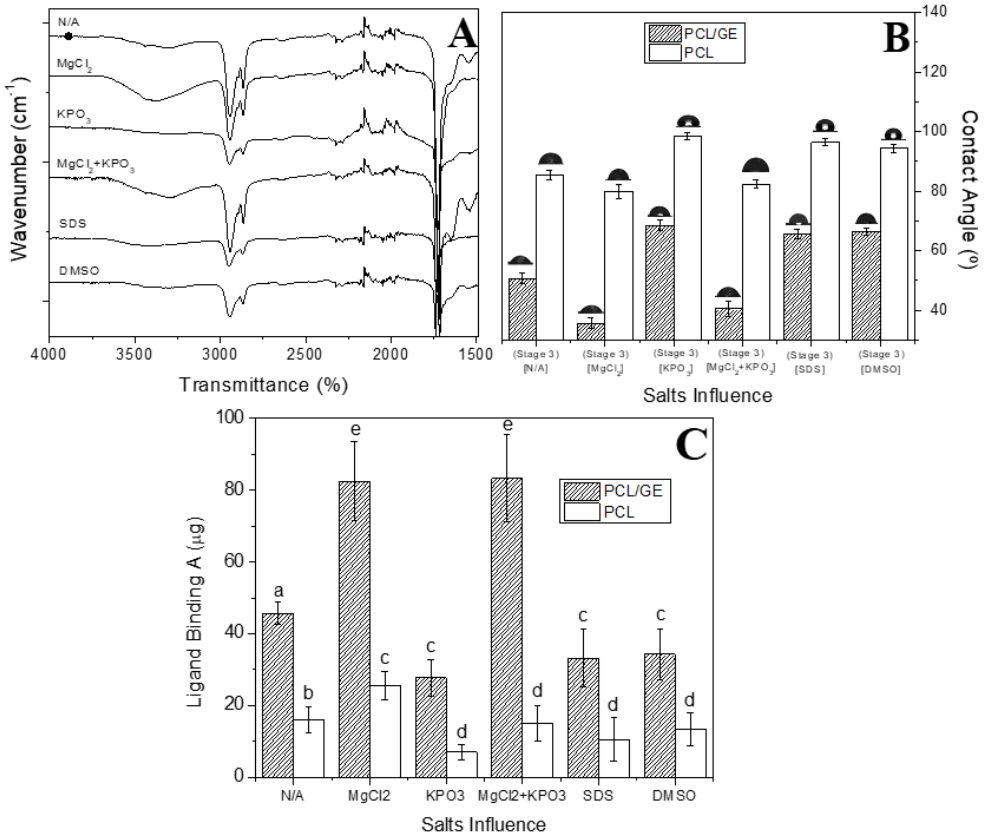

Figure 5.11. FTIR profiles, water contact angle measurements and template binding results obtained for PCL and PCL/GE scaffolds after performing the MI process including different salts in the template solution ($MgCl_2$, KPO_3, $MgCl_2$+KPO_3, SDS and DMSO)

Different considerations can be noted out from the results obtained (Figure 5.11). First, the addition of $MgCl_2$ produced an increase in the typical protein peaks observed in the FTIR spectra (Figure 5.11A), especially remarkable in the broad peak at ca. 3300 cm^{-1} (3276 cm^{-1}). In addition, both the PCL/GE- and PCL neat-based scaffolds presented a lower contact angle compared to the reference one (with no salts added) (Figure 5.11B). These results show a higher protein rebinding compared to the reference system, tested and corroborated with the template binding analysis, showing a protein rebinding two times higher than the

reference for the PCL/GE system and 1.25 times higher for the PCL neat scaffold (Figure 5.11C). In conclusion, the *salting in* effect (fomented by the addition of $MgCl_2$) promoted the protein rebinding, which was more remarkable for the PCL/GE system.

On the other hand, the opposite result occurred when using KPO_3 (*salting out* effect). Figure 5.11C showed a decrease in the template binding compared to the reference data (28 instead of 45 µg and 9 instead of 18 µg for the PCL/GE and PCL systems, respectively). These quantitative results are corroborated by the decrease observed in the intensity of the protein peaks in the FTIR spectrum when including KPO_3 to the template solution and the increase in the contact angle of both systems (PCL/GE- and PCL neat-based), as a consequence of obtaining a more hydrophobic system, i.e., with a lower proportion of rebound protein. These results could be due to the fact that the *salting out* effect leads to the aggregation of the protein and, therefore, the formation of big aggregates which cannot fit in the cavities previously formed.

The influence of the combination of both effects was also studied by the immersion of the scaffolds in a template solution with $MgCl_2$, followed by the immersion in another template solution with KPO_3. The results were called $MgCl_2$+KPO_3 and are also shown in Figure 5.11. In general, both the FTIR profile and contact angle values obtained are similar to the ones obtained with the addition of only $MgCl_2$. This can be verified by the template binding results (Figure 5.10C), which have no significantly different values from the ones obtained for the *salting in* effect. In conclusion, once the protein rebinding occurs, the addition of *salting out* molecules does not promote the subsequent release of the rebound protein.

Apart from *salting in/out* salts, other substances were also evaluated to study their influence on the MI process (SDS and DMSO). Considering the results obtained in both cases, the contact angle values obtained were not significantly different from the values obtained during the *salting out* effect for both the PCL/GE and PCL neat scaffolds. In addition, the FTIR profiles show a softening of the characteristic protein peaks, which could be due to a lower protein rebinding efficiency. To verify this, the template binding was also analyzed, showing results similar to those obtained for *salting out* and, once again, lower ligand binding results comparing these values with the reference ones. It can be concluded that a similar effect takes place when using substances which promote protein unfolding, such as SDS or DMSO (Bhuyan, 2010). Unfolding of the protein promotes its aggregation (Azuaga et al., 2002; Jahn and Radford, 2008) and, subsequently, the formation of big aggregates which cannot fit in the template cavities of the target.

On the other hand, the concentration of the salt can affect the *salting in/out* process (Grundl et al., 2017). In this sense, different concentrations of $MgCl_2$ were evaluated to analyze the influence of the salt concentration on the *salting in/out* process. Figure 5.12 shows the ligand binding results of PCL/GE and PCL structures under the influence of $MgCl_2$ at different concentrations (10, 100 and 1000 mg/mL). No significant differences are observed when a small amount of $MgCl_2$ is included (10 mg/mL). However, a marked increase is observed when the salt concentration is higher (100 mg/mL). Nevertheless, the improvement of the template binding is not linear with the salt concentration, as can be seen when the salt concentration is 1000 mg/mL with a dramatic decrease of the template binding.

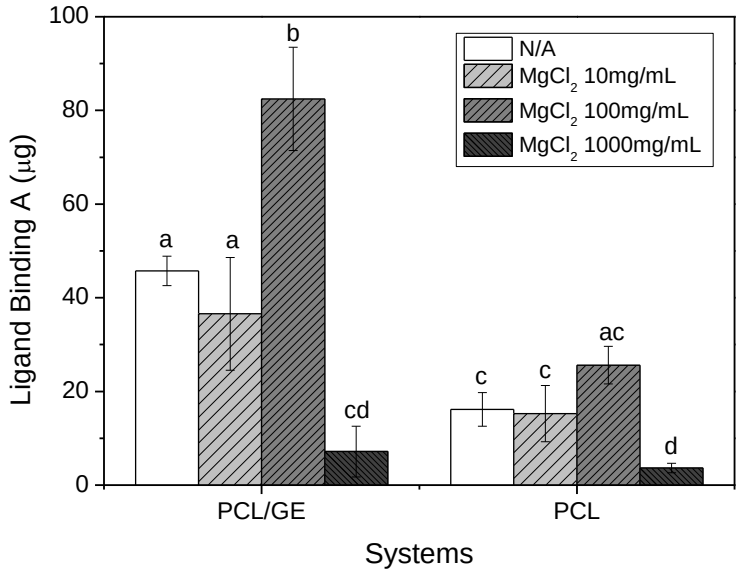

Figure 5.12. Template binding of PCL/GE and PCL-based scaffolds after performing the MI process including MgCl2 at different concentrations in the template solution (0, 10, 100 and 1000 mg/mL)

These results suggest that there is an optimal salt concentration which enhances the *salting in* effect, whereas an excessive salt concentration reverses the process, improving a *salting out* effect, and thus decreasing the ligand binding (Arakawa and Timasheff, 1984).

5.3.5.3. Target

Apart from studying the template used, the target was also analysed. Different polymers were selected to evaluate the influence of the hydrophobicity of the target on the process (Figure 5.13). Specifically, for PCL, the higher the molecular weight, the higher its hydrophobicity according to the results shown in Chapter 4 (Section 4.3.1, Figure 4.10). Therefore, polymers with different hydrophobicity were studied by performing the process on PCL with different molecular weight (80; 45 and 14 kDa).

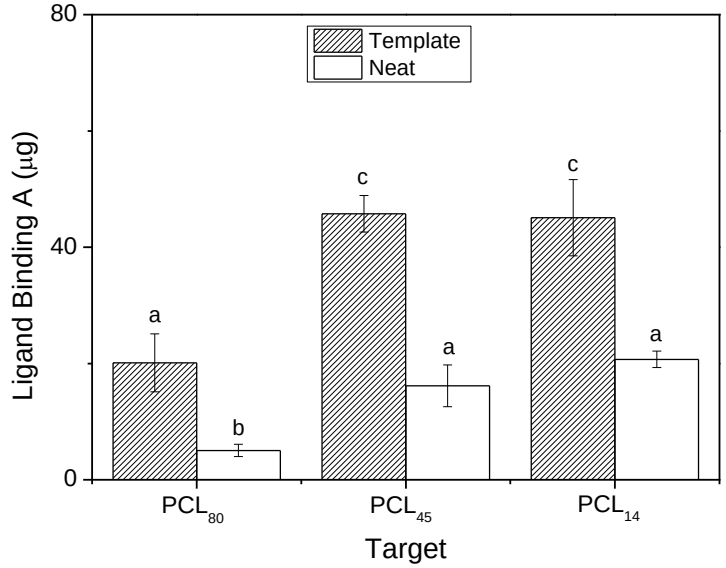

Figure 5.13. Ligand binding of PCL/GE and PCL-based scaffolds using PCL of different molecular weights as target (PCL80, PCL45, PCL14)

The differences found in the protein binding were analysed by using a ratio comparing the protein rebinding in the polymer neat scaffold (white column) and the polymer/gelatin scaffold (striped column). This ratio was calculated with the Ligand binding results obtained for the PCL/GE and PCL-based scaffolds according to the following equation (Eq. 5.2):

$$Ratio = \frac{Ligand\ Binding\ A\ (PCL/GE)}{Ligand\ Binding\ A\ (PCL)} \qquad (5.2)$$

The results are shown in the following table (Table 5.10):

Table 5.10. **Ligand binding ratio between the polymer neat and the polymer+gelatin scaffold**

POLYMER	**PCL80**	**PCL45**	**PCL14**
Ratio	3.26	2.79	2.18

Conclusion: Protein binding is favored by using hydrophilic polymers:

$$PCL_{14}>PCL_{45}>PCL_{80}$$

However, according to the ratio included in the previous table, the use of a hydrophobic polymer induced significant differences in the MI process when carrying out the process with the polymer/gelatin scaffold compared to the polymer neat system.

5.4 Concluding remarks

As a general conclusion, the different behaviors shown in this study for protein deposition on PCL scaffolds versus scaffolds made with PCL and gelatin allowed corroborating that a process of molecular imprinting takes place on the latter. In addition, it is an alternative molecular imprinting process, since it was carried out with polymeric structures, previously processed via electrospinning, instead of using crosslinkers and monomers as is traditionally conducted.

Carrying out the process with different proteins allowed determining the high selectivity of the process, since the best results were obtained when carrying out the process with the same protein with which it was initially blended with PCL (i.e., gelatin). However, good results are obtained by carrying out Stage 3 with collagen, with the possibility of using gelatin as a dummy template.

The kinetics of the process was evaluated with different immersion times, obtaining a polynomial trend reaching a plateau region after two hours, since from that time there was no increase in protein rebinding.

The study of the efficiency revealed that a decrease in the concentration of the template solution results in an enhancement in the overall efficiency of the process, but with the disadvantage of the decrease in the net amount of rebound protein. In addition, the MI process was tested by repeating this process with successive cycles (C1, C2 and C3), obtaining similar results, thus discarding the idea of a traditional protein deposition. In the same way, when carrying out a new solvent extraction after each process, it is possible to verify the reversibility of the process by obtaining the same initial systems again.

On the other hand, the process took place due to ionic interactions between both polymers, as demonstrated by the variation in protein

rebinding by modifying the pH of the template solution, thus modifying the surface charges of the protein. Furthermore, the MI process is shown to be favored when using hydrophobic targets and with the addition of substances that promote the *salting in* effect. However, the addition of molecules that promote the aggregation of the template (*salting out* effect) led to a worsening of the protein rebinding during the MI process. The study of different targets revealed that protein binding is favored by using hydrophilic polymers. However, the use of a hydrophobic polymer induced significant differences in the MI process when carrying out the process with the polymer/gelatin scaffold compared to the polymer neat system.

Consequently, the search for new techniques for the fabrication of scaffolds such as the molecular imprinting method opens a new stage in the development of scaffolds. The combination with electrospinning, apart from having a lower associated cost for the scaffolds, opens up the possibility of fine-tuning their properties. All this driving scaffolds to have a promising future in Regenerative Medicine and, specifically, in Tissue Engineering.

Acknowledgements

The authors gratefully acknowledge Complex Tissue Regeneration Department and especially to Dr. Lorenzo Moroni and Dr. Paul Wieringa (Maastricht University) for their supervision, assistance and help during the research stay in which most of these studies have been developed.

Related publications

References

Allam, E., Bottino, M.C., Al-Shibani, N., Jack Windsor, L., 2012. Collagen scaffolds: Tissue engineering and repair, Type I Collagen: Biological Functions, Synthesis and Medicinal Applications.

Arakawa, T., Timasheff, S.N., 1984. Mechanism of Protein Salting In and Salting Out by Divalent Cation Salts: Balance between Hydration and Salt Binding. Biochemistry 23, 5912–5923.

Azuaga, A.I., Dobson, C.M., Mateo, P.L., Conejero-Lara, F., 2002. Unfolding and aggregation during the thermal denaturation of streptokinase. Eur. J. Biochem. 269, 4121–4133.

Bhuyan, A.K., 2010. On the mechanism of SDS-induced protein denaturation. Biopolymers 93, 186–199.

Braunschweig, A.B., Huo, F., Mirkin, C.A., 2009. Molecular printing. Nat. Chem. 1, 353–358.

Cai, D., Ren, L., Zhao, H., Xu, C., Zhang, L., Yu, Y., Wang, H., Lan, Y., Roberts, M.F., Chuang, J.H., Naughton, M.J., Ren, Z., Chiles, T.C., 2010. A molecular-imprint nanosensor for ultrasensitive detection of proteins. Nat. Nanotechnol. 5, 597–601.

Cebi, N., Durak, M.Z., Toker, O.S., Sagdic, O., Arici, M., 2016. An evaluation of Fourier transforms infrared spectroscopy method for the classification and discrimination of bovine, porcine and fish gelatins. Food Chem. 190, 1109–1115.

Chen, L., Wang, X., Lu, W., Wu, X., Li, J., 2016. Molecular imprinting: Perspectives and applications. Chem. Soc. Rev. 45, 2137–2211.

Chen, L., Xu, S., Li, J., 2011. Recent advances in molecular imprinting technology: current status, challenges and highlighted applications. Chem. Soc. Rev. 40, 2922–2942.

Chronakis, I.S., Milosevic, B., Frenot, A., Ye, L., 2006. Generation of molecular recognition sites in electrospun polymer nanofibers via molecular imprinting. Macromolecules 39, 357–361.

Ertürk, G., Mattiasson, B., 2017. Molecular imprinting techniques used for the preparation of biosensors. Sensors (Switzerland) 17, 1–17.

Fasihi, J., Ammari Allahyari, S., Shamsipur, M., Sharghi, H., Charkhi, A., 2011. Adsorption of uranyl ion onto an anthraquinone based ion-imprinted copolymer. React. Funct. Polym. 71, 803–808.

Frenot, A., Chronakis, I.S., 2003. Polymer nanofibers assembled by electrospinning. Curr. Opin. Colloid Interface Sci. 8, 64–75.

Ghorani, B., Tucker, N., Yoshikawa, M., 2015. Approaches for the assembly of molecularly imprinted electrospun nanofibre membranes and consequent use in selected target recognition. Food Res. Int. 78, 448–464.

Grundl, G., Müller, M., Touraud, D., Kunz, W., 2017. Salting-out and salting-in effects of organic compounds and applications of the salting-out effect of Pentasodium phytate in different extraction processes. J. Mol. Liq. 236, 368–375.

Gümüşderelioğlu, M., Dalkıranoğlu, S., Aydın, R.S.T., Çakmak, S., 2011. A novel dermal substitute based on biofunctionalized electrospun PCL nanofibrous matrix. J. Biomed. Mater. Res. Part A 98A, 461–472.

Hardy, J.G., Römer, L.M., Scheibel, T.R., 2008. Polymeric materials based on silk proteins. Polymer (Guildf). 49, 4309–4327.

Hayden, O., Dickert, F.L., 2001. Selective Microorganism Detection with Cell Surface Imprinted Polymers. Adv. Mater. 13, 1480–1483.

Jahn, T.R., Radford, S.E., 2008. Folding versus aggregation: Polypeptide conformations on competing pathways. Arch. Biochem. Biophys. 469, 100–117.

Kadhirvel, P., Machado, C., Freitas, A., Oliveira, T., Dias, R.C.S., Costa, M.R.P.F.N., 2015. Molecular imprinting in hydrogels using reversible addition-fragmentation chain transfer polymerization and continuous flow micro-reactor. J. Chem. Technol. Biotechnol. 90, 1552–1564.

Muyonga, J.H., Cole, C.G.B., Duodu, K.G., 2004. Fourier transform infrared (FTIR) spectroscopic study of acid soluble collagen and gelatin from skins and bones of young and adult Nile perch (Lates niloticus). Food

Chem. 86, 325–332.

Turiel, E., Martin-Esteban, A., Fernandez, P., Perez-Conde, C., Camara, C., 2001. Molecular recognition in a propazine-imprinted polymer and its application to the determination of triazines in environmental samples. Anal. Chem. 73, 5133–5141.

Whitcombe, M.J., Kirsch, N., Nicholls, I.A., 2014. Molecular imprinting science and technology: A survey of the literature for the years 2004-2011, Journal of Molecular Recognition.

Woodruff, M.A., Hutmacher, D.W., 2010. The return of a forgotten polymer—Polycaprolactone in the 21st century. Prog. Polym. Sci. 35, 1217–1256.

Wulff, G., Schauhoff, S., 1991. Enzyme-analog-built polymers. 27. Racemic resolution of free sugars with macroporous polymers prepared by molecular imprinting. Selectivity dependence on the arrangement of functional groups versus spatial requirements. J. Org. Chem. 56, 395–400.

Ye, L., Weiss, R., Mosbach, K., 2000. Synthesis and Characterization of Molecularly Imprinted Microspheres. Macromolecules 33, 8239–8245.

Yoshikawa, M., 2001. Molecularly imprinted polymeric membranes. Bioseparation 10, 277–286.

Yoshikawa, M., Izumi, J., Kitao, T., Koya, S., Sakamoto, S., 1995. Molecularly imprinted polymeric membranes for optical resolution. J. Memb. Sci. 108, 171–175. https://doi.org/https://doi.org/10.1016/0376-7388(95)00160-8

Yoshikawa, M., Tanioka, A., Matsumoto, H., 2011. Molecularly imprinted nanofiber membranes. Curr. Opin. Chem. Eng. 1, 18–26.

Zhang, Z., Li, J., Song, X., Ma, J., Chen, L., 2014. Hg2+ ion-imprinted polymers sorbents based on dithizone–Hg2+ chelation for mercury speciation analysis in environmental and biological samples. RSC Adv. 4, 46444–46453.

Chapter 6: Biological evaluation of scaffolds

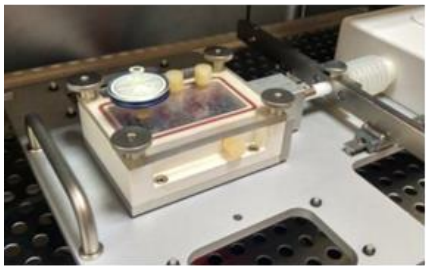

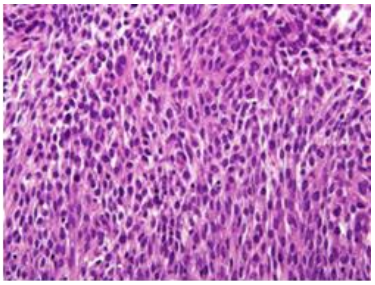

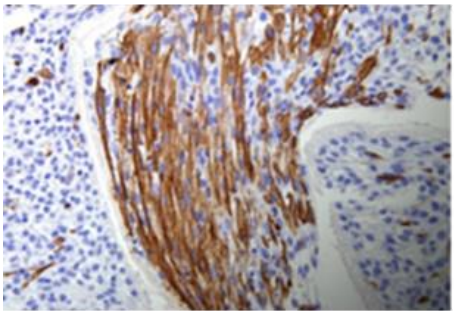

6.1 Introduction

The formation of skeletal muscle tissue *in vitro* is one of the topics of greatest interest in recent years in the field of biomedical research and, although great advancements have been made, nowadays, finding the optimal biophysical conditions that must be applied in the cellular environment is still a challenge (Aghaee-Afshar et al., 2009; Bisson et al., 2015; Frudinger et al., 2010; Saihara et al., 2009).

The nature of musculoskeletal diseases is complex and little known. They encompass a wide spectrum of pathologies that affect different connective tissues of the skeletal system, including bones, cartilage, muscles, tendons and ligaments. Due to the lack of knowledge about the etiopathology of many of these diseases, treatment options are limited in most cases to the control of their symptoms rather than to their cure or prevention (Pimentel et al., 2017).

The total muscle tissue represents 40% of the human body and its structure is greatly adapted to its function, which limits its ability to restore itself after damage. The nature of musculoskeletal diseases is poorly understood, which restricts the treatment of patients. Therefore, the creation of skeletal muscle tissue *in vitro* is a major topic of current interest in the field of biomedical research.

For the creation of skeletal muscle tissue *in vitro*, it is necessary to know the formation process of its basic structural unit, the skeletal muscle cell, also known as muscle fiber. Muscle fibers are grouped in parallel (fascicles), with a thickness that varies according to muscle activity; each part is surrounded by connective tissue septa with abundant collagen fibers, capillaries and nerve fibers (perimysium). Fascicles are grouped to form muscles and they are surrounded by a band of irregular dense connective tissue with abundant type I and II collagen fibers and elastic

fibers called epimysium, which is continuous, with tendons and muscle insertions. Through the epimysium, the arteries and nerves penetrate the muscles, branching through the perimysium and endomysium to bring irrigation and innervation to the muscle fibers (Clark et al., 2002).

Skeletal muscle cells are cylindrical and very elongated, their size varies from 10 to 100 μm and their length varies from 1 to 50 mm. The plasma membrane (also called sarcolemma) is surrounded by a basal membrane consisting of a basal lamina and a layer of reticular fibers. Each muscle cell contains numerous nuclei elongated in the direction of the fiber and arranged in its periphery (Paniagua, 2007).

Efforts have been made to evaluate the effect of scaffold characteristics on cellular behavior (Jafari et al., 2017). There are many studies in the literature about the use of both artificial and natural polymers in the manufacture of scaffolds for biomedical applications. In the case of synthetic polymers, it is relatively easy to control the characteristics of scaffolds manufactured from synthetic polymers, although this involves certain problems related to their immunogenicity and the inflammation they cause once they are grafted into the organism (Taylor et al., 1994).

In addition, nowadays, there are still unsolved challenges in obtaining multifunctional scaffolds, mainly related to vascularization, nerve regeneration, electromechanical coupling, and structural, mechanical and electrophysiological properties that allow for a better contractile function of the cells. The main disadvantage, particularly in the production of musculoskeletal tissues, is the absence of physiological and mechanical stimuli during their formation, which prevents adequate cellular regulation and spatial development of the tissue, with the consequent decrease in its mechanical quality (Barrère et al., 2008; Lee et al., 2001). Furthermore, it has been proved that the culture of cells in

2D does not reproduce the anatomy or physiology of a tissue, whereas in 3D culture in static growth, although it allows the proliferation and differentiation in the surface by being in direct contact with the culture medium, the cell nucleus becomes hypoxic, and less active or necrotic areas appear. Therefore, the current methodology of 3D sowing, instead of static growth, uses bioreactors that recreate the proper conditions of muscle tissue *in vivo*, subjecting the seeded scaffold to mechanical stimulations that promote more efficient cellular repopulation, differentiation and remodeling of the scaffold (Wang et al., 2013).

Therefore, in order to achieve a greater expansion of cells in culture, thus increasing the production of tissue *in vitro*, as well as an improvement of its properties, we propose in this study the introduction of a bioreactor that provides these mechanical load stimuli.

6.2 Material and methods

6.2.1. Materials

Among the scaffolds produced with the different techniques explained in the previous sections, the electrospun scaffolds were selected as the most promising to perform further biological analysis.

Therefore, PCL/GE 16/4 scaffolds were selected to carry out the biological analysis, assessing the influence of this system with different alignments (random, semi-aligned and aligned) on the growth and proliferation of skeletal muscle cells.

6.2.2. Biological study

Cell culture

A suitable synergy is necessary between the type of cells used, the environment subjected and the architecture and properties of the scaffold in order to obtain *ex vivo* skeletal muscle tissue. The cell lines mostly used for the creation of *ex vivo* muscle tissue were C2C12 (mouse) and L6 (rat), obtaining great advances with the latter.

Thus, cell culture was carried out using Rattus norvegicus skeletal muscle cells, cell line L6 (ATCC ® CRL-1458™). Cells were grown in Minimum Essential Medium α (MEM α, 12571-063, Gibco), supplemented with 10% fetal bovine serum (F7524, Sigma Aldrich) and 1% streptomycin penicillin (15140-122, Gibco) and they were kept in an incubator with controlled temperature and carbon dioxide (37 °C and 5% CO_2).

Cell seeding on scaffolds

The cells were subcultured using 0.05% trypsin / EDTA (25300-062, Gibco) when 85-90% confluence was reached. Then, they were planted on the scaffolds, which were previously sterilized. Seeding was

performed once $10x10^6$ cells were quantified and incorporated in each scaffold. The samples were left inside the incubator for 2 hours to allow the anchoring of the cells to the scaffold.

Bioreactor stimulation

After 2 h in the incubator, the scaffolds were placed in the bioreactor's culture chamber. The culture chamber was filled with 45 ml of the growth medium, which was replaced after 72h. During the following 48 hours, in order to allow cells to differentiate in the scaffold, the media was replaced with differentiation culture media (MEM α) supplemented with 2% horse serum (S0910, Biowest) and 17.8 mM NaHCO3 (S6297, Sigma-Aldrich), after washing the scaffold with PBS (phosphate buffer saline, L0615, Linus).

6.2.2.1 "In vitro" evaluation

When the two weeks of culture were reached, the scaffolds of the *in vitro* studies were extracted from the culture chamber for fixation and histological and immunohistochemical evaluation.

Hematoxylin-Eosin staining (H&E)

Hematoxylin (GHS316 Hematoxylin Solution, Gill No. 3) and eosin (HT110116 500ML: Eosin Y Solution) staining was carried out. In this way, blue and purple dyeing of acidic structures such as the cell nucleus is achieved, whereas with eosin it is possible to dye the alkaline structures pink, such as cellular cytoplasms.

Immunohistochemical staining (IHC)

Immunohistochemical staining was performed with the smooth muscle actin antibody (Actin, Smooth Muscle (1A4) Mouse Monoclonal Antibody, Cell Marque). With this procedure, it is possible to identify the protein that has specifically bound to the antibody. The smooth

muscle actin antibody was used to detect the muscle cells and determine their degree of differentiation.

6.2.2.2 "In vivo" evaluation

The scaffolds implanted in the animal model, at the *in vivo* stage, were extracted on the day that the surgical procedure was performed.

The scaffolds were implanted into female Wistar rats weighing between 230~280 g. They were anesthetized by intraperitoneal injection of Ketamine and Xylazine, at doses of 80 and 10 mg per kg of weight, respectively. The puncture was carried out with a hypodermic needle (lateral to the midline), close to the vertex of the bladder. All the animals were analgesiated with Meloxicam (1mg/Kg every 24 hours) and kept in separate cages.

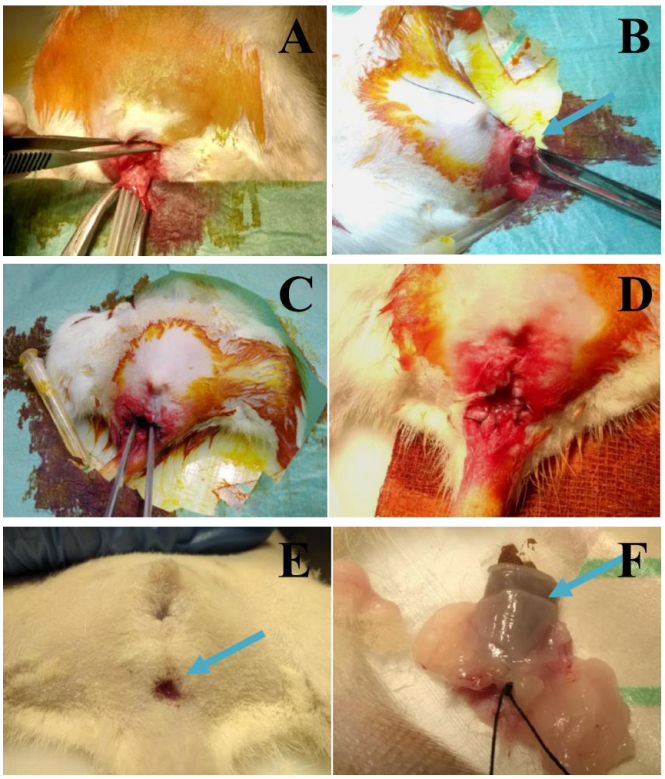

Figure 6.1. Stages of the surgical procedure performed to the rats

The first step of the surgery was to perform a perineal amputation of the sphincter and rectum complex (Figure 6.1A). After the anorectal amputation, the cultured scaffold was placed on the anterior surface of the rectum in the form of a hemi-sphincter with two Vicryl 4/0 stitches (Figure 6.1B). Finally, a recto-cutaneous anastomosis with Vicryl 4/0 stitches was performed, reconstructing the natural anal canal orifice again (Figures 6.1C and 6.1D). After the surgery, the animals were left for 30 days with water and free feed. Once a week they were weighed, and the number of bowel movements was counted each week. The animals were sacrificed one month after the surgery by injection of thiobarbital sodium (diluted in physiological serum) to avoid the pain caused by the irritation in the peritoneum, at a dose of 1 mL. During the autopsy, the final section of the rectum and the perineum were extracted and fixed in 4% formaldehyde to be processed (Figures 6.1E and 6.1F).

6.2.3. Statistical analysis

Student´s t-test and one-way analysis of variance ($p<0.05$) were performed using PASW Statistics for Windows (Version 18: SPSS, Chicago, IL). Standard deviations were calculated for selected parameters.

6.3. Results and Discussion

6.3.1. "In vitro" evaluation

The in vitro evaluation consisted of studying and analyzing:

- Cell proliferation, obtained by performing nuclear counting.
- Cell viability, calculated by estimating the percentage of living cells with respect to the areas of necrosis.
- Cell occupation on the scaffold
- Degree of differentiation in the scaffolds by analyzing immunohistochemical images.

Hematoxylin-Eosin staining (H&E):

The images of the H&E staining are shown in Figure 6.2. Figures 6.2A and 6.2B show the resulting images for the random system at 10x and 40x, respectively. It is possible to see foci of necrosis, with indicators of cell death such as rounded morphology, eosinophilic cytoplasm and retracted and pyknotic nuclei, although generally viable cells with a good cell density and cells in different phases of cell division predominate. Moreover, it can be observed that it has a lower alignment, corresponding to its properties.

Moreover, Figures 6.2C and 6.2D show the semi-aligned system after the staining. Minimal foci of necrosis are observed; the rest are viable cells well distributed homogeneously with a good cell density and cells in different phases of cell division.

On the other hand, the images corresponding to the aligned system (Figures 6.2E and 6.2F) show viable cells homogeneously distributed; however, more foci of necrosis can be seen in different areas. The morphology of the cells indicates that there are many of them which are in the stage prior to cell death.

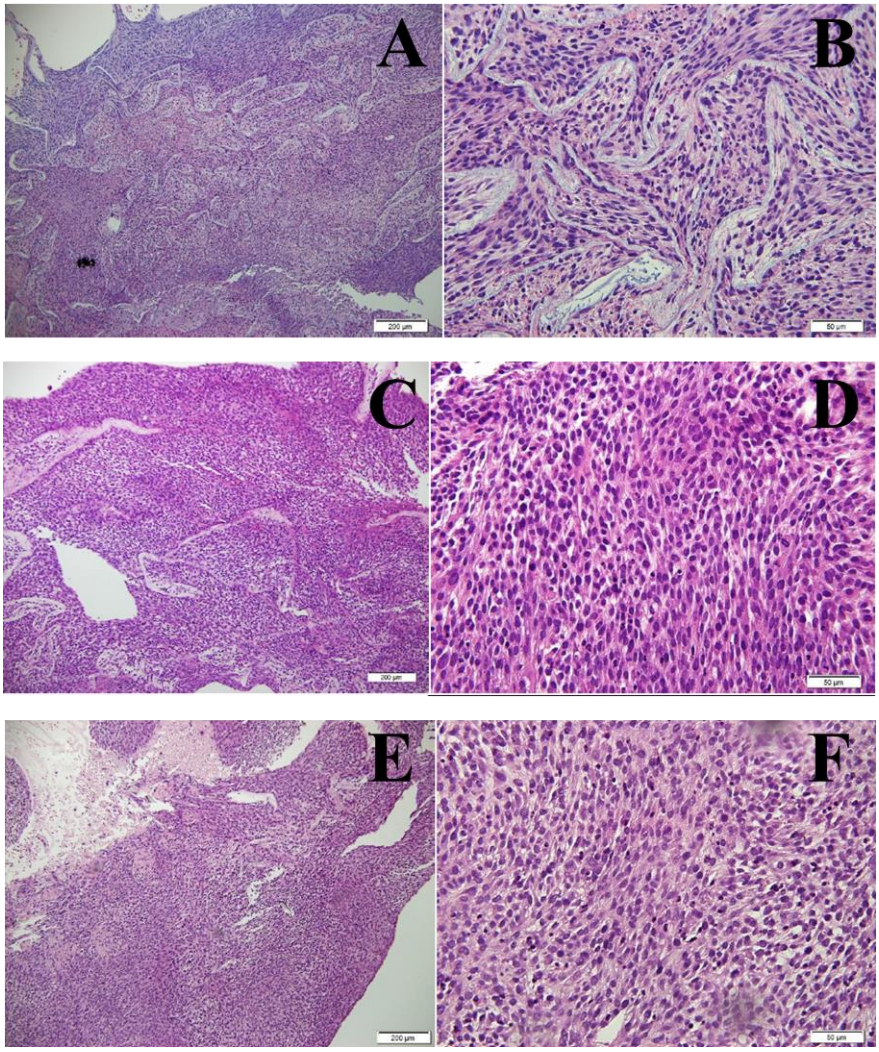

Figure 6.2. H&E staining images of the different scaffolds processed with different alignments: random (A and B), semi-aligned (C and D) and aligned (E and F) at 10x and 40x, respectively

After analyzing the different images obtained, the nuclear count, cell area and occupation were calculated, as well as the cell viability for each type of scaffold. The results are summarized below (Table 6.1). Considering the results obtained, fiber alignment did not influence cell population or occupation. However, improvements were obtained in cell viability and

cell area when an intermediate alignment was used (semi-aligned systems).

Table 6.1. Comparative results (cell population, cell viability, cell area and occupation) obtained staining image of the different scaffolds processed with different alignments: random, semi-aligned and aligned

SYSTEMS	Cell Population	Cell Viability (%)	Cell Area (μm^2)	Occupation (%)
Random	1217^{α}	71.7^{A}	23.96^{a}	22^{I}
Semi-aligned	1220^{α}	86.7^{B}	27.86^{b}	23^{I}
Aligned	1194^{α}	57.5^{C}	26.59^{ab}	21^{I}

Immunohistochemical staining (IHC):

Apart from the H&E staining, immunohistochemical staining (IHC) was also carried out to study the degree of cell differentiation with smooth muscle actin antibody. The results for the three systems evaluated are shown in Figure 6.3.

The results showed that the random scaffold (Figures 6.3A, $6.3A_1$ and $6.3A_2$) had areas where the desired protein is expressed, although very scarcely and mostly by the edges of the scaffold. There were few fusiform cells, characteristic of myotubules, that may be due to the low percentage of alignment, which does not favor the fusion of the cells. However, the cells seeded in the semi-aligned scaffolds expressed the desired protein, since the actin antibody was recognized. The expression of the desired protein was slightly higher in the aligned scaffolds with respect to the random system; however, it was similar to that obtained for the semi-aligned system. In this case, it predominated at the edges. In the images taken at higher magnification (Figures $6.3C_1$ and $6.3C_2$), some isolated cells with fusiform shaped can be observed.

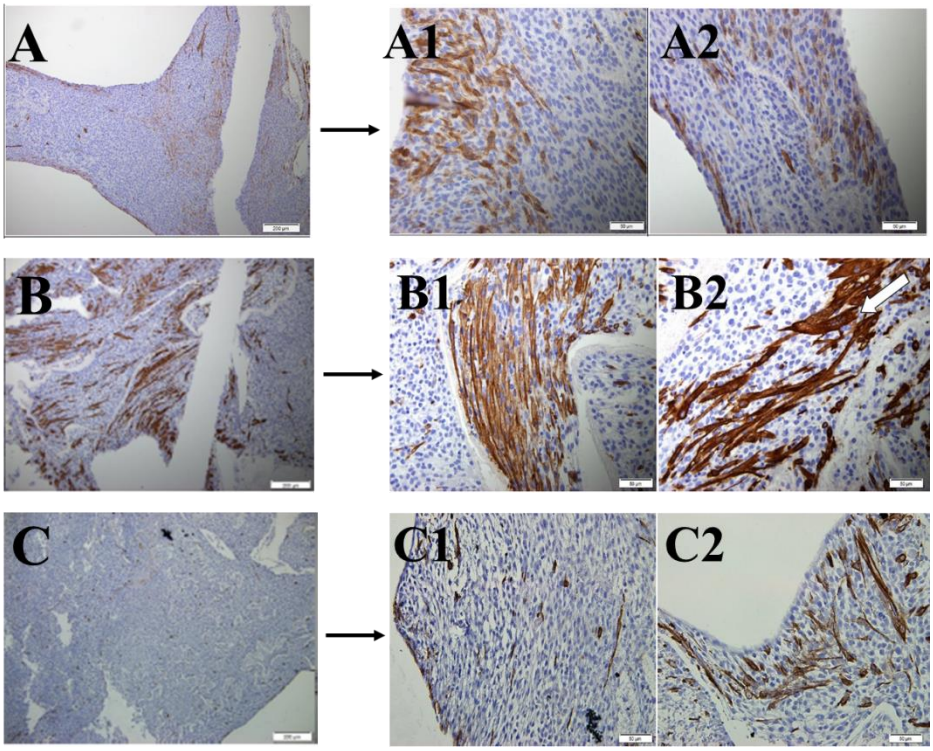

Figure 6.3. IHC staining images of the different scaffolds processed with different alignments at 10x: (A) random, (B) semi-aligned and (C) aligned; and at 40x: (A1-A2) aligned, (B1-B2) semi-aligned and (C1-C2) aligned

6.3.2. "In vivo" evaluation

Preliminary analysis:

First, the mortality was evaluated without noticing any deaths during the implant surgery and the postoperative period. In addition, a study of the evolution of the weight of the rats and the number of their depositions was carried out throughout the experiment to analyze whether the implanted scaffold influenced the general health state of the animal. The results are shown in Figure 6.4:

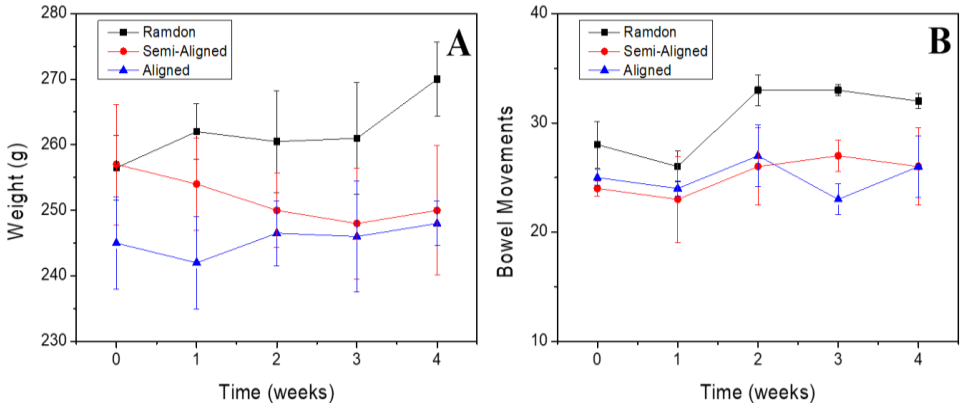

Figure 6.4. (A) Weight variation and (B) bowel movements of the rats after the surgery during the four week-experiment

Figure 6.4A shows the evolution of the weight of the rats during the four week-experiment and moments before the final surgery (week 4). The weight of the rats remained constant with no significant changes throughout the experiment; thus, a dramatic decrease in the weight produced by the surgery was not observed. Furthermore, there is a correct opening of the anus and of the neo-sphincter from the implantation of the scaffold, since there was not a significant drop in the bowel movements according to the results shown in Figure 6.4B.

Macroscopic evaluation:

First of all, in all the sacrificed rats, the correct healing of the recto-cutaneous anastomosis and the opening of the neo-sphincter was observed (see Figure 6.5):

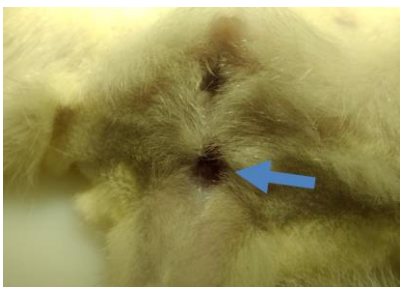

Figure 6.5. Image evidencing the correct opening of the rat's anus before sacrifice

Figure 6.5 shows the correct healing of the recto-cutaneous anastomosis and its opening, which was observed in all the sacrificed rats. Thus, anal stenosis (narrowing of the anus due to scar tissue in the anal canal, which may cause pain and other problems) was not observed.

Microscopic evaluation:

At the microscopic level, different variables were studied:

- Inflammatory reaction: by studying the presence of multinucleated giant cells, histiocytes, etc.
- Location of the scaffold in the histological section and its retraction.
- Muscular structure creation.

The histopathological study of all the systems showed chronic granulomatous inflammation, with the presence of multinucleated giant cells, histiocytes, macrophages, plasma cells and lymphocytes, in a lower proportion. This inflammation is characteristic of a reaction to foreign bodies, which may be due to the presence of suture wire, both from the scaffold and from the recto-cutaneous anastomosis, as can be observed in all the samples (see Figure 6.6).

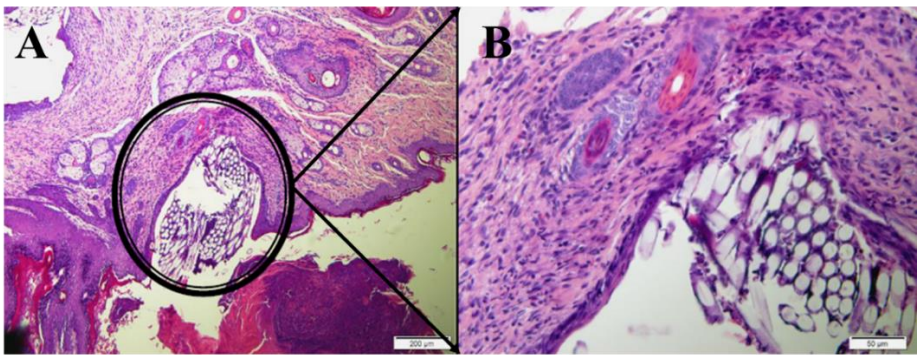

Figure 6.6. Suture with granulomatous chronic inflammatory reaction at two magnifications: (A) 10x and (B) 40x

However, locating the scaffold could only be possible for the semi-aligned and aligned systems, as shown in Figure 6.7. However, in none of these two systems, or around them, were muscle cells located; only the cells corresponding to the inflammatory reaction were found.

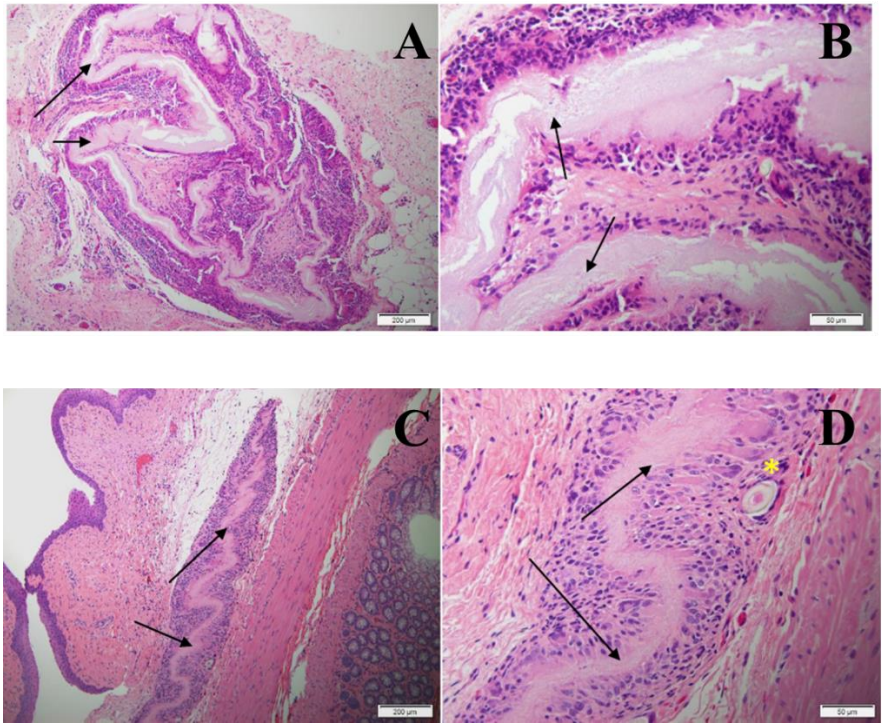

Figure 6.7. Histopathologic study of the semi-aligned (A and B) and aligned (C and D) systems at two different magnifications (10x and 40x, respectively). Arrows show the scaffold and * shows stitches

This is also confirmed by immunohistochemistry (Figure 6.8), showing that the scaffold is marked nonspecifically, and the labeled cells are inflammatory cells (noticing the absence of muscle cells in the scaffold). Necrotic or degenerated cells also show nonspecific staining. By histologically analyzing the samples taken from the neo-sphincter, it can be considered that the cells involved in the granulomatous inflammatory reaction are degrading the material; therefore, these cells have

phagocytosed the muscle cells implanted in the scaffold, thus justifying their absence.

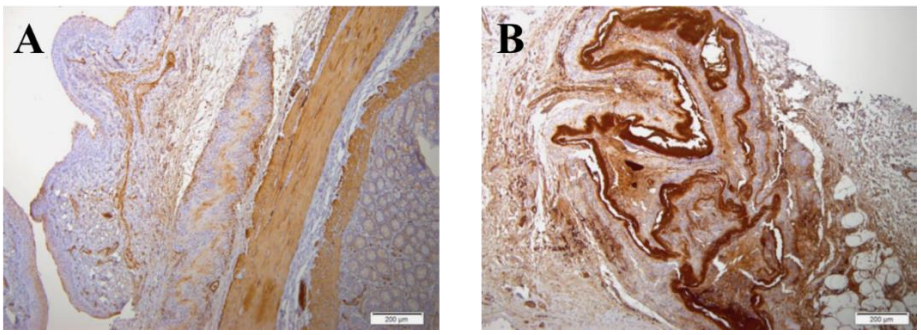

Figure 6.8. Non-specific immunohistochemistry of rat (A) semi-aligned and (B) aligned scaffolds

6.4 Concluding remarks

As a general conclusion, the creation of *ex vivo* skeletal muscle tissue through the use of a bioreactor as well as its perirectal implantation as a neo-sphincter were obtained by using PCL/GE 16/4 (4%) electrospun scaffolds.

Fiber alignment did not influence cell proliferation *in vitro*. However, the alignment of the fibers played an important role in cell growth and viability. Cell viability and differentiation were promoted to a greater extent in the semi-aligned scaffolds as compared to the random and aligned scaffolds.

It was possible to implant the cell-seeded scaffolds in an animal model. The implantation of the scaffolds did not produce any anal stenosis in the rats and, consequently, no obstructive defecation or weight variation was observed. However, chronic granulomatous foreign body inflammation was shown in all the systems, together with the absence of muscle cells. Future research in this project can be carried out with the improvement of the *in vitro* phase to obtain a more mature muscle tissue prior to implantation, which can survive the possible inflammatory reaction of the animal. Therefore, the next step will be to carry out tests increasing the time of the scaffolds in the bioreactor.

Acknowledgements

The authors gratefully acknowledge the Department of General and Digestive Surgery, Colorrectal Surgery Unit, from the "Virgen del Rocío" University Hospital (IBiS/CSIC/University of Seville), especially to Yaiza Yuste, who carried out the biological study under the supervision of Professor Dr. Fernando de la Portilla de Juan.

Related publications

References

Aghaee-Afshar, M., Rezazadehkermani, M., Asadi, A., Malekpour-Afshar, R., Shahesmaeili, A., Nematollahi-mahani, S.N., 2009. Potential of human umbilical cord matrix and rabbit bone marrow-derived mesenchymal stem cells in repair of surgically incised rabbit external anal sphincter. Dis. Colon Rectum 52, 1753–1761.

Barrère, F., Mahmood, T.A., de Groot, K., van Blitterswijk, C.A., 2008. Advanced biomaterials for skeletal tissue regeneration: Instructive and smart functions. Mater. Sci. Eng. R Reports 59, 38–71.

Bisson, A., Freret, M., Drouot, L., Jean, L., Le Corre, S., Gourcerol, G., Doucet, C., Michot, F., Boyer, O., Lamacz, M., 2015. Restoration of anal sphincter function after myoblast cell therapy in incontinent rats. Cell Transplant. 24, 277–286.

Clark, K.A., McElhinny, A.S., Beckerle, M.C., Gregorio, C.C., 2002. Striated muscle cytoarchitecture: an intricate web of form and function. Annu. Rev. Cell Dev. Biol. 18, 637–706.

Frudinger, A., Kolle, D., Schwaiger, W., Pfeifer, J., Paede, J., Halligan, S., 2010. Muscle-derived cell injection to treat anal incontinence due to obstetric trauma: pilot study with 1 year follow-up. Gut 59, 55–61.

Jafari, M., Paknejad, Z., Rad, M.R., Motamedian, S.R., Eghbal, M.J., Nadjmi, N., Khojasteh, A., 2017. Polymeric scaffolds in tissue engineering: a literature review. J. Biomed. Mater. Res. B. Appl. Biomater. 105, 431–459.

Lee, C.H., Singla, A., Lee, Y., 2001. Biomedical applications of collagen. Int. J. Pharm. 221, 1–22.

Paniagua, R., 2007. Citología e histología vegetal y animal, Vol. 2, 4th ed, Citología e histología vegetal y animal: biología de las células y tejidos animales y vegetales. McGraw-Hill Interamericana de España S.L.

Pimentel, M.R., Falcone, S., Cadot, B., Gomes, E.R., 2017. In Vitro Differentiation of Mature Myofibers for Live Imaging. J. Vis. Exp. DOI: 10.3791/55141

Saihara, R., Komuro, H., Urita, Y., Hagiwara, K., Kaneko, M., 2009. Myoblast transplantation to defecation muscles in a rat model: a possible treatment strategy for fecal incontinence after the repair of imperforate anus. Pediatr. Surg. Int. 25, 981.

Taylor, M.S., Daniels, A.U., Andriano, K.P., Heller, J., 1994. Six bioabsorbable polymers: in vitro acute toxicity of accumulated degradation products. J. Appl. Biomater. 5, 151–157.

Wang, B., Wang, G., To, F., Butler, J.R., Claude, A., McLaughlin, R.M., Williams, L.N., de Jongh Curry, A.L., Liao, J., 2013. Myocardial scaffold-based cardiac tissue engineering: application of coordinated mechanical and electrical stimulations. Langmuir 29, 11109–11117.